Doctoral Dissertation
Doctoral Program in Metrology (34th Cycle)

Innovative methods and metrological aspects applied to food safety: case studies of OTA and SO_2

By

Iris Cagnasso

******

Supervisors:
Prof. Fabrizio Giorgis ,Supervisor
Dr. Francesca Durbiano, Co-Supervisor

Doctoral Examination Committee:
Prof. Laura Anfossi , Referee, Università degli Studi di Torino
Dr. Pietro Giuseppe Gucciardi, Referee, Istituto per i Processi Chimico Fisici - CNR Messina
Dr. Michela Sega, Istituto Nazionale di Ricerca Metrologica (INRiM)
Prof. Ornella Abollino, Referee, Università degli Studi di Torino
Prof. Elena Tresso, Politecnico di Torino

Politecnico di Torino
2022

Declaration

I hereby declare that, the contents and organization of this dissertation constitute my own original work and does not compromise in any way the rights of third parties, including those relating to the security of personal data.

Iris Cagnasso

2022

* This dissertation is presented in partial fulfillment of the requirements for **Ph.D. degree** in the Graduate School of Politecnico di Torino (ScuDo).

Abstract

Food is an essential component in our daily life since it provides essential nutrients for life. The access to healthy food is a fundamental human right. However, from a chemical point of view, foods may contain some substances that affect their composition, quality and safety. These substances are food contaminants and food additives. For this reason, growing attention from the scientific community is placed on the issue of food safety. Given their potential impact on consumer health, contaminants and additives are subjected to specific legislations that establish their concentration limits in food products intended for human consumption. To ensure the food quality, many analytical methods have been developed or are under study. Nowadays, the challenge is to improve the reproducibility and the limit of detection of these methods and to reduce their uncertainties. Within this framework metrology in chemistry is placed, which has among its main objectives the production of certified reference materials (CRM).

In this thesis, two main targets were considered: the ochratoxin A (OTA), which is a food contaminant, and the sulfur dioxide (SO_2), which is a food additive. These two case studies were tackled by considering different analytical techniques and trying to provide a characterization of several aspects. However, some similarities were present in the approaches used to study the two molecules.

About OTA, in order to test one of the most used technique, firstly the HPLC-FLD method was used to quantify its concentration in a CRM of red wine. Then, a comprehensive description of the behaviour of OTA in aqueous solutions was performed in a range of pH from 1 to 12.5. Under conditions from acid to neutral, its two acid dissociation constants were evaluated by two independent techniques. Under alkaline conditions, the most probable degradation pathway of OTA was defined by experimental findings flanked by theoretical simulations. Furthermore, the conditions of reversibility of this process was studied. Another activity regarded a feasibility study for OTA identification by Raman and a SERS spectroscopy. Raman spectroscopy was useful to obtain a reference spectrum of solid OTA and to identify its most relevant peaks. An in liquid label-free SERS method taking advantage of AgNPs as a substrate for the identification of OTA was developed and tested. Lastly, a work for culturing, isolation, and purification of OTA for reference material production was performed during a Secondment at the NRC – Canada.

About SO_2, a measurement comparison among nine specialized laboratories was conducted to evaluate its maximum recovery from a wine simulant by applying the official OIV-OENO 591A-2018 method. Moreover, a rigorous evaluation of the measurement uncertainty associated to the free SO_2 concentration achieved by this method was performed to be in support to the procedure stated by the International Organisation of Vine and Wine (OIV). For these studies, a candidate CRM of free SO_2 in wine simulant was produced and a first characterization attempt was carried out. Another work was the development of an in liquid SERS method for the quantification of total SO_2 in wine. Tests of interaction between the AgNPs and the SO_2 were performed and then six wines were analysed. A comparison between this innovative method and the OIV-OENO 591B-2018 method, taken as a reference, was conducted.

In order to develop the SERS methods for both the analytes, AgNPs with three different average sizes (4, 30 and 55 nm) have been carefully synthesized, characterized and tested.

In conclusion, the main aspects covered in this research activity were the characterization of the analytes and of the AgNPs, the improvement of the knowledge in specific areas regarded both the analytes, the development of new analytical methods, the evaluation of the measurement uncertainty and the preliminary studies for the future production of certified reference materials of both OTA and SO_2.

Contents

1. Introduction 1
1.1 Metrology issues 1
1.2 Food safety 3
1.3 Food contaminants and food additives 4
1.4 Topics and structure of my PhD thesis 7
2. Silver nanoparticles (AgNPs) 10
2.1 Introduction 10
2.2 Chemicals 14
2.3 Synthesis 15
2.4 Methods for AgNPs characterization (instrumental setup) 19
2.4.1 UV-Vis 19
2.4.2 Transmission Electron Microscopy (TEM) 19
2.4.3 Inductively Coupled Plasma – Mass Spectrometry (ICP-MS) 19
2.5 Results and discussion 20
2.6 Surface Enhanced Raman Scattering (SERS) 23
2.7 Use of AgNPs for in liquid SERS analysis in this thesis 24
3. Ochratoxin A (OTA) 28
3.1 Introduction to mycotoxins 28
3.2 Description and characteristics of OTA 29
3.3 Quantification of OTA in a CRM of red wine by High Performance Liquid Chromatography with Fluorescence Detection (HPLC-FLD) 32

3.3.1 Scope of the work 32
3.3.2 Chemicals.....33
3.3.3 Solution for HPLC-FLD 33
3.3.4 Preparation of calibration solutions of OTA.....33
3.3.5 Pre-treatment of the CRM of OTA in red wine 34
3.3.6 High Performance Liquid Chromatography with Fluorescence Detection (HPLC-FLD).....35
3.3.7 Densimeter 35
3.3.8 Results and discussion 35
3.3.9 Conclusion and future perspectives 41
3.4 Comprehensive study of OTA behaviour in aqueous solution.....42
3.4.1 Scope of the work 42
3.4.2 Chemicals.....43
3.4.3 UV-Vis spectrophotometry with a stoichiometric approach 44
3.4.4 Fluorescence spectroscopy coupled with a chemometric approach45
3.4.5 Theoretical method by Density Functional Theory (DTF) 46
3.4.6 Results and discussion 47
3.4.7 Conclusion and future perspectives 63
3.5 Feasibility study of OTA identification by Raman spectroscopy and label-free in liquid SERS method 64
3.5.1 Introduction to SERS for the determination of mycotoxins 64
3.5.2 Scope of the work 65
3.5.3 Chemicals.....66
3.5.4 Preparation of OTA samples for Raman measurements.....67
3.5.5 Synthesis and characterization of AgNPs colloidal suspensions....67
3.5.6 Preparation of of OTA samples for SERS measurements 67
3.5.7 Raman spectroscopy 68
3.5.8 Label-free in liquid SERS method.....68

3.5.9 Results and discussion 69
3.5.10 Conclusion and future perspectives 78
3.6 Abroad experience: Skills Broadening Secondment on OTA 79
3.6.1 Introduction 79
3.6.2 Skills Broadening Secondment on OTA at NRC - Canada 80
3.6.3 Results 80
3.6.4 Conclusion 84
4. Sulfur dioxide (SO_2) 85
4.1 Introduction to sulfites 85
4.2 SO_2 in wine 87
4.3 OIV-OENO 591A-2018 method: free SO_2 maximum recovery in wine simulant solution 89
4.3.1 Scope of the work 90
4.3.2 Chemicals 90
4.3.3 Preparation of wine simulant solution with a specific concentration of SO_2 92
4.3.4 Measurement procedure and INRiM apparatus 92
4.3.5 Organization of the comparison 96
4.3.6 Results and discussion 97
4.3.7 Conclusion and future perspectives 101
4.4 Evaluation of measurement uncertainty 103
Part of the work described in this chapter was also published in the paper: “Evidence of a systematic underestimation of free sulfur dioxide by the aeration-oxidation method approved by OIV” published on Measurement in 2022 [303]. 103
4.4.1 Scope of the work 103
4.4.2 Chemicals 104
4.4.3 Preparation of wine simulant solution with a specific concentration of SO_2 104

4.4.4 Measurement procedure and INRiM apparatus 105
4.4.5 The measurement uncertainty 105
4.4.6 Results and discussion 107
4.4.7 Conclusion and future perspectives 119
4.5 In liquid SERS quantification of SO_2 in wine 121
4.5.1 Scope of the work 121
4.5.2 Chemicals 123
4.5.3 Preparation of wine simulant solution 123
4.5.4 Synthesis and characterization of AgNPs colloidal suspensions 123
4.5.5 Pre-cleaning of wine samples and preparation of the AgNPs – SO_2 mix for wine sample analysis 123
4.5.6 UV-Vis spectroscopy 124
4.5.7 SERS method 124
4.5.8 OIV method 126
4.5.9 Results and discussion 126
4.5.10 Conclusions and future perspectives 143
5. Final conclusions and future perspectives 145
6. References 151

List of Figures

Figure 1: Application of nanoparticles. 12

Figure 2: Approaches and methods for the synthesis of nanoparticles 13

Figure 3: Main parameters of the nanoparticles 14

Figure 4: Scheme of stepwise size-controlled synthesis of AgNPs 15

Figure 5: Setup for the AgNPs synthesis 16

Figure 6: Characterization of 4, 30 and 55 nm AgNPs 21

Figure 7: The pH dependent OTA forms in aqueous solutions 30

Figure 8: Chromatogram of standard 1 of OTA used to create the calibration curve 36

Figure 9: Calibration curve of OTA standards with HPLC-FLD 38

Figure 10: Chromatograms of the two samples from the CRM of OTA in red wine 40

Figure 11: UV-Vis spectra of OTA solution in function of the pH 47

Figure 12: Behaviour of ε in function of the pH for the OTA forms 48

Figure 13: EEMs of OTA solutions at different pH 51

Figure 14: Emission loadings from the two component PARAFAC model and experimental emission spectra extrapolated from the EEMs 52

Figure 15: Scatter scores plot in function of the pH 53

Figure 16: Experimental excitation spectra extrapolated from the EEMs and intensities ratio curve as a function of the pH 54

Figure 17: Deconvolutions of monoanionic and dianionic peaks in the excitation spectra 55

Figure 18: Diagram of percentage distribution of the three forms of OTA in function of the pH 56

Figure 19: EEMs of OTA solutions and OTα solution under alkaline conditions 57

Figure 20: Fluorescence excitation spectrum of the RM of OTα under alkaline conditions....58

Figure 21: Theoretical most probable degradation pathway....60

Figure 22: EEM of OTα solution at pH 1.0 62

Figure 23: Scheme of the degradation pathway of OTA that lead to the inactivation of its toxicity 63

Figure 24: Raman accessory for in liquid measurements 69

Figure 25: Raman spectrum of solid OTA on a substrate....70

Figure 26: Subdivision of OTA into smaller molecules 71

Figure 27: Principal peaks of solid OTA in the Raman spectrum 74

Figure 28: Spectrum of OTA by label-free in liquid SERS method....77

Figure 29: The Mycotoxin Metrology CBKT project of the BIPM....79

Figure 30: Wheat inoculation....81

Figure 31: Pictures of the flasks in the incubator....82

Figure 32: Wheat inoculation and wheat extracts 83

Figure 33: Percentage distribution of sulphites forms 86

Figure 34: Chemical equilibria of sulfites in wine....87

Figure 35: OIV apparatus for SO_2 determination....93

Figure 36: Homogeneity and long term stability studies of SO_2 in wine simulant solutions 97

Figure 37: Measurement comparison on free SO_2 concentration in wine simulant solution....99

Figure 38: Percentage recovery of free SO_2 concentration....100

Figure 39: Average and standard deviation of the results achieved in the comparison....101

Figure 40: Uncertainty contributions 107

Figure 41: Distributions histograms for the molar mass of SO_2 108

Figure 42: Distributions histograms for the molar mass of KHP....113

Figure 43: AgNPs – SO_2 interaction in hydroalcoholic solution 127

Figure 44: Progressive blue shift of 4 nm AgNPs LSPR 128

Figure 45: AgNPs – SO_2 interaction in wine simulant solution and comparison with hydroalcoholic solution 130

Figure 46: Quantification of SO_2 in wine simulant solution 131

Figure 47: Details of the three SERS peaks of Figure 46 in wine simulant solution at different SO_2 concentration 133

Figure 48: Cuvette with 4 nm AgNPs – wine mix 136

Figure 49: AgNPs – wine interaction 136

Figure 50: Quantification of total SO_2 in Chardonnay white wine by in liquid SERS method 137

Figure 51: Quantification of total SO_2 in Grillo white wine by in liquid SERS method 138

Figure 52: Quantification of total SO_2 in Favorita white wine by in liquid SERS method 138

Figure 53: Quantification of total SO_2 in Dolcetto red wine by in liquid SERS method 139

Figure 54: Quantification of total SO_2 in Chianti red wine by in liquid SERS method 139

Figure 55: Quantification of total SO_2 in Freisa red wine by in liquid SERS method 140

Figure 56: The comparison of the results 142

List of Tables

Table 1: Characteristics of the three AgNPs of different sizes. 22

Table 2: Experimental values of the two acid dissociation constants of OTA reported in literature.....31

Table 3: Real concentration and area of the peaks of the six standards of OTA 37

Table 4: Concentration and recovery of OTA in the samples of CRM of red wine.....40

Table 5: Values of λ_{max} and ε_{max} of the three OTA forms obtained in this study (by experiment and calculation) and reported in literature. 50

Table 6: Attribution of solid OTA peaks in Raman spectrum. The main peaks are highlighted with colours 72

Table 7: Results obtained by the 9 laboratories in the measurement comparison on free SO_2 concentration in wine simulant solution.....98

Table 8: Volume of nominal 1×10^{-2} M NaOH solution needed for the titration of Flask B solutions obtained by the 6 repetitions.....109

Table 9: The atomic weights of the elements of KHP and their distributions 113

Table 10: Volume of NaOH solution needed for the standardization against 4.000×10^{-3} l of nominal 1×10^{-2} M KHP solution obtained by the 9 repetitions of the titration.....115

Table 11: Values, distributions and standard uncertainties of the six variables which contributed to the calculation of c_{NaOH}.....116

Table 12: Values, distributions and standard uncertainties of the four variables which contributed to the total calculation of $y_{SO2.OIV}$ 118

Table 13: Assignment of the vibrational modes and positions of the peaks of SO_2, citrates and ethanol.....129

Table 14: Average SERS intensity, standard deviation and relative standard deviation (RSD) of the 620 cm^{-1} and 928 cm^{-1} peaks at increasing SO_2 concentration in wine simulant solution. 132

Table 15: Concentration of SO_2 in red wine before and after the SPE pre-cleaning step obtained by OIV methods. 135

Table 16: SO_2 quantifications in red and white wines by the proposed in liquid SERS method and by the official OIV-OENO 591B-2018 method. 141

Chapter 1

Introduction

1.1 Metrology issues

Metrology is defined as the "science of measurement and its application" by the International vocabulary of metrology – Basic and general concepts and associated terms (VIM) [1]. Metrology is one of the oldest science, which was dated back to the ancient world [2] It evolved over the time since measurements recover a key role in any society. Modern metrology was born at the end of the 18^{th} century during the France revolution. In fact, the need of standardize units led to the foundation of a decimal-based metric system, To develop, spread and uniform this system between the countries, in 1875 the Metre Convention established the Bureau International des Poids et Mesures (BIPM), which is an intergovernmental organization with the aim of coordinate the international metrology. In 1960, the metric system was evolved into the International System of Units (SI). Nowadays, the role of metrology is to provide standardization and quality assurance practices, establishing the traceability of the measurement results to the SI units. Three subfields of metrology can be distinguished:

- applied, which deals with the industrial measurement instruments,
- legal, which regards the regulatory aspects of measurements,
- scientific, which establishes, realizes, and maintains the SI units and develops new measurement methods and standards. In several countries, this last metrological subfield is the prerogative of the National Metrology Institutes (NMI).

The definition of metrology provided by the BIPM is “the science of measurement, embracing both experimental and theoretical determinations at any level of uncertainty in any field of science and technology” [3] This statement stress the fundamental role covered by the uncertainty in a measurement process. The Guide to the expression of uncertainty in measurement (GUM) defined the measurement uncertainty as a “parameter, associated with the result of a measurement, that characterizes the dispersion of the values that could reasonably be attributed to the measurand” [4]. As a consequence, a measurement results should be expressed by the value of the quantity and its uncertainty. Thus, the evaluation of the measurement uncertainty represents a crucial stage in a measurement procedure and ensures the comparability in time and space of the measurement result.

Metrology plays an essential role in all scientific fields and its repercussions on the quality of the daily life of each of us are manifold [5]. One of the most recently developed branches of this science is chemical metrology [6], [7]. The role of metrology in chemistry is to develop measurement procedures and to provide reference materials to ensure the metrological traceability of the measurement results. According to the VIM, the measurement traceability is a “property of a measurement result whereby the result can be related to a reference through a documented unbroken chain of calibrations, each contributing to the measurement uncertainty” [1]. Given the growing need for their production, one of the most current topics of analytical and metrological chemistry is covered by reference materials [8]–[10]. Indeed, in recent years the scientific community has been paying increasing attention to these materials. The definitions of the two types of these materials are reported in the standard ISO 17034:2016 – “General requirements for the competence of reference material producers” released by the International Organization for Standardization (ISO) [11]. A Reference Material (RM) is a “material, sufficiently homogeneous and stable with respect to one or more specified properties, which has been established to be fit for its intended use in a measurement process”. A Certified Reference Material (CRM) is a “reference material (RM) characterised by a metrologically valid procedure for one or more specified properties, accompanied by an RM certificate that provides the value of the specified property, its associated uncertainty, and a statement of metrological traceability”. These materials are principally used for calibrate measurement instruments, for validate analytical methods and to perform quality control tests. In particular, CRMs are a fundamental tool to attest the reliability of measurement results and provide the guarantee of traceability to SI units. The potential

reference materials to be produced are almost infinite but their production is rather long and laborious. For this reason the reference materials (both RMs and CRMs) currently available only partially satisfy their growing demand from users.

One of the most relevant topics in the chemical field is that related to food. Food metrology represents an emerging area of interest and, in fact, the Technical Committee 23 – "Metrology in Food and Nutrition" of the International Measurement Confederation (IMEKO) was founded in the 2006 [12]. The main areas of development of food metrology concern:

- development and validation of new analytical methods for food analyses,
- identification and determination of constituents and chemicals in food intended for human consumption,
- evaluation of the measurement uncertainty associated with the analytical result of food analyses,
- development of RMs and CRMs related to food (pure substances or chemicals in food matrices).

1.2 Food safety

Food is of undeniable importance to humans. In fact, since the dawn of human existence, food has played a central role in the daily aspects of life, both from the nutritional and cultural point of view.

Nowadays, access for all the population to an adequate amount of safe food is a fundamental right. Indeed, food is the source of nutrients, which are essential substances for the proper and healthy functioning of the human body. Nutrients are classified as macro-nutrients (carbohydrates, proteins and fats) and micro-nutrients (vitamins and minerals).

Nutrition is strictly related to food safety and food security. It is estimated that the cases of foodborne illness generate in a year by unsafe food are 600 million and that they result fatal for 420000 people [13]–[15]. The foodborne diseases are more than 200, between acute and chronic, and go from infections and diarrhoea to cancers [13], [16], therefore representing a relevant factor of mortality and morbidity [17]. The World Health Organization (WHO) prepared a "Five keys to safer food manual" [18] to disseminate to as many people as possible the main hygienic practices to be adopted to prevent states of illness. Food-related pathological states are widespread worldwide but their occurrence represents a

burden especially in developing countries. This issue aggravates the situation of poverty in these countries and makes the achievement of the Sustainable Development Goals established by the 2030 Agenda [19] more challenging. Furthermore, in addition to the clinical aspect, diseases deriving from food also negatively affect the economic sector compromising its growth [17], [20]. Moreover, the production of unsafe food forces the destruction of foodstuffs, causing scarcity of available food, the drastic decline of foodstuffs exportation and a relevant loss of productivity, especially in the emerging economies. Considering the continuous increase of the world population and the problems generated by the climate changes, this reality is even less sustainable from an environmental and social point of view [15]. Hence, in an world struggling with climate change and pollution and increasingly globalized, attention to food safety must concern all relevant aspects of the production, handling, transport and storage chain. To emphasize this concept, the WHO in 2015 promotes the slogan: "From farm to plate, make food safe" [21]. Furthermore, to provide scientific advice on food-related risks along the entire food chain, the European Food Safety Authority (EFSA) was established in 2002. It is an agency of the European Union (EU) based in Italy in Parma. In their review, Kleter and Marvin report some examples of identification of hazards along the entire food production chain [22].

The past General Director of the Food and Agriculture Organization of the United Nations (FAO) José Graziano da Silva claimed that: "There is no food security without food safety, which is the base for healthy diets and lives" [15]. Food security is the condition for which the entire population, at all times, has access to the amount of healthy food necessary for an active life, both physically and economically [23], [24]. Food security is based on four dimensions: availability of healthy food, access to food, utilization of safe food and stability of supplies. Food safety is a constituent element essential for food security and affects all its aspects [15]. Indeed, food safety implies the absence of chemical and/or biological substances in food or their presence in concentrations that do not cause food-related disease [23].

1.3 Food contaminants and food additives

As already mentioned, unsafe food is responsible for a variety of foodborne diseases, which represent a global burden. Therefore, ensuring food safety is a priority for modern society.

In this scenario, it is crucial to identify and study thoroughly the chemicals which affects food making it unsafe: the contaminants. Environmental contaminants representing an hazard for the human health are extremely diverse and are responsible of numerous adverse effects. Indeed, food contaminants represent a global challenge, as stated by the WHO [17], [25]. The contamination is defined as the presence of something foreign and not intentionally added to the normal composition of food. The contamination can occur during the entire food production chain and can makes it unsuitable for human and/or animal consumption since it poses a risk to humans [26]. It can be physical, chemical or biological.

Food contaminants are mainly divided in the following categories [27], [28]:

- Heavy metals and metalloids. Metals are environmental contaminants that represent a significant hazard to human because their capacity of bioaccumulation and concentration along the food chain. Metals are natural substances but their concentrations are considered to increase due to anthropic activities. Among the most dangerous metals there are mercury, lead, arsenic and cadmium [29];
- Residues of veterinary drugs. They are used for the care of animals for slaughter and to improve and increase productivity. As a representative example, the presence of residues in the meat is due to the absence of suspension of these drugs within the time limits established by law and therefore to their incomplete disposal by the animal's metabolism. Drug contamination of food occurs daily and is much more dangerous than is commonly thought. For example, due to food intake and continuous and not correct exposure to antibiotics, more and more pathogens are becoming resistant to them [30], [31];
- Pesticides and other agrochemicals, such as herbicides, insecticides, fungicides, fertilizers, surfactants, etc. All these substances are globally used in agriculture sector to protect the crops from different types of pest infestations and improve the productivity. The toxicity of these heterogeneous group of chemical agents are often not confined to the target organisms and thus they represent environmental and food hazards and are dangerous to humans [32];
- Dioxins. They include a variety of compounds with a similar basic chemical structure. Dioxins are particularly stable and are accumulated throughout the food chain [33];

- Polycyclic aromatic hydrocarbons (PAHs). They are by-products of partial organic compounds combustion and derive mainly from industrial activities. PAHs are genotoxic and carcinogenic [33];
- Microbial pathogens. This category includes bacteria, viruses and protozoa. They compromise the human health via microbiological contamination of food and are responsible of numerous foodborne diseases. Examples of widespread pathogens are *Salmonella* and *Escherichia coli* [34], [35];
- Mycotoxins. They are toxins naturally produced by the secondary metabolism of fungi and molds. To date, over 300 of these toxins have been classified. Mycotoxins proliferate in a wide range of foodstuff commodities especially in certain conditions of favorable temperature and humidity. Given the extreme toxicity of these molecules and their widespread presence all over the world, mycotoxins represent a serious scourge for society [36];
- Radionuclides. They are radioactive isotopes of elements and can have a natural or anthropogenic origin. Radionuclides spread in nature can contaminate food and provoke risks to human health as a consequence of DNA damage. Thus, the concentration of these contaminants in food should be reduce to the minimal [37], [38];
- Micro- and nano-plastics. These types of very small-sized plastics are recently included in the contaminants list due to their dramatic impact on the global environment. The massive use of plastics in fact leads to the accumulation of poorly biodegradable plastic debris in water and soils [39]. The toxicological consequences of food contamination by these plastics debris are still under study due to the difficulties in achieving small fraction separation and characterization of them [40].

In summary, it is possible to define as food contaminant a substance foreign to the natural composition of the food or a harmful microorganism [27]. It is important to underline that some substances classified as food contaminants occurred naturally and are not originated from anthropic actions. Examples of these contaminants are mycotoxins and microrganisms.

In addition to food contaminants, other substances can also be present in food, known as food additives. Food additives are substances intentionally added to foodstuffs because their properties positively affect the characteristics of the products. The addition of additives to food products represents a technological

need resulting from industrial development and changes in eating habits. As a consequence, today the various stages of the production cycle (production, storage and distribution) of foodstuffs can be made in different geographical areas thanks to the use of additives. For example, additives are adopted to preserve texture and flavor, to maintain the desired color, to obtain certain organoleptic characteristics, to decelerate the aging process of food and to ensure a long shelf life of the products [41]. A characteristic of additives is that usually they are not eaten alone as a food [42]. Food additives can derive from synthetic process or from natural sources (minerals, plants or animals) and must satisfy chemical purity and safety requirements. Additives are included in the ingredients list of the food products and, in the European Union are labeled with an "E number" code [43]. Among the high quantities of additives, there are very diffused antioxidants, sweeteners, emulsifiers and preservatives. Although they are permitted substances, the presence of additives in food is regulated by law. In fact, excessive amounts of additives can cause adverse effects on humans, such as allergies and respiratory symptoms [44], [45]. The Joint FAO/WHO Expert Committee on Food Additives (JECFA) is responsible for safety assessment related to the use of food additives [15]. Thus, only food additives approved by JECFA and in concentration level established by law are allowed in foodstuffs suitable for global market [46].

The monitoring of food contaminants and food additives currently represents a priority for the international scientific community. Indeed, many resources are exploited for the in-depth knowledge of contaminants and additives chemical-physical characteristics, occurrence and toxicology. Furthermore, the correct and reliable quantification of their levels appear to be of essential importance to guarantee food safety to the global community.

Most countries have implemented regulatory limits for additives and contaminants in food and feed to protect their populations.

1.4 Topics and structure of my PhD thesis

In this thesis I faced some chemical and metrological aspects related to the food safety topic.

In particular, I worked on two categories of chemicals which affect the food safety: food contaminants and food additives. For this reason, I decided to organized the chapters of my thesis on the basis of the two molecules that I took

as case studies: the ochratoxin A, which is a food contaminant, and the sulfur dioxide, which is a food additive.

Below, the topics that have been treated in each chapter, considering their order of appearance, are summarized.

Chapter 2 was devoted to the silver nanoparticles (AgNPs). The subjects treated were:

- the syntheses of AgNPs with three nominal dimensions: 4, 30 and 55 nm;
- the characterization of such AgNPs by: UV-Vis spectrophotometry, Transmission Electron Microscopy, Inductively Coupled Plasma - Mass Spectrometry.

The synthesis of the AgNPs was located before the other chapters since this work was conducted during the duration of the PhD and the AgNPs were used for develop a Surface Enhanced Raman Spectroscopy method in both the case studies.

Chapter 3 dealt with a characterization of ochratoxin A (OTA) under various aspects:

- a quantification of OTA concentration in a CRM of red wine by High Performance Liquid Chromatography coupled with fluorescence detection;
- a comprehensive description of the behaviour of OTA in aqueous solutions in a wide range of pH. This study was divided into two part. Under acid to neutral condition, the two acid dissociation constants were determined by two independent techniques: the UV-Vis spectrophotometry and the fluorescence spectroscopy. Under alkaline conditions, the degradation of OTA and the reversibility of such process were investigated experimentally by fluorescence spectroscopy and theoretically by Density Functional Theory calculations;
- the acquisition of a reference spectrum of solid OTA by Raman spectroscopy with the attribution of the vibrational modes of its main peaks and a feasibility study for OTA identification by an in liquid label-free SERS method with AgNPs as a substrate;

- a work for culturing, isolation, and purification of ochratoxin A for reference material production, along with metrological characterization of the material, which was performed during a Secondment at the NRC – Canada.

Chapter 4 was dedicated to the study of sulfur dioxide (SO_2) under various aspects:

- the evaluation of the maximum recovery of free SO_2 from a sample of wine simulant by applying the official OIV-OENO 591A-2018 method. To delve into this topic, a measurement comparison among specialized laboratories was conducted;
- a rigorous evaluation of the measurement uncertainty associated to the free SO_2 concentration achieved by the official OIV-OENO 591A-2018 method;
- the production and a first attempt of characterization of a candidate CRM of free SO_2 in a wine simulant matrix;
- the investigation of the interaction between SO_2 and AgNPs and the develop and validation of an in liquid SERS method for total SO_2 quantification in wine.

In conclusion, with this thesis I tried to improve the knowledge on this two analytes in different areas and to develop new analytical methods. Moreover, I tackled two of the main aspects of metrology in chemistry: the evaluation of the measurement uncertainty and the production of certified reference materials.

Chapter 2

Silver nanoparticles (AgNPs)

Part of the work described in this chapter was also published in the paper: “Direct quantification of sulfur dioxide in wine by Surface Enhanced Raman Spectroscopy” published on Food Chemistry in 2020 [47].

2.1 Introduction

On December 29, 1959, the Nobel Prize in Physics Richard Feynman prophesied the arrival of the age of nanotechnology with the words "There’s plenty of room at the bottom" [48]. In these sixty years, considerable progress has been made and, in recent years, nanotechnology has become one of the leading sectors of research worldwide. Nanotechnology is based on the combination of technological and scientific skills for the development of materials at the nanoscale [49]. Thanks to their properties and to their dimensions, the nanomaterials are widely used in many technological fields and allow new innovative applications.

In these emerging fields, there is a need of standardization and, currently, a common definition of the word “nanomaterial” has not yet been achieved [50]. The nanomaterials are classified by the International Organization for Standardization (ISO) in [51]:

- Nano-objects, which are “discrete pieces of material with one, two or three external dimensions in the nanoscale”;

- Nanostructured materials, which are “materials having internal structure or surface structure in the nanoscale”;

where nanoscale is intended from 1 to 100 nm.

According to their size and shape, the nano-objects are divided in [51]:

- Nanoparticles (NPs), which are “nano-objects with all dimensions at the nanoscale where the lengths of the longest and shortest axes of the nano-objects do not differ significantly”;
- Nanofibers, which are “nano-objects with two external dimensions at the nanoscale and the third dimension significantly larger”;
- Nanoplates, which are “nano-objects with one external dimension in the nanoscale and the other two dimensions significantly larger”.

In particular, nanoparticles have acquired considerable importance in many scientific fields. Indeed, just to name a few, they are used in the biomedical sector [52], [53], in the food industry [54]–[56], in environmental applications [57], [58], in the catalysis systems [49] and in the optoelectronic field [59]. A broader representation of the possible applications is reported in Figure 1.

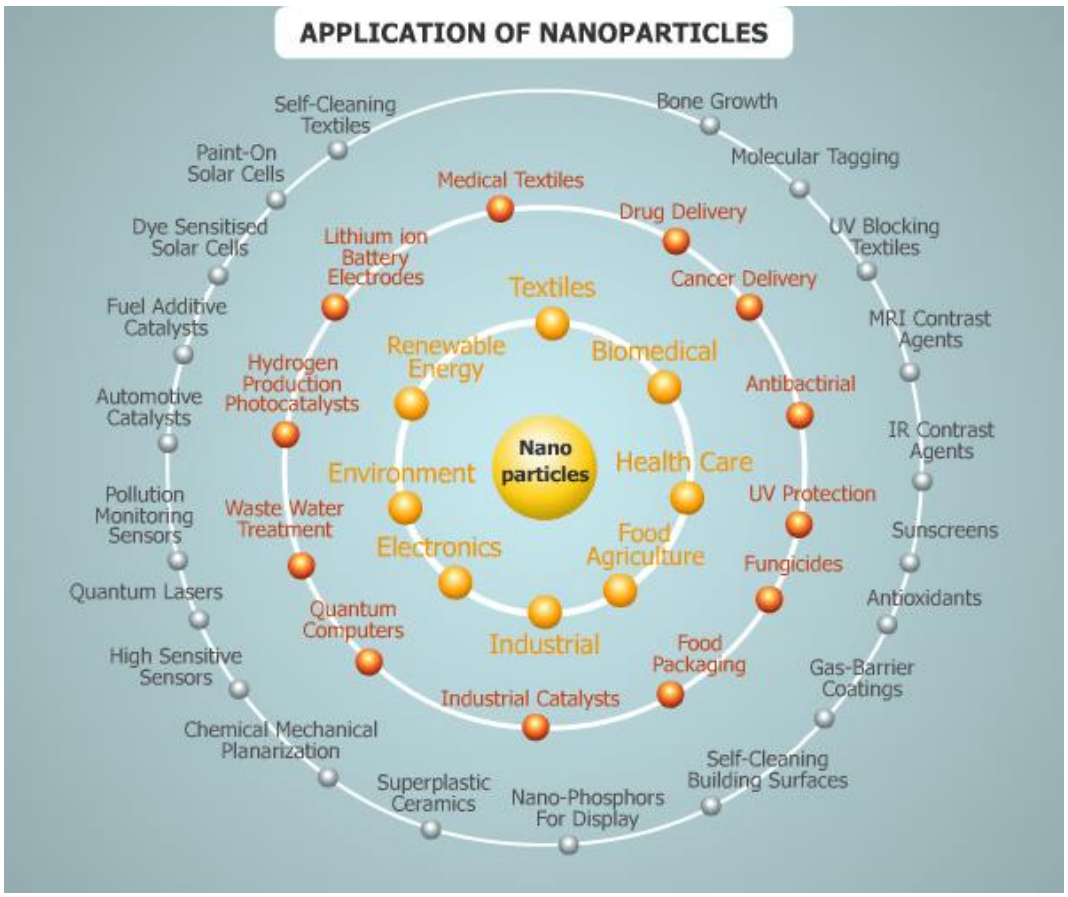


Figure 1: Application of nanoparticles.

Figure 1: Examples of applications of nanoparticles in fields that concern daily life. Image taken from [60]

There are two opposite approaches to the synthesis of nanoparticles: the top – down and the bottom – up, as schematized in Figure 2. The top – down approach starts from bulk materials and, following their breaking down or miniaturizing, conducts to nanoparticles, while the bottom – up approach starts from atoms and molecules and produces nanoparticles through the assembly of building blocks. Among these two approaches, there are many methods for the synthesis of nanoparticles. These methods can be physical, chemical or biological [61], as summarized in Figure 2.

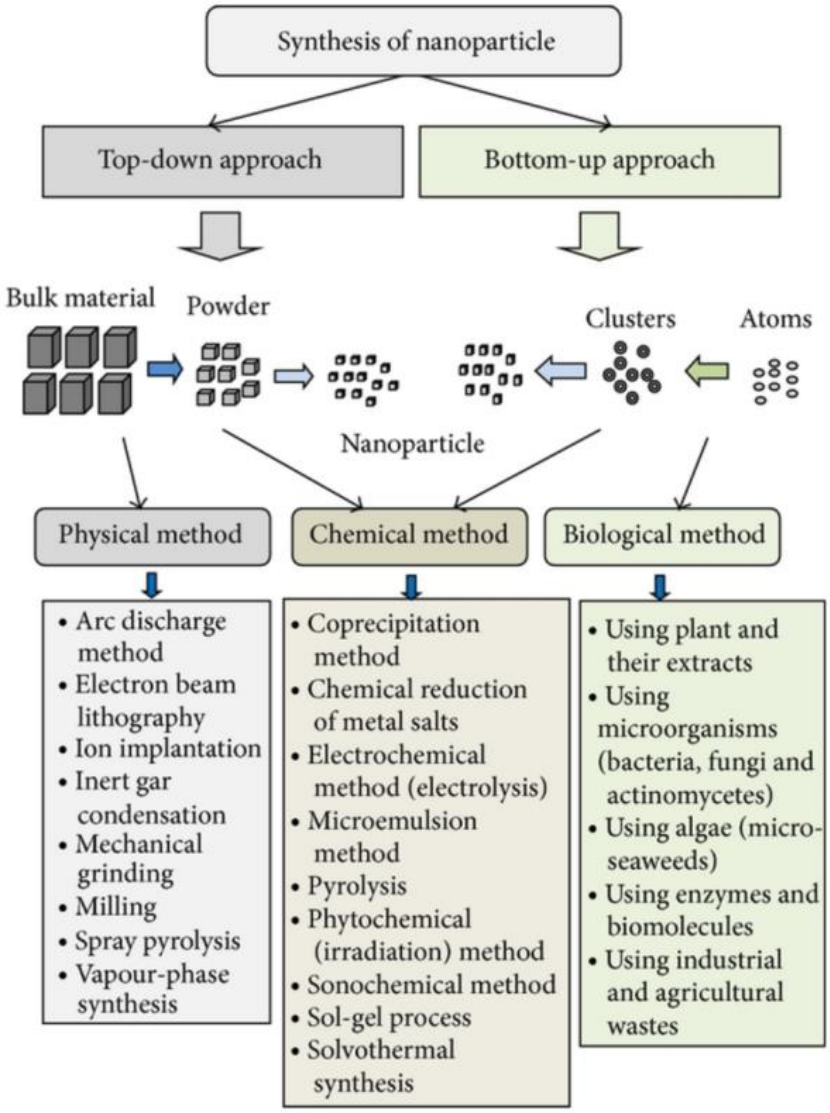


Figure 2: Approaches and methods for the synthesis of nanoparticles

Figure 2: The two approaches for the synthesis of nanoparticles (top – down and bottom – up) and the three categories of methods (physical, chemical and biological). Image taken from [62]

From these methods, many types of nanoparticles can be obtained. The nanoparticles are mainly characterized by their size, their shape, the material which constitutes them and their properties at the surface, as shown in Figure 3.

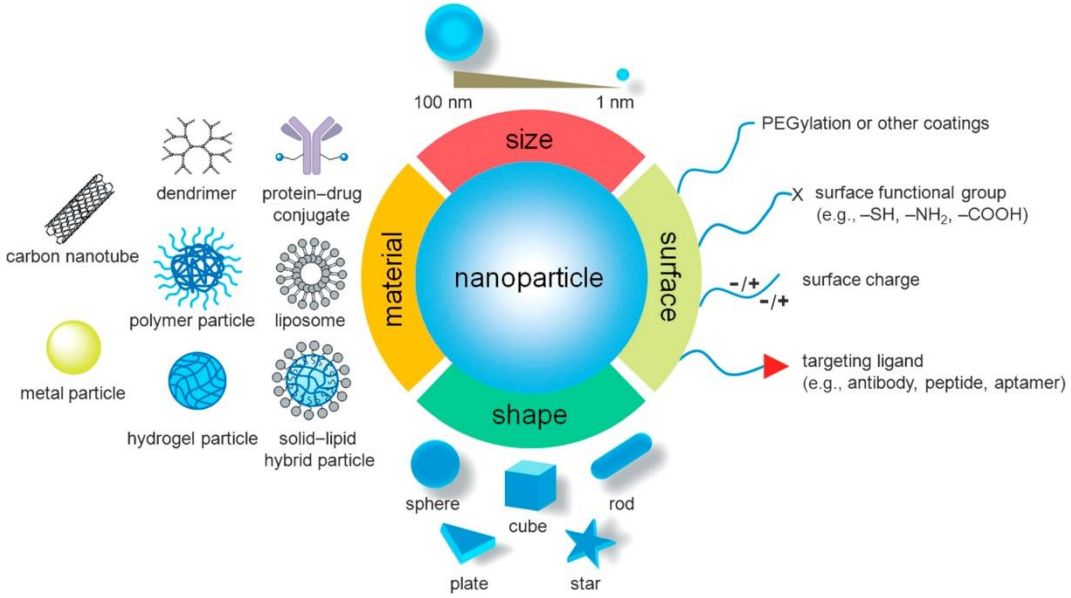


Figure 3: Main parameters of the nanoparticles

Figure 3: The characterization of a nanoparticles in terms of the material, the size, the shape and the surface. Image taken from [63]

In this Chapter, the focus are the silver nanoparticles (AgNPs). In this thesis, the AgNPs were synthetized by chemical synthesis exploiting a bottom-up strategy. In particular, a stepwise seeded growth method was adopted for their synthesis. These AgNPs were exploited as a substrate for the analytical determination of chemical molecules in food related matrices.

2.2 Chemicals

For the syntheses of 4, 30 and 55 nm spheroidal AgNPs in colloidal suspensions, ultra-pure water and reagent at high purity level were adopted. Before syntheses, the whole glassware was cleaned twice with aqua regia, which is composed of HCl and HNO_3 in 3:1 ratio, and then thoroughly washed with ultra-pure water and dried with nitrogen. HCl and HNO_3 were both acquired from Carlo Erba. The reagent adopted for the syntheses were silver nitrate — $AgNO_3$, purchased by Panreac, sodium borohydride — $NaBH_4$ from Acros Organics and sodium citrate tribasic dehydrate — $HOC(COONa)(CH_2COONa)_2 \cdot 2H_2O$ bought from Sigma-Aldrich.

2.3 Synthesis

A stepwise seeded growth method was adopted for the syntheses of AgNPs of 4, 30 and 55 nm as nominal diameter. The three protocols for the different dimensions of AgNPs are optimized starting from the procedure reported by Wan et al. [64]. This latter match the classical synthesis proposed by Lee-Meisel [65] with growth steps of the seeds. The initial step regarded the synthesis of the smallest AgNPs which are denominated seeds. Larger nanoparticles were subsequently obtained by growing up the seeds, as schematized in Figure 4.

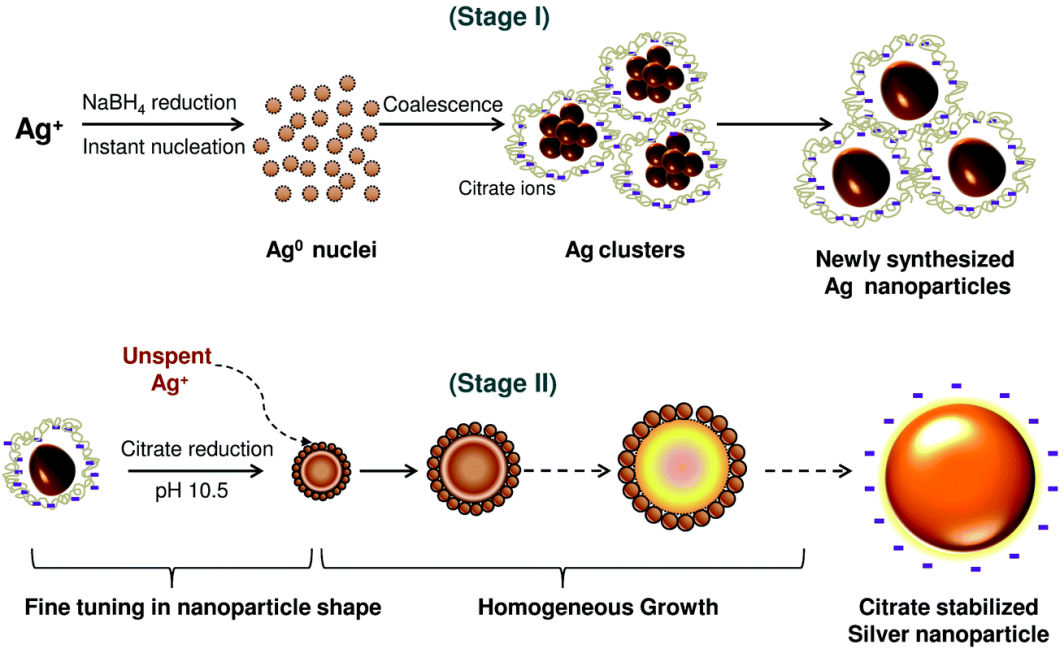


Figure 4: Scheme of stepwise size-controlled synthesis of AgNPs

Figure 4: Representation of the steps involved in the stepwise seeded growth method exploited for the syntheses of AgNPs with nominal diameter of 4, 30 and 55 nm. Image taken from [66]

In all these syntheses, the AgNPs were in colloidal suspensions. As a result of the method of synthesis, a shell of citrates is weakly bounded on the AgNPs surface [67]. The negative charge of the citrates causes the repulsion among the nanoparticles. This repulsion stabilizes the AgNPs and allows them to remain in suspension [68].

The setup used for all the three syntheses was reported in Figure 5. It is composed by a heating plate upon which there was a vessel containing an oil bath.

A round bottom flask was dipped into the vessel in order to keep the temperature constant during the syntheses. This flask, in which the synthesis took place, was equipped with two necks: one of them was connected to a water-cooled condenser and the other was used to control the temperature through a probe inserted in the holey cap. A magnetic stir bar was placed in the flask. The syntheses were conducted in a laboratory with an active control of the temperature at 23 ± 3 °C.

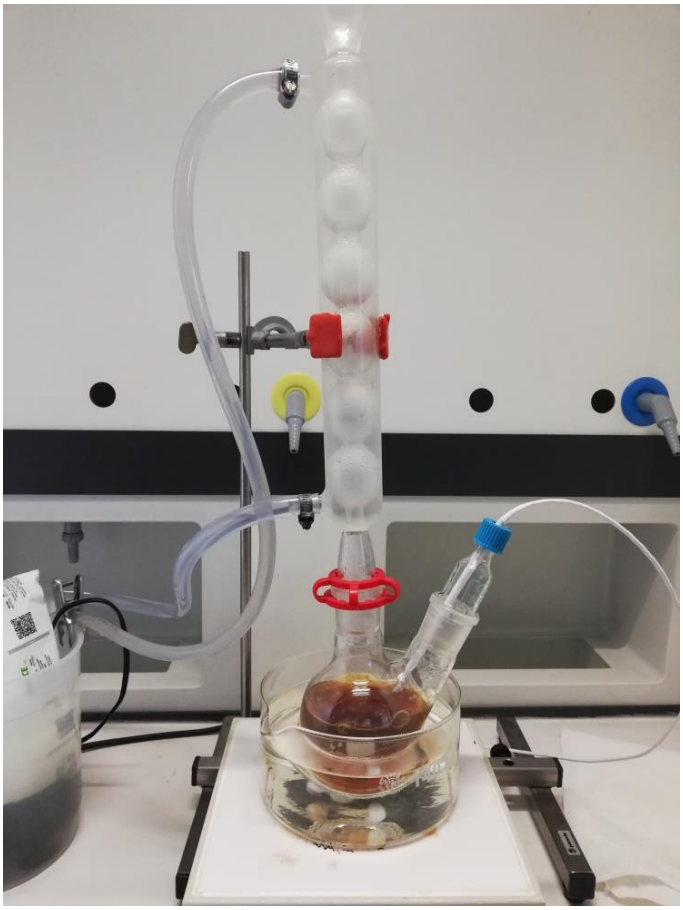


Figure 5: Setup for the AgNPs synthesis

Figure 5: Glassware used for the synthesis of the three sizes of AgNPs. It consists of a heating plate, an oil bath, a two necks round bottom flask, a magnetic stir bar, a water-cooled condenser and a temperature probe

Protocol for nominal 4 nm AgNPs synthesis:

- During the whole synthesis, stir the solution at 430 rpm;

- Bring to 70 °C a solution containing 75 ml of ultra-pure water and 20 ml of sodium citrate 1% w/v and keep at this temperature for 15 minutes;
- Add 1.7 ml of solution of $AgNO_3$ 1 % w/v and 2 ml of $NaBH_4$ 0.1 % w/v freshly prepared;
- Keep the colloidal suspension at 70 °C for 1 hour;
- Cool it to room temperature;
- Bring the colloidal suspension to 100 ml of volume with ultra-pure water.

Protocol for nominal 30 nm AgNPs synthesis:

- During the whole synthesis, stir the solution at 430 rpm;
- Bring to 100 °C a solution containing 75 ml of ultra-pure water and 2 ml of sodium citrate 1% w/v and keep at this temperature for 15 minutes;
- Add 10 ml of 4 nm AgNPs started seeds solution and 1.7 ml of solution of $AgNO_3$ 1% w/v;
- Keep the colloidal suspension at 100 °C for 1 hour;
- Add 2 ml of sodium citrate 1% w/v and 1.7 ml of solution of $AgNO_3$ 1% w/v;
- Keep the colloidal suspension at 100 °C for 1 hour;
- Add again 2 ml of sodium citrate 1% w/v and 1.7 ml of solution of $AgNO_3$ 1% w/v;
- Keep the colloidal suspension at 100 °C for 1 hour;
- Cool it to room temperature;
- Bring the colloidal suspension to 100 ml of volume with ultra-pure water.

Protocol for nominal 55 nm AgNPs synthesis:

- During the whole synthesis, stir the solution at 450 rpm;
- Bring to 80 °C a solution containing 80 ml of high pure H_20 and 2 ml of sodium citrate and keep at this temperature for 15 minutes;
- Add 10 ml of 30 nm AgNPs solution and 1.7 ml of solution of $AgNO_3$ 1% w/v;
- Keep the colloidal suspension at 80 °C for 2 hours;
- Cool it to room temperature;

- Bring the colloidal suspension to 100 ml of volume with high pure H_20.

All the variables involved in theses synthesis protocols can affect the dimensions of the AgNPs. In particular:

- The most affecting parameter is the temperature since a difference of even a few degrees leads to a change in the final dimension of the AgNPs. In the setup for the AgNPs synthesis (see Figure 5), the accurate control of the temperature is not trivial. Moreover, the oil bath causes an inertia between the heating of the plate and the actual temperature of the suspension. To optimize the control of this parameter, a temperature probe immersed in the suspension and connected to the heating plate was employed. This system allowed both to set the desired temperature and to monitor the real temperature of the system inside the flask;
- The second most important aspect that affects the syntheses is the evaporation of the water during the process. The water-cooled condenser represents an essential component of the setup and it is fundamental that the water inside is very cold. Indeed, if a considerable volume of the water evaporates during the synthesis, the concentration of the reagent in the flask change in an uncontrolled way which can be reflected in a difference in the final dimensions of the AgNPs. In order to limit the evaporation, the use of a temperature probe inserted in a specially perforated cap (as in Figure 5) is preferable to placing a thermometer inside the open neck of the flask;
- Another relevant parameter is the time. The duration of every step of each synthesis must be respected. However, time is easily managed;
- It is important to prepare the reagent solutions at the correct concentrations, paying particular attention in the $NaBH_4$ which must be freshly prepare and maintained in ice bath until its use. However, working carefully, the concentrations of the reagents is not a problematic factor;
- Before starting the synthesis process, the stirring speed should be optimized considering the dimension of the two necks round bottom flask and of the magnetic stir bar. In fact, the stirring speed must be adjusted in order to allow the homogenization of the suspension components but to avoid the formation of a vortex inside the flask.

Once optimized, the same flask and magnetic stir bar are adopted for the syntheses.

2.4 Methods for AgNPs characterization (instrumental setup)

2.4.1 UV-Vis

UV-Vis spectra were obtained by a DR 5000 UV-Vis spectrophotometer from Hach company. Since the AgNPs solutions as they are provoked saturation of the absorbance signals, 4 nm AgNPs were diluted 1:10 in water while both 30 nm and 55 nm AgNPs were brought to 1:40 ratio. These diluted solutions were placed in cuvettes made by polystyrene with a path length of 10 mm and analysed in a range from 200 to 1100 nm.

2.4.2 Transmission Electron Microscopy (TEM)

A JEM 3010 ultrahigh resolution Transmission Electron Microscope by JEOL was used to acquire the images of the three dimensions of AgNPs. The instrument had a thermo-ionic with mono-crystal of LaB_6 source and 0.17 nm as point resolution. The voltage adopted was 300 kV. Before each TEM analysis, a thin film of perforate carbon was used to cover a copper grid of 3 mm. Then, for each of the three AgNPs size, a drop of solution was put on the described grid and left to dry. The dimensions of the particles were measured by TEM micrographs on around 200 AgNPs for each size. The software used was ImageJ [69].

2.4.3 Inductively Coupled Plasma – Mass Spectrometry (ICP-MS)

The used ICAP-Qs Inductively Coupled Plasma-Mass Spectrometer was purchased from Thermo Fisher Scientific. The mass analyser is composed by a quadrupole with a collision/reaction cell. The calibration of the ICP-MS was performed for ^{107}Ag and adopting internal standard (100 ug/l of ^{45}Sc, ^{89}Y, ^{159}Tb). For the calibration, 6 points were used to build the curve with a coefficient of linear correlation > 0.999. Collision cell in He mode with kinetic energy discrimination (He - KED) was operated in order to eliminate the polyatomic ions interferences. The instrument parameters adopted were: 1450 w for the RF power, 15 l/min for the main argon flow, 1.0 l/min for the flow of auxiliary argon, 0.90 l/min for the nebulized flow, 5.0 ml/min for the flow of helium in the chamber of collision.

This instrument was used to quantify the amount of Ag in the synthetized colloidal suspensions. Before the dissolution, the samples of AgNPs were pre-treated as follow: sonication at 80 W for 20 minutes, filtration through nylon filter of 0.2 μm and three centrifugations with ultra-pure water for washing the NPs. For each of the three size of AgNPs, hot HNO_3 was used to dissolve 0.5 ml of NPs solution. Each of these samples were then diluted 1:10000 and contained 2 % w/w HNO_3.

2.5 Results and discussion

The first evidence about the three size AgNPs is that the colloidal suspensions were differently coloured, as proved by the cuvettes in Figures 6 from a to c. The position of the Local Surface Plasmon Resonance (LSPR), which is characteristic of each type of AgNPs [70], was evinced from the UV-Vis spectra of Figure 6. A Mie model for the SPR, that is the collective oscillation of the electrons in the conduction band of metallic NPs, could be implemented. Indeed, the mathematical Mie theory is widely used to simulate the interaction of the electromagnetic wave with homogeneous spherical particles. The LSPR of NPs strictly depends from their size, shape and composition. In this case, the composition (silver) and the shape (spheroidal) were the same while the parameter that varied was the size of the nanoparticles. The experimental evidence suggested that the LSPR red shifted increasing the AgNPs dimensions [71], [72]. In particular, it was positioned at 391 nm for 4 nm AgNPs, at 397 nm for 30 nm AgNPs and at 417 nm for 55 nm AgNPs, as shown in Figure 6 from d to f. These findings were in agreement with the general conclusion reported in literature for the Mie theory [73], [74] which modelled a red shift of the spectral position of the LSPR as the size of the nanoparticles increased.

UV-Vis spectra offered also some information regarding the size distribution, the state of agglomeration and the shape of the nanoparticles. As shown in Figure 6, the absorption peaks of 4 nm and 30 nm AgNPs are narrow and symmetric, attesting a good homogeneity of the size and suggesting an almost spheroidal shape. These evidences were also confirmed by TEM images, as reported in Figure 6 g and h. Furthermore, in inset i) in Figure 6, a distance of 2.4 Å was measured between two crystallographic planes, in accordance with literature data [75]. The UV-Vis spectrum of 55 nm AgNPs had instead a shoulder of the principal peak positioned at around 370 nm. The presence of this shoulder can be attributed to due phenomena that could occurred in the last synthesis: a further

nucleation or a growth of the already formed AgNPs in an asymmetrical way. This fact was already observed by Wan et al. [64] and was confirmed by TEM images, in Figure 6 i, which showed some not-spherical shaped AgNPs. Inset ii) and iii) in Figure 6 evidenced the five-fold multiple twinned decahedron crystal. This very probable multiple twin configuration suggested an Ostwald ripening of the Ag nuclei which led to the formation of the larger AgNPs [66], [76]. The average diameters of the batches of nanoparticles analysed by TEM were 6 ± 3 nm for the nominal 4 nm AgNPs, 30 ± 6 nm for the nominal 30 nm AgNPs and 52 ± 7 nm for the nominal 55 nm AgNPs. However, the average diameters of the AgNPs may change slightly between syntheses repetitions. Since in UV-Vis spectra of all the AgNPs, the peaks at high wavelength were not generated, it can be affirmed that aggregation of the AgNPs had not occurred.

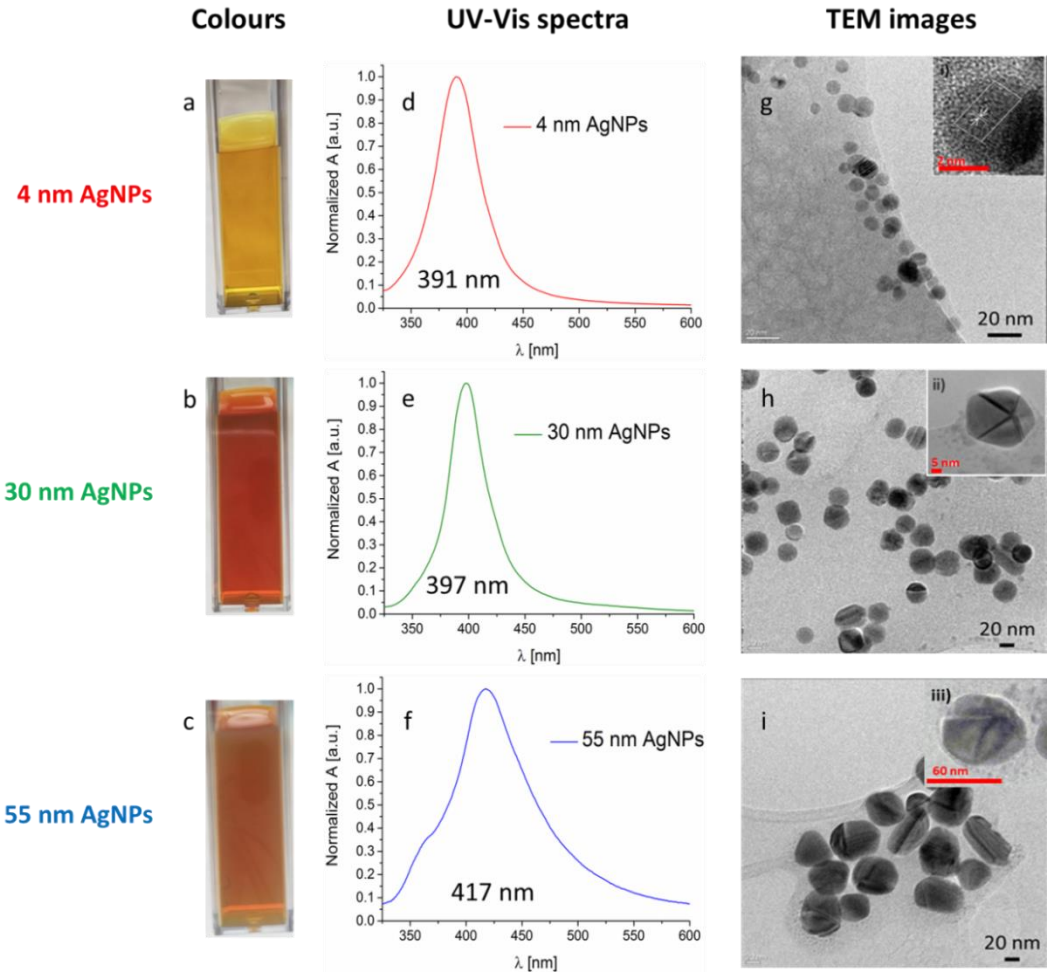


Figure 6: Characterization of 4, 30 and 55 nm AgNPs

Figure 6: From a to c: colours of the colloidal suspensions of 4, 30 and 55 nm AgNPs respectively; from d to f: normalized UV-Vis spectra of 4, 30 and 55 nm AgNPs respectively (diluted in water in ratio 1:10 for 4 nm AgNPs and 1:40 for both 30 e 55 nm AgNPs); form g to i: TEM images of 4, 30 and 55 nm AgNPs respectively. Inset i): High Resolution TEM image of the lattice fringes of a 4 nm AgNPs. Inset ii) and iii): TEM images of the shape of a 30 nm and 55 nm AgNPs respectively. Image taken from [47] and adapted.

Based on the information achieved by the described techniques, it was possible to obtain further information about the characteristics of the three types of AgNPs. The results are summarized in Table 1. The values reported in Table 1 were calculated assuming a spherical shape for all the three dimensions of AgNPs.

Table 1: Characteristics of the three AgNPs of different sizes.
Table taken from [47] and adapted.

AgNPs nominal size (nm)	**Diameter by TEM (nm)**	**λ of LSPR (nm)**	**[Ag] by ICP-MS (ug/ml)**	**Single AgNPS surface area (nm^2)**	**Quantity of AgNPs (NPs/ml)**	**Total surface area (nm^2/ml)**	**Specific surface area (nm^2/ug)**
4	6 ± 3	391	152 ± 2	1.13×10^{2}	1.28×10^{14}	1.45×10^{16}	9.52×10^{13}
30	30 ± 6	398	424 ± 12	2.83×10^{3}	2.86×10^{12}	8.1×10^{15}	1.9×10^{13}
55	52 ± 7	419	208 ± 4	8.49×10^{3}	2.54×10^{11}	2.3×10^{15}	1.1×10^{13}

The values reported in Table 1 were obtained applying the following formulas:

- Single AgNPs surface area in nm^2

$$S_{sphere} = 4\pi r^2$$

- Quantity of AgNPs in *NPs/ml*

$$\frac{NPs}{ml} = \frac{[Ag]}{m_{single\ AgNP}}$$

- Where the average $m_{\text{single AgNPs}}$ in g was obtained by

$$m_{single\ AgNP} = V_{sphere} \times Ag_{density}$$

in which $V_{sphere} = \frac{4}{3}\pi r^3$ and $Ag_{density}$ is 1.05×10^{-20} g/nm^3. Then the result was converted from g to µg by applying a multiplicative factor

- Total surface area in nm^2/ml

$$A_s = S_{sphere} \times \frac{NPs}{ml}$$

- Specific surface area in nm^2/µg

$$A_{s-specific} = \frac{S_{sphere}}{average\ m_{single\ AgNP}}$$

As evinced in Table 1, the specific surface area of 4 nm AgNPs was the highest. In fact, with respect to them, 30 nm and 55 nm AgNPs showed around a 5 times and 9 times lower specific surface area. Also the amount of AgNPs in NPs/ml followed the same trend: 4 nm > 30 nm > 55 nm AgNPs.

2.6 Surface Enhanced Raman Scattering (SERS)

In recent years, the vibrational spectroscopies were widely used for the analysis of food additives and contaminants for their simplicity, the rapidity of the analyses and because they are non-destructive methods [77], [78].

In particular, Raman spectroscopy is a technique which detects the inelastic scattering of light. Since the frequencies of the Raman scattered photons bring information about the samples, this technique provide the structural fingerprint of the analytes and allow their chemical identification [79]. The main advantages of the Raman technique are the minimal pre-treatment needed for the samples, the high selectivity allowed by the characteristic molecular fingerprint, the fast time of the detection and the absence of water interferences.

Moreover, the Raman sensitivity can be enhanced by several order of magnitude exploiting a variation of the traditional technique: the Surface Enhanced Raman Scattering (SERS) [80]–[83]. SERS exploits metal nanoparticles as a substrate to amplify the Raman signals. When illuminated by a monocromatic light, the excitation of the peculiar LSPR [70] of these metal nanoparticles produces hot spots that generate a local increase of the electromagnetic field. Thus, when molecules are adsorbed onto or in close proximity to metallic nanostructures, which are plasmonically active, the produced hot spots allow to increase the sensitivity of the technique [67], [84].

Recently, the SERS technique is acquiring a role of considerable importance in the panorama of analytical methods for the quantification of additives and contaminants in food matrices [85]–[88]. Indeed, thanks to the chemical interaction between the colloidal NPs and the analytes, which provide considerable sensitivity and specificity, SERS can be considered as a prominent candidate for the food control analyses [89].

2.7 Use of AgNPs for in liquid SERS analysis in this thesis

During my PhD, I produced many batches of AgNPs with the three nominal diameter of 4, 30 and 55 nm. These AgNPs were used by the whole group of Physical Chemistry and Nanotechnology of INRiM for different research activities, such as the evaluation of their antimicrobial properties [90], the quantification of organotin compounds [91] and of dithiocarbamate fungicide thiram by SERS techniques.

For the detection of additives and contaminants in food matrices, numerous SERS techniques were proposed in literature. The main SERS strategies can be summarized in the following categories:

- The use of solid SERS substrates, with nanostructures directly fabricated on it or with metal nanoparticles immobilized on it [92], on which the analyte extracted from the matrix is deposited and mapped. These substrates can be obtained in many ways, such as the nano-lithography or the soft-lithography [93], [94], self-assembly of colloidal NPs on the substrate [95]–[97], porous membranes or substrates with colloidal NPs [84], [98], [99], flexible or free standing nanowires or pillars obtained by reactive ion etching [100] and active plasmonic nanostructures produced *in situ* [101]. These solid substrates generally have SERS hot spots due to NPs homogeneously distributed and thus signal that are reproducible in a large portion of the substrate. Moreover, the high enhancement factor of SERS effect allows the detection of analytes in traces. Usually, the results achieved with these solid substrates are good but their fabrications involve high costs, long time and high skills. The main disadvantage of these structures is that the analytes are often distributed on the substrates in an inhomogeneous way and this fact can limit the reproducibility of their quantifications [102], [103]. Moreover, to quantify the analytes on their surface, it is necessary to provide time consuming 2D

mapping.

- The detection of the analytes directly *in situ*, such as on the peels of fruits. For this kind of measurements, a first option is the use of metallic or bi-metallic core-shell colloidal NPs as a sort of dust to cover the surface of analysis [104]–[106]. Sensitive detection of the analytes is obtained but these methods suffer the lack of reproducibility and accuracy caused by the random distribution of the NPs colloidal on the matrices surface. A second option is the use of SERS substrates where analytes are recovered from the matrices surface and directly analysed them [107], [108]. These structures are transparent and flexible and have plasmonic features homogeneously distributed [107], [109]–[111]. They allow to achieve more reproducible measurements compared to the dust of NPs. However, their main disadvantage is that, with this approach, only limited portions of the surfaces can be sampled and thus it is difficult to carry out a reliable quantification of the analytes.
- The in liquid analysis of mixture of the analytes from the matrices and the colloidal suspensions of metallic NPs. This approach exploits the specific interaction of the analyte with the NPs surface and the hot spots generated by the agglomeration of the colloids to obtained a huge enhancement of the signals. To promote this mechanism, the chemical properties of the NPs surface and the addition of salts or molecules, which changes the ionic strength and the pH of the mixtures, can be considered [47], [91], [112]–[114]. The in liquid SERS measurements can be performed *in situ* and the low cost of the production of the NPs suspensions make the application of this approach convenient. The principal advantage of the in liquid SERS method is the good homogeneity achieved by the mixed suspension of analyte and NPs, which is a condition that can improve its repeatability [113]. Nevertheless, it is necessary to pay attention at the dynamics which can occur in the mix during the analysis in order to optimize the agglomeration of the NPs and maximize the SERS signals.

Therefore, each of the described SERS methods has advantages and disadvantages and the optimal method has yet to be found. It should be the best compromise between excellent sensitivity and satisfactory reproducibility of the measurements.

For my PhD, I decide to use AgNPs for the development of in liquid SERS methods. I tested all the three sizes of AgNPs and I selected the most suitable substrate for each specific analyte. In this thesis, this approach was used for:

- a feasibility study of the determination of ochratoxin A (Section 3.5);
- the development and the application of an innovative in liquid SERS method for the quantification of sulfur dioxide in wine (Section 4.5).

From these studies, which were extensively described in the next chapters, I experimented many of the advantages and disadvantages of the in liquid SERS approach described in literature [115].

The main advantages of the use of in liquid SERS method are [115]:

- absence or minimal pre-treatment of the sample is required;
- it provides the characteristic molecular fingerprint of the analytes, allowing the chemical identification [79]. This results in high selectivity and specificity of the method;
- the reduced time of the detection, since the acquisition of a single spectrum requires seconds or minutes;
- the absence of water interferences which allows analysis of aqueous solutions;
- high sensitivity thanks to the use of metal nanoparticles. Indeed, the Raman sensitivity can be enhanced by several order of magnitude exploiting this approach [80]–[83];
- suitable for a large variety of food analyses thanks to the chemical interaction between the analytes and the colloidal NPs [89];
- need for a very small volume to analyse;
- very low use of solvents;
- it is a portable *in situ*, allowing fast analyses also in agricultural fields, warehouses, ports and at all stages of processing and distribution of food products;
- it does not require hard working conditions (high vacuum, temperature, etc.).

On the other hand, the main drawbacks of the in liquid SERS method are [115]:

- need to produce and characterize metal nanoparticles with defined properties (composition, shape, dimension, surface);
- need to provide a study to select the best typology of NPs for the specific analyte;
- the stability of the nanoparticle colloids suspensions. It depends on the type of NPs and on the stabilizing agents;
- not always satisfactory reproducibility in practical applications. This is mainly due to the agglomeration of NPs which leads to a heterogeneity of the enhancement of the electromagnetic field;
- the mixing of the sample with the nanoparticles often leads to a clustering of these last, resulting in an unstable suspension. These clusters were subjected to fluctuation over time and the density variation of them led to differences in the SERS signals intensities;
- the fabrication of suitable substrates often requires their functionalization with recognition ligands [116].

Chapter 3

Ochratoxin A (OTA)

3.1 Introduction to mycotoxins

Mycotoxins are small-size secondary metabolites with molecular weight usually lower than <1000 Da [117]–[119]. They are naturally produced by filamentous fungi and molds of the genera Aspergillus, Penicillium and Fusarium [117], [120] and contaminate a large variety of foodstuffs such as corn, barley, wheat, rice, dried fruit, spices, cocoa, coffee, fruit, vegetables, milk, wine, beer, ecc. [121], [122]. From a chemical point of view, mycotoxins are a heterogeneous group of molecules. Nowadays, around 300 mycotoxins are acknowledged and their number is constantly increasing [36], [123]. The most abundant and dangerous are aflatoxins, trichothecenes, zearalenone, fumosinins, deoxynivalenol, patulin and ochratoxins [119], [122], [123]. Molds can be able to produce one or more mycotoxins, but not all the molds produce toxins as well as not the whole secondary metabolites are toxic [123].

Mycotoxins can exert a wide range of biological effects relating to the target organs they affect. In general, they are able to provoke acute toxic effects and can be carcinogenic, genotoxic, teratogenic, mutagenic, nephrotoxic, hepatotoxic and immunosuppressive to animals and humans [36], [124].

Although there are several information regarding the toxicological properties of mycotoxins, it is often still uncertain what is their biological role, in general, as secondary metabolites of fungi. On the whole, the prevalent hypothesis is that mycotoxins play a role in the colonization processes allowing fungi to survive in a

specific trophic niche [125]. Indeed, it seems that the fungi able to produce mycotoxins are favored in their ecological niche because they are better shielded against further organisms living in the same environment [122].

In addition to the implications on human health, the foodstuffs contamination by mycotoxins has important repercussions also on the economic sector [121], [123], [126]. Indeed, FAO reported that mycotoxins worldwide affect food crops in the relevant percentage of up to 25 % [127], [128].

3.2 Description and characteristics of OTA

Ochratoxin A (OTA) is a mycotoxin produced by the metabolism of fungi of the genus Aspergillus carbonarius, Aspergillus ochraceus and Penicillium verrucosum [117], [129]. OTA was first isolated and identified by Van der Merwe in South Africa in 1965 by Aspergillus ochraceus, from which it takes its name [130], [131], and, since then, considerable advances have been made in the study of this molecule [132].

It consists of a dihydroisocumaric ring linked to β-phenylalanine via an amide bond with the carboxyl group (Figure 7) [133]. The chemical formula of OTA is $C_{20}H_{18}O_6ClN$ and its IUPAC name is (N - [[(3R) -5-chloro-8-hydroxy-3-methyl-1-oxo-7-isochromanyl] carbonyl] -3-phenylL-alanine) [132].

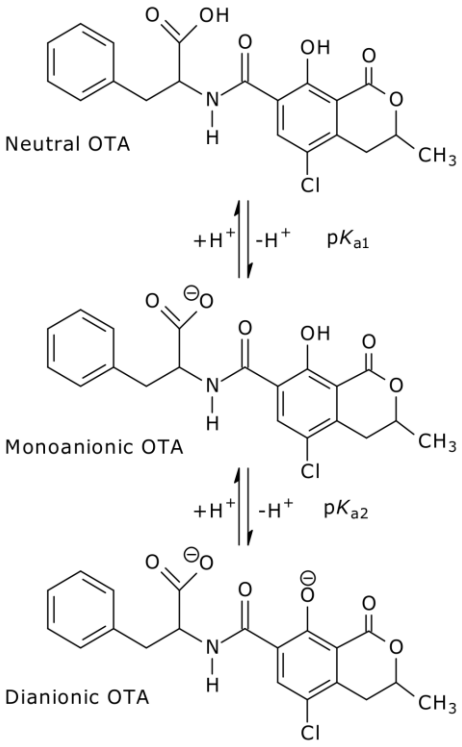


Figure 7: The pH dependent OTA forms in aqueous solutions

Figure 7: From neutral to monoanionic OTA (pK_{a1}) and from monoanionic to dianionic OTA (pK_{a2}). Image taken from [134]

In literature some metabolites of OTA are reported [135]:

- ochratoxin B (OTB), obtained by dechlorination of OTA;
- ochratoxin C (OTC), obtained by esterification of OTA with ethyl;
- ochratoxin α (OTα), an isocoumaric derivative of OTA.

Nevertheless, OTA is the most toxic and the most abundant and thus most of the studies on ochratoxins refer to this molecule.

Solid OTA is a colorless crystalline with a molecular weight (MW) of 403.8 g/mol. It is non-polar and soluble in solvents such as acetonitrile and benzene, in fact its octanol/water partition coefficient ($Log K_{O/W}$) is equal to 4.6 [118]. OTA can be purchased in solid form or in solution but, due to the high toxicity of the powder, it is highly recommended to prefer the liquid form, if possible. In laboratory practices, it is generally degraded using 5% sodium hypochlorite solutions [136], [137].

As shown in Figure 7, in aqueous solution OTA shows three level of protonation which depend on the pH through the two acid dissociation constants ($pK_{a1,2}$). In details, under acid condition OTA is present in the neutral form, increasing the pH the monoanionic OTA becomes present (following a loss of a proton from the phenylalanine carboxylic group) and reaching the neutral pH the dianionic form becomes prevalent (following a loss of a second proton from the phenolic group). The two acid dissociation constants (pK_a) for OTA reported in the literature are summarized in Table 2.

Table 2: Experimental values of the two acid dissociation constants of OTA reported in literature

Table taken from [134] and adapted.

Reference	pK_{a1}	pK_{a2}
[138]	-	7.0
[139]	-	7.0 ± 0.02[a]
[140]	-	7.05 – 7.1
[141]	4.4	7.3
[142]	-	7.05 – 7.10[b]
[143]	-	7.04[c]
[144]	-	7.1

[a] In 0.1 mol/l phosphate buffer, [b] in 0.16 mol/l KCl, [c] in 0.16 mol/l; at 25 °C.

The growing attention paid to OTA in recent years is due to its contamination of a large variety of foodstuffs, such as cereals, coffee, spices and wine. In the last evaluation of OTA performed by the Joint FAO/WHO Expert Committee on Food Additives (JECFA), a Provisional Tolerable Weekly Intake (PTWI) of 100 ng/kg body weight of OTA was established. This maximum value is normally respected. Indeed, it is estimated that the effective amount of OTA to which humans in Europe are exposed in consequences of a weekly normal diet is between 8 and 17 ng/kg body weight [145]. The maximum levels of OTA in different foods are

established by REGULATION (EC) No. 1881/2006 [146] for Europe and range from 0.5 to 10 μg/kg. This regulation is adopted also in Italy and the threshold value for wine is 2 μg/kg.

The toxic properties of OTA generate nephrotoxic, teratogenic, carcinogenic and immunosuppressive activity in many animals[147], [148] and the IARC classifies OTA as a possible human carcinogen (group 2B) [149], [150].

The relevance of OTA characterization and quantification is connected to its extreme toxicity and its broad-spectrum contamination of foodstuffs. Various analytical methods have been developed and optimized [151]. Among the traditional techniques there are high performance liquid chromatography coupled with fluorescence spectroscopy (HPLC-FLD), which is considered the method of choice for the determination of OTA [152]–[157], high performance liquid chromatography coupled with mass spectrometry (HPLC-MS) [157], thin layer chromatography (TLC) [158], [159], fluorescence spectroscopy [160]–[163] and enzyme linked immunosorbent assay (ELISA) [152], [164]. There are also other alternative OTA analysis techniques, more recently applied, such as, for instance, vibrational spectroscopy [165]–[168] and electrochemical methods [169]–[171].

3.3 Quantification of OTA in a CRM of red wine by High Performance Liquid Chromatography with Fluorescence Detection (HPLC-FLD)

3.3.1 Scope of the work

HPLC-FLD is the analytical technique most commonly used for the determination of OTA in food matrices [152]–[156].

I performed an experiment of OTA quantification by HPLC-FLD in order to evaluate the advantages and disadvantages of this technique. It was carried out in the Chemical Laboratory of the Agenzia delle Dogane e dei Monopoli of Turin. For this work, a CRM of ochratoxin A in red wine was used as a sample. Indeed, some recent papers on the determination of OTA in wine by HPLC-FLD were reported in literature [153], [155], [172]–[175]. The legal limit for OTA in wine is established by COMMISSION REGULATION (EC) No 1881/2006 [146] at 2 μg/kg. For the measurements, the protocol EN 14133:2009 entitled “Foodstuffs - Determination of ochratoxin A in wine and beer - HPLC method with immunoaffinity column clean-up” [176] was adapted and used.

3.3.2 Chemicals

All the solutions were prepared in ultra-pure water and high purity reagents were used. For the preparation of the solutions for the analysis, the following reagents were used: acetonitrile — CH_3CN (Carlo Erba), glacial acetic acid — CH_3COOH (Sigma Aldrich), phosphoric acid — H_3PO_4 (Sigma Aldrich), sodium hydrogen carbonate — $NaHCO_3$ (Sigma Aldrich), sodium chloride — NaCl (Carlo Erba), polyethylene glycol (Merk), methanol — CH_3OH (Panreac). Sodium hypochlorite — NaClO (Sigma Aldrich) was used to clean the glassware.

An analytical standard solution of OTA in acetonitrile with concentration of (10 ± 0.20) µg/ml was acquired from Sigma Aldrich. The solutions of OTA were obtained from it by dilutions.

A CRM of ochratoxin A in red wine with concentration of (0.52 ± 0.11) µg/l (ERM-BD476) was acquired from the Federal Institute for Materials Research and Testing (BAM) and used as a sample.

3.3.3 Solution for HPLC-FLD

For the HPLC-FLD analysis, the following solutions were prepared:

- Diluting solution: 100 ml of ultra-pure water with 1 g of polyethylene glycol and 5 g of sodium hydrogen carbonate;
- Washing solution: 500 ml of ultra-pure water with 12.5 g of sodium chloride and 2.5 g of sodium hydrogen carbonate;
- Mobile phase: 49.5 % of ultra-pure water, 49.5 % of acetonitrile and 1 % of glacial acetic acid. This solution was sonicated for 1 hour before use.

3.3.4 Preparation of calibration solutions of OTA

A solution of OTA in acetonitrile at 2 mg/l was obtained from dilution in acetonitrile of the analytical standard of the purchased OTA. This solution was then used to prepare six calibration solutions in the mobile phase (called standard from 1 to 6) that were exploited to build a calibration curve. The six standards were prepared with the following expected concentrations (according to the protocol EN 14133:2009 [176]): 0.6, 2.0, 6.0, 20, 40, 60 µg/l. The real

concentrations of these standards were calculated by considering the volumetric mass of the mobile phase of 0.91261 g/ml and are reported in Table 3.

The range of concentration of the OTA standards used for the calibration curve was studied to include the final concentration (following the pre-treatment of the CRM) of the samples to analyse.

3.3.5 Pre-treatment of the CRM of OTA in red wine

The CRM of OTA in wine was used as a sample to evaluate the recovery with this technique.

A pre-treatment of the CRM was necessary to purify it from possible interferers, such as tannins. Firstly, the wine was filtrated with quartz filters from PallFlex. Then, Ochraprep immunoaffinity columns (IAC) from R-Biopharm Rhône LTD, which had a recovery reported by the producer > 85 %, were used. Thanks to the high specificity of the antigen (in this case OTA) - antibody interaction, the IAC columns [153] allowed the selective retention of the analyte of interest.

The pre-treatment procedure was constituted by the following steps:

- mixing 20 ml of CRM of red wine with 20 ml of diluent solution and filtration of the obtained solution on a quartz filter;
- subdivision of the filtrated solution into two aliquots of 20 ml each called sample 1 and sample 2;
- conditioning of two IAC columns with the liquid contained within them;
- parallel passage of the two samples on the two IAC columns with a flow rate of about 1 drop/s;
- washing of the two IAC columns with 5 ml of washing solution and 5 ml of water with a flow rate of approximately 1-2 drops/s;
- drying of the two IAC columns;
- elution of the OTA retained by the two IAC columns with 2 ml of methanol in ~~a~~ two vials at a flow rate of about 1 drop/s;
- evaporation of methanol from the two vials at 50 ° C under a nitrogen flow until the OTA was completely dry;
- re-dissolution of crystallized OTA into the two vials with 500 µl of mobile phase;

- transfer of the two solutions into two smaller vials suitable for the HPLC autosampler;
- injection of 10 µl of each of the two samples into the instrument and analysis.

Following this procedure, the OTA in the two samples was concentrated 20 times as compared to the CRM of OTA in red wine. As a consequence, the nominal concentration of OTA in the two samples deriving from the CRM was 10.4 µg/l.

3.3.6 High Performance Liquid Chromatography with Fluorescence Detection (HPLC-FLD)

An HPLC-FLD from Waters was used for the analysis. The instrument was equipped with a C18 reverse phase column from Phenomenex Kinetex. The column characteristics were: length of 150 mm, internal diameter of 3 mm, particle size of 2.6 µm, pore size of 100 Å and it was thermostated at 35 °C. The eluent used for the analysis was composed by 80 % mobile phase and 20 % ultra-pure water. The eluent flow rate was of 0.35 ml/min. The injection volume of the samples was 10.00 µl and the run time of each analysis was of 40 minutes.

3.3.7 Densimeter

To calculate the volumetric mass of the mobile phase, a DMA 4500 M electronic densimeter from Anton Paar was used.

3.3.8 Results and discussion

This experiment was performed once to test one of the most commonly used methods for OTA determination. There were no replicas of these analyses as they did not represent the main purpose of my thesis. In Figure 8 the chromatogram of the standard 1 with a known concentration of OTA is reported. The chromatograms of the other standards used to obtain the calibration curve were similar to this one.

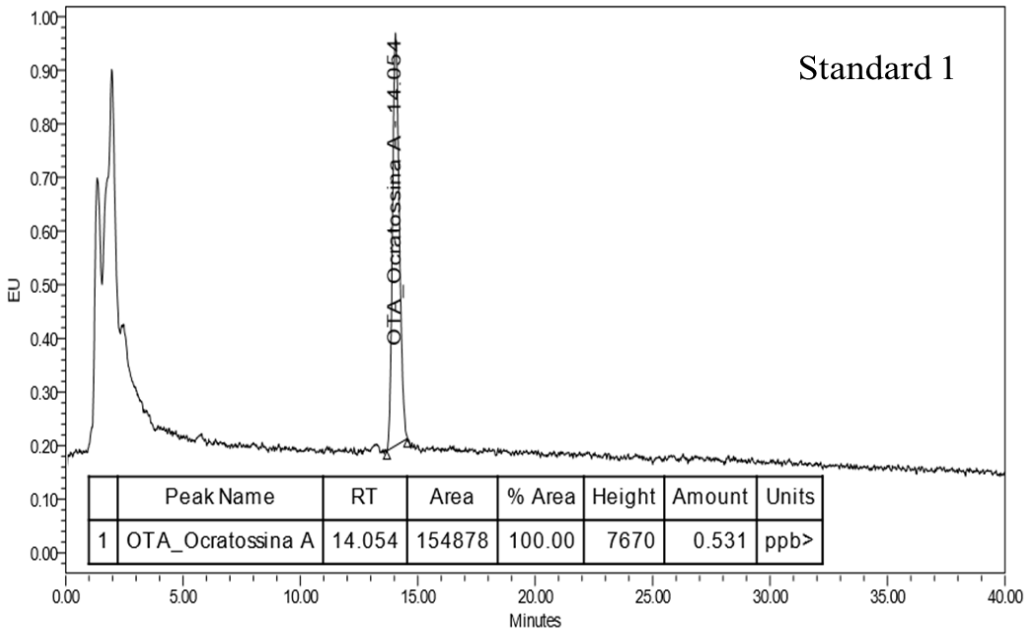


Figure 8: Chromatogram of standard 1 of OTA used to create the calibration curve

Figure 8: Standard 1 with a known concentration of OTA of 0.53 µg/l. The chromatograms of the other standards were similar to this one. The area of the peak is expressed in unit of emission (EU)

As can be seen in the chromatogram of Figure 8, OTA had a retention time of about 14 min. From the area of this elution peak, the concentration of OTA was quantified using the fluorescence detector. For these fluorescence measurements, the classical wavelengths reported in the literature [153] were set on the instrument, namely λ_{ex} = 333 nm and λ_{em} = 460 nm. These wavelengths are those specific of the OTA molecule in the monoanionic form because the pH of the mobile phase is ~ 4. The area of the peaks in the chromatograms of the six standards of OTA are summarized in Table 3. As already mentioned, no replicates of these measures were performed. I was aware that the HPLC method should be validated by following definite and accepted rules, which included replicates of the measures. However, this experiment can be interpreted as one more test I did to broaden the scenario on the OTA analysis in my thesis. This test was only functional for the other studies I worked on and its results did not claim to be valid in themselves. This activity allowed me to evaluate some advantages and disadvantages of this technique with respect to the methods that I had dealt with during my PhD.

Table 3: Real concentration and area of the peaks of the six standards of OTA

Standard n°	Real concentration of OTA [µg/l]	Area of the peak of OTA in the chromatogram [EU]
Standard 1	0.53	154878
Standard 2	1.89	546300
Standard 3	5.83	1691431
Standard 4	20.03	5867645
Standard 5	40.41	11878714
Standard 6	55.60	16818479

In Figure 9 is shown the calibration curve obtained by plotting the real concentrations of OTA standards versus the peaks area. The linear fit had R^2 of 0.9996 and proved the high sensitivity of the instrument and an accurate preparation of the standard solutions.

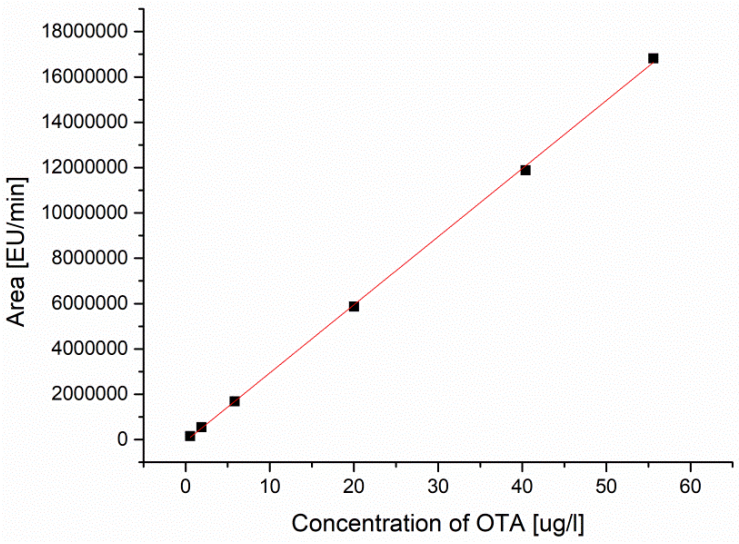
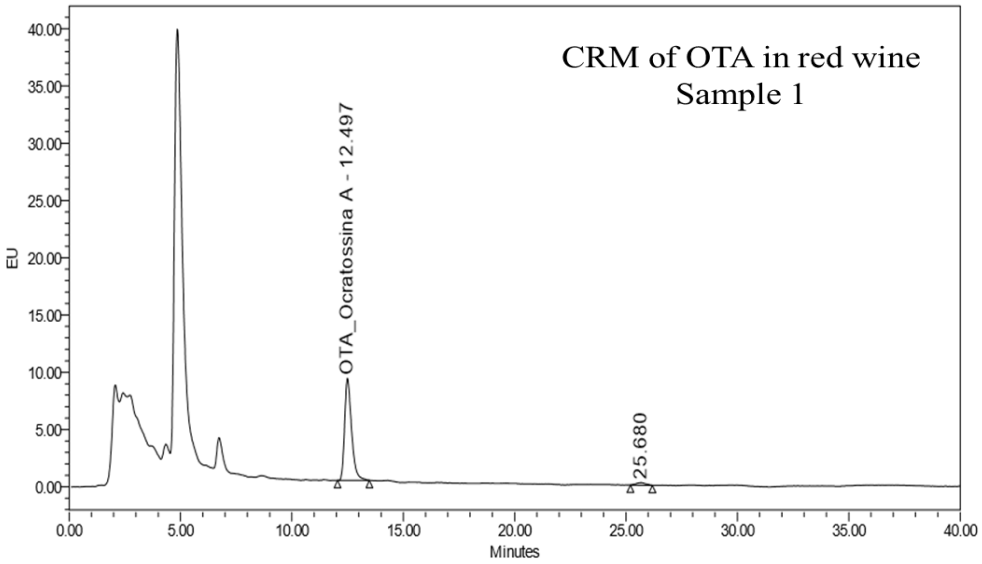


Figure 9: Calibration curve of OTA standards with HPLC-FLD

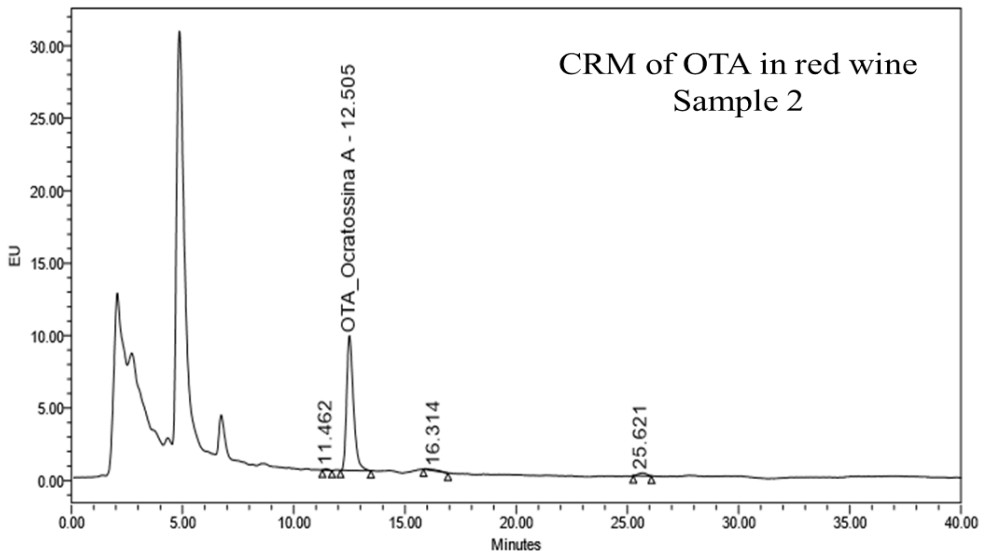
Figure 9: Linear fit (R^2 = 0.9996) obtained by plotting the peaks area as a function of the real concentrations of the six OTA standards.

Then, the two samples obtained from the pre-treatment of the CRM of OTA in red wine were analysed with the same analytical conditions. In Figure 10 are reported their chromatograms. In the chromatograms of the samples, the elution peaks of the OTA shifted to 12.5 min with respect to the 14 min of the standards. This shift could be probably attributed to:

- the matrix effect of the wine, whose composition is strongly different from the standard solutions. The interference of the chemical compounds present in wine could influence the position of the chromatographic peak of OTA. As can be observed in the chromatograms of Figure 10, other low intensities peaks were present, probably due to some residual chemical component of the wine. Moreover, the matrix effect in real samples also had repercussions on the width of the chromatographic peaks. Indeed, width of the OTA peaks in the CRM samples were larger than those in the standards.
- the effect of the pre-treatment that was applied only to the samples and not to the standards.



	Peak Name	RT	Area	% Area	Height	Amount	Units
1	OTA_Ocratossina A	12.497	1935653	96.88	89053	6.664	ppb>
2		25.680	62240	3.12	2179		



	Peak Name	RT	Area	% Area	Height	Amount	Units
1		11.462	12503	0.60	902		
2	OTA_Ocratossina A	12.505	1985797	95.27	92909	6.831	ppb>
3		16.314	33263	1.60	813		
4		25.621	52845	2.54	2007		

Figure 10: Chromatograms of the two samples from the CRM of OTA in red wine

Figure 10: Samples, obtained from the pre-treatment of CRM of OTA in red wine, with concentration of 10.4 µg/l. The areas of the peaks are expressed in unit of emission (EU)

The area of OTA peaks in the chromatograms was related to the nominal concentration of 10.4 µg/l obtained following the pre-treatment ($[OTA]_{\text{sample}}$) (Section 3.3.5). The effective OTA concentration was calculated using the following formula:

$$[OTA]_{\text{quantified}} = \frac{[OTA]_{\text{CRM}} * [OTA]_{\text{chromatrogram}}}{[OTA]_{\text{sample}}}$$

and the percentage recovery was calculated, as reported in Table 4.

Table 4: Concentration and recovery of OTA in the samples of CRM of red wine

Sample	Concentration of OTA declared in the CRM of red wine ($[OTA]_{\text{CRM}}$) [µg/l]	Concentration of OTA obtained from the chromatogram ($[OTA]_{\text{chromatogram}}$) [µg/l]	Concentration of OTA quantified in the sample after correction ($[OTA]_{\text{quantified}}$) [µg/l]	Recovery %
1	0.52	6.66	0.33	63.46
2	0.52	6.83	0.34	65.38

For the CRM of OTA in red wine, the mean recovery was 64.42 % with a standard deviation of 1.36 %. However, it should be considered that the uncertainty associated with the concentration of OTA in this CRM was of 21.15 %, thus the recovery could be significantly higher or lower.

The most critical aspects, which probably influenced the performance of OTA quantification of the experiment, were:

- The passage of the CRM in the IAC column. During this phase, in fact, it was necessary to set an optimal flow rate to allow the antigen-

antibody reactions. If the set flow rate was too fast, the analyte did not have time to react with the antibody of the column affecting the percentage of retained OTA. Moreover, the percentage recovery reported by the producer was > 85 %, which meant that potentially the recovery of OTA following this step could not be quantitative;

- The evaporation of methanol. This step was particularly delicate because there was the risk that the nitrogen flow, by mechanical action, would extract together with the solution part of the OTA, reducing the amount of it that was deposited into the vial. For this reason, it was necessary to adjust the gas flow to allow only the evaporation of the solvent. This passage was also the most dangerous for the operator's health as the evaporation of the solvent led OTA to the crystalline form which is the most toxic;
- The re-dissolution of the crystallized OTA and the transfer of the solution into a vial for HPLC analysis. If the re-dissolution is not complete, this phase can also affect the final OTA recovery;
- The relevant uncertainty on the concentration value stated for the CRM. This uncertainty reflected on the quantification since the recovery could be significantly higher or lower;
- The strong matrix interference for OTA in wine. Indeed, wine is a quite complex matrix and contains a large variety of organic compounds such as organic acids, polysaccharides, polyphenols (tannins, anthocyanins and flavonols) [177]. These molecules could affect the quantification performance, maybe especially during the pre-treatment, by interacting with OTA. However, since this evidence derived from a single test, further studies was needed to confirm and deepen the effect of this matrix interference on OTA quantification.

3.3.9 Conclusion and future perspectives

HPLC-FLD is considered the official technique for the determination of OTA thanks to its good sensitivity and selectivity and the availability of official methods [159]. However, it presents some critical aspects in the procedure that require the employment of skilled operators [152]. Moreover, the sample pre-treatment procedure is quite long (a few hours) and the entire analysis involves the use of high volumes of solvents. Last but not least, the step of evaporation of

the solvent resulting in a crystallization of the solid OTA exposes the health of the operator to a non-negligible risk.

For these reasons, in recent years, the new frontier is the study of faster alternative methods, which require less pre-treatment of the samples and which offer the possibility of working *in situ* with portable instrumentation. Among these there are, for example, the enzyme-linked immunosorbent assay (ELISA) [178] and the SERS methods [179].

3.4 Comprehensive study of OTA behaviour in aqueous solution

Part of the work described in this Section was also previously published in the paper: "Comprehensive study on the degradation of ochratoxin A in water by spectroscopic techniques and DFT calculations" published on RSC Advances in 2019 [134].

3.4.1 Scope of the work

Contamination of crops from OTA is a serious problem worldwide. It is therefore of primary importance to increase the level of knowledge about this mycotoxin. In this context, a comprehensive study of the behaviour of OTA in aqueous solution was performed.

In the first part of this study, the protonation equilibria of ochratoxin A were investigated. Indeed, pK_a is a relevant physicochemical parameter in the characterization of a substance[180], [181]. The two pK_a of the molecule were evaluated by the following techniques:

- UV-Vis spectrophotometry with a stoichiometric approach. This part was performed in collaboration with Prof. Agnese Giacomino and Prof. Silvia Berto of the University of the Study of Turin,
- Fluorescence spectroscopy coupled with a chemometric approach.

The used experimental conditions were detailed since this information were often scarce or not available in literature.

In the second part of this study, the behaviour of OTA under alkaline conditions was thorough. In particular, the degradation pathway was monitored and the reaction products were identified. pH and time were the variables of this

experiment. Since this degradation process led to molecules less toxic than OTA, the conditions of irreversibility of the OTA toxicity deletion were investigated by bringing back the pH of the solution towards acidity. These evaluations were performed by:

- Experimental evidenced obtained by fluorescence spectroscopy,
- Theoretical studies using the Density Functional Theory (DTF). This part was performed by Prof. Glauco Tonachini and Prof. Andrea Maranzana thanks to the collaboration with the University of the Study of Turin.

The complete identification of the forms of OTA and of its degradation products in aqueous solutions from pH 1 to pH 12.5 was of paramount importance. Indeed, the chemical structure of the molecules strongly affected their toxicological properties and influenced their biological behaviour [140], [143], [144], [162], [182]. Therefore, this comprehensive OTA assessment reported here may supply helpful information for toxicological studies on this harmful and widespread mycotoxin.

3.4.2 Chemicals

A solution at 1 g/l of OTA in dimethyl sulfoxide — C_2H_6OS was purchased from Sigma-Aldrich as a reference material. The solutions of OTA used for the experiment derived from this material as follow:

- aliquots of OTA in dimethyl sulfoxide were directly diluted into aqueous solutions and prepared for spectrophotometric measurements;
- an aliquot of it was diluted into an aqueous solution to reach the OTA concentration of 0.001 g/l. This latter was then used to prepare the analytical solutions for the fluorescence experiments.

Aqueous solutions at different pH were prepared using:

- aliquots of 0.1 mol/l HCl solution in water for acidic conditions (with 0.1 mol/l KCl to fixed the ionic strength);
- aliquots of 0.1 mol/l sodium phosphate monobasic — NaH_2PO_4 and 0.1 mol/l disodium phosphate — Na_2HPO_4 for neutral condition (with 0.4 mol/l as ionic strength due to the phosphate buffer). The phosphate buffer was also useful for the stabilization of OTA neutral solutions.
- aliquots of standardized 0.01 mol/l or 0.5 mol/l NaOH solution in water and, if necessary, aliquots of 0.1 mol/l HCl solution to adjust the

pH for basic conditions (with 0.1 mol/l KCl to fixed the ionic strength).

OTA solutions were prepared by adding the analyte to these differently pH aqueous solutions. The OTA concentrations chosen for the experiments were 8 mg/l (which corresponded to 2×10^{-5} mol/l) in the case of UV-Vis spectrophotometry and 50 μg/l (which corresponded to 1.24×10^{-7} mol/l) in the case of fluorescence spectroscopy.

The standardized 0.01 mol/l NaOH solution was used to perform the spectrophotometric titration.

A solution at 10.2 ± 0.1 mg/l of OTα in acetonitrile — CH_3CN was purchased from LGC Standards and was adopted as a standard in fluorescence measurements.

To investigate the OTA degradation reversibility, aliquots of HCl 37% was added to acidify the solutions.

Milli-Q ultra-pure water was used to prepare all the solutions used in the experiments. The glassware used to store OTA and OTα solutions were previously conditioned with sulphuric acid — H_2SO_4 2 M for at least 6 hours and then accurately washed with ultra-pure water. OTA and OTα solutions were preserved at a temperature of 4 °C and in amber glassware to guarantee the dark conditions. To remove trace of OTA from the used glassware, 5 % active chlorine sodium hypochlorite — NaClO (commercial bleach) was adopted [136], [137].

3.4.3 UV-Vis spectrophotometry with a stoichiometric approach

The UV-Vis spectra of OTA solutions were collected to estimate the two pK_a of the molecule.

A V550 UV-Vis double-beam spectrophotometer from Jasco was used to acquire the UV-Vis spectra of OTA solutions. The instrument was equipped with quartz cuvettes with a path length of 10 mm from Hellma for the flow-through measurements. A potentiometer model 713 with a resolution of 0.001 pH units acquired from Metrohm was used to measure the pH of the OTA solutions. The potentiometer was equipped with a model 6.0259.100 combined glass electrode from Metrohm, which was calibrated with respect to the concentration of H^+ every day. ESAB2M program [183] was employed to elaborate the slope and the $E°$ formal potential in the Nernst equation. A flow of nitrogen in the cuvette allowed

to obtained an atmosphere without oxygen. The solutions were stirred and kept at the constant temperature of 25 °C by a D1-G thermocryostat from Haake.

Before the measurement, 20 ml of 2×10^{-5} mol/l OTA solution was brought to pH 3 by adding aliquots of the HCl solution. Then, a 765 Dosimat burette from Metrohm with a resolution of 1 µl was used to add the 0.01 M NaOH solution until the pH of the solution reached about 7.5. Each of the consecutive aliquots were of 10 µl and corresponded to a rise of the pH of about 0.1/0.2 units.

The HypSpec software [184], [185] was used to elaborate the UV-Vis spectra. It worked on the basis of the stoichiometric principles, considering the equations of the mass and of the charge balance and applying the Lambert-Beer's law. In this work, 45 spectra were collected.

3.4.4 Fluorescence spectroscopy coupled with a chemometric approach

The fluorescence spectroscopy is a useful technique for the evaluation of the composition and the quality of food products [186]. In this study, it was employed both in the estimate of the two pK_a of the OTA and in the assessment of its degradation process under alkaline conditions.

The model FL3-21 of the Fluorolog-3 spectrofluorometer from the Horiba Scientific was used. It was equipped with quartz cuvettes with a path length of 10 mm from Hellma. The right angle geometry was selected [186]. Excitation-Emission Matrices of fluorescence (EEMs) were acquired for the solutions of OTA at the various pH. The excitation ranged from 310 to 395 nm and the emission ranged from 400 to 475 nm, both with wavelength resolution of 1 nm. For both the excitation and the emission the slits were 2 nm and the integration time selected was of 1 second. For the determination of the pK_{a1}, 12 EEMs of solutions of OTA in the pH range from 1.0 to 6.0 were recorded. The pH values of the solutions were: 1.0, 1.5, 2.0, 2.5, 2.9, 3.4, 3.8, 4.0, 4.3, 4.8, 5.2, 6.0. For the determination of the pK_{a2}, 7 EEMs of solutions of OTA in the pH range from 4.8 to 8.3 were recorded. The pH values of the solutions were: 4.8, 5.2, 6.0, 6.6, 7.1, 7.6, 8.3.

To evaluate the pK_{a1}, Parallel Factor Analysis (PARAFAC) [187]–[191] was employed for the elaboration of the fluorescence EEMs. PLS Toolbox from (Eigenvector Research, Inc.) for MatLab R2015a (Mathworks) was used. The array of the EEMs used had the following dimensions: 12 (samples) × 86

(emission wavelengths) × 76 (excitation wavelengths). For the preprocessing of the data, the multiway center was used. Non-negativity and unimodality constrains were imposed.

The Monte Carlo method was employed to evaluate and propagate the fits' uncertainty.

3.4.5 Theoretical method by Density Functional Theory (DTF)

DFT studies were performed to support the experimental evidences. Indeed, DFT established the values of maximum absorption wavelength (λ_{max}) of the three OTA forms in solution from acid to neutral and the most probable degradation pathway for OTA in alkaline conditions. Furthermore, it provided a theoretical confirmation of the laboratory findings and allowed the identification of the molecules in solutions.

Gradient procedures [192]–[196] within DFT [197] were used to determine all the stationary points on the energy hypersurface. The functional used was wB97XD [198]–[205]. For DFT optimizations and for the vibrational analysis, where both included the solvent effects, the Pople's basis set 6-311++G(d,p) was chosen [206], [207]. It was used to check the critical points nature. The Solvation Model based on Density (SMD) [208], [209] and the Integral Equation Formalism – Polarizable Continuum Model (IEF-PCM) schemes [210] were used to consider the molecules as a solute in water (the polarized continuum). Since water cooperated in a hydrogen transfer which helped the bond cleavage [211]–[213], in the steps TI1-4 and TI2-5, one explicit water molecule was taken into account to avoid the overestimation of these barriers. The relative Gibbs free energies (ΔG) in solution were estimated at a temperature of 298 K and were expressed in kcal/mol.

Single point time dependent – DFT calculations [214]–[219] were used to calculate the excitation energies. The functional used was O3LYP [220] and the basis set 6-311++G(d,p) [206], [207] were chosen.

The procedure reported in [221] was adopted to obtain the simulated UV-Vis absorption spectra.

The GAUSSIAN 09 system of programs [222] were employed for the optimization of the geometry and the thermochemistry calculations.

3.4.6 Results and discussion

Determination of the two pK_a of OTA

In Figure 11 the UV-Vis spectra of an OTA solution as a function of the pH are shown.

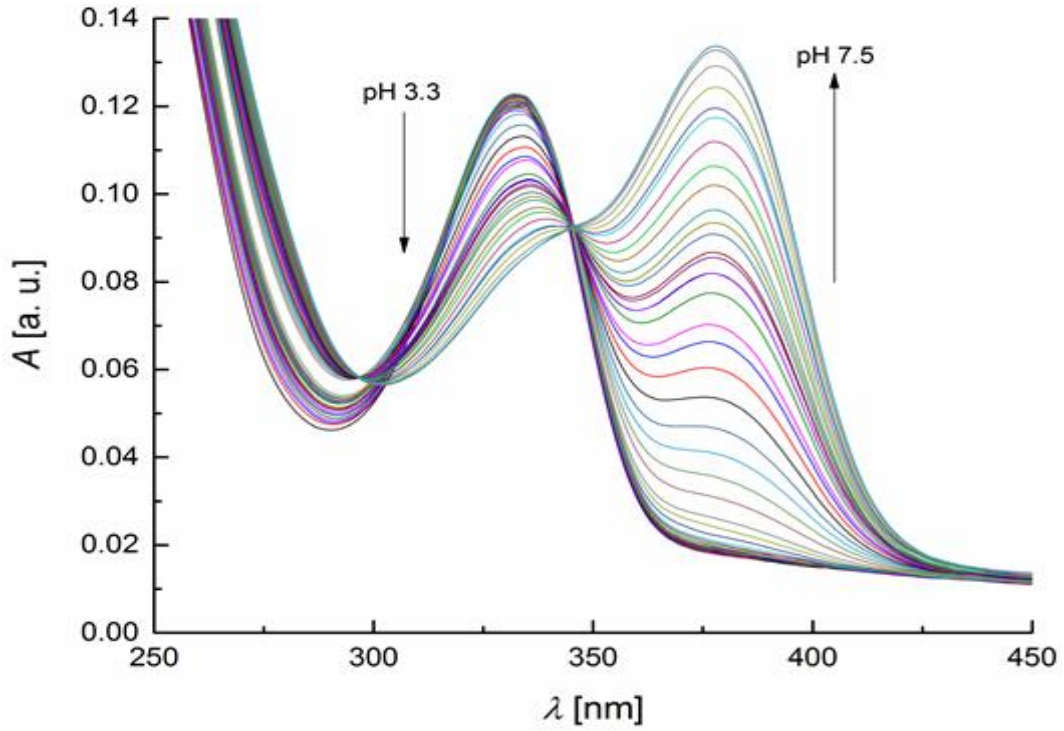


Figure 11: UV-Vis spectra of OTA solution in function of the pH

Figure 11: The OTA solution used had a concentration of 8 mg/l. The range of pH tested went from 3.3 to 7.5 by adding ach time 10 µl of 0.01 M NaOH solution. Each spectrum corresponded to an increment of about 0.1 – 0.2 pH units. Image taken from [134]

In Figure 11, two isosbestic points (specific wavelengths at which the absorbance of a sample does not change during a physical change of the sample) were observed (346 nm and 297 nm). This suggested the presence of two forms of the molecule in solution in this range of pH. However, the forms of OTA were three, as schematized in Figure 7. Indeed, there were two peaks whose intensities varied with the pH of the solution:

- The peak on the left (at 332 nm), that was attributable both to the neutral and the monoanionic forms of OTA, since their λ_{max} were the same;
- The peak on the right (at 378 nm), that was relative to the dianionic form of OTA.

These results were in agreement with the information reported in literature which stated that there was no difference between the neutral and the monoanionic OTA absorption spectra [162], [223], as reported in Table 5. However, these two forms can be distinguished by a small difference in the molar absorptivity (ε) value. The ε of a chemical species represent the specific absorbance of a solution with a unitary molar concentration, at a given wavelength, through a unitary optical path length. The HypSpec software [184], [185] was used to deduce the ε value of the three forms of OTA, as shown in Figure 12, and the two acid dissociation constants. This is a commercial software, whose formulas are not published, that worked on the basis of the stoichiometric principles, considering the equations of the mass and of the charge balance and applying the Lambert-Beer's law.

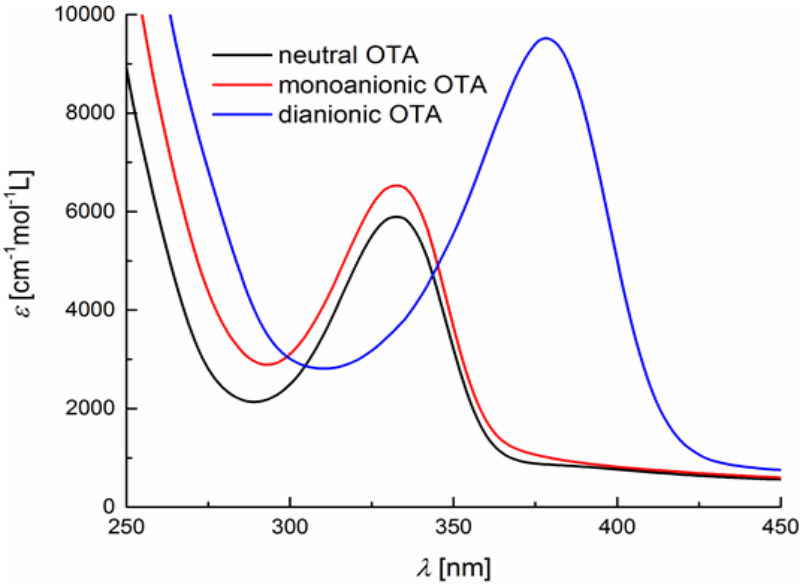


Figure 12: Behaviour of ε in function of the pH for the OTA forms

Figure 12: ε values obtained by the HypSpec software for neutral, monoanionic and dianionic OTA. Image taken from [134]

DFT can simulate the entire UV-Vis spectra of the neutral, monoanionic and dianionic OTA, as shown in [134]. The match of the calculation data with the experimental data depended on many factors: the calculation method (a DFT in this case), the base set, the way in which the vertical transition was simulated (TD-DFT in this case). These factors affected the shape of the spectrum, the position of the absorption maximum and the intensity of absorption. Differences of 10-35 nm between experimental data and calculation was considered normal and accepted. Those specific functional DFT and basis sets were chosen because the computed spectrum was very similar to the experimental one that was used as a reference. The absorption spectra could be simulated even better, but at significantly higher computational costs. Indeed, calculation times depended heavily on the size of the molecule, and more refined calculations were prohibitive. The best time/accuracy ratio was chosen.

In general, the shape of the molecule (conformational isomerism) can affect the spectrum in the whole spectral region. However, in this case there are not many conformational isomers and, above all, the chromophore was located in the rigid part of the molecule, i.e. the aromatic portion. The spatial position of the "outer" phenyl is quite irrelevant to the absorption spectrum.

DFT could also provide information in this deep-UV region by setting the number of excited states to consider. The program calculates all the possible electronic transitions (bands) starting from the ground state up to the nth excited state, with the relative intensities. The bands can fall into the visible or into the deep-UV.

In Table 5 the values of λ_{max} and ε_{max} obtained by the elaboration of the experimental UV-Vis spectra and by the theoretical DFT calculation are reported together with the data already published in literature, which show a good agreement. To the best of my knowledge, no information on the ε_{max} of the monoanionic form of OTA was present.

Table 5: Values of λ_{max} and ε_{max} of the three OTA forms obtained in this study (by experiment and calculation) and reported in literature.

Table taken from [134] and adapted

Source	Neutral form		Monoanionic form		Dianionic form	
	λ_{max} [nm]	ε_{max} [$cm^{-1}mol^{-1}l$]	λ_{max} [nm]	ε_{max} [$cm^{-1}mol^{-1}l$]	λ_{max} [nm]	ε_{max} [$cm^{-1}mol^{-1}l$]
This study – exp	332	5990	332	6544	378	9682
This study – calc	329	-	333	-	375	-
[162]	332	6650	332	-	380	10970
[223]	330	6600	330	-	379	9115

Concerning the two acid dissociation constants, the UV-Vis spectra were modelled with the HypSpec software [184], [185] considering both the protonation equilibria together. To obtain reliable results and to find the conditions that minimize the standard deviation, some evaluations and tests on pK_{a1} and pK_{a2} were needed. Initially, the software was run considering different fixed value of pK_{a1} and the outputs were evaluated. The minimum standard deviation for pK_{a1} was found in the range from 4.3 to 4.5. Then, in this range, fixed and free pK_{a2} were considered for ten elaborations and both the pK_a mean values were returned by the HypSpec software. The mean values for pK_{a1} and pK_{a2} and their associated standard deviations were 4.4 ± 0.1 and 7.09 ± 0.01, respectively. The distance between the λ_{max} of monoanionic and of dianionic OTA allowed to estimate the second pK_a with a higher number of digits compared to the case between neutral and monoanionic OTA where the λ_{max} values were the same.

In Figure 13 some of the fluorescence EMMs of OTA solutions acquired at different pH are reported. In these fluorescence maps, the emission wavelengths are reported on the *x* axis while the excitation wavelengths are reported on the *y* axis . The colour scales are shown on the right of each map. The three forms of

OTA were fluorophores and were identified by bands at specific excitation/emission wavelengths ($\lambda_{Ex/Em}$).

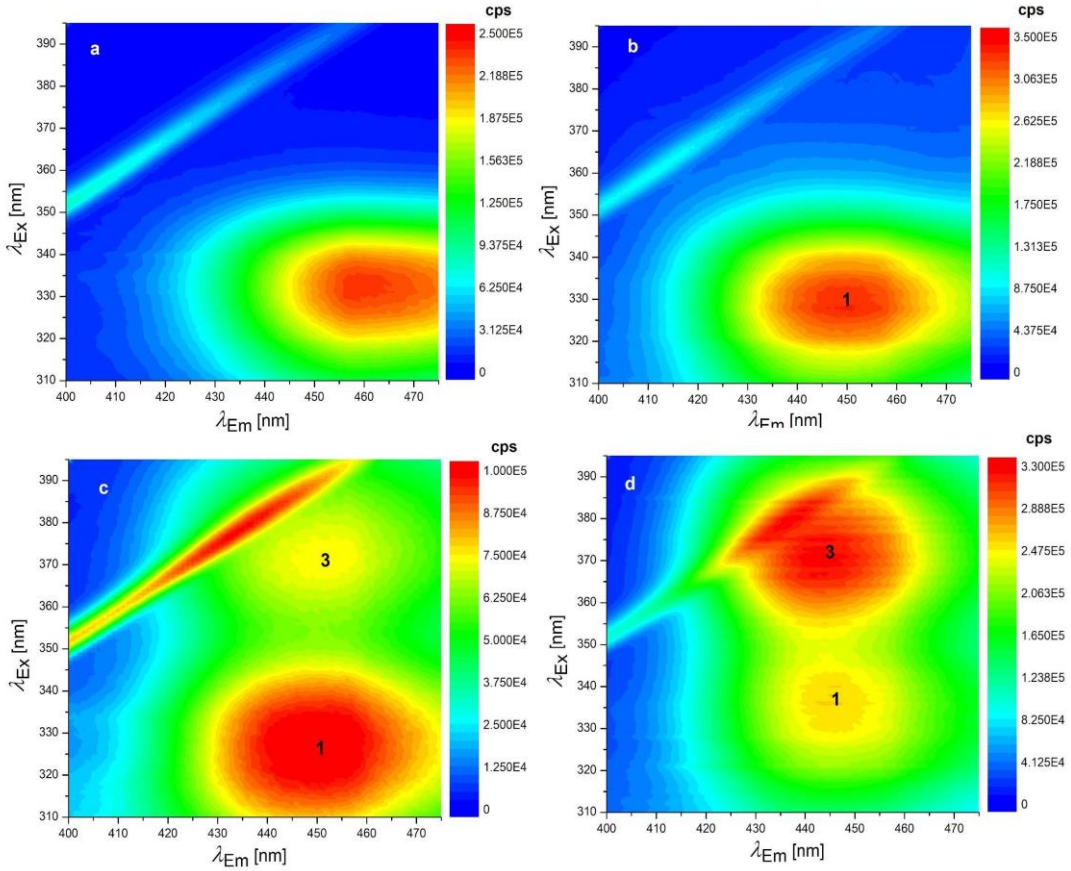


Figure 13: EEMs of OTA solutions at different pH

Figure 13: OTA solution with concentration of 50 µg/l. a) pH 1.0; b) pH 4.8; c) pH 6.6; d) pH 7.1. The numbers reported on the bands corresponded to the molecular structures of OTA in the scheme of Figure 21. Image taken from [134]

In the range of pH 1.0 – 6.0, the neutral and the monoanionic forms of OTA were present, while the dianionic form was not observed. A single band was observed at $\lambda_{Ex/Em}$ of 332/458 nm (Figure 13 a), attributable to the neutral form, which gradually shifted to $\lambda_{Ex/Em}$ of 328/446 nm (Figure 13 b), attributable to the monoanionic form, by increasing the pH.

As for the UV-Vis spectra in which the absorption wavelengths were the same for neutral and monoanionic OTA, also for the EEMs the bands were partially overlapped. For this reason, a two component PARAFAC model was employed to separate the two forms. A variance of 61.1 % and a core consistency of 100 %

was obtained for this model. The emission loadings profile resulted from PARAFAC are reported in Figure 14 a and represented the best approximation of experimental spectra of emission for pure OTA. Two components were present: the first, that represented the neutral form of OTA, with a λ_{Em} of 459 nm, and the second, that represented the monoanionic form of OTA, with a λ_{Em} of 536 nm. These emission loadings were in agreement with the normalized experimental raw emission spectra, extracted at λ_{Ex} of 332 nm from the EEMs of OTA in solutions from pH 1.0 to 6.0, reported in Figure 14 b. By these experimental spectra, the λ_{Em} of the neutral and of the monoanionic forms resulted of 458 nm and 446 nm, respectively.

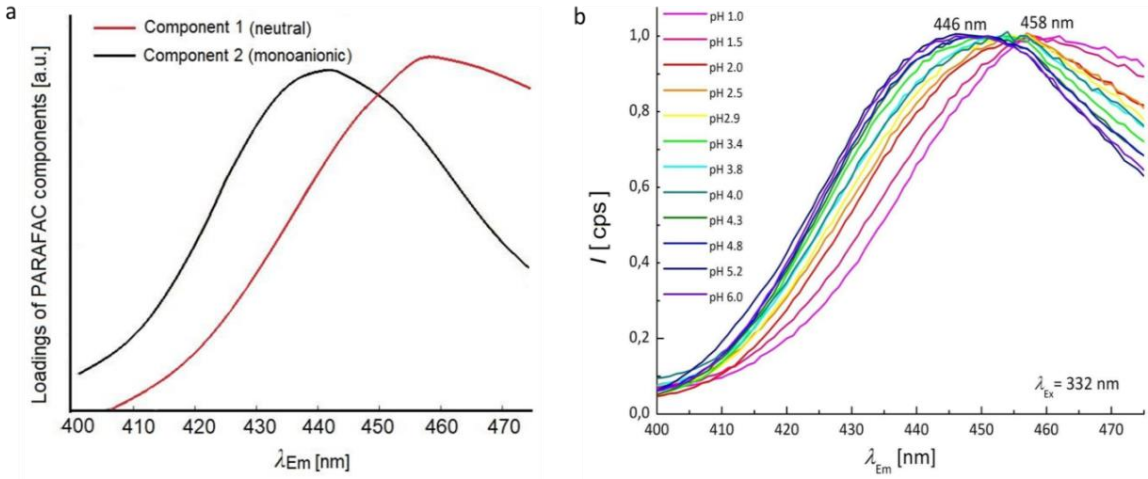


Figure 14: Emission loadings from the two component PARAFAC model and experimental emission spectra extrapolated from the EEMs

Figure 14: a) modeled emission spectra. Red line: neutral OTA with a λ_{Em} of 459 nm; black line: monoanionic OTA with a λ_{Em} of 536 nm; b) normalized experimental raw emission spectra extracted at λ_{Ex} of 332 nm from the EEMs of OTA in solutions from pH 1.0 to 6.0. Image taken from [134] and adapted.

Thanks to the slight difference of the λ_{Em} values for the two OTA forms, the scores obtained by the PARAFC model estimated the amount of these two forms in the solutions at various pH. The results are shown in Figure 15. The scores of the component 1, that represented the neutral OTA, was fitted with a linear fit, while the scores of the component 2, that represented the monoanionic OTA, was fitted by a second order polynomial fit.

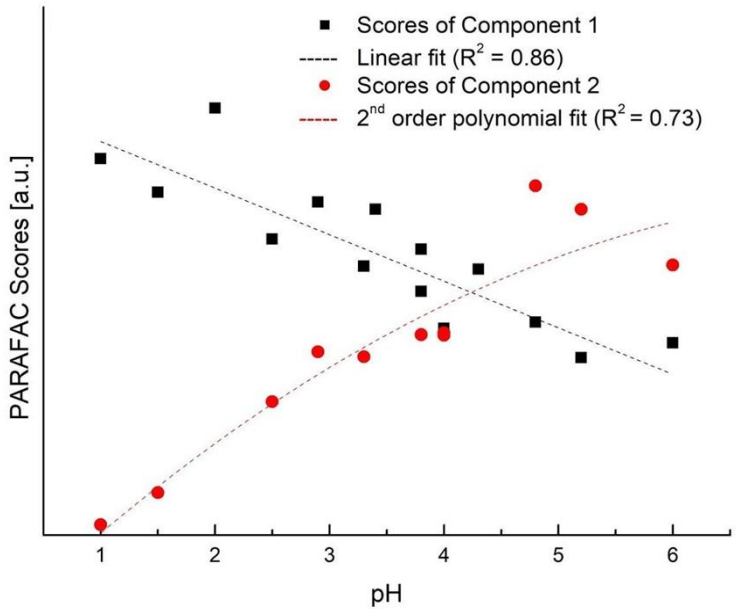


Figure 15: Scatter scores plot in function of the pH

Figure 15: Scores of the PARAFAC model with two components: component 1, that represented the neutral OTA and was fitted with a linear fit, and component 2, that represented the monoanionic OTA and was fitted by a second order polynomial fit. Image taken from [134] and adapted.

The point of intersection of these two fits represented the pK_{a1}. The value resulted by this method for the pK_{a1} was 4.2 and the associated fit uncertainty was 0.9.

In the range of pH 4.8– 8.3, the monoanionic and the dianionic forms of OTA were present. In particular, with the rise of the pH of the solutions, the decrease of the monoanionic form band (labelled with 1 in Figure 13) and the rise of a new band located at $\lambda_{Ex/Em}$ of 372/443 nm and attributable to the dianionic form (labelled with 3 in Figure 13) was observed, as shown in the maps of Figure 13 c and d. In this case, for the evaluation of the pK_{a2}, the use of PARAFAC model was not necessary. Indeed, both the forms of OTA had almost the same λ_{Em} but sufficiently distinguished λ_{Ex}. Thus, the excitation spectra at different pH were isolated from the EEMs at λ_{Em} of 446 nm and are reported, normalized and fitted, in Figure 16 a.

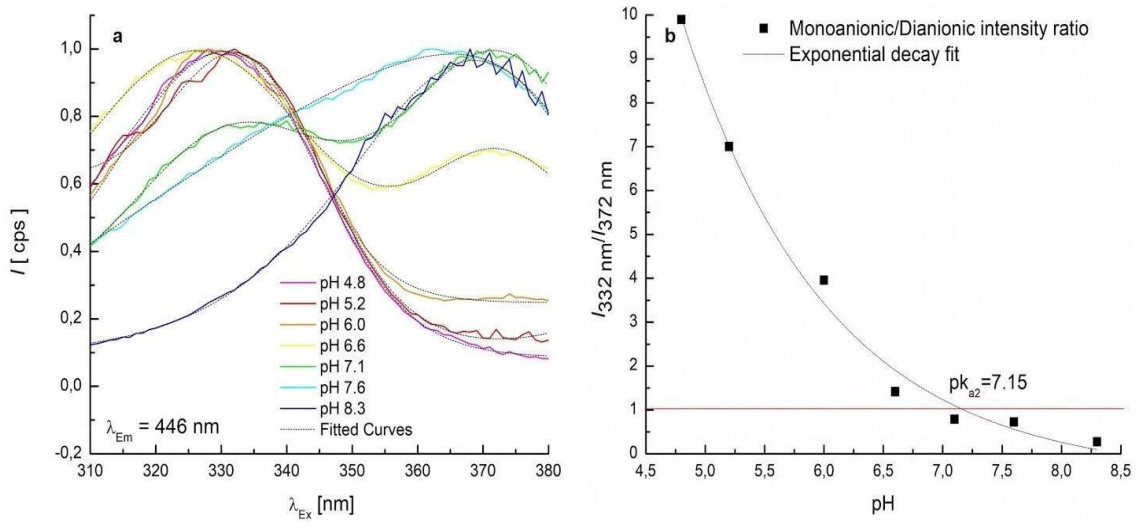


Figure 16: Experimental excitation spectra extrapolated from the EEMs and intensities ratio curve as a function of the pH

Figure 16: a) Normalized and fitted spectra isolated from the EEMs at different pH at λ_{Em} of 446 nm; b) Intensities ratio curve of the monoanionic and dianionic peaks (I_{332} and I_{372}, respectively) and evaluation of the pK_{a2}. Image taken from [134]

Two maxima of λ_{Ex} were observed: one at 332 nm due to the monoanionic form and another at 372 nm due to the dianionic form. However, from pH 6.6 to pH 7.1, the λ_{Ex} of monoanionic OTA was shifted towards higher wavelength, as appreciable in Figure 13 c and d. This phenomenon was attributable to a partial overlap of the monoanionic band with the band of the dianionic form at λ_{Em} of 446 nm. The deconvolutions of the two peaks in the spectra isolated from the EEMs at λ_{Em} of 446 nm are reported in Figure 17 a for pH 6.6 and in Figure 17 b for pH 7.1. They showed the correct position of the λ_{Ex} for both monoanionic and dianionic forms of OTA.

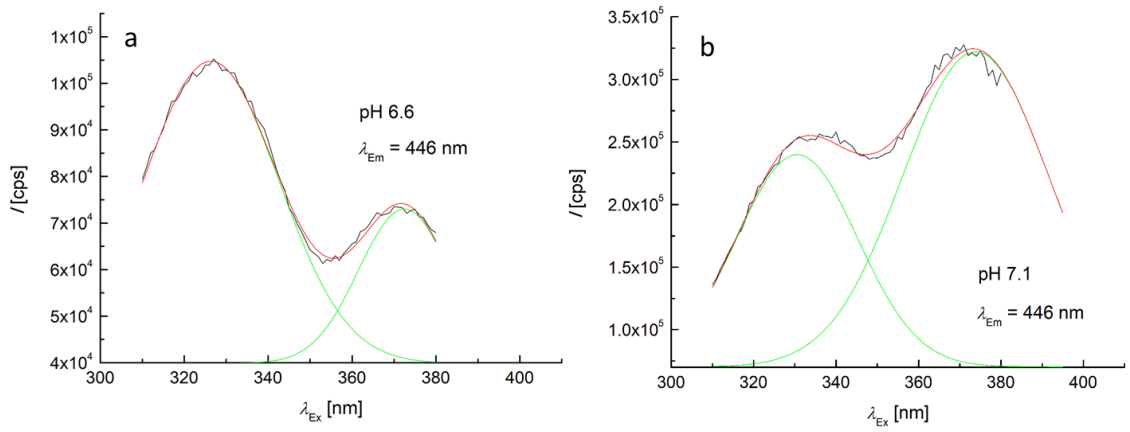


Figure 17: Deconvolutions of monoanionic and dianionic peaks in the excitation spectra

Figure 17: Spectra isolated from the EEMs at λ_{Em} of 446 of Figure 13 c and d. a) pH 6.6; b) pH 7.1. Image taken from [134] and adapted.

The intensities ratio of the monoanionic and dianionic peaks (I_{332} and I_{372}, respectively) of Figure 16 a was calculated for each pH. The experimental points obtained were fitted by an exponential decay function and the resulted curve is reported in Figure 16 b. The value at which this curve intersected the line positioned at $I_{332}/I_{372} = 1$, that is the point of inversion of the prevalence of one form on the other, corresponded to the pK_{a2}, as shown in Figure 16 b. However, the estimated value (7.15) was achieved with an ionic strength of 0.4 mol/l. In order to express the pK_{a2} at a value of ionic strength of 0.1 mol/l (as usually found in literature and also in agreement with the UV-Vis determination in this work), the extended Debye-Hückel equation [224] was applied. The resulted value of pK_{a2} was 7.0 and the fit uncertainty associated was 0.4.

The two values achieved by UV-Vis spectrophotometric titration and by fluorescence spectroscopy for pK_{a1} (4.4 and 4.2 respectively) and pK_{a2} (7.09 and 7.0 respectively) were consistent. From these values, the diagram of distribution as a function of the pH of the three forms of OTA was obtained (Figure 18).

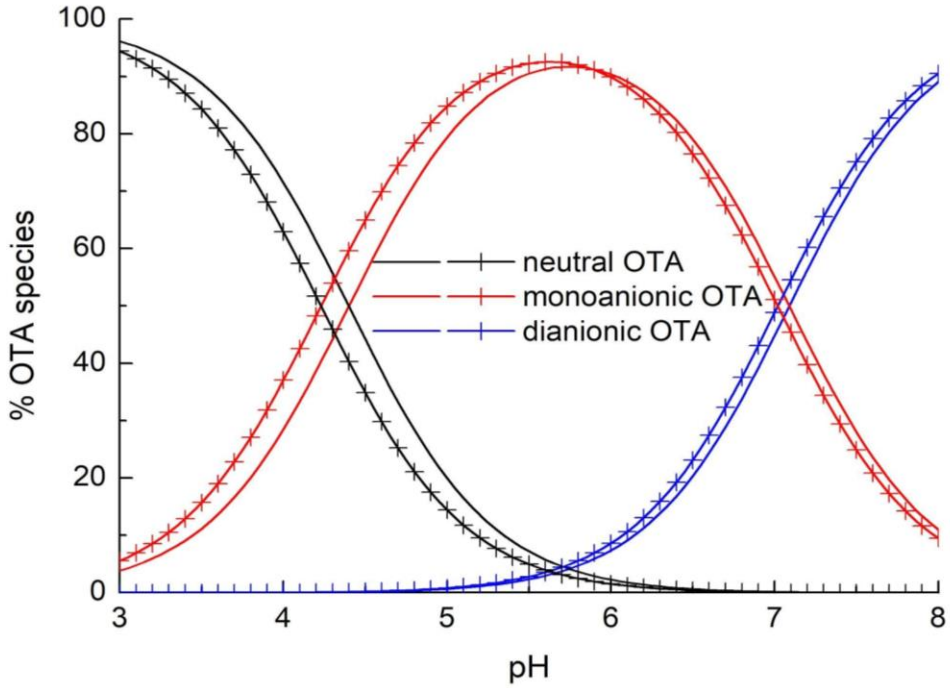


Figure 18: Diagram of percentage distribution of the three forms of OTA in function of the pH

Figure 18: Solid lines: distribution obtained from the elaboration of the UV-Vis spectrophotometric titration; lines with crosses: distribution obtained from the elaboration of the fluorescence spectroscopy. Black lines: neutral OTA; red lines: monoanionic OTA; blue lines: dianionic OTA. Image taken from [134] and adapted.

Degradation of OTA

To experimentally follow the degradation process of OTA, many fluorescence EEMs were collected of alkaline solutions freshly prepared and monitored over time. Four of them are reported in Figure 19. Unlike what happened in acid and neutral environments, under alkaline conditions the EEMs were rather noisy and therefore the bands were jagged and flickering.

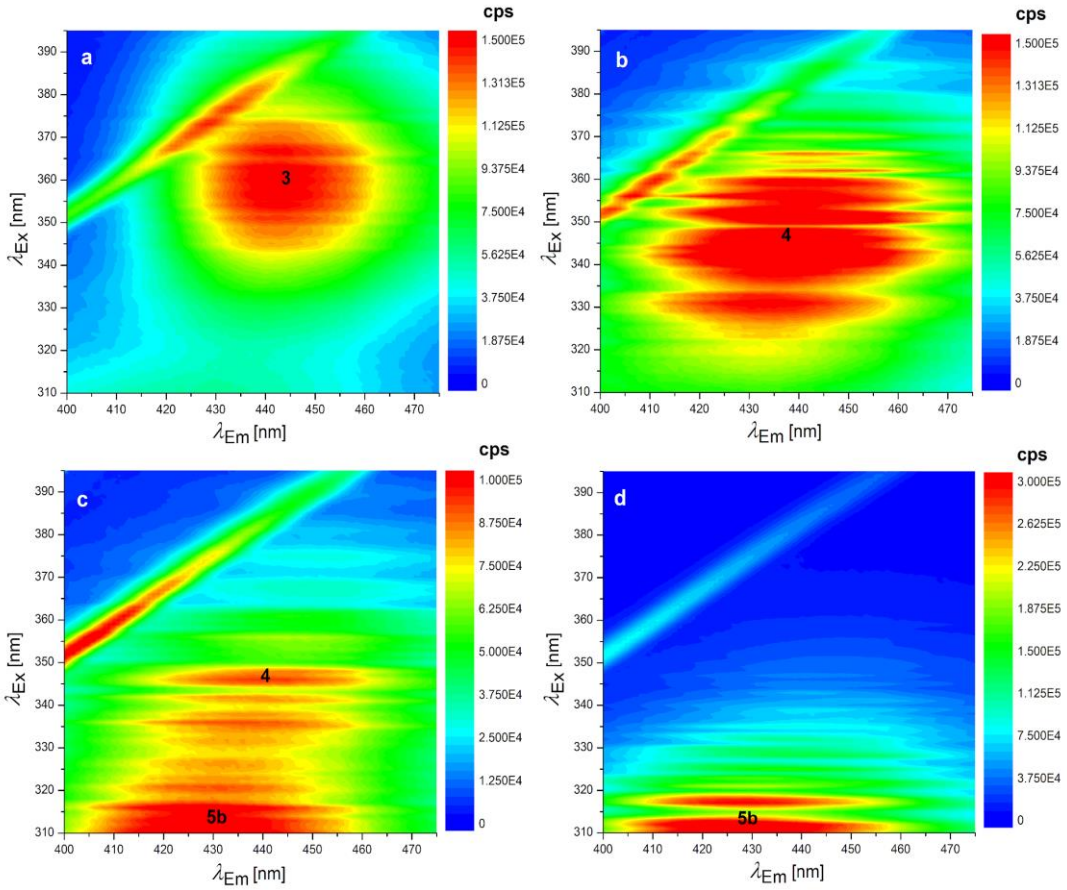


Figure 19: EEMs of OTA solutions and OTα solution under alkaline conditions

Figure 19: OTA solution with concentration of 50 µg/l: a) pH 11.6, fresh solution; b) pH 12.5, fresh solution; c) pH 12.5, solution at day 7. OTα solution with concentration of 50 µg/l: d) pH 12.5, fresh solution. The numbers reported on the bands corresponded to the molecular structures of OTA and OTα in the scheme of Figure 21. Image taken from [134]

In Figure 19 a, a freshly prepared solution of OTA at pH 11.6 was tested. A band positioned at $\lambda_{Ex/Em}$ of 365/443 nm and attributable to the dianionic form (labelled with 3 in Figure 19) was observed. An analogous OTA solution freshly prepared at pH 12.5 was analysed (Figure 19 b). In this case, a new very large band positioned at $\lambda_{Ex/Em}$ of 346/440 nm was observed and was attributable to a form of OTA with the lactone ring hydrolysed (labelled with 4 in Figure 19). This evidence was in agreement with the λ_{max} of 345 nm reported by Xiao et al. [139] and with the theoretical λ_{max} value for this molecule of 346 nm obtained in this work (molecule 4 in Figure 21) but in disagree with the λ_{max} of 385 nm stated by Bazin et al. [225]for pH ≥ 11. However, the band in the map was quite broad,

indicating that the OTA was still undergoing a degradation process. For this reason, this last solution of OTA at pH 12.5 was stored in fridge at 4 °C in dark condition and was monitored over the time. In Figure 19 c the EEM acquired after 7 days is reported. Here the band due to the form of OTA with the lactone ring hydrolysed was still present and a new band at $\lambda_{Ex/Em}$ of 313/430 nm appeared. The hypothesis was that this band was due to the OTα with the lactone ring hydrolysed (labelled with 5b in Figure 19). An EEM of a RM of OTα was acquired in the same experimental condition (Figure 19 d) and confirmed the assignment of this band. In this EEM, two separate bands appeared to be present. However, the tested solution was a RM whose label stated to contain only OTα. To evaluate if this output was simply due to an instrumental factor linked to the duration of the measurement, a fluorescence excitation spectrum of this material under the same alkaline condition was registered at a fixed λ_{Em} of 430 nm. The obtained spectrum is shown in Figure 20 and demonstrated that only OTα was present.

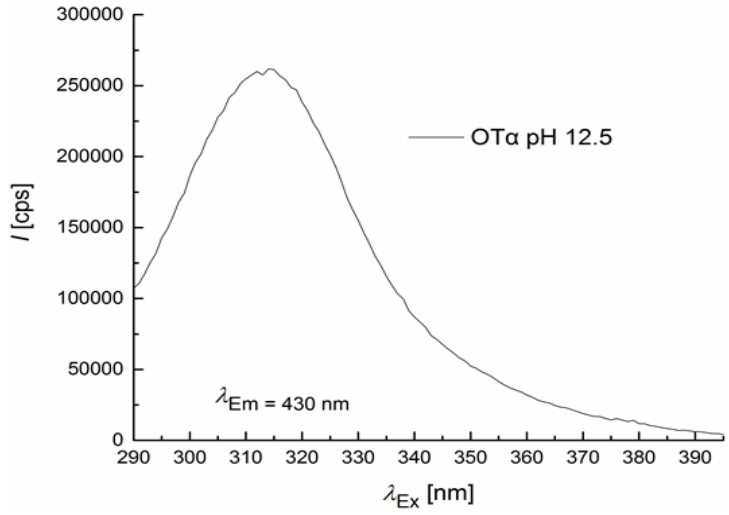


Figure 20: Fluorescence excitation spectrum of the RM of OTα under alkaline conditions

Figure 20: OTα solution with concentration of 50 µg/l freshly prepared at pH 12.5 solution. Spectrum acquired at fixed λ_{Em} of 430 nm. Image taken from [134]

Thus, under alkaline condition, OTα derived from the form of OTA with the lactone ring hydrolysed by the hydrolysis of the amide, as shown in Figure 21. This fragmentation led to two reaction products:

- the OTα with the lactone ring hydrolysed, which is less toxic than the precursor;
- the phenylalanine (labelled with 5a in Figure 21), which is an amino acid and consequently non-toxic. The band of phenylalanine should be positioned at $\lambda_{Ex/Em}$ of 258/284 nm [226] that was outside of the range of wavelength scanned in this work.

These experimental findings were flanked by theoretical calculations of the most probable degradation pathways for OTA under alkaline conditions. The calculations were performed with a DFT method at the Chemistry Department at the University of the Study of Turin by Prof. Andrea Maranzana and Prof. Glauco Tonachini of the Organic Group. The details of this part can be found in the article published [134].

Several reaction pathways were explored [134]. Among them, the most probable one is schematized in Figure 21. This pathway started from the monoanionic OTA (labelled with 1), passed through the dianionic OTA (labelled with 3) and conducted to the OTA with the lactone ring hydrolysed (labelled with 4). From the hydrolysis of the amide group of this molecule, two products were obtained: the phenylalanine (labelled with 5a) and the OTα with the lactone ring hydrolysed (labelled with 5b). This modelled pathway found confirmation in the experimental results already explained. Moreover, in the scheme of Figure 21 the theoretical wavelength of absorption/excitation of the different molecules which intervened in the process were also reported. These values were in agreement with experimental λ_{Ex} obtained from the above mentioned fluorescence EEEMs.

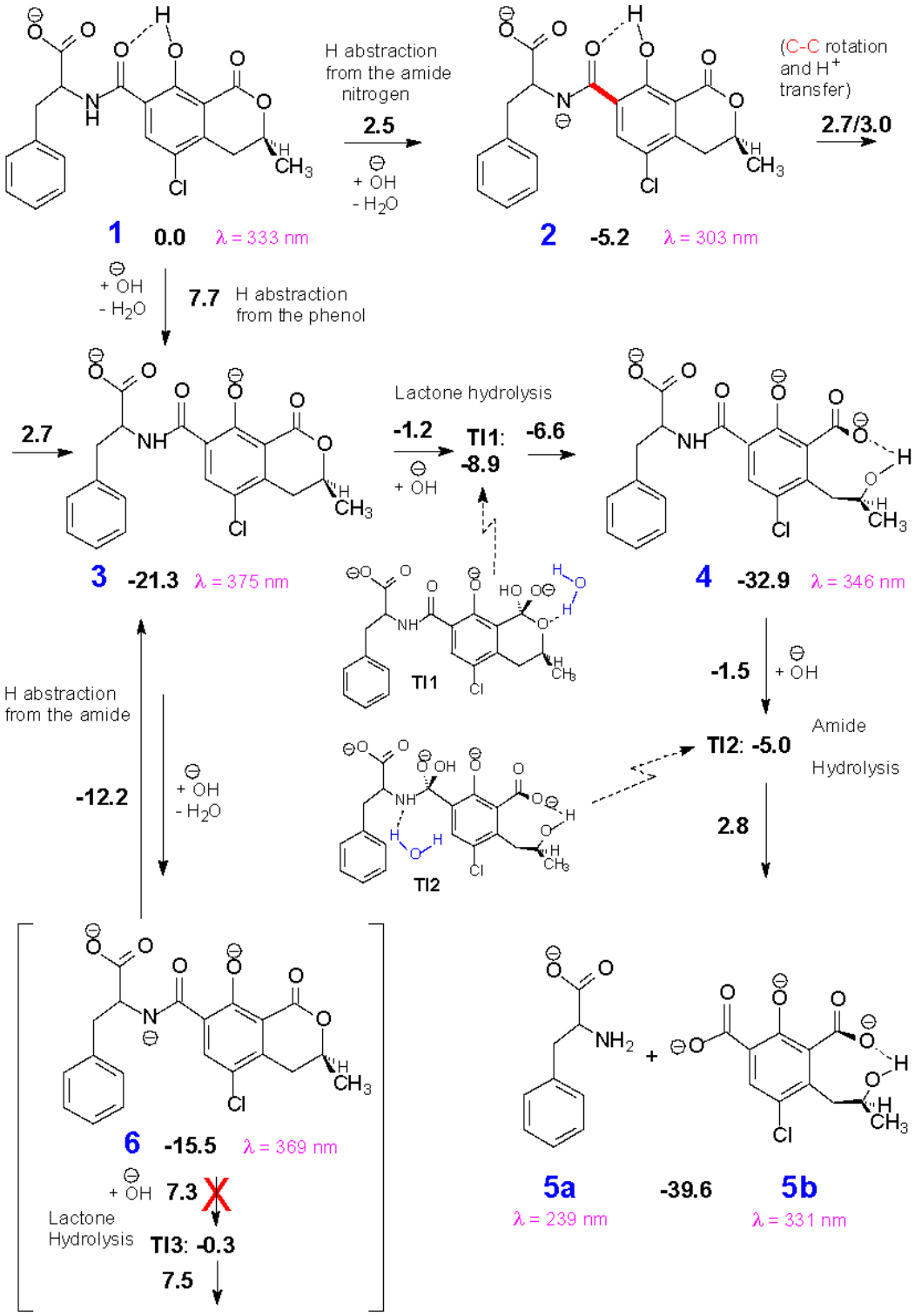


Figure 21: Theoretical most probable degradation pathway

Figure 21: DFT calculation of the most viable reactions occurred to OTA under alkaline conditions and which conducted to the generation of OTα and phenylalanine. The Gibbs free energies were reported in kcal/mol as differences compared to the monoanionic form of OTA labelled with 1. Image taken from [134]

Furthermore, in Figure 21, the OH^- molecules that intervened in the reactions were explicitly reported. Their concentration in the solutions had a key role in the whole process. The two last passages of the described pathway presented estimated energy barriers quite high and therefore the corresponding reactions happened slowly. This output was in agreement with the experimental evidences and, consistently, a relevant difference was noticed on the basis of the pH. Indeed, at pH 11.5 the reactions of degradation started after some days and evolved in a much slower way (many weeks) compared to pH 12.5 where the degradation started from day 1 and prosecuted faster.

Moreover, reversibility studies of this degradation process was performed. To do this, the solutions used for the EEMs of Figure 13 and Figure 19 were promptly acidified to pH 1.0 just after the measurement. The results achieved strongly depended on the molecules initially present in solutions. The solution at pH 7.1 of Figure 13 d, which contained both the monoanionic and the dianionic OTA, after acidification presented only the band related to the neutral form of Figure 13 a ($\lambda_{Ex/Em}$ of 332/458 nm). The OTA with the lactone ring hydrolysed of Figure 19 b was still brought back to neutral OTA when the pH became 1.0. The acidification of the solution containing OTα with the lactone ring hydrolysed of Figure 19 c, instead, did not conducted to the neutral OTA but led to neutral OTα, as shown in Figure 22. Indeed, after the fragmentation occurred, it was not possible to recreate OTA from the two degradation products. The band of neutral OTα of Figure 22 was positioned at $\lambda_{Ex/Em}$ of 333/443 nm. The same results were achieved by the theoretical calculation [134].

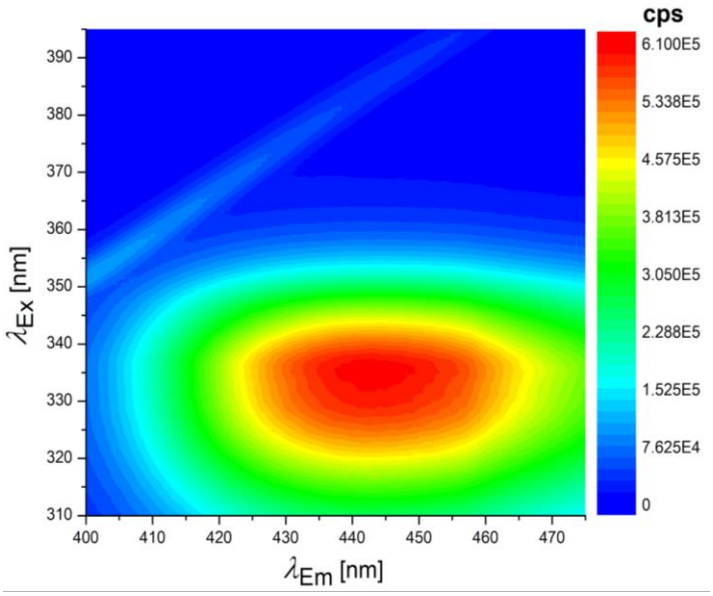


Figure 22: EEM of OTα solution at pH 1.0

Figure 22: OTα solution with concentration of 50 µg/l. The solution analysed was freshly prepared at pH 12.5 and then acidified at pH 1.0. Image taken from [134]

To summarize the most relevant passages of the degradation pathway and to highlight the reversible and irreversible steps, the Figure 23 was reported. Here, it was clearly shown by the red harrow that the reaction between OTA and OTA with the lactone ring hydrolysed was reversible and thus the toxicity of OTA was still harmful. The reaction of fragmentation of OTA with the lactone ring hydrolysed into phenylalanine and OTα with the lactone ring hydrolysed was responsible of OTA irreversible toxicity inactivation. The irreversibility was symbolized by the black arrow with the green cross and the less toxicity (OTα) or non-toxicity (phenylalanine) of the products by the green tick.

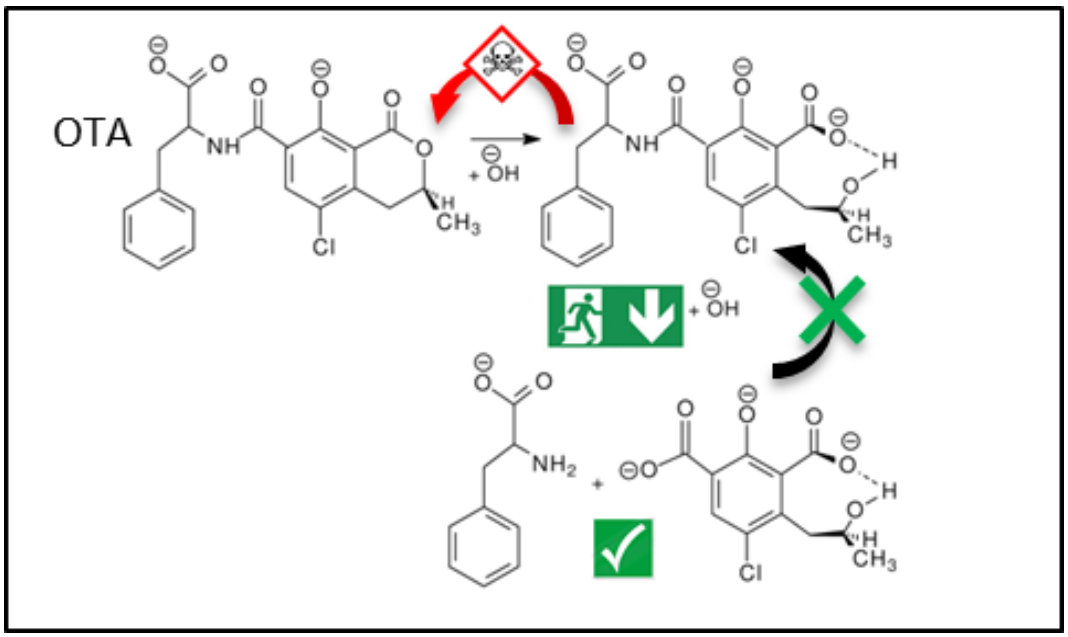


Figure 23: Scheme of the degradation pathway of OTA that lead to the inactivation of its toxicity

Figure 23: The most relevant passages of the degradation pathway of OTA. The red arrow indicates the reversibility of the reaction which re-conducts to toxic OTA. The black arrow with the green cross indicates that that reaction is irreversible. The final products are labelled with a green tick that represents their less toxicity (OTα) or non-toxicity (phenylalanine). Image taken from [134]

3.4.7 Conclusion and future perspectives

A wide range of pH (from 1 to 12.5) was investigated in order to provide a comprehensive description of the behaviour of OTA in aqueous solutions.

In solutions under acidic to neutral conditions, the two acid dissociation constants of the molecule were determined by two independent techniques: the UV-Vis spectrophotometry and the fluorescence spectroscopy. pK_{a1} involved the passage from the neutral to the monoanionic form of OTA and resulted 4.4 ± 0.1 and 4.2 ± 0.9, respectively. pK_{a2} involved the passage from the monoanionic to the dianionic form of OTA and resulted 7.09 ± 0.01 and 7.0 ± 0.4, respectively. These results achieved with different techniques were consistent.

In solution under alkaline conditions, the degradation of OTA was studied. To the best of my knowledge, this was the first work which reported its most probable degradation pathway both by experimental findings and theoretical

calculations. This pathway started from the monoanionic and dianionic forms of OTA, passed through a form of OTA with the lactone ring hydrolysed and conducted to the degradation product OTα with the lactone ring hydrolysed. These two latter molecules are less toxic compared to OTA [142]. However, special attention should be paid on the reversibility of the degradation pathway. Indeed, the reversibility studies under acidic conditions showed that the outcome depended from the molecules initially present in solution. Dianionic OTA and OTA with the lactone ring hydrolysed were able to return to neutral OTA if the pH of the solutions were quickly acidified. OTα with the lactone ring hydrolysed, instead, derived from the fragmentation of OTA and thus, in this case, the reaction was irreversible and acidifying the solution only OTα was achieved. However, the irreversible fragmentation of OTA in strongly alkaline conditions occurred after some days and can be considered completed only after more than one week. In the meantime, an effective inactivation of OTA toxicity was not achieved. As a consequence, the reversibility of the degradation pathway showed that higher attention of OTA handling should be paid.

This work lays the foundations for future toxicological studies relating to the various forms of the molecule. Moreover, the acquired knowledge on the behaviour of OTA in solution at different pH and on the degradation times may be useful for the development and future production of CRMs of OTA in different forms.

3.5 Feasibility study of OTA identification by Raman spectroscopy and label-free in liquid SERS method

3.5.1 Introduction to SERS for the determination of mycotoxins

In recent years, a growing number of SERS methods have been developed also for the detection of OTA [165], [167], [227]–[229] and multiple mycotoxins [230]–[233]. These methods can be summarized in three categories according to the sensing strategy adopted [231]:

- Label-free SERS detection, which allows low cost analysis, easy preparation of the substrates and the direct detection of the analytes. This most direct approach can be based on the use of colloidal suspensions of noble metals [234]–[236] or of substrate constituted by a surface of nanostructured metals [237], [238]. However, the label-

free SERS detection may suffer from insufficient sensitivity and reproducibility and from the possible interference of other substances present in the food matrix;

- SERS detection by metallic substrates modified with specific recognition elements, which help to refine the specific identification and quantification of target mycotoxins. These recognition elements can be classified into three main categories. The first are the SERS-based immunoassays [103], [239], [240] and the SERS immunosensors [233], that exploit antibody-antigen-antibody structures to perform sensitive and specific analyses of mycotoxins. The second are the SERS aptasensors, which exploit ligands consisting of single-stranded DNA, i.e. the aptamers, to create specific binding with target mycotoxins [167], [241]–[245]. The third are the SERS molecularly imprinted polymers (MIPs) sensors, which, thanks to the use of specific template molecules for their production, provide high affinity to the target mycotoxins [246], [247].
- SERS combined with other techniques to improve their performances and allow the determination of mycotoxins in complex food matrices. Even if the research in this field is of recent development, some examples of the methods exploited are here reported. The first are the separation techniques, such as the thin layer chromatography (TLC) [248] and the supported liquid membrane (SLM) extraction [228], which allow the pre-treatment and the purification of the samples before the analysis. The second example is the later flow immunoassay (LFIA) [249], which enables a simultaneous multiple detection of mycotoxins. The last example of method are the microfluidic systems or “lab on a chip”, that represent low cost, portable and disposable suitable tools for the analysis of mycotixins in food [229].

3.5.2 Scope of the work

In literature, only a few spectra of solid OTA are reported [165], [229]. Moreover, in these mentioned works the analysed spectral range is only partial and the attribution of the vibrational modes of just some peaks are explained. Indeed, in all the cases in which a biosensor is used for the detection of the analyte, the

peaks of interest are those of the free biosensor and of the biosensor binding with the analyte.

However, I was interested in getting a reference spectrum of pure OTA and in having a more detailed understanding of OTA peaks, also to be able to address SERS measures. For this reason, the first goal of this work was to obtain a reference spectrum of pure solid OTA, which represented the OTA fingerprint. An accurate attribution of the vibrational modes of the most relevant peaks in the spectrum was the second goal.

To the best of my knowledge, in literature only two papers report the identification and quantification of OTA with label-free AgNPs solid substrates by SERS [227], [228]. In the work of Kutsanedzie et al. [227], AgNPs were synthetized in a range of pH from 4 to 12 and those at pH 11 were selected and spotted on a silicon platform for the preparation of a solid substrate. This substrate was used for the SERS detection of OTA in cocoa beans with good performances and low limit of detection (LOD). In the work of Rostami et al. [228], Ag-capped silicon nanopillars were used as substrates for the detection of OTA in wine. A preliminary SLM extraction of OTA from the samples were performed. However, this method reached LOD in wine matrices two order of magnitude higher than the European legal limits [146] and thus it needed further improvements.

About SERS technique, in my thesis I was interested in the development of in liquid methods for fast, easy and portable *in situ* determination of analytes, as already mentioned in Section 2.7. To the best of my knowledge, no paper about a label-free in liquid SERS method for OTA quantification was available in literature. For this reason, I provided a feasibility study for the development of an in liquid label-free SERS method with AgNPs for OTA identification.

3.5.3 Chemicals

Ochratoxin A in solid form was purchase from Acros Organics and then diluted in acetonitrile (Sigma Aldrich) to obtain a standard solution of OTA at 1000 mg/l.

The used solutions and the AgNPs suspensions were prepared with ultra-pure water. The adopted reagents were at high purity level. The reagents used for the synthesis of AgNPs are described in Section 2.2.

Solutions of 5 g/l of tartaric acid — $C_4H_6O_6$ (Carlo Erba) was used as aggregating agent in SERS measurements.

3.5.4 Preparation of OTA samples for Raman measurements

The substrates used for the Raman measurements were of two types:

- A monocrystalline Si covered with 280 nm of SiO_2, which was bought from Si-Mat;
- The previous commercial Si/SiO_2 substrate coated by an adhesion layer of 5 nm of Ti (Alfa Aesar) and above a 90 nm Au (Alfa Aesar) plamonic layer, both deposited by sputtering [250].

Before the depositions of Ti and then of Au, both the substrates were accurately cleaned by sonication for 5 minutes in acetone and 5 minutes in ethanol and dried under hood by a flow of nitrogen.

On both the substrates, 3 µl of OTA solution at 1000 mg/l were deposited, covered by a glass coverslip (Carlo Erba) and left to air dry under the hood. The coverslip was used to limit the dispersion of this toxic substance during drying, handling and analysis of samples.

These two substrates were tested to obtain the Raman spectrum of solid OTA, as described in Section 3.5.9.

3.5.5 Synthesis and characterization of AgNPs colloidal suspensions

AgNPs were synthetized with nominal diameter of 4, 30 and 55 nm according to the procedures described in Section 2.3. The AgNPs of three dimensions were characterized with the methods reported in Section 2.4

3.5.6 Preparation of of OTA samples for SERS measurements

Several analytical conditions were tested to provide a feasibility study of OTA determination by a label-free in liquid SERS method. The best conditions were here reported.

The blank for the analysis was prepared in a microtube (from Eppendorf) according to the following procedure:

- 200 µl of 30 nm AgNPs colloidal suspension,

- 100 µl of acetonitrile,
- 5 seconds of vortex,
- 100 µl of tartaric acid,
- 10 seconds of vortex.

The mix for the analysis was prepared in microtube (from Eppendorf) according to the following procedure:

- 200 µl of 30 nm AgNPs colloidal suspension,
- 100 µl of OTA solution in acetonitrile at 1000 mg/l,
- 5 seconds of vortex,
- 100 µl of tartaric acid,
- 10 seconds of vortex.

The concentration of OTA in the mix was 250 mg/l.

After the preparations, both the liquid samples were transferred into a 96 well plates (from Sigma Aldrich) and analysed by SERS.

3.5.7 Raman spectroscopy

A DXR Raman spectrometer form Thermo Fischer Scientific was used to collect the solid OTA spectra. It was equipped with a 532 nm wavelength excitation laser source and with charge-coupled device (CCD) as detector. A calibration tool that is software-controlled was used weekly to calibrate the instrument. It provided the calibration of wavelength by multiple neon emission lines, of laser frequency by multiple polystyrene Raman peaks and of intensity of CCD by white light source. After optimization of the signals, the instrument set up was: objective 20x, laser power at 9 mW, 50 µm of pinhole aperture, spectral range of 200 – 3500 cm^{-1}, 1 s for 500 scans as acquisition time.

3.5.8 Label-free in liquid SERS method

The same DXR Raman spectrometer of Section 3.5.7 was used to collect SERS spectra. It was equipped with a 532 nm wavelength excitation laser source and with charge-coupled device (CCD) as a detector. The in liquid measurements were conducted in a quartz cuvette with the help of a specific accessory reported in Figure 24. This accessory was a holder with a parabolic mirror that collected the light that passed several times through the sample and reflected it back,

maximizing the collection and the illumination. It was positioned in the Raman spectrometer in place of the objective.

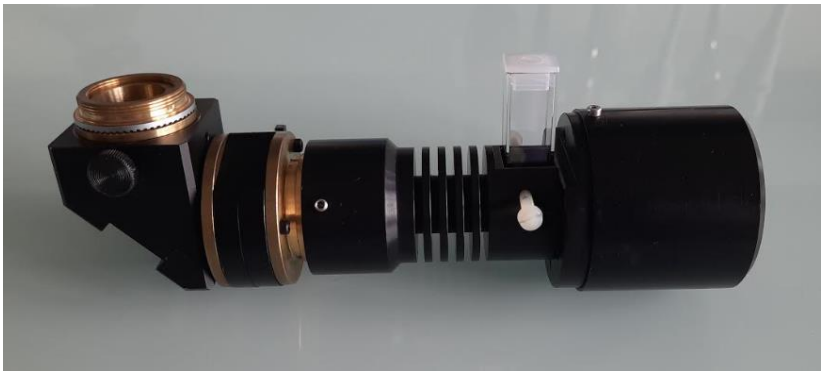


Figure 24: Raman accessory for in liquid measurements

Figure 24: The Raman accessory consisted in a holder with a parabolic mirror inside which a quartz cuvette was inserted

The instrument set up was: laser power at 10 mW, 50 μm of rectangular aperture, spectral range of 50 – 3500 cm^{-1}, 1 s for 50 exposures of acquisition time.

3.5.9 Results and discussion

Raman spectrum of solid OTA

The two substrates mentioned in Section 3.5.4 were tested to obtain the Raman spectrum of solid OTA. The intensity of the OTA spectra on the substrate covered by the Au layer resulted one order of magnitude higher than the intensity on the Si/SiO_2 substrate. Indeed, probably, the combination of the following factors favoured the use of the substrate with the gold surface:

- The Au layer was chemically inert and it had no SERS effect, as demonstrated in [250];
- The Au layer partially covered the bands related to Si, which could interfere with the OTA signals in the fingerprint region;
- For a question of hydrophilicity/hydrophobicity, the way the drop of OTA landed on the substrate was different. In particular, on the Au layer the OTA solution was distributed homogeneously, reaching the edges of the coverslips where it was determined. On the other hand, on Si/SiO_2

substrate the drop of OTA solution remained more concentrated in the center and formed lumps under the coverslip, making it difficult to analyse.

For these reasons, the substrate with the Au layer was selected to acquire the Raman spectrum of solid OTA taken as a reference that is reported in Figure 25.

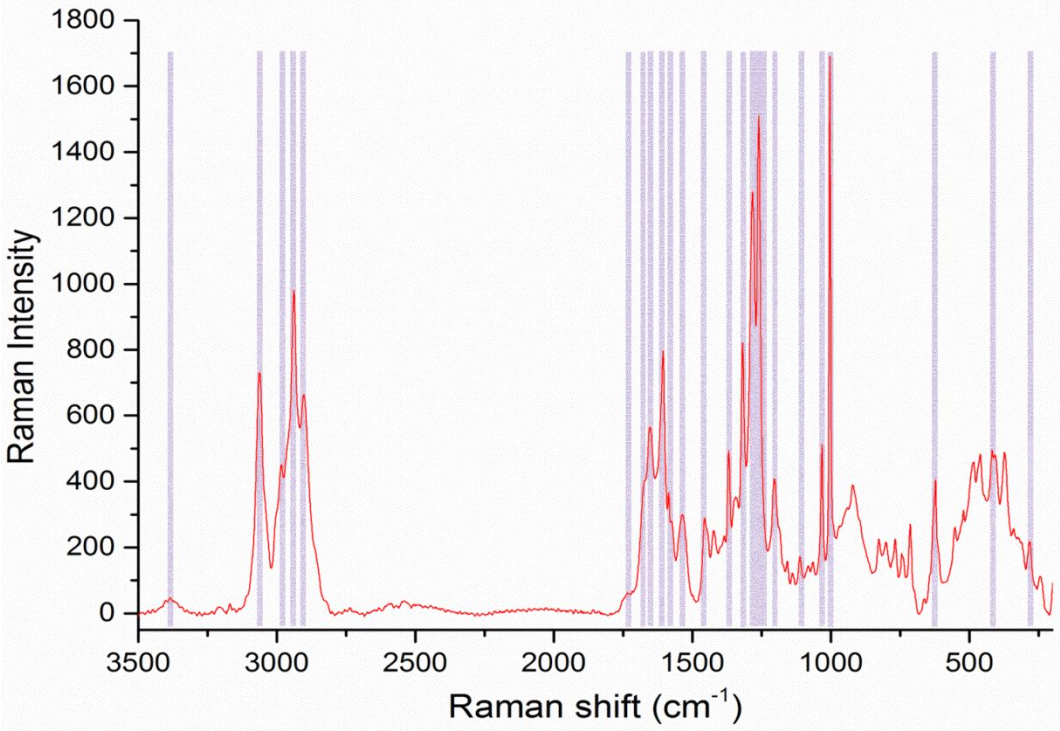


Figure 25: Raman spectrum of solid OTA on a substrate

Figure 25: Raman spectrum of solid OTA acquired after evaporation of the solvent on a Si/SiO_2 substrate coated by an adhesion layer of 5 nm of Ti and above a 90 nm Au plasmonic layer

The spectrum of Figure 25 presented several peaks. To provide the attribution of most of these, I have carried out extensive research in literature. To better understand which parts of the OTA molecule were involved in the vibrational modes, it was useful to consider the functional groups and the molecules contained in the structure of the OTA. The subdivision of OTA into the principal smaller molecules is reported in Figure 26 where different colours were used to border them. In particular, the phenylalanine was highlighted in violet, the secondary amide in green, the salycilamide in orange and the lactone in blue.

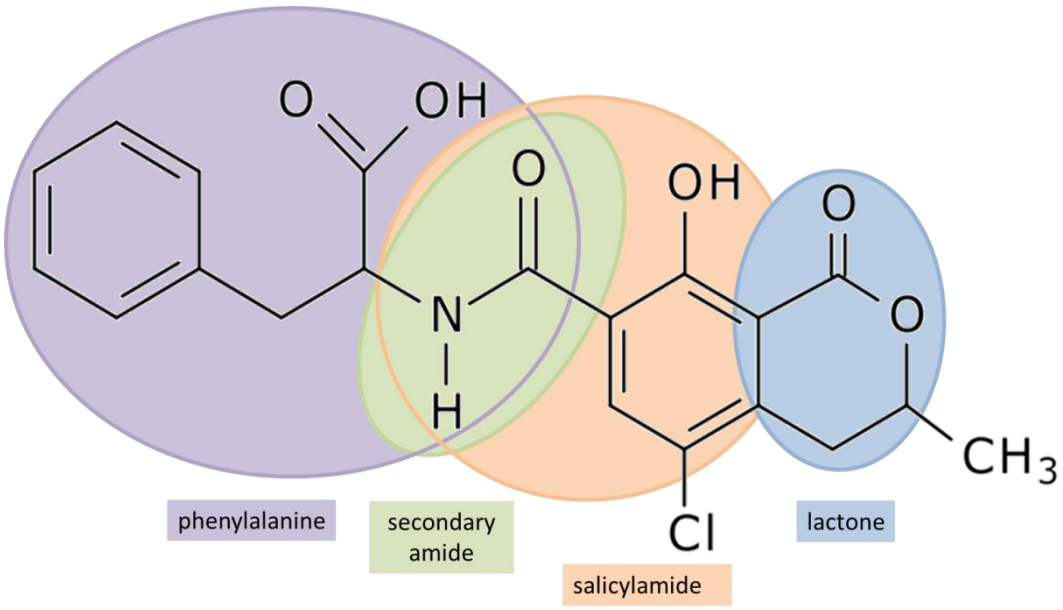


Figure 26: Subdivision of OTA into smaller molecules

Figure 26: Molecules contained in the OTA structure: phenylalanine in violet, secondary amide in green, salicylamide in orange and lactone in blue.

In Table 6, the vibrational modes attributed to the peaks of solid OTA highlighted in grey in Figure 25 are reported. To confirm the following attributions and to differentiate the Raman modes of the various forms of OTA, a DFT simulation could be useful.

Table 6: Attribution of solid OTA peaks in Raman spectrum. The main peaks are highlighted with colours

Raman shift [cm^{-1}]	**Vibrational mode**	**Reference**
3384	Stretching N-H amide (halogenated salicylamide)	[251]
3062	Stretching C-H of aromatic ring	[252]
2984	Stretching asym CH_3 (EtOH)	[253]
2938	Stretching sym CH_3 (EtOH)	[253]
2902	Stretching sym CH_2 (EtOH)	[253]
1717	Stretching COOH	[251]
1673	Stretching carbonyl of lactone	[229]
1653	Amide	[229], [251]
1606	Aromatic breathing mode	[251]
1586	Phenyl ring bond – stretching vibrations (phenylalanine)	[254]
1535	Amide	[133], [229], [251]
1456	CH_2 bonds scissor vibration	[252]
1369	Lactone ring	[255]
1318	Stretching aromatic ring	[229]
1283	Secondary amide (doublet)	[165]

1261	Secondary amide (doublet)	[165]
1205	Stretching C-C benzene and C-CH_2 side chain (phenylalanine)	[254]
1112	Aromatic C-H deformation of phenol	[252]
1032	Stretching C-Cl	[229]
1003	Deformation of aromatic ring / Phenyl ring angular bending vibrations (phenylalanine)	[228], [229], [254]
622	Monosubstituted benzene in plane ring deformation / phenyl ring angular breathing vibrations (phenylalanine)	[252], [254]
418	In plane bending vibration of aromatic C-OH bond	[252]
283	C-Cl deformation	[252]

Among these peaks, four were pointed out with colours in Table 6. They were:

- The aromatic breathing mode at 1606 cm^{-1};
- The stretching of C-Cl at 1032 cm^{-1};
- The deformation of aromatic ring also named the phenyl ring angular bending vibrations, which is related to the phenylalanine portion, at 1003 cm^{-1};
- The monosubstituted benzene in plane ring deformation also named phenyl ring angular breathing vibrations, which is related to the phenylalanine portion, at 622 cm^{-1}.

Although some other peaks were intense, these selected peaks can be considered as the most useful for OTA identification. They are highlighted in

Figure 27 with the same colours of the Table 6. Indeed, as reported later about the explored label-free in liquid SERS method, in some region of the spectral range the signals related to OTA were not visible.

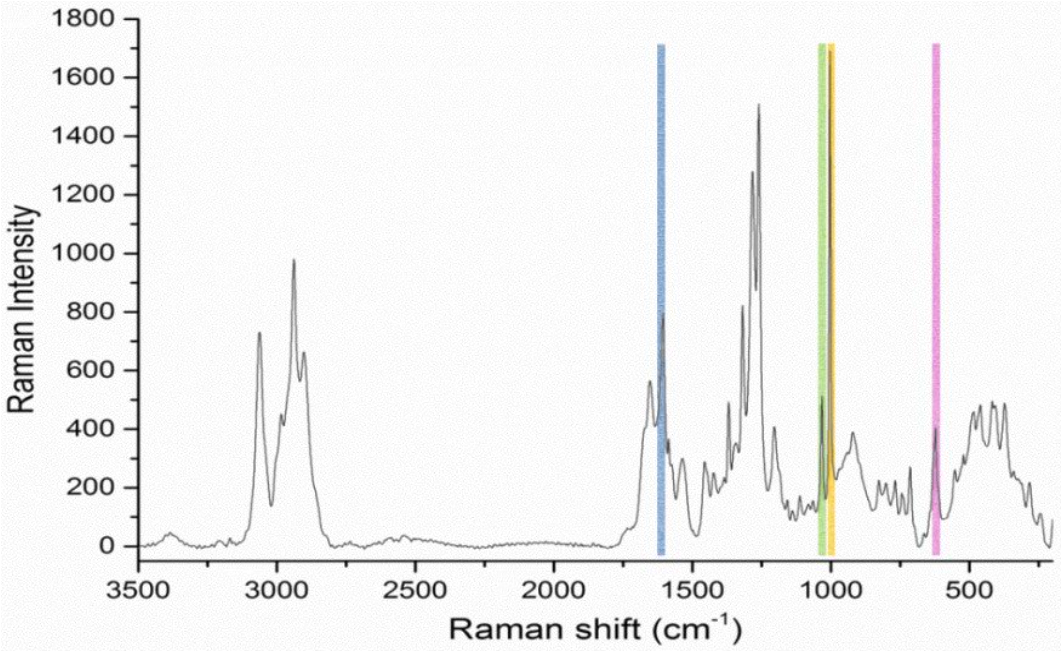


Figure 27: Principal peaks of solid OTA in the Raman spectrum

Figure 27: Blue band: at 1606 cm^{-1}, the aromatic breathing mode; green band: at 1032 cm^{-1}, the stretching of C-Cl; orange band: at 1003 cm^{-1}, the deformation of aromatic ring also named the phenyl ring angular bending vibrations, pink band: at 622 cm^{-1}, the monosubstituted benzene in plane ring deformation also named phenyl ring angular breathing vibrations.

This work was necessary to obtain a satisfactory reference spectrum of OTA and to identify the principal peaks. However, the main issue of solid OTA was its toxicity. In fact, obtaining and handling these samples was very dangerous if I did not take in consideration specific precautions.

Feasibility study of a label-free in liquid SERS method with AgNPs colloids for OTA identification

The aim of this part of the work was to provide a feasibility study of a label-free in liquid SERS method for the identification of OTA with AgNPs colloids.

The different tested experimental conditions were:

- 3 sizes of AgNPs (4, 30 and 55 nm);
- Level of concentration of AgNPs: as they are, 2 fold, 5 fold and 10 fold concentrated;
- Absence (water) or adoption (tartaric acid or sodium sulfate) of aggregating agents. This aspect also reflected on the pH of the solution (acid for tartaric acid, slightly acid for water, slightly basic for sodium sulfate);
- Order of addition of the reagents in the procedure for the mixes preparation;
- Range of OTA concentration from thousands of mg/l to μg/l.

The first experiments were conducted with analytical mixes containing OTA with a concentration of 250 mg/l.

About the nanoparticles, the different sizes of AgNPs that I produced (Chapter 2) were tested in the above mentioned experimental conditions. With 4 nm AgNPs, no peaks related to OTA were observed. With 55 nm AgNPs, some peaks attributable to OTA were present and, in particular, these peaks were visible when the 2 fold concentrated 55 nm AgNPs was used. However, with concentrated NPs, a considerable portion of the spectral range of blank subtracted spectra presented negative bands, especially when aggregating agents were used. These negative bands were due to the differences in the agglomeration of the AgNPs between the blank and the sample. Since the negative bands influenced the peaks in their proximity, the use of concentrated AgNPs was avoided. The best size of AgNPs resulted to be the 30 nm. In this case, the four principal peaks of OTA were observed. Thus, the size of 30 nm AgNPs, as they are, was selected.

Regarding the pH, in their publication [227], Kutsanedzie et al. used AgNPs synthetized at pH 11 to create a solid substrate. However, in my case, I worked in liquid and therefore the pH of the colloidal suspension had a great impact on the mix of analysis. As explained in Section 3.4.6, at pH 11 OTA was mostly present in the form with the lactone ring hydrolysed and the degradation process was still ongoing. Even if the process of degradation was quite long, the solution at this alkaline pH was instable. For these reasons, I did not test this extreme condition of work. A slightly basic solution was achieved with the adoption of sodium sulfate as aggregating agent. However, no appreciable improvement of the SERS signals

was obtained, thus leading to the exclusion of this type of aggregating agent. Working in water (slightly acid pH), an insufficient agglomeration of AgNPs occurred and no OTA peaks were detected. Instead, the use of tartaric acid as an agglomerating agent (acid pH) proved to be a good solution to enhance the SERS signals of OTA, as already demonstrated in the case of sulfur dioxide (Section 4.5.9) [47]. Furthermore, under acidic conditions, OTA was stable in solution. For these reasons, the tartaric acid was used in the analysis.

The order with which the reagents were added to create the mix was also investigated. The chosen sequence involved first inserting the AgNPs and the OTA and vortexing, in order to promote the interaction between the substrate and the analyte. Only then, tartaric acid was added to stress the agglomeration of the nanoparticles.

Lastly, different concentrations of OTA were tested. The drawback I found in this case was to go down in concentration up to the legal limit of OTA in the real matrices. Indeed, I was unable to obtain SERS spectra at OTA concentrations below 250 mg/l.

From all these experiments, the best analytical conditions resulted to be: use of 30 nm AgNPs as they are, addition of tartaric acid as an aggregating agent and concentration of OTA of 250 mg/l. In Figure 28, the SERS spectrum of OTA achieved by this label-free in liquid SERS method is reported. Even if not all peaks have been assigned, many of the peaks of Figure 28 were the same listed in Table 6, especially in the range 1000 – 1600 cm^{-1}. Moreover, as can be noticed, the principal peaks found in the above mentioned Raman spectrum of solid OTA were observed also in this SERS spectrum, showing the potentiality of this method. In Figure 28 they were highlighted with the same colours of Figure 27 and Table 6.

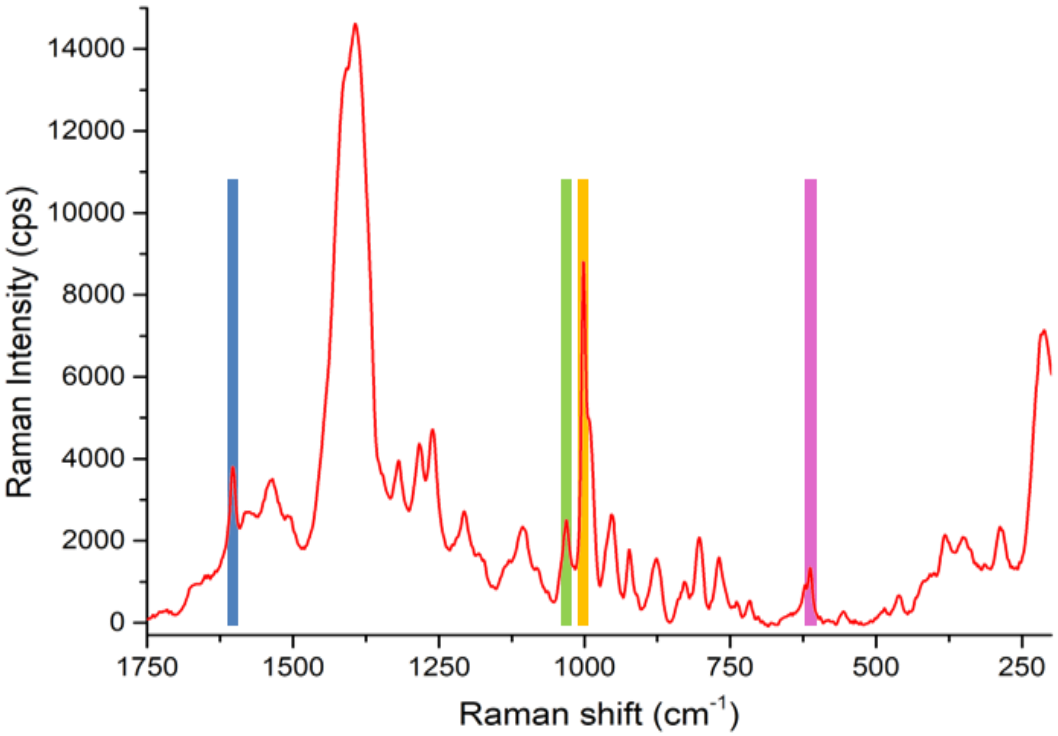


Figure 28: Spectrum of OTA by label-free in liquid SERS method

Figure 28: This spectrum is blank subtracted. Sample mix: 30 nm AgNPs, OTA 250 mg/l and tartaric acid as an aggregating agent. Blue band: at 1606 cm^{-1}, the aromatic breathing mode; green band: at 1032 cm^{-1}, the stretching of C-Cl; orange band: at 1003 cm^{-1}, the deformation of aromatic ring also named the phenyl ring angular bending vibrations, pink band: at 622 cm^{-1}, the monosubstituted benzene in plane ring deformation also named phenyl ring angular breathing vibrations.

The spectrum of Figure 28 was blank subtracted, where the blank sample was constituted by AgNPs, tartaric acid and acetonitrile in the same ratio of the OTA sample. Nevertheless, the peaks of OTA in the spectral region around 1400 cm^{-1} were covered by a very intense and broad band. Indeed, this band was very high in the blank spectrum and, despite the subtraction, it remained intense in the SERS spectrum of the OTA sample. This band was probably attributable to the modes of CO stretching combined with OH deformation of the citrates on the AgNPs surface, as explained in Section 4.5.9. This interference of the citrates, derived from the method of synthesis adopted (Section 2.3), was already discovered in my study of the in liquid SERS method for the determination of sulfur dioxide [47]. Thus, the peaks of OTA that were positioned in this same

spectral range cannot be considered for its identification by this label-free in liquid SERS method.

3.5.10 Conclusion and future perspectives

Despite the high toxicity of solid OTA, a reference Raman spectrum of the molecule on a substrate was achieved. The assignment of the vibrational modes for most of the peaks was performed. This allowed to identify the most characteristic peaks of OTA, which are those at 1606, 1032, 1003 and 622 cm^{-1}. This work was useful for all Raman and SERS studies involving the direct identification of OTA. An interesting future perspective could be represented by DFT simulation of Raman spectra of OTA in order to assign the vibrational modes of its different forms. It could be very useful for dedicated pH-related Raman and SERS studies.

Moreover, a feasibility study of OTA identification by in a label-free in liquid SERS method was performed. Several analytical conditions were tested and the 30 nm AgNPs with tartaric acid as an aggregating agent was selected. A OTA concentration of 250 mg/l was analysed. The SERS spectrum showed the same principal peaks identified in the Raman spectrum of solid OTA. This work can be considered as a proof of concept study and can represent a first approach to the development of this label-free in liquid SERS method. Certainly, its sensitivity still had to be greatly improved. Indeed, at the moment, I was not able to provide the detection of OTA in a range of concentration close to the legal limits in foodstuffs. In general, I can summarize that I consider rather difficult to optimize the in liquid SERS method maintaining its characteristic of being extremely simple, fast and without pretreatment of the sample.

Although this method needed to be greatly improved in order to be of applicative interest, the obtained information could be useful for future studies on the subject.

3.6 Abroad experience: Skills Broadening Secondment on OTA

3.6.1 Introduction

The Bureau International des Poids et Mesures (BIPM) in 2016 started the project of Capability Building and Knowledge Transfer (CBKT): Metrology for Safe Food and Feed – Mycotoxins [256].

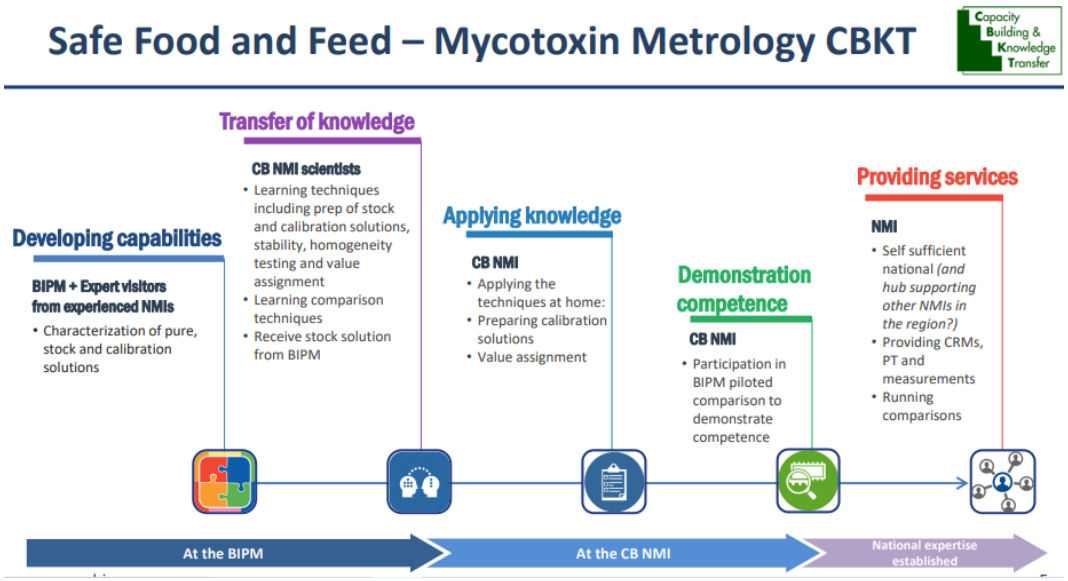


Figure 29: The Mycotoxin Metrology CBKT project of the BIPM
Figure 29: Description of the steps of the programme. Image taken from [257], [258]

As described in Figure 29 [257], [258], this project involved the National Metrology Institutes (NMIs) with the aim of improve the metrological capabilities on mycotoxins. Thanks to the collaboration between the scientists from different institutes, a greater spread of knowledge and a shared growth of skills on this topic were achieved. The final goals were the characterization of samples constituted of pure mycotoxins, the achievement of calibrants for mycotoxins and materials for proficiency tests and the production of reference materials or certified reference materials (CRM) of mycotoxins [259].

3.6.2 Skills Broadening Secondment on OTA at NRC - Canada

During the course of my PhD, I had the opportunity to take part of one of these projects. Indeed, I was selected for a Skills Broadening Secondment, as part of the BIPM's Mycotoxin Metrology Capacity Building and Knowledge Transfer (CBKT) Programme. The Secondment was focused on culturing, isolation, and purification of ochratoxin A for reference material production, along with the metrological characterization of the material. It was hosted by the National Research Council (NRC) of Canada in Ottawa, Canada, where I was received as volunteer visitor. There I worked in the group of Organic Chemical Metrology headed by Dr Jeremy E. Melanson and I was trained by Dr Adilah Bahadoor. My period of work on the project was supposed to last six months. However, due to the pandemic, the project was temporarily interrupted and my return had to be brought forward.

3.6.3 Results

In this Section the purpose of the project is reported without details. This choice is due to the fact that the work was suddenly interrupted by the pandemic and it has not yet been completed. Furthermore, as the intellectual property of the project belongs to Canadian researchers, I am not authorized to disclose sensitive data.

I completed the work on the culturing and isolation of ochratoxin A for subsequent reference material production, developing my expertise on fundamental techniques in fungal cultures to produce mycotoxins. Furthermore, for the first time, I learned how to handle biological material and experimented with the procedures for working in a sterilized environment under a laminar flow hood. Before and after each of the steps that I will illustrate, it was in fact necessary to sterilize the glassware in an autoclave and clean the hood. Furthermore, it was necessary to provide to the correct disposal of biologically contaminated waste.

The inoculation process started by filling Erlenmeyer flasks with a specific amount of wheat kernels bought from a local market. Each of the flasks were inoculated with a fresh *Penicillium verrucosum* culture. The flasks were capped and stored in the dark at fixed temperature in an incubator for the whole period of the wheat inoculation. The maintenance of the optimal humidity conditions for the spores was carried out by introducing water periodically into the flasks. The scheduling of the water additions and the right quantity were previously

established. Thus, during the wheat inoculation time, all the flasks were repeatedly subjected to the following treatment: opening under hood, water addition, turning of wheat kernels, re-cap and positioning in the incubator. In Figure 30 was reported the evolution of the kernels fermentation during the wheat inoculation time.

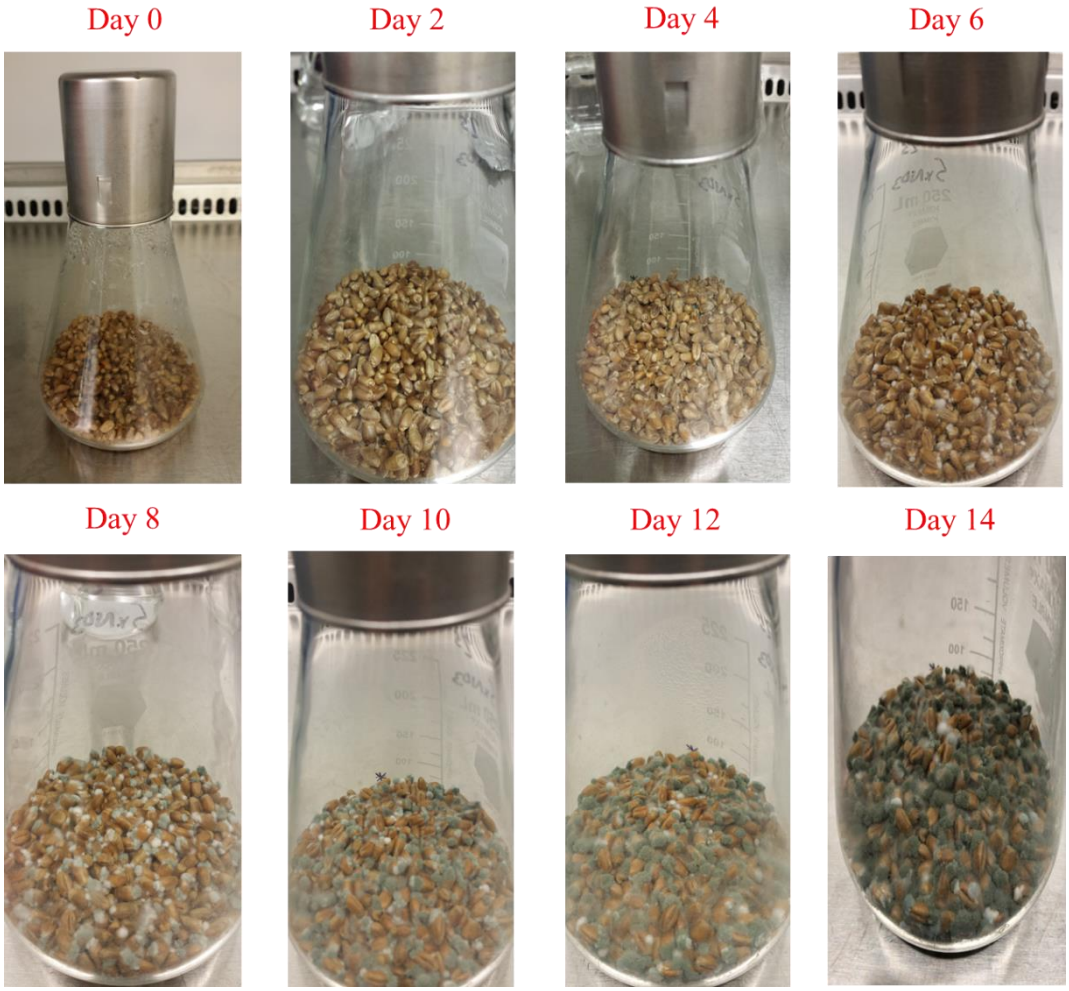


Figure 30: Wheat inoculation

Figure 30: Pictures of the wheat inoculation over the 14 days in the incubator

The duration of the wheat fermentation process was previously optimized. The fourteenth day was selected as the best compromise between the highest OTA concentration and the lowest interfering molecules formation. For monitoring the concentration of OTA during rounds of culturing, liquid chromatography – high resolution mass spectrometry (LC-HRMS) was employed.

As shown in Figure 31, one of the flask was dedicated to the blank sample. It was prepared following the same protocol of the other flasks and was subjected to the same procedural steps without the agar plug. The blank sample was used as a check. Indeed, the flask with the blank was handled at the end of each inoculation treatment. If no spores spread during the treatments under hood the blank sample remained uncontaminated by OTA. Another result of obtaining an uncontaminated blank sample was that no other source of OTA interfered in this mycotoxin production.

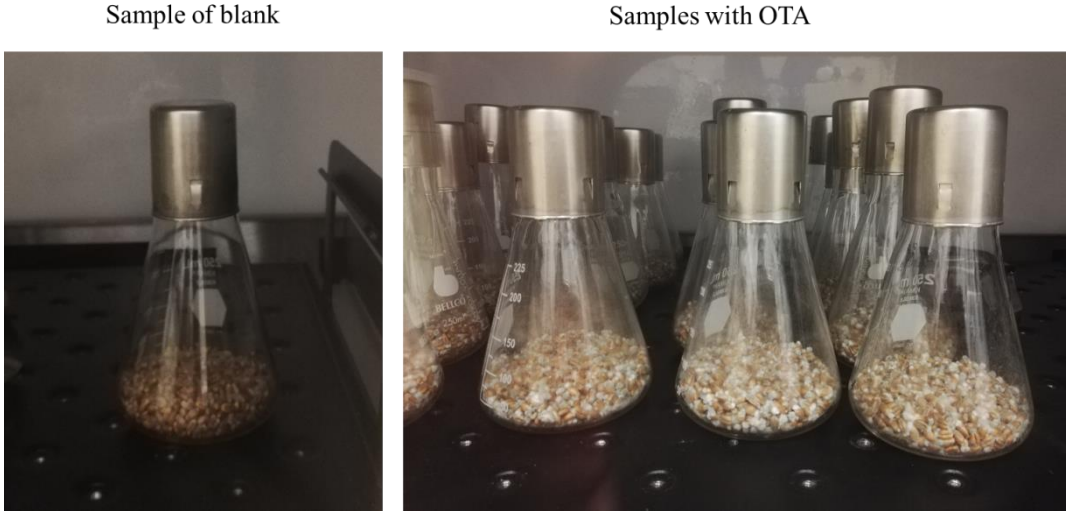


Figure 31: Pictures of the flasks in the incubator

Figure 31: On the left: flask with the blank sample; on the right: flasks contaminated by OTA

After the period of wheat inoculation, as third step, the samples were harvested and purified [260]. The OTA harvesting procedure involved the preparation of the extraction solvent and the extraction of the content of the flasks with an optimized protocol. At the end of this extraction phase, the liquid wheat extracts were capped and stored in fridge. The entire harvesting procedure was carried out keeping the OTA contaminated samples separate from the blank sample. In Figure 32 are reported the sample of blank and one of the flask with the sample contaminated by OTA on day 14 with their relative wheat extracts. The wheat extracts had different colours: yellow for the blank sample and orange for the sample with OTA. This showed that the blank sample was not appreciably contaminated by OTA.

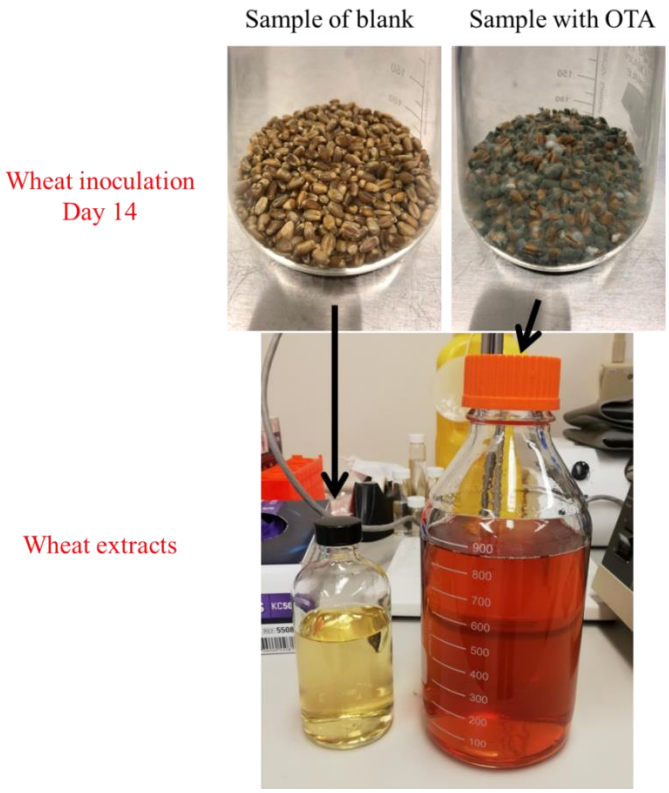


Figure 32: Wheat inoculation and wheat extracts

Figure 32: Pictures of the sample of blank and of the one sample contaminated with OTA on day 14 of wheat inoculation and relative wheat extracts

At this point, the extracts were subjected to liquid-liquid extraction and successively to evaporation to dryness.

The described whole process of OTA production was repeated three times. The aim was to obtain around 2 g of solid OTA from this large scale production.

The evaluation of the impurity and the purification of OTA had to be performed with LC-HRMS. For a fine characterization of the molecule [251] and the purity assignment, quantitative nuclear magnetic resonance (qNMR) spectroscopy was planned, as already done for the other mycotoxins [261]. I started practice on NMR performance tests, such as temperature calibration test, line shape test and sensitivity test, which was indispensable for the evaluation of the correct machine operating. Unfortunately, the training was cut short due to the pandemic.

At the end of the entire project, it was expected to have high purity OTA.

3.6.4 Conclusion

In conclusion, during the PhD, I was selected for a Skills Broadening Secondment on OTA at NRC – Canada lasting six months. I took part actively in the culturing and isolation of OTA from wheat kernels fermentation, learning the fundamental techniques of manipulation of biological materials and, in particular, of fungal cultures. Furthermore, I started training with the analytical techniques planned for the project, that were LC-MS and NMR.

Due to pandemic, the project was temporarily interrupted and I could not continue it. Currently the project has restarted and is still in progress.

Chapter 4

Sulfur dioxide (SO_2)

4.1 Introduction to sulfites

Sulfites are worldwide employed in the food and beverage sector [262]. They can be found as additives in a large variety of food commodities: meat products, seafood, shrimps and other crustaceans, preserved vegetables, fruit juices, jams, jellies, died fruits, wine, wines vinegars, beers and many others [263], [264]. Sulfites can be added to foods as sulfiting agents in various forms: such as sulfur dioxide (E220), sodium sulphite (E221), sodium or potassium metabisulfite (E223 and E224, respectively), etc. In water solutions, sulfites can be present in different forms which are pH dependent, as reported in the diagram of Figure 33.

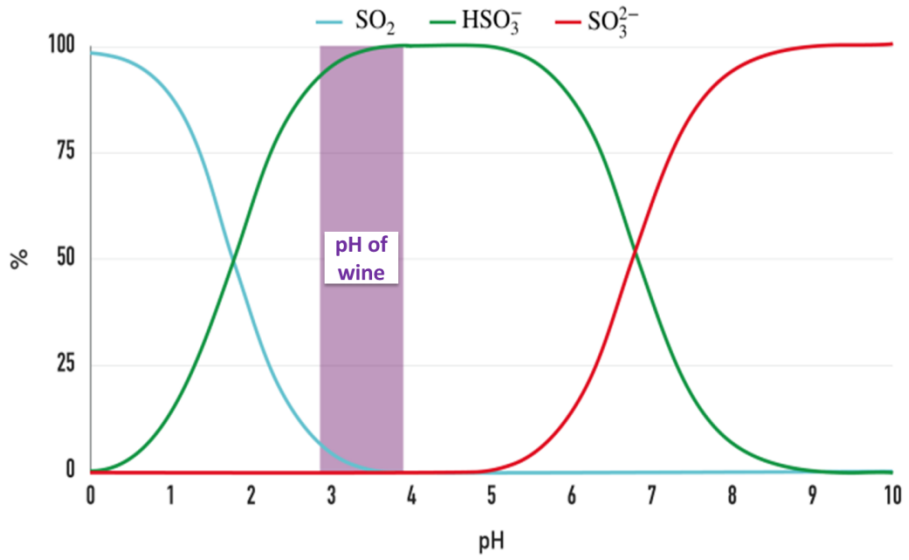


Figure 33: Percentage distribution of sulphites forms

Figure 33: Percentage distribution of the forms of sulphites in an aqueous solution from pH 0 to pH 10 (where pK_{a1} = 1.81 and pK_{a2} = 6.91). Image taken and adapted from [262]

In food, sulfites carry out two prominent activities which contributed to increase the shelf life of food products. Indeed, they are:

- broad-spectrum antimicrobial agents, in particular in sulfur dioxide molecular form (SO_2). This role is useful for curtail the proliferation of yeast and bacteria, which are responsible of the foodstuffs contamination [262],
- antioxidant agents, especially in the bisulfite form (HSO_3^-). This property inhibits reactions of food oxidation and safeguards its quality [265].

Thus, sulphites represent one of the most used additives from antiquity thanks to their preservative properties [263].

Despite sulfites are widely and commonly used as additives in various food matrices, they are classified as allergens to humans. In fact, in hypersensitive individuals, they can provoke problems at the respiratory system, such as bronchial spasms and bronchoconstriction. Furthermore, they can be responsible of episodes of hives [44], [45], [266], [267]. As a consequence, the concentration of sulfites in food is monitored and regulated in many food commodities.

4.2 SO_2 in wine

Among the food commodities already mentioned, wine deserves a particular mention. In fact, sulfites are the most used preservatives in the oenological sector. This beverage has been produced and drunk from the dawn of human civilization.

The chemical components of wine influence its quality. To preserve the organoleptic characteristics and to extend the storage shelf life of wine, the level of sulfites, naturally produced by yeasts, are usually adjusted during the vinification process by the addition of sulfiting agents [268], [269]. In wine, the addition of sulfiting agent generates a complex variety of pH-dependent forms of sulfur-containing species, schematized in Figure 34.

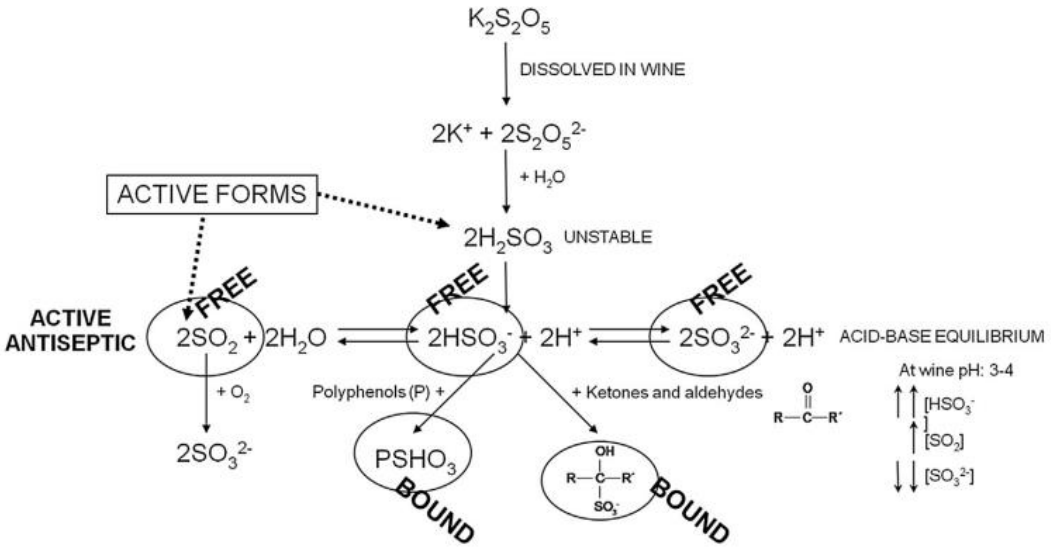


Figure 34: Chemical equilibria of sulfites in wine

Figure 34: Chemical equilibria of sulfites in wine following the addition of potassium metabisulfite. Image taken from [44]

The term “sulfites” implies a class of molecules, which, in the oenological context, generally refers to sulfur dioxide (SO_2). Furthermore, SO_2 in wine is distinguished in:

- free SO_2, which includes molecular SO_2 and bisulfites ion HSO_3^-,
- bound SO_2, which includes the sulfite forms combined with the organic compounds of the wine matrix, in particular with the carbonyl

groups such as acetaldehyde. This form is less active in the vinification process [270].

The sum of free SO_2 and combined SO_2 defines the total SO_2.

Although some alternatives to the use of SO_2 are currently under study [271]–[275], nowadays in oenological sector it is still the most worldwide used additive thanks to its technological advantages. Thus, SO_2 is added to almost all wines in order to limit the microorganisms proliferation and to slow down the oxidative process and the sensory deterioration.

As in many other food commodities, the components of wines must comply with legal regulations. The Commission Delegated Regulation (EU) 2019/934 of 12 March 2019 [276] regulated the legal requirements to be respected in the oenological sector. These limits for total SO_2 corresponded to 150 mg/l for red wines and 200 mg/l for white wines.

To determine the concentration of SO_2 in wine, many measurement methods were proposed [263]. Among these there are: iodometric titration [277], [278], colourimetry [279]–[282], electrochemistry [283], [284], chemiluminescence [285], chromatography [286], [287], fluorometry [288], infrared spectrometry [289] and enzymatic method [290]. In addition to the aforementioned techniques, there are official analytical methods for SO_2 determination released by the International Organisation of Vine and Wine (OIV). OIV is an intergovernmental organisation of a scientific and technical nature with the scope of creating harmonised standards for several parameters in the oenological sector. Among the official methods drew up in a specific Compendium, those related to SO_2 quantification are:

- Resolution OIV-OENO 591A-2018 for free sulfur dioxide [291];
- Resolution OIV-OENO 591B-2018 for total sulfur dioxide [292];
- Method OIV-MA-AS323-04B of Resolution OENO 377/2009 for sulfur dioxide by iodometry [293];
- Method OIV-MA-AS323-04C of Resolution OENO 377/2009 for sulfur dioxide by molecular method [294].

Among those above mentioned, the aeration-oxidation official method, described in Resolution OIV-OENO 591A-2018 and Resolution OIV-OENO 591B-2018, is internationally considered the election method for the quantification of sulfur dioxide in wine. It is commonly used in analysis

laboratories and wineries for its simplicity, robustness and not high cost. This aeration-oxidation method is also employed for the SO_2 quantification in other food commodities, such as shrimp, vegetables, potatoes, jams, apple juice and dried apricots [263], [264].

Concerning the evaluation of repeatability and reproducibility of the results, the OIV Resolution OIV-OENO 591B-2018 [292] suggests the adoption of multiplicative coefficients which should be applied to the achieved results. Monro stated that the aeration-oxidation method provides reproducible results within 5 % [279]. In general, in analytical chemistry, the evaluation of the measurement uncertainty associated with an analytical result can be provided by using the Horwitz equation in specific range of concentration and, out of this range, by the Thompson corrections [295]–[297]. The resulting model for the evaluation of the reproducibility standard deviation is:

$$\sigma_r = \begin{cases} 0.22c & \text{when} \quad c < 1.2\times10^{-7} \\ 0.02c^{0.8495} & \text{when} \quad 1.2\times10^{-7} \le c \le 0.138 \\ 0.01c^{0.5} & \text{when} \quad c > 0.138 \end{cases}$$

where c is the mass fraction of the analyte and is $0 \le c \le 1$ [297].

Indeed, the Horwitz equation allows to evaluate the percentage standard deviation regardless of the nature of the analyte, the method of measurement used, the measurement conditions and the matrix of the analyte. In the case of wine, this approach was adopted by Jain [264] and Fazio [263]. However, these indications suggest a wide and generic range of the results repeatability but do not take into account the other uncertainty sources, such as those due to the equipment used by the laboratories and the measurement capabilities.

4.3 OIV-OENO 591A-2018 method: free SO_2 maximum recovery in wine simulant solution

The work devoted to the organization of the measurement comparison, described in this chapter, was published in the Istituto Nazionale di Ricerca Metrologica (INRiM) Technical Report n° 15/2021: “Confronto di misura sulla determinazione della concentrazione dell’anidride solforosa libera in una soluzione di similvino” [298].

4.3.1 Scope of the work

Among the official methods reported in Section 4.2, the aeration-oxidation one described in Resolution OIV-OENO 591A-2018 of the International Organization of Vine and Wine (OIV) is the reference method for determining the concentration of free SO_2 in wine.

However, from research in the literature and from experiments performed on wine simulant solutions with SO_2 present only in the free form, it was plausible that with this method it was not possible to determine the SO_2 total concentration. Consequently, to verify whether this hypothesis was true, a measurement comparison was planned by INRiM and conducted involving nine Piedmont laboratories with ascertain skills in this measurement method. The comparison was conducted on a sample of wine simulant. This simplified version of wine was chosen for an initial investigation since it was necessary to limit the number of variables and verify if, without matrix effects typical in wine, the recovery of free SO_2 was complete. Moreover, this model system allowed a better comprehension of the parameters that mostly affect the measurement result and the identification of the weaknesses of the method.

Furthermore, since the wine simulant sample was prepared gravimetrically, it was possible to evaluate the maximum recovery of free SO_2 obtained by the OIV method. A concentration of SO_2 close to the legal limit for red wines was considered, and in this case free and total SO_2 were equivalent.

4.3.2 Chemicals

All the solutions were freshly prepared using ultra-pure water (Milli-Q).

The wine simulant solution used for the measurement comparison and for the evaluation of the measurement uncertainty (Section 4.4) had the composition of an average wine [299], [300]. It was prepared at INRiM and contained:

- 12 % v/v of EtOH (Carlo Erba), since an average range of 10 – 14 % v/v of ethanol is the typical alcohol content in wine [268];
- 5 g/l of tartaric acid — $C_4H_6O_6$ (Carlo Erba), since an average range of 2 – 6 g/l of tartaric acid is the typical content in wine. This polyprotic and non-volatile acid is one of the prevalent acids in wine

[268]. It is useful both to reach the right pH of wine and to simulate the organic composition of wine.

- 1 M NaOH solution (Panreac), necessary to buffer the pH at 3.2, peculiar value for wine;
- potassium metabisulfite — $K_2S_2O_5$, in powder form (Acros Organics), that represents the most employed sulfiting product in the wine sector. Taking into account the stoichiometric ratio, the addition of potassium metabisulfite leads to a known concentration of SO_2 in wine simulant (see Section 4.3.3) [268], [301]. This reagent was added as a last step to avoid loss of SO_2 during the preparation of the wine simulant.

In this type of wine simulant, SO_2 was present only in the free form.

For the application of the OIV method according to the Resolution OIV-OENO 591A-2018, the following solutions were used:

- phosphoric acid — H_3PO_4 at 85 % m/v (Honeywell Fluka), necessary to acidify the sample and promote the volatilization of SO_2;
- indicator reagent, which contained 1.00×10^{-1} g of Methyl Red (Merck) and 5.0×10^{-2} g of Methylene Blue (Merck) in 5.0×10^{-2} l of ethanol ≥ 95 % (v/v) and ultra-pure water up to a volume of 1.00×10^{-1} l [291], [302];
- indicator solution, named Flask B solution. It must be freshly prepared adding in sequence: diluted hydrogen peroxide — H_2O_2 solution (from 10 volumes to 3 volumes), 3 drops of indicator reagent (at this stage the overall solution was violet) and drops of 1×10^{-2} M NaOH solution to neutralize this indicator solution and switch it to green.

For the titration of sulfuric acid — H_2SO_4 resulting from the OIV measurement, the following solutions were used:

- 1×10^{-2} M NaOH solution, obtained from anhydrous pellets (Panreac) and standardized against a 1×10^{-2} M potassium hydrogen phthalate — $C_8H_5KO_4$ solution (Alfa Aesar). The standardization of this solution and the evaluation of its uncertainty are reported in detail in Section 4.4.6;
- Phenolphthalein indicator reagent, employed in the standardization procedure of NaOH solution. 5.0×10^{-2} l of this indicator reagent was

obtained by dissolving 2.5×10^{-1} g of phenolphthalein in 50 % EtOH hydroalcoholic solution.

4.3.3 Preparation of wine simulant solution with a specific concentration of SO_2

For the measurement comparison and for the evaluation of the measurement uncertainty (Section 4.4), wine simulant solutions with a specific concentration of SO_2 were gravimetrically prepared. Mass of potassium metabisulfite was dissolved in hydroaloholic solution, following the procedure described in Section 4.3.2.

From $K_2S_2O_5$, the sulfur dioxide is generated according to the following reaction:

$$K_2S_2O_5 + 2\ H^+ \rightarrow 2\ SO_2 + H_2O + 2\ K^+$$

The gravimetric concentration of SO_2, $y_{SO2.g}$, expressed in mg/l, was obtained applying the equation (1):

$$y_{SO2.g} = \frac{m_{K2S2O5} \cdot P_{K2S2O5} \cdot 10^3}{V} \cdot \frac{MM_{SO2}}{MM_{K2S2O5}} \cdot 2 \qquad (1)$$

where:

- m_{K2S2O5} is the mass, expressed in g, of potassium metabisulfite weighted for the preparation of wine simulant solution,
- P_{K2S2O5} is the purity of potassium metabisulfite,
- 10^3 is a multiplicative factor for the conversion from g to mg,
- MM_{SO2}, expressed in g/mol, is the molar mass of sulfur dioxide,
- 2 is a multiplicative factor related to the stoichiometric ratio between potassium metabisulfite and sulfur dioxide,
- V is the volume, expressed in l, of the wine simulant solution prepared,
- MM_{K2S2O5}, expressed in g/mol, is the molar mass of potassium metabisulfite.

4.3.4 Measurement procedure and INRiM apparatus

As already mentioned, the wine simulant used for these experiments contained only free SO_2, thus the method applied was the OIV-OENO 591A-2018 [291].

The schematic apparatus proposed by the OIV [291] is reported in Figure 35 a. At INRiM, the apparatus (Figure 35 b) was located in a laboratory with an active control of the temperature at (21 ± 3) °C in order to keep the temperature in the range proposed by the OIV method (18 – 24) °C. The INRiM apparatus was slightly modified with respect to the one described by the OIV Resolution. In fact, the most important implementation regarded the addition of a mass flow controller located on the left side of the apparatus, which pull a constant flow of nitrogen gas through the apparatus and facilitates the extraction of SO_2 and channelling into the Flask B where it is collected and then quantified. Instead in Figure 35 a, on the right hand part there is a water pump which sucks air, risking to take part of the SO_2 out of the apparatus without it being quantified.

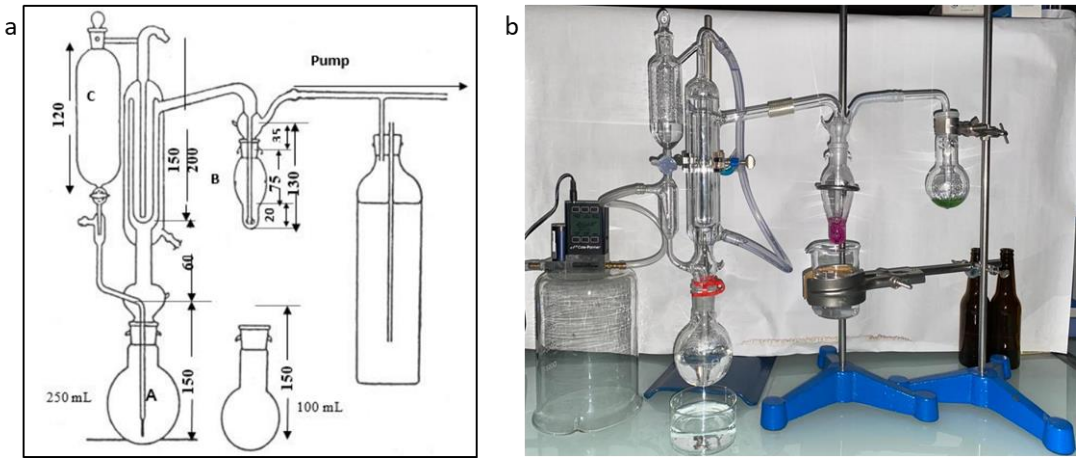


Figure 35: OIV apparatus for SO_2 determination

Figure 35: a) OIV schematic configuration proposed by OIV-OENO 591A-2018 method [291], b) picture of the INRiM apparatus

The measurement procedure consisted in placing 5×10^{-2} l of wine simulant into the Flask A, 3×10^{-3} l of indicator solution both in the Flask B and in the Flask C (as explained below) and 1.5×10^{-2} l of phosphoric acid into the Reservoir. By opening the glass tap of the Reservoir, phosphoric acid was added to wine simulant provoking the lowering of the pH under 1. This acidification of the wine simulant solution promoted the volatilization of the SO_2. The constant flow of nitrogen set at (6.67×10^{-1} ± 7×10^{-3}) l/min driven by the mass flow controller (Cole-Palmer) facilitated the SO_2 transport into Flask B. In the Flask B, the oxidation of sulfur dioxide into sulfuric acid caused by hydrogen peroxide

provoked the switch of the solution colour from green to violet [302]. The two reactions that occurred were:

$$SO_2 + H_2O_2 \rightarrow SO_3 + H_2O$$

and

$$SO_3 + H_2O \rightarrow H_2SO_4$$

In the OIV Resolution, the phase of SO_2 extraction from the sample lasted 15 minutes. Nevertheless, at INRiM, the adoption of two consecutive rounds of 15 minutes each, with the two relative acidification steps by phosphoric acid, was preferred in order to guarantee the theoretically complete SO_2 extraction.

With respect to the OIV scheme, the INRiM apparatus presented some differences which were made with the purpose of improve the performances of the method and of better control the system (Figure 35). These modifications to the apparatus were:

- the already mentioned flow of nitrogen upstream which allowed the gurgle of the wine simulant solution in Flask A, promoting the extraction of SO_2 and channelling it into the Flask B solution;
- a Flask C in series with the Flask B. The Flask C contained the same indicator solution of Flask B (Flask B solution) and represented a negative control. Indeed, the Flask B solution before the measurement was green and became violet after the oxidation of SO_2 into H_2SO_4. If the Flask B solution contained into the Flask C did not became violet after the two phases of SO_2 extraction, then no SO_2 into the Flask C was collected. As a consequence, Flask C certified that the SO_2 stream did not pass beyond Flask B and therefore was not lost downstream;
- Flask A and Flask B dipped in water baths. This shrewdness minimized the temperature variations of the contained solutions.

Before the titration, Flask B was detached from the apparatus and ultra-pure water was used to rinse the pipes close to it in order to collect all the possible residues of SO_2. Then, the sulfuric acid produced in Flask B was titrated with the standardized 1×10^{-2} M NaOH solution. The acid-base titration was performed according to the reaction:

$$H_2SO_4 + 2\ NaOH \rightarrow Na_2SO_4 + 2\ H_2O$$

Since SO_2 and H_2SO_4 are related by a stoichiometric ratio of 1:1, as reported in the two chemical reactions previously described, in the next formula MM_{SO2} will be used instead of MM_{H2SO4}. To get the concentration of SO_2 obtained by the OIV method, $y_{SO2.OIV}$, expressed in mg/l, the subsequent equation (2) was exploited:

$$y_{SO2.OIV} = MM_{SO2} \cdot \frac{V_{NaOH} \cdot c_{NaOH}}{2 \cdot V_{wine}} \cdot 10^3 \quad (2)$$

where:

- V_{NaOH} is the volume, expressed in l, of NaOH solution necessary for the titration of sulfuric acid,
- c_{NaOH} is the molar concentration, expressed in mol/l, of NaOH solution (nominal value of 1×10^{-2} mol/l),
- V_{wine} is the volume, expressed in l, of the wine simulant sample,
- 10^3 is a multiplicative factor for the conversion from g to mg,
- 2 is the stoichiometric factor related to the ratio between NaOH and SO_2 (or H_2SO_4).

Equation (2) was enforced at INRiM to provide the result of $y_{SO2.OIV}$, instead of using the approximations suggested by the OIV Resolution. For the measurement comparison, the estimate of $y_{SO2.OIV}$ was obtained by a series of 6 repetitions of the measurement. Particular attention was paid in reducing the repeatability contribution. In fact, in addition to the methodological and instrumental improvements already described, the following precautions were adopted:

- Experiments performed in a laboratory with an active control of the temperature at (21 ± 3) °C;
- Solution freshly prepared before the measurement campaigns;
- NaOH solution used in the titration was specially standardized with potassium hydrogen phthalate;
- Experiments performed consecutively to prevent the possible degradation of the wine simulant;
- Apparatus accurately washed with ultra-pure water between the experiments to recreate the same starting conditions of the measurement;

- Characterization of the volumetric pipette used to take the wine simulant solution and place it into the Flask A. The volume established by this characterization was ($4.9800\times10^{-2} \pm 5.0\times10^{-5}$) l instead of 5.0000×10^{-2} l. This error was taken into account.
- Titrations performed by the same operator.

Furthermore, equation (2) was also chosen as equation model to evaluate the measurement uncertainty of the result, as described in Section 4.4.

4.3.5 Organization of the comparison

The comparison was planned and coordinated by the group of Physical chemistry and nanotechnology of INRiM. The participants were 9 laboratories of Piedmont: INRiM, 3 different departments of the Centro di Ricerca Viticoltura ed Enologia (CREA), the Department of Agricultural, Forest and Food Sciences of University of the Study of Turin (UNITO), Bi.lab., Enocontrol S.c.a.r.l., Centro per l'enologia S.r.l. and Sinergo. The laboratories signed a document attesting their participation in the measurement comparison and their commitment to respect the deadlines. Each laboratory was required to carry out a minimum of 5 repetitions of the measurement within 8 days from the date of receipt of the sample to comply with the stability requirement of the solution. The method employed had to be attributable to the OIV-OENO 591A-2018. Information about transport, unpacking, storage and handling of the sample was provided to the laboratories together with the measurement instructions. At the end of the experiments, each laboratory had to send its sheet filled in with the measurement results to the coordinator. In this form, the participants had to report, in addition to the measurement results, any changes made to the official method, the photograph of the apparatus used and a description of the used procedure.

Before the preparation of the sample for the comparison, studies on the homogeneity and on the long term stability of wine simulant solutions with nominal 200 mg/l and 150 mg/l of free SO_2 respectively were performed. For the homogeneity study, (Figure 36 a) the solution with nominal 200 mg/l of free SO_2 was distributed in bottles which were subsequently hermetically sealed. 8 bottles were then opened and analyzed (4 in day 1 and 4 in day 2). For the long term stability test (Figure 36 b), two measurements were made on each designated bottle and, for each day of analysis, a new bottle was opened and used in order to preserve its composition.

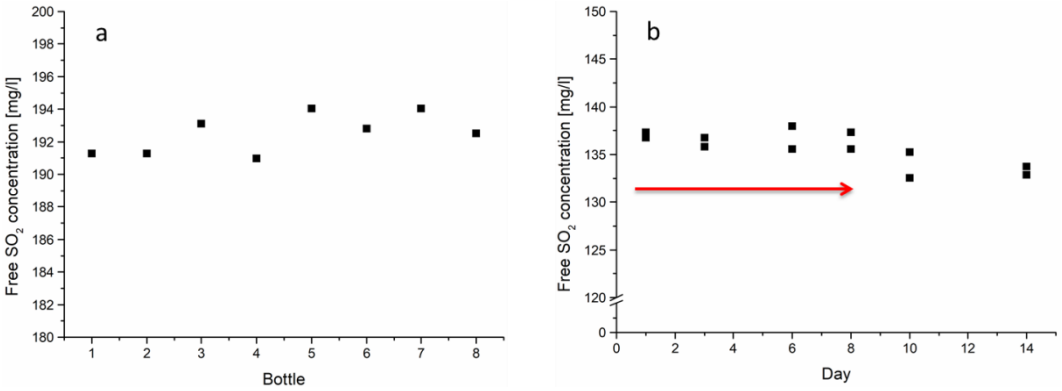


Figure 36: Homogeneity and long term stability studies of SO_2 in wine simulant solutions

Figure 36: a) Homogeneity study of wine simulant solution with nominal free SO_2 concentration of 200 mg/l (legal limit for white wines); b) Long term stability study of wine simulant solution with nominal free SO_2 concentration of 150 mg/l (legal limit for red wines)

For the homogeneity test, a mean value of 192.5 mg/l and a percentage standard deviation of 0.6 % were obtained. For the long term stability test, a mean value of 136.6 mg/l and a percentage standard deviation of 0.7 % were obtained. On the base of the measurement capabilities of the coordinating laboratory, a sufficient stability of the solution within a period of 8 days was established and a good homogeneity of the solution between bottles was verified.

After these tests, a wine simulant solution was gravimetrically prepared with a concentration of free SO_2, $y_{SO2.g}$, of 150.1 mg/l for the measurement comparison as described in Section 4.3.3. This value of free SO_2 concentration was taken as a reference because gravimetric measures are consolidated over time and reliable. Moreover, a calibrated balance was employed for the preparation of this solution, thus ensuring metrological traceability. The solution was accurately prepared, divided into different bottles, which then were hermetically sealed and distributed among the participating laboratories.

4.3.6 Results and discussion

The 9 laboratories provided their measurement results within the time established by the comparison. Each of them applied the OIV method according to its capabilities and filled in the results sheet specifying any differences made with respect to it. These modifications were considered acceptable by the coordinator

of the comparison. The results of this comparison were summarized in Table 7. The measurements were conducted from each laboratory according to their capabilities and the results were provided as usual for them. The results are therefore quoted with different numbers of significant digits. No uncertainty evaluation was required to the participants. Only the standard deviation was calculated as a repeatability contribution.

Table 7: Results obtained by the 9 laboratories in the measurement comparison on free SO_2 concentration in wine simulant solution

Measure n°	Lab 1 [µg/l]	Lab 2 [µg/l]	Lab 3 [µg/l]	Lab 4 [µg/l]	Lab 5 [µg/l]	Lab 6 [µg/l]	Lab 7 [µg/l]	Lab 8 [µg/l]	Lab 9 [µg/l]
1	133	128.00	138	134	141	144.8	143.90	144	145.92
2	136	138.88	137	135	138	143.2	143.00	144	147.20
3	132	132.80	139	136	139	142.4	143.30	144	147.84
4	134	128.96	139	144	137	143.5	143.30	144	147.84
5	132	139.52	137	133	139	142.4	143.00	144	147.84
6	131	138.56	-	142	-	-	143.30	-	-
7	-	-	-	144	-	-	-	-	-
8	-	-	-	138	-	-	-	-	-
Average	133	134.45	138	138	139	143.3	143.30	144	147.33
Standard deviation	1.79	5.23	1.00	4.50	1.48	0.99	0.33	0.00	0.83
Average recovery %	88.61	89.58	91.94	92.11	92.48	95.45	95.47	95.94	98.16

These data were graphically reported in Figure 37. The legal limit of SO_2 for red wines (150 mg/l) is highlighted in red and the gravimetric concentration of SO_2 in wine simulant obtained by gravimetry is reported in green (150.1 mg/l).

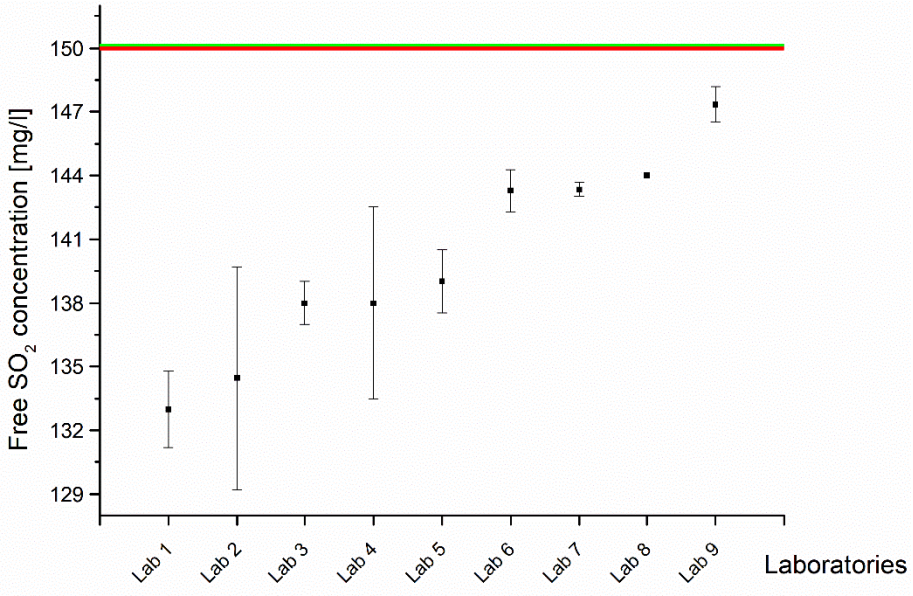


Figure 37: Measurement comparison on free SO_2 concentration in wine simulant solution

Figure 37: Results and standard deviations obtained by the 9 laboratories. Red line: legal limit for SO_2 in red wines (150 mg/l); green line: gravimetric concentration of SO_2 in the wine simulant (150.1 mg/l). Image taken from [303] and adapted.

From this comparison, the most prominent result was that the 100 % recovery of free SO_2 was not achieved by any of the laboratories, as well observed in Figure 38.

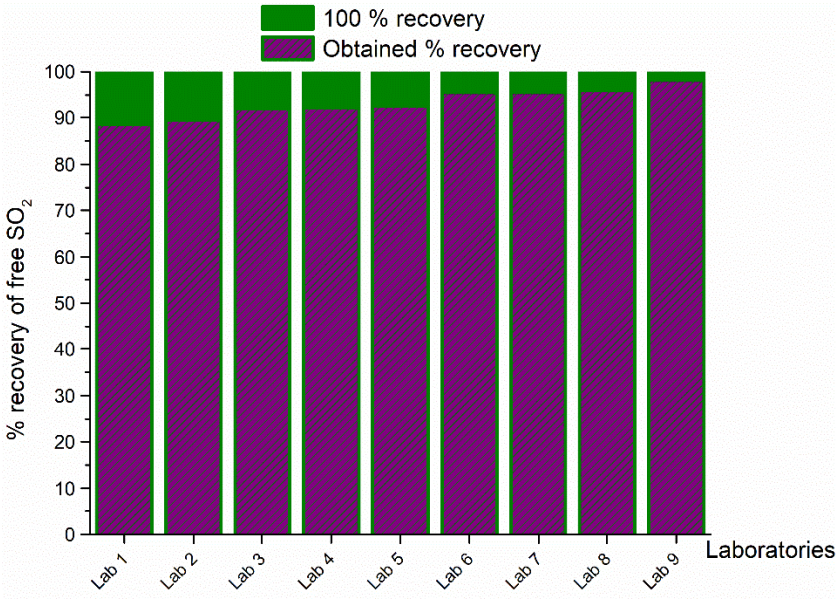


Figure 38: Percentage recovery of free SO_2 concentration

Figure 38: Percentage recovery of free SO_2 concentration for each laboratory, in purple, with respect to the total percentage amount, highlighted by the green rectangles

In fact, by the comparison the average recovery of free SO_2 was settled on 93.1 % which means an average concentration of 139.8 mg/l for free SO_2 (the blue line in Figure 39). The wide differences between the average result obtained by the comparison and by the gravimetric method underlined a criticality in the application of the OIV method.

A second output highlighted in Figure 39 was the standard deviation of the average concentration considering all the results reported by the 9 participants (dashed blue lines). It was equal to ± 5.2 mg/l, and thus provided a fairly wide range of values reasonably attributable to the measurand. This number reflected the variety of interpretations of the official OIV method and the consequent implication in the slightly difference approaches adopted by the laboratories.

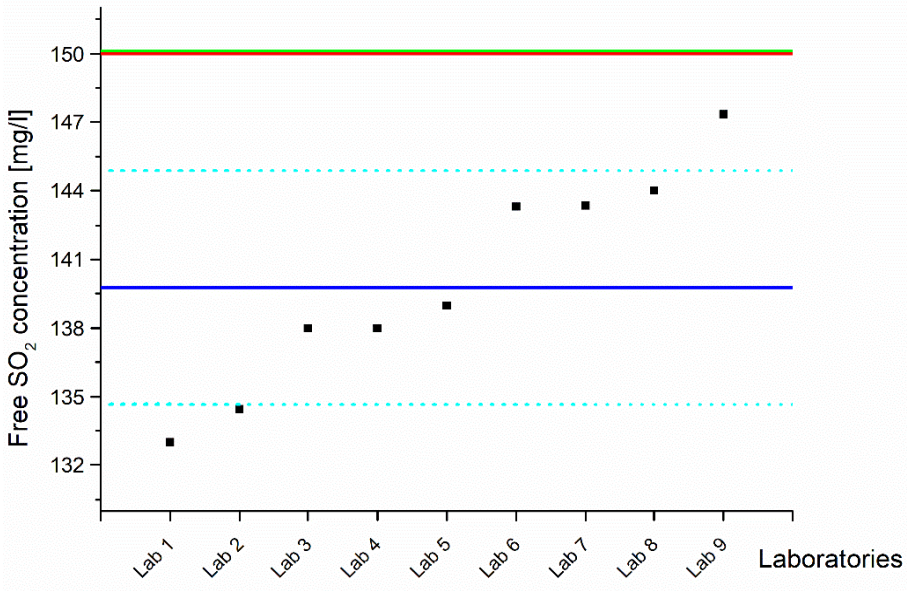


Figure 39: Average and standard deviation of the results achieved in the comparison

Figure 39: The blue line indicates the average value obtained on the basis of all the free SO_2 concentration estimates obtained by the laboratories (139.8 mg/l), the dashed blue lines indicate the extremes of the corresponding standard deviation and black dots indicate the mean values declared by the laboratories. The red line represents the value of the legal limit for red wines (150 mg/l) and the green line represents the value of the sample containing the SO_2 concentration obtained by gravimetric method (150.1 mg/l).

The average value of $y_{SO2.OIV}$ achieved at INRiM was 143.3 mg/l, which corresponded to 95.5 % of free SO_2 recovery respect to $y_{SO2.g}$. For the comparison, only the uncertainty contribution related to the standard deviation (repeatability), as calculated by the other laboratories, was taken into account. Nevertheless, for INRiM equipment, the measurement uncertainty was calculated, as reported in Section 4.4.

4.3.7 Conclusion and future perspectives

A measurement comparison on the official OIV-OENO 591A-2018 method was planned and coordinated by INRiM among nine laboratories that explicate a control role for wine in the commercial community. The sample analysed in this comparison was a wine simulant solution containing free SO_2 in concentration close to the legal limit of total SO_2 for red wine. It was produced via gravimetry,

spread among the participants and analysed with respect to the free SO_2 concentration achieved by OIV method.

The most important result obtained by this comparison was the confirmation that, with the official OIV method, the determination of the concentration of free SO_2 in wine simulant is only partial. In fact, the average value of free SO_2 was equal to 139.8 mg/l instead of 150.1 mg/l, which meant an underestimation of 6.9 %. This experimental value, far from the gravimetric one and always underestimated, highlighted the relevance of the evaluation of SO_2 recovery, since it is not considered in the OIV method. Thanks to this comparison, this problem was unearthed and the oenological community has become aware of this systematic underestimation. From a metrological point of view, this outcome was not acceptable. This topic should be deeply studied to understand if, with some instrumental and technological expedients, it is possible to reach a recovery that is closer to the concentration value determined by the gravimetric method. In addition, a policy aimed at disseminating metrological knowledge and the importance of concepts such as data quality and metrological traceability of the measurement results should be widely promoted. Indeed, if the SO_2 concentration is underestimated, producers risk to add potassium metabisulfite in excess to wine during the vinification process. Moreover, erroneous quantification can involve the marketing of batches of wine with a concentration of sulfur dioxide exceeding the legal limits, putting at risk the health of consumers.

A second output regarded the great variability of the standard deviation achieved by the laboratories, which was reflected in the value of 5.2 mg/l for the standard deviation of the average concentration of SO_2. This variability could be attributable to different interpretations and approaches to the OIV method carried out by the laboratories. It is undeniable that the use the official OIV method in a more harmonized way could lead to more coherent results. This outcome can be achieved by a better exchange of useful information and tips among analytical laboratories with a view to increasing the transfer of knowledge and skills.

Considering the definition of accuracy (“closeness of agreement between a measured quantity value and a true quantity value of a measurand”) and precision (“closeness of agreement between indications or measured quantity values obtained by replicate measurements on the same or similar objects under specified conditions”) stated by the VIM [1], it can be concluded that the results of this measurement comparison were neither accurate nor precise. As a conclusion, a reliable correction should be investigated to be applied to the measurement results

obtained by OIV-OENO 591A-2018 method. This becomes of primary importance since this kind of measurements are routinely carried out by laboratories and wineries to assess compliance with the legal limits for sulfur dioxide in wine and therefore to authorize its sale. To do this, further investigations are necessary. In fact, the same approach should be used on a real wine matrix, where free SO_2 and total SO_2 have to be determined, and besides, interferences can possibly occur. Therefore, it will be necessary first of all switch to a more realistic and complicated solution containing all the form of SO_2 (free and bound, with together are the total) in order to investigate both the OIV-OENO 591A-2018 and OIV-OENO 591B-2018 methods. Then, the collected information should be employed to establish the reliable correction on real samples.

The evaluation of the recovery of free SO_2 in a wine simulant by a measurement comparison is only the first part of a comprehensive assessment on the OIV method. Indeed, to make the measurement results reliable and anchored to the SI units, an evaluation of the measurement uncertainty is indispensable. This second part is the subject of the Section 4.4.

4.4 Evaluation of measurement uncertainty

Part of the work described in this chapter was also published in the paper: "Evidence of a systematic underestimation of free sulfur dioxide by the aeration-oxidation method approved by OIV" published on Measurement in 2022 [303].

4.4.1 Scope of the work

Nowadays, the analytical laboratories are required to improve the quality of their results and to provide measurement uncertainties associated to these results. Indeed, the estimation of the measurement uncertainty is one of the key steps in the procedure for the validation of an analytical technique. However, currently, for many methods, only the standard deviation of the measurements is reported. Also in the case of the Resolutions OIV-OENO 591A-2018 and OIV-OENO 591B-2018 a rigorous evaluation of the measurement uncertainty is not required since the adoption of generic multiplicative coefficients are recommended.

For these reasons, in this work a rigorous evaluation of the measurement uncertainty of free SO_2 concentration in a wine simulant solution by the OIV-OENO 591A-2018 method was performed. To do this, the INRiM apparatus was

considered. Thanks also to the measurement comparison carried out on the same matrix (see Section 4.3), the critical issues and the variables that had the greatest influence on the method were investigated.

To the best of my knowledge, there were only a few papers devoted to the detailed assessment of SO_2 measurement uncertainty in food matrices [304] and none on wine. This rigorous evaluation is needed to assess the reliability of measurement results and establish the level of confidence that can be placed in them. Without such an indication, measurement results cannot be compared, neither among themselves nor with reference values given in a specification or standard. This work aimed to lay the foundations for anchoring the free SO_2 measurement results to the International System of Units (SI) by assessing the uncertainty evaluation of the OIV-OENO 591A-2018 method. By establishing the SI traceability, it is possible to ensure measurement comparability in time and space. The evaluation of the measurement uncertainty improves the reliability of the results and strengthens the work carried out by the OIV. Moreover, the evaluation of the measurement uncertainty associated with the estimate of SO_2 concentration also enables a validation process for other techniques by comparing the results. Besides, a reliable assessment of the estimate and measurement uncertainty of SO_2 concentration with the official OIV method is necessary to wineries both for routine detection of SO_2 in wine and in case of potential legal disputes.

4.4.2 Chemicals

Since this activity was the subsequent part of the work described in the measurement comparison of Section 4.3, the same chemicals of Section 4.3.2 was used.

4.4.3 Preparation of wine simulant solution with a specific concentration of SO_2

Since the solution of wine simulant adopted for the evaluation of the measurement uncertainty of $y_{SO2.OIV}$ was the same of the one employed in the measurement comparison, please refer to Section 4.3.3 for details.

4.4.4 Measurement procedure and INRiM apparatus

The INRiM apparatus and the measurement procedure used for the evaluation of the measurement uncertainty of $y_{SO2.OIV}$ were the same described in Section 4.3.4.

4.4.5 The measurement uncertainty

When a measurement result has to be expressed, it should be reported as a value of the measurement quantity accompanied by its measurement uncertainty. In this work, the measurand was represented by the concentration of free SO_2 in the wine simulant solution. After accurately established the correction to be applied to the concentration of SO_2, as described in Section 4.3, the measurement result still remained only an estimate of the SO_2 value in wine simulant solution. Thus, a rigouous evaluation of the measurement uncertainty was necessary. The uncertainty of a measurement is formally defined as a "parameter, associated with the result of a measurement, that characterizes the dispersion of the values that could reasonably be attributed to the measurand" [1], [4]. To assess its evaluation, the framework provided by the Guide to the expression of uncertainty in measurement (GUM), which is responsibility of the International Bureau of Weights and Measures (BIPM) [4], was employed. In fact, the GUM allows to estimate the total measuement uncertainty of a measurement result and highlights which are the most critical empirical inputs in terms of reliability.

Two types of evaluation of uncertainty are possible: type A, which is based on the statistical analysis of measurement repetitions, or type B, which derives from scientific judgments about the variables based on the information available [1], [4]. The steps to deal with to provide an uncertainty evaluation can be summarized as follows:

- Describe in detail the measurement procedure,
- Establish the model equation,
- Identify the sources of uncertainty. It may be helpful to use an Ishikawa fishbone diagram to visually summarize them,
- Quantify all the sources of uncertainty as standard uncerainties,
- Combine the standard uncertainties of each variable to obtaine the combined uncertainty of each variable,
- Convolute all the uncertainty contributions to obtaine the combined uncertainty of the measurand,

- Calculate the expanded uncertainty to provide an interval that may be expected to encompass a large fraction of the distribution of values that could reasonably be attributed to the measurand.

The propagation law of the uncertainty was applied to calculate the uncertainty from the standard uncertainty of the input estimates, as suggested by the GUM. This uncertainty is based on the equipment used by the laboratories and the measurement capabilities and expertise. Therefore, the expanded standard uncertainty provided in this study should be interpreted as the minimum value achievable by a skilled operator.

Talking about the molar masses and the uncertainties of sulfur dioxide and potassium hydrogen phtalate, they were estimated by the Monte Carlo method [305], as recommanded by the GUM [306]. The values of standard atomic weights of the elements stated in 2013 by the Commission on Isotopic Abundances and Atomic Weights of the International Union of Pure and Applied Chemistry (IUPAC) [307] were used as input to calculate the molar mass of this two molecules.

These masses of the elements were reported either as weight intervals, whose distributions were considered uniform (rectangular) or as average values with their uncertainties, whose distributions were considered normal (Gaussian). For the evaluation of the measurement uncertainty, the Monte Carlo method is the recommended approach when the probability density function of the input quantities involved in the calculations significantly differs from a normal distribution, such as the uniform distribution. While the sum of as few as three independent rectangular distributions of similar variance could be considered approximately normal [4], this was not the case for SO_2. The Monte Carlo method was therefore applied for the calculation of the molar masses of SO_2 and potassium hydrogen phthalate, i.e. $C_8H_5O_4K$. The number of trials for the Monte Carlo method, M, was chosen according to the guidelines indicated in Supplement 1 of the GUM [306] at paragraph 7.2, and was therefore set to $M = 10^4/(1-p) = 10^6$ for p = 99 %, where p is the coverage probability, also termed level of confidence. It represents the “probability that the set of true quantity values of a measurand is contained within a specified coverage interval”.

4.4.6 Results and discussion

The equation (2), already mentioned in Section 4.3.4 and here reported for semplicity, was also adopted as model equation for the uncertainty evaluation of $y_{SO2.OIV}$.

$$y_{SO2.OIV} = MM_{SO2} \cdot \frac{V_{NaOH} \cdot c_{NaOH}}{2 \cdot V_{wine}} \cdot 10^3 \qquad (2)$$

The evaluation of the measurement uncertainty contribution was reported for each variable of the model equation since all the variables affected the uncertainty budget. The sources of uncertainty which contributed to each of the variables were identified using the cause and effect analysis and were summarized in the Ishikawa fishbone diagram of Figure 40.

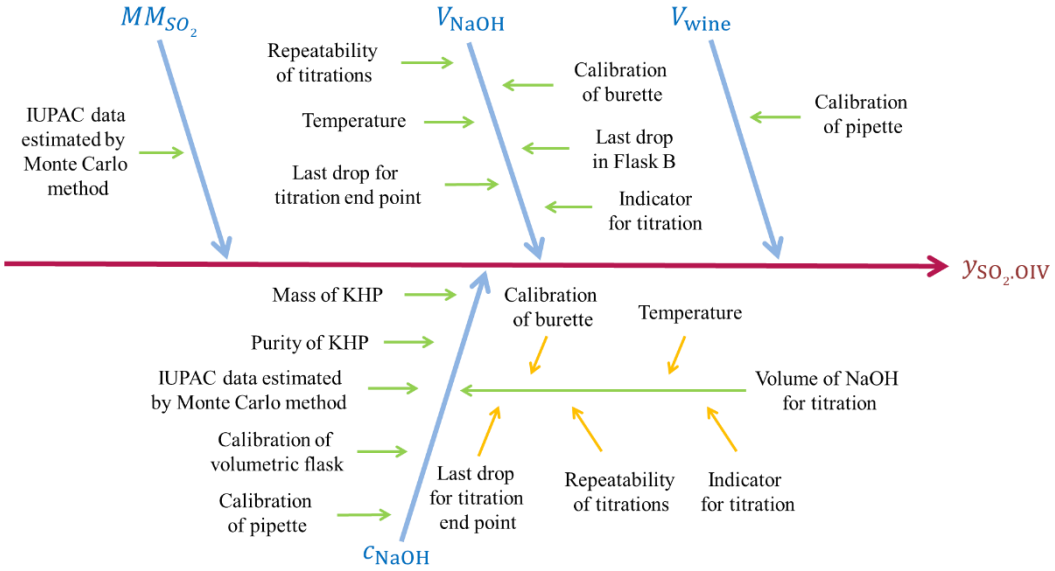


Figure 40: Uncertainty contributions

Figure 40: Diagram of Ishikawa used to idenity the sources of uncertainty

The values of the uncertainty contributions were reported considering 2 significant digits. The correspondent values of the estimated quantities were reported accordingly, even in the case in which the related instruments were equipped with a lower number of digits.

According to the order of appearance of variables in the equation (2), the uncertainty contributions were the following:

- MM_{SO2} was calculated as the sum of three uniform distributions, with the element O ranging in the interval (15.99903, 15.99977) g/mol, and S ranging in the interval (32.059, 32.076) g/mol. Since the interval of the sulfur was much larger than that of the oxygen, the distribution of the sum of the three atoms in the Monte Carlo evaluation yielded an almost-rectangular distribution with a similar width to that of the sulfur. Figure 41 shows the input and output quantities distribution histograms in the calculations of the molar masses of SO_2. The resulting average MM_{SO2} was 64.0663 g/mol and its standard uncertainty (standard deviation on the trials), u(MM_{SO2}), was 4.9×10^{-3} g/mol.

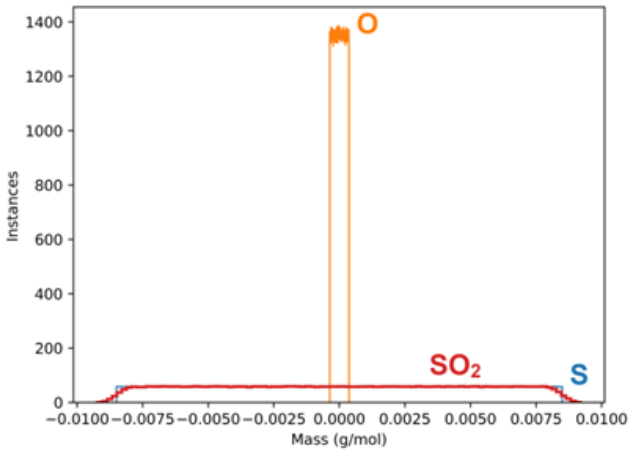


Figure 41: Distributions histograms for the molar mass of SO_2

Figure 41: Input and output quantities distributions histograms in the calculation of the molar mass of SO_2 with the Monte Carlo method (10^6 trials per molecule, represented with 100 bins per distribution); with annotations of their corresponding colour for each (output quantities in red). All distributions are centered to zero for mutual comparison. Image taken from [303] and adapted

- To V_{NaOH} contributed six sources of uncertainty:

  The first source of uncertainty was associated to the repeatability of the titrations. The repetitions reported here in Table 8 were the same used in Section 4.3.6 for the comparison but, in this case, the volume of nominal 1×10^{-2} M NaOH solution was the variable taken into consideration instead of the concentration of SO_2. These 6 titration measurements gave an experimental standard deviation of the mean, *u(Rep)*, of **2.2×10^{-5} l**, which was calculated by dividing the

standard deviation of the repetitions by the square root of the number of repetitions.

Table 8: Volume of nominal 1×10^{-2} M NaOH solution needed for the titration of Flask B solutions obtained by the 6 repetitions

Table taken from [303]

Titration n°	**Volume of nominal 1×10^{-2} M NaOH solution [l]**
1	0.023800
2	0.023650
3	0.023700
4	0.023700
5	0.023650
6	0.023700
Average	0.023700
Standard deviation	$5.5\text{x}10^{-5}$

The second source of uncertainty was related to the calibration of the burette, $u(Cal)$. The accuracy of the delivered volume was reported by the manufacturer. For the 2.5000×10^{-2} l burette, this value was $\pm\ 3.0\times10^{-5}$ l. The standard uncertainty was evaluated assuming a triangular distribution. $u(Cal) = 3\times10^{-5}/\sqrt{6} =$ **1.2×10^{-5} l**.

The third source of uncertainty was due to the difference between the temperature at which the experiments were conducted and that at which the burette calibration was performed, $u(\Delta T)$. It was estimated to be ± 3 °C with a 95 % confidence (corresponding to a coverage factor, k, of 2 for the evaluation of the standard uncertainty). Using the coefficient of volume expansion for aqueous solution as 2.1×10^{-4} °C^{-1}

and considering a mean value of 2.3700×10^{-2} l of the NaOH solution required for the titration of the Flask B solution, the following value was given for $u(\Delta T) = 2.3700\times10^{-2}\times2.1\times10^{-4}\times3/2 =$ **7.5×10^{-6} l**.

The fourth source of uncertainty regarded the fractionation of the last drop of nominal 1×10^{-2} M NaOH solution used to neutralize the H_2O_2 solution present in Flask B before starting the SO_2 extraction process. In this case, the last drop (5.00×10^{-5} l) of the NaOH solution was included in the uncertainty calculation. To minimize this contribution, 1.0000×10^{-1} l of Flask B solution were prepared and neutralized with 1.50×10^{-3} l of 1×10^{-2} M NaOH solution. 3.00×10^{-3} l of this solution already neutralized were placed in Flask B. With 1.0150×10^{-1} l of neutral solution it was possible to carry out 33.83 experiments. A fraction of drop with respect to this number of experiments was considered. A rectangular distribution was associated with this contribution and thus, $u(Flask\ B) = 5.00\times10^{-5}/(33.83\times2\times\sqrt{3})$ = **4.3×10^{-7} l**.

The fifth source of uncertainty was related to the last drop of 1×10^{-2} M NaOH solution from the burette used to reach the end point detection in the titration. This last drop added to the Flask B solution was included in the uncertainty calculation considering that potentially not the whole drop was needed for the titration of H_2SO_4. In this case, considering a rectangular distribution, $u(E\text{-}P) = 5.0\times10^{-5}/2\sqrt{3}$ = **1.4×10^{-5} l**.

The sixth source of uncertainty was due to the pH difference of the end point showed by the indicator from the equivalence point, $u(Ind)$ [308]. This contribution was evaluated considering the resolution of the burette of 5.0×10^{-5} l and a rectangular distribution. Thus, $u(Ind) = 5.0\times10^{-5}/2\sqrt{3} =$ **1.4×10^{-5} l** [309], [310].

The standard uncertainty of V_{NaOH}, $u(V_{NaOH})$, was evaluated normally distributed by combining these six uncertainty contributions:

$$u(V_{NaOH}) =$$

$$\sqrt{(u(Rep)^2 + u(Cal)^2 + u(\Delta T)^2 + u(Flask\ B)^2 + u(E-P)^2 + u(Ind))} =$$

3.4×10^{-5} l

- To evaluate the uncertainty related to c_{NaOH} it was necessary to consider the standardization process of the nominal 1×10^{-2} M NaOH solution with the potassium hydrogen phthalate.

The molar concentration of NaOH in a solution and its uncertainty were determined by a titrimetric method. The solution was standardised against the primary standard potassium hydrogen phthalate — $C_8H_5O_4K$ (KHP) following the procedure reported in QUAM [311]. The measurand was the concentration of the NaOH solution. For this acid-base titration, the end point was determined by phenolphthalein as indicator.

The concentration of the potassium hydrogen phthalate solution, c_{KHP}, was determined on the base of equation (3):

$$c_{KHP} = \frac{m_{KHP} \cdot P_{KHP}}{MM_{KHP} \cdot V_{Sol-KHP}} \quad (3)$$

where:

- m_{KHP} is the mass, expressed in g, of potassium hydrogen phthalate,
- P_{KHP} is the purity of potassium hydrogen phthalate,
- MM_{KHP} is the molar mass, expressed in g/mol, of potassium hydrogen phthalate
- $V_{Sol-KHP}$ is the volume, expressed in l, of the solution of potassium hydrogen phthalate prepared.

After drying, a mass of KHP of 1.02280 g was weighed and added to 5.000×10^{-1} l of ultra-pure water. A solution of KHP with concentration of 1.002×10^{-2} mol/l was obtained.

Once obtained the value of c_{KHP}, c_{NaOH} was determined on the base of equation (4):

$$c_{NaOH} = \frac{c_{KHP} \cdot V_{KHP}}{V_{NaOH.St}} \quad (4)$$

where:

- V_{KHP} is the volume, expressed in l, of the solution potassium hydrogen phthalate in the flask used for the titration,
- $V_{NaOH.St}$ is the volume, expressed in l, of NaOH needed for the titration.

A NaOH solution with nominal concentration 1×10^{-2} mol/l was prepared starting from NaOH pellets.

9 repetitions of titration were conducted using the NaOH solution in the burette and 4.000×10^{-3} l aliquots of the KHP solution in a flask. From these repetitions, the obtained mean value of $V_{NaOH.St}$ corresponded to 4.261×10^{-3} l.

The measurand c_{NaOH} was estimated to be **9.40×10^{-3} mol/l**.

For the uncertainty evaluation, the following contributions, reported in the order of appearance in the equation (3) and (4), were taken into account.

m_{KHP}, as well as the other masses weighted in this work, was weighed on a balance with a last digit of 1.0×10^{-4} g. For the uncertainty evaluation associated with the balance, only the linearity was considered. The calibration certificate of the balance quoted ± 3.0×10^{-4} g. The uncertainty was taken as having a normal distribution ($k = 2$), so the standard uncertainty $u(m_{KHP})$ was **1.5×10^{-4} g**.

P_{KHP} was quoted to be within the range of 99.95 % and 100.05 %. Therefore, $P_{KHP} = 1.00000 \pm 0.00050$. The uncertainty was taken as having a rectangular distribution, so the correspondent standard uncertainty $u(P_{KHP})$ was evaluated as $5.0\times10^{-4}/\sqrt{3}$ = **2.9×10^{-4}**.

MM_{KHP} and its uncertainty were calculated by the Monte Carlo method from the values reported in Table 9 [307], [312] and the distributions shown in Figure 42. Most atomic weights were declared as intervals, implying a rectangular distribution; however, potassium was reported as an average value with an expanded uncertainty, and was therefore treated as normally distributed ($k = 2$). The resulting MM_{KHP} ($C_8H_5O_4K$) was calculated as 204.2206 g/mol, with an approximately normal distribution and a standard uncertainty, $u(MM_{KHP})$, of **1.7×10^{-3} g/mol**.

Table 9: The atomic weights of the elements of KHP and their distributions
Table taken from [303]

Element	Distribution	Atomic weight (g/mol)
H	Uniform	(1.00784, 1.00811)
C	Uniform	(12.0096, 12.0116)
O	Uniform	(15.99903, 15.99977)
K	Normal	39.0983 ± 0.0001

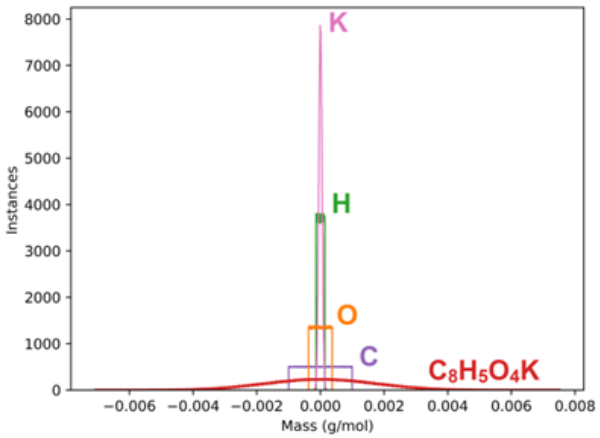


Figure 42: Distributions histograms for the molar mass of KHP

Figure 42: Input and output quantities distributions histograms in the calculation of the molar mass of KHP with the Monte Carlo method (10^6 trials per molecule, represented with 100 bins per distribution); with annotations of their corresponding colour for each (output quantities in red). All distributions are centered to zero for mutual comparison. Image taken from [303] and adapted

For $V_{\text{Sol-KHP}}$, the uncertainty was evaluated considering the limits of accuracy of the volumetric flask, reported by the manufacturer. For the 5.0000×10^{-1} l volumetric flask used this value was ± 5.0×10^{-4} l. Assuming a triangular distribution, the experimental standard deviation of the mean was $u(V_{\text{Sol-KHP}}) = 5.0\times10^{-4}/\sqrt{6} = \mathbf{2.0\times10^{-4}}$ **l**.

For V_{KHP}, the uncertainty contribution was determined on the basis of the accuracy of the delivered volume reported by the manufacturer. For a 1.000×10^{-3} l pipette, this value was $\pm\ 1.00\times10^{-4}$ l. Assuming a triangular distribution, a standard uncertainty $u(V_{KHP}) = 1.00\times10^{-4}/\sqrt{6} =$ **4.1×10^{-5} l**.

To $V_{NaOH.St}$ five uncertainty sources were associated:

The first one regarded the uncertainty of the burette calibration, $u(Cal.st)$, as already reported for the case of the determination of V_{NaOH}. Thus, $u(Cal.st) =$ **1.2×10^{-5} l**.

The second one was associated to the difference between the temperature in the laboratory and that of the calibration, $u(\Delta T.st)$, as already reported for the case of the determination of V_{NaOH}. In this case the mean value of the volume of NaOH solution for the standardization was 4.2611×10^{-3} l (see Table 10) and $u(\Delta T.st) =$ **1.4×10^{-6} l**.

The third one was due to the end point detection, $u(E\text{-}P.st)$. As described for the case of V_{NaOH}, $u(E\text{-}P.st) =$ **1.4×10^{-5} l**.

The fourth one was due to the repeatability of the 9 titration measurements carried out, as reported in Table 10. The experimental standard deviation of the mean, $u(Rep.st)$, was calculated by dividing the standard deviation of the repetitions by the square root of the number of repetitions. $u(Rep.st) =$ **1.1×10^{-5} l**.

Table 10: Volume of NaOH solution needed for the standardization against 4.000×10^{-3} l of nominal 1×10^{-2} M KHP solution obtained by the 9 repetitions of the titration

Table taken from [303]

Titration n°	**Volume of nominal 1×10^{-2} M NaOH solution [l]**
1	0.004250
2	0.004250
3	0.004250
4	0.004300
5	0.004250
6	0.004250
7	0.004300
8	0.004300
9	0.004200
Average	0.004261
Standard deviation	3.3×10^{-5}

The fifth one was related to the use of phenolphthalein as a visual indicator for the end point of the titration. Since there is a difference between the equivalent point and the end point, the uncertainty due to this visual indicator, $u(Ind.\mathrm{st})$, was evaluated to be $\mathbf{3\times10^{-5}}$ **l** accordingly to what reported by Forigua & Meija [309], [310].

The standard uncertainty of $V_{\mathrm{NaOH.St}}$, $u(V_{\mathrm{NaOH.St}})$, was evaluated normally distributed by combining the five uncertainty contributions:

$$u(V_{\mathrm{NaOH.St}}) =$$

$$\sqrt{(u(Cal.\mathrm{st})^2 + u(\Delta T.\mathrm{st})^2 + u(Rep.\mathrm{st})^2 + u(E-P.\mathrm{st})^2 + u(Ind.\mathrm{st}))} =$$

$$\mathbf{3.7\times10^{-5}\ l}$$

In Table 11 the values and the standard uncertainty of the six variables which contributed to the total calculation of c_{NaOH} are summarized.

Table 11: Values, distributions and standard uncertainties of the six variables which contributed to the calculation of c_{NaOH}

Table taken from [303]

Variable	Description	Value, X	Distribution	Standard uncertainty, u	Unit
$\boldsymbol{m_{\mathrm{KHP}}}$	Weight of KHP	1.02280	Normal	1.5×10^{-4}	g
$\boldsymbol{P_{\mathrm{KHP}}}$	Purity of KHP	1.00000	Uniform	2.9×10^{-4}	
$\boldsymbol{MM_{\mathrm{KHP}}}$	Molar mass of KHP	204.2206	Normal	1.7×10^{-3}	g/mol
$\boldsymbol{V_{\mathrm{Sol\text{-}KHP}}}$	Volume of KHP solution	5.0000×10^{-1}	Triangular	2.0×10^{-4}	l
$\boldsymbol{V_{\mathrm{KHP}}}$	Volume of KHP used for the titration	4.000×10^{-3}	Triangular	4.1×10^{-5}	l
$\boldsymbol{V_{\mathrm{NaOH.St}}}$	Volume of NaOH used for the titration	4.261×10^{-3}	Normal	3.7×10^{-5}	l

The combined uncertainty of c_{NaOH}, $u(c_{\mathrm{NaOH}})$, was evaluated applying the uncertainty propagation law. The partial derivatives, called sensitivity coefficients c_i, describe the weight of each contribution i on the estimated c_{NaOH} and make the units of each contribution homogeneous. $u(c_{\mathrm{NaOH}})$ resulted normally distributed by:

$$u(c_{\mathrm{NaOH}}) = \sqrt{(c(m_{\mathrm{KHP}})^2 \cdot u(m_{\mathrm{KHP}})^2 + c(P_{\mathrm{KHP}})^2 \cdot u(P_{\mathrm{KHP}})^2 + c(MM_{\mathrm{KHP}})^2 \cdot u(MM_{\mathrm{KHP}})^2 + \cdots}$$

$$\overline{\ldots + c(V_{\mathrm{Sol-KHP}})^2 \cdot u(V_{\mathrm{Sol-KHP}})^2 + c(V_{\mathrm{KHP}})^2 \cdot u(V_{\mathrm{KHP}})^2 + c(V_{\mathrm{NaOH.St}})^2 \cdot u(V_{\mathrm{NaOH.St}})^2}$$

where:

- $c(m_{\mathrm{KHP}}) = \frac{\partial(C_{\mathrm{NaOH}})}{\partial(m_{\mathrm{KHP}})} = 0.00920023465 \ \frac{mol}{g \cdot l}$
- $c(P_{\mathrm{KHP}}) = \frac{\partial(C_{\mathrm{NaOH}})}{\partial(P_{\mathrm{KHP}})} = 0.00941 \ \frac{mol}{l}$
- $c(MM_{\mathrm{KHP}}) = \frac{\partial(C_{\mathrm{NaOH}})}{\partial(MM_{\mathrm{KHP}})} = -0.0000460776239 \ \frac{mol^2}{g \cdot l}$
- $c(V_{\mathrm{Sol-KHP}}) = \frac{\partial(C_{\mathrm{NaOH}})}{\partial(V_{\mathrm{Sol-KHP}})} = -0.01882 \ \frac{mol}{l^2}$
- $c(V_{\mathrm{KHP}}) = \frac{\partial(C_{\mathrm{NaOH}})}{\partial(V_{\mathrm{KHP}})} = 2.3525 \ \frac{mol}{l^2}$
- $c(V_{\mathrm{NaOH.St}}) = \frac{\partial(C_{\mathrm{NaOH}})}{\partial(V_{\mathrm{NaOH.St}})} - 2.208920188 \ \frac{mol}{l^2}$

in which all of the digits were retained for further calculations.

Applying equations (3) and (4), c_{NaOH} resulted as **9.40×10^{-3} mol/l** and the combined uncertainty as **1.3×10^{-4} mol/l**.

- Resuming the topic of the uncertainty calculation of $y_{\mathrm{SO2.OIV}}$, the uncertainty of V_{wine} was evaluated considering the limits of accuracy of the volumetric pipette, reported by the manufacturer. For the volume value of 4.9800×10^{-2} l this value was $\pm\ 5.0\times10^{-5}$ l. Assuming a triangular distribution, a standard uncertainty $u(V_{\mathrm{wine}}) = 5.0\times10^{-5}/\sqrt{6} =$ **2.0×10^{-5} l**.

In Table 12 the values and the standard uncertainty of the four variables which contributed to $y_{\mathrm{SO2.OIV}}$ was summarized.

Table 12: Values, distributions and standard uncertainties of the four variables which contributed to the total calculation of $y_{SO2.OIV}$

Table taken from [303]

Variable	Description	Value, X	Distribution	Standard uncertainty, u	Unit
MM_{SO2}	Molar mass of SO_2	64.0663	Almost-rectangular	4.9×10^{-3}	g/mol
V_{NaOH}	Volume of NaOH used for the titration	2.3700×10^{-2}	Normal	3.4×10^{-5}	l
c_{NaOH}	Concentration of NaOH solution	9.40×10^{-3}	Normal	1.3×10^{-4}	mol/l
V_{wine}	Volume of wine simulant sample	4.9800×10^{-2}	Triangular	2.0×10^{-5}	l

By the uncertainty propagation law, the combined uncertainty of $y_{SO2.OIV}$, $u(y_{SO2.OIV})$ was:

$$u(y_{\mathrm{SO2.OIV}}) = \sqrt{(c(MM_{\mathrm{SO2}})^2 \cdot u(MM_{\mathrm{SO2}})^2 + c(V_{\mathrm{NaOH}})^2 \cdot u(V_{\mathrm{NaOH}})^2 + c(c_{\mathrm{NaOH}})^2 \cdot u(c_{\mathrm{NaOH}})^2 + \cdots \overline{\ldots + c(V_{\mathrm{wine}})^2 \cdot u(V_{\mathrm{wine}})^2})}$$

where:

- $c(MM_{\mathrm{SO2}}) = \frac{\partial(y_{\mathrm{SO2.OIV}})}{\partial(MM_{\mathrm{SO2}})} = 2.237369725\ \frac{mol}{l}$
- $c(V_{\mathrm{NaOH}}) = \frac{\partial(y_{\mathrm{SO2.OIV}})}{\partial(V_{\mathrm{NaOH}})} = 6048.101266\ \frac{g}{l^2}$
- $c(c_{\mathrm{NaOH}}) = \frac{\partial(y_{\mathrm{SO2.OIV}})}{\partial(c_{\mathrm{NaOH}})} = 15232.73114\ \frac{g}{mol}$
- $c(V_{\mathrm{wine}}) = \frac{\partial(y_{\mathrm{SO2.OIV}})}{\partial(V_{\mathrm{wine}})} = -2878.313253\ \frac{g}{l^2}$

in which all of the digits were retained for further calculations.

$y_{SO2.OIV}$ resulted of 143.3 mg/l and the combined uncertainty of 1.9 mg/l. The expanded uncertainty ($k = 2$) was evaluated of 3.9 mg/l.

The expanded uncertainty is defined by the VIM as the "product of a combined standard measurement uncertainty and a factor larger than number one" where "the factor depends upon the type of probability distribution of the output quantity in a measurement model and on the selected coverage probability" [1]. Therefore, the expanded uncertainty provides an interval that may be expected to encompass a large fraction of the distribution of values that could reasonably be attributed to the measurand. In general, the main contributes of a total uncertainty budget are due to repeatability, instrumental resolution, the use of CRM and/or the instrument calibration. In chemistry, usually, the only considered contribute is the measurement repeatability, which is expressed as a standard deviation, as shown in the comparison of Section 4.3. This is justified by the fact that it is usually the most relevant contribution. However, the repeatability represents only one of the numerous sources of uncertainty that affect a measure and thus a rigorous assessment of the measurement uncertainty associated with a measurement result should always be performed.

4.4.7 Conclusion and future perspectives

In addition to the definition of the maximum recovery of free SO_2 concentration achieved by the official OIV-OENO 591A-2018 method, the evaluation of the measurement uncertainty of the results obtained on a specific batch using INRiM apparatus in particular repeatability conditions was performed. This allowed to anchor the measurement results of sulfur dioxide concentration to the SI Units.

For this purpose, the measurement uncertainty associated with the $y_{SO2.OIV}$ value achieved in the comparison by the INRiM equipment was strictly determined. Applying the OIV method during the comparison, the value of $y_{SO2.OIV}$ reached at INRiM was 143.3 mg/l, against the gravimetric value of 150.1 mg/l. Therefore these measurements were precise but not accurate with respect to the gravimetric value taken as a reference. The associated expanded uncertainty was established equal to 3.9 mg/l, that meant the 2.7 %.

By the law of uncertainty propagation, it was possible to establish the contribution that affect the most the final result. It was made by considering, for each variable, the product of its sensitivity coefficients for the corresponding

standard uncertainty. It resulted that the most impactful contribution was the molar concentration of NaOH solution needed for the titration of sulfur acid.

To the best of my knowledge, the most detailed and complete evaluation of the measurement uncertainty of sulfur dioxide in the wine simulant solution to date has been described in this work. The accurate estimate of free SO_2 concentration achieved by the measurement comparison and the evaluation of the measurement uncertainty here described were fundamental output to strengthen the effort provided by the OIV and to enhance the reliability of the results. This is a crucial issue since the OIV method is internationally recognised as the official one for the quantification of SO_2 in wine matrices.

As a future perspective, this work could be extended to the evaluation of the measurement uncertainty of SO_2 in free and total forms in real samples of wine. This study would be essential to provide reliability and comparability in time and space of the results obtained applying the OIV official methods for SO_2 determination.

Moreover, this performed activity can be also considered from another point of view: as a feasibility study for a future production of a certified reference material (CRM) for the concentration of SO_2 in wine simulant. For the comparison of Section 4.3 and for the evaluation of the measurement uncertainty here tackled, a home-made wine simulant solution was used as a sample since no reference material of sulfur dioxide in wine or wine simulant were available. This wine simulant solution can be considered as a sort of candidate CRM. Given the need of certified reference materials and their growing demand in the wine sector, a future perspective is to face the metrological steps to produce such CRMs at INRiM. The equation model used to determine the estimate of the CRM, x_{CRM}, was the following:

$$x_{CRM} = x_{char} + \delta x_{bb} + \delta x_{stab}$$

where:

- x_{char} is the value of the property obtained from the characterization, which corresponded to $y_{SO2.OIV}$ reached at INRiM in this case;
- δx_{bb} is the error term related to the homogeneity test,
- δx_{stab} is the error term related to the long term stability test.

The error terms were usually zero but their uncertainties had to be considered.

In this respect, the already mentioned homogeneity and stability tests (Section 4.3.5) and the skills acquired during this work will be of paramount importance. Indeed, even if the criteria prescribed by the UNI CEI EN ISO 17034:2017 [313] have not been completely addressed, this work can be considered as a feasibility study for the future production of CRMs of SO_2 in wine simulant. The commutability of the wine simulant solutions used for the homogeneity and the stability studies with the wine simulant solution used for the comparison and the evaluation of the measurement uncertainty was considered acceptable. The uncertainty contributions of homogeneity and stability were reported respect to the $y_{SO2.OIV}$ achieved at INRiM, i.e. 143.3 mg/l, and resulted 0.9 mg/l and 1.0 mg/l respectively. Therefore, it was possible to assume a value of expanded uncertainty for that batch of hypothetic CRMs of SO_2 in wine simulant, u_{CRM}, of 4.8 mg/l. This result was obtained by the formula:

$$u_{\mathrm{CRM}} = \sqrt{u^2_{y_{\mathrm{SO2.OIV}}} + u^2_{\mathrm{Hom}} + u^2_{\mathrm{Stab}}}$$

where:

- $u_{ySO2.OIV}$ is the uncertainty of free SO2 quantification in wine simulant solution with the INRiM apparatus by the OIV-OENO 591A-2018 method achieved in this work,
- u_{Hom} is the uncertainty related to the homogeneity study on wine simulant solution (Section 4.3.5),
- u_{Stab} is the uncertainty related to the long term stability study on wine simulant solution (Section 4.3.5).

4.5 In liquid SERS quantification of SO_2 in wine

The work described in this chapter was also published in the paper: “Direct quantification of sulfur dioxide in wine by Surface Enhanced Raman Spectroscopy” published on Food Chemistry in 2020 [47].

4.5.1 Scope of the work

Although OIV provides official methods for the determination of sulfur dioxide in wine and some other techniques are available, as reported in Section 4.2, the development of methods that require minimal pre-treatment of the sample and a more rapid and *in situ* quantification of SO_2 are still required.

A technique that meets these requirements is the Surface Enhanced Raman Spectroscopy (SERS). Moreover, SERS provides high selectivity, due to the typical molecular fingerprint supply by Raman spectroscopy, and high sensitivity, due to the enhancement of the signal generated by the use of plasmonic metal nanostructures [67], [84]. For these reasons, SERS technique is applied in food analysis [89]. Two examples of its application for sulfites determination in wine with solid substrates were already published in literature [314], [315]. They used ZnO nanostructures with a sea urchin-like shape and covered by AuNPs as substrate for the detection of SO_2.

As explained in Section 2.7, in this work a liquid SERS method for the direct determination of total SO_2 in wine with AgNPs colloidal suspension was presented. This approach did not require preliminary extraction of SO_2 from the samples but only a pre-cleaning of the matrices by cartridges for solid-phase extraction (SPE) to limit the presence of interference molecules. The interaction in hydroalcoholic solution of the SO_2 analyte with colloidal suspensions of AgNPs with nominal diameters of 4, 30 and 55 nm was investigated and the smallest AgNPs resulted the best substrate for this in liquid SERS analysis. Thus, 4 nm AgNPs were used for further inquiries in wine simulant solution and then for quantification of SO_2 in red and white wines. To limit the interferences of the matrices in the analyses, the method of standard additions was chosen.

The official OIV-OENO 591B-2018 method [292] was applied at CREA of Asti on the same wine samples. The results achieved at INRiM by the in liquid SERS method was compared with those obtained applying the OIV method.

In this work, a rigorous evaluation of the measurement uncertainty was not performed for the following reasons:

- This work was performed before the evaluation of measurement uncertainty of free SO_2 concentration at INRiM on the basis of the OIV method,
- The results obtained by the official OIV method were provided by CREA of Asti, where the measurement uncertainty was not carried out since it is not required by the method,
- The evaluations reported in Section 4.4 concerned only the free form of SO_2 in wine simulant while in this work the total SO_2 in real matrices of wine was considered,

- The evaluation of the measurement uncertainty related to a complex system such as the in liquid SERS was not yet performed.

For these reasons, the standard deviation was considered as the only uncertainty contribution to compare the results obtained by the two techniques.

4.5.2 Chemicals

The solutions and the AgNPs suspensions were prepared with ultra-pure water. The reagents adopted were at high purity level. The reagents used for the synthesis of AgNPs are described in Section 2.2. The hydroalcoholic solution used as the most simplified model contained water and ethanol (Carlo Erba) at 12 % v/v. The reagents for the wine simulant solution and for the application of the OIV method are reported in Section 4.3.2.

4.5.3 Preparation of wine simulant solution

The wine simulant solution used in this study was prepared according to the protocol reported in Section 4.3.2. Solutions with different concentrations of SO_2 were achieved by applying equation (1) in Section 4.3.3.

4.5.4 Synthesis and characterization of AgNPs colloidal suspensions

AgNPs were synthetized with nominal diameter of 4, 30 and 55 nm according to the procedures described in Section 2.3. The AgNPs with the three dimensions were characterized with the methods reported in Section 2.4.

4.5.5 Pre-cleaning of wine samples and preparation of the AgNPs – SO_2 mix for wine sample analysis

The wine samples were purchased in a local market. They were Chardonnay, Grillo and Favorita (white wines) and Dolcetto, Chianti and Freisa (red wines).

Before the analyses, wine samples were pre-cleaned using cartridges for solid-phase extraction. The cartridges ISOLUTE C18 (EC) 1 g/6 ml from Biotage were adopted. This type of cartridges contains a retentive and non-polar sorbent able to extract acidic, neutral and basic analytes from aqueous matrices. The non-polar retention mechanism is exploited to enhance the level of purity of the extracted wine samples.

The procedure for using the cartridges was:

- Activate with 5 ml of methanol,
- Wash with 5 ml of water,
- Pass 5 ml of the wine sample at atmospheric pressure,
- Wash with 5 ml of water.

At the end of this process, the wine samples resulted in a dilution factor of 1:2. Then, each AgNPs – SO_2 mix for analysis was prepared by adding in sequence 1.50 ml of AgNPs liquid suspension, 1.45 ml of pre-treated wine and a spike of 50 µl of hydroalcoholic solution with high concentration of SO_2. After these steps, the wine samples reached an overall dilution factor of 4.14. The final concentrations of SO_2 solutions obtained in the mix solutions for these standard additions of sulfites were 10 mg/l, 20 mg/l, 30 mg/l, 40 mg/l, 50 mg/l.

All the wines were analysed in triplicate.

4.5.6 UV-Vis spectroscopy

The UV-Vis spectra were acquired with the instrument and the setup described in Section 2.4.1.

The UV-Vis spectra of diluted AgNPs were obtained as described in Section 2.4.1. The other UV-Vis spectra were obtained as followed:

- for the two simplified models of wine (hydroalcoholic and wine simulant solutions) used in this work and for all the three sizes of nanoparticles, the interaction AgNPs – SO_2 was analysed by mixing the two liquid components in ratio 1:1 and then diluted accordingly to Section 2.4.1,
- for all the wine samples with different concentration of added sulfites and for all the three sizes of nanoparticles, the AgNPs – SO_2 mixes of Section 4.5.5 were used for analysis.

4.5.7 SERS method

A DXR Raman spectrometer of Thermo Fischer Scientific was used to collect SERS spectra. It was equipped with a 532 nm wavelength excitation laser source and with a charge-coupled device (CCD) as a detector. A calibration tool that is software-controlled was used weekly to calibrate the instrument. It provided the

calibration of wavelength by multiple neon emission lines, of laser frequency by multiple polystyrene Raman peaks and of intensity of CCD by white light source. The 5 cm^{-1} of grating resolution was considered as frequency uncertainty while intensity uncertainty was < 5 %.

The in liquid measurements were conducted in quartz cuvette with the help of a specific accessory, as described in Section 3.5.8 and shown in Figure 24. The AgNPs – SO_2 mix for analysis was prepared as followed:

- for the two simplified models of wine (hydroalcoholic and wine simulant solutions) used in this work and for all the three sizes of nanoparticles, by mixing the two component in ratio 1:1,
- for all the wine samples with different concentration of added sulfites and for all the three sizes of nanoparticles, as reported in Section 4.5.5.

The instrument set up was: laser power at 10 mW, 50 μm of rectangular aperture, spectral range of 50 – 3400 cm^{-1}, 1 s for 50 exposures of acquisition time.

At least three repetitions of each measurement was performed to establish the repeatability. The intensity of the SERS peaks of the AgNPs – SO_2 mixes were plotted as a function of the increasing concentration of sulfur dioxide. The CCC software developed at INRiM [316] was employed to calculate the linear fit by weighted total least square (WTLS) regression. WTLS was employed to maximize the efficiency of the parameter estimation in cases where the data should not be treated equally due to their varying quality. The weights associated to each observation reflected the precision of the information contained in them and their contribution to the final estimate. This approach was useful for small data sets, as in this case [317]. With the CCC software, the standard deviation on the y axis, related to the measurement repeatability, was considered. The concentrations of SO_2 initially present in the wine samples were calculated by negative extrapolation to $y = 0$ and multiplied for the dilution factor. The NIST Uncertainty Machine [318] was exploited to propagate the uncertainty fit by the Monte Carlo method, as reported in the guidelines of the GUM [306].

For each sample of wine, the limit of detection (LOD) was calculated by the formula $LOD = 3sd_{blank}/b$ [319], where sd_{blank} was the standard deviation of the data obtained on the sample of blank and b was the slope of the experimental fit.

4.5.8 OIV method

A comparison between the quantification achieved by the proposed in liquid SERS innovative method and the results obtained applying the official OIV method for total SO_2 [292] was carried out on the same samples.

This experimental part was performed at CREA thanks to the collaboration with Dr Maurizio Petrozziello. The apparatus used by this institute was the same that they employed for the measurement comparison of Section 4.3. However, in this case, the procedure adopted was the one for the total SO_2 [292]. It differed from the procedure for free SO_2 for the operative temperature, which was 100 °C.

4.5.9 Results and discussion

Characterization of AgNPs colloidal suspensions

The results of the characterization of nominal 4, 30 and 55 nm AgNPs were reported in Section 2.5.

AgNPs – SO_2 interaction in hydroalcoholic solution

As mentioned in Section 2.6, if there is a good affinity between the analyte and the nanoparticles, the agglomeration of the latter leads to an appreciable SERS signal [113].

As a first model system to investigate the interaction between the AgNPs and the sulfites, the hydroalcoholic solution was chosen since it is the most simplified version of wine. In this environment, it was possible to assess the different reactivity of the AgNPs of different size with respect to the specific analyte SO_2. It was performed by UV-Vis and SERS spectra, as shown in Figure 43.

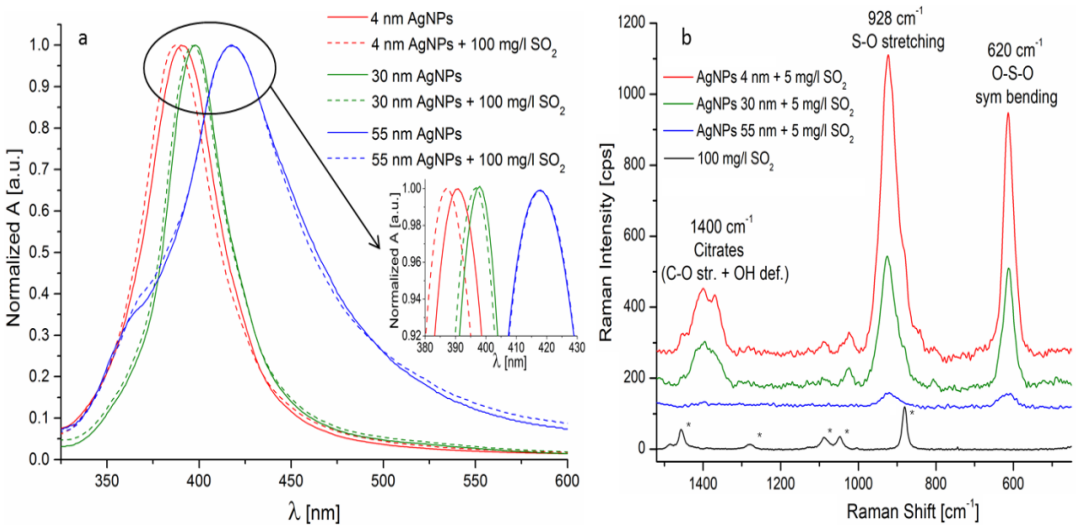


Figure 43: AgNPs – SO_2 interaction in hydroalcoholic solution

Figure 43: a) Normalized UV-Vis spectra of diluted 4, 30 and 55 nm AgNPs colloidal suspensions (solid lines) and of the mix 4, 30 and 55 nm AgNPs – SO_2 100 mg/l solution (dash lines); b) SERS spectra of 4, 30 and 55 nm AgNPs – SO_2 5 mg/l solution and Raman spectrum, without NPs, of SO_2 100 mg/l. The * labeled peaks referred to EtOH. (In Table 13 the assignment of the vibration modes of SO_2, citrates and ethanol were summarized). Image taken from [47]

In Figure 43 a, the normalized UV-Vis spectra of diluted 4, 30 and 55 nm AgNPs colloidal suspensions were reported with red, green and blue solid lines, respectively. The spectra of the same 4, 30 and 55 nm AgNPs mixed with SO_2 solution at 100 mg/l were reported in red, green and blue dash lines, respectively. In Figure 43 b, SERS spectra of 4, 30 and 55 nm AgNPs mixed with SO_2 solution at 5 mg/l were reported in red, green and blue lines, respectively. The SO_2 concentration of 5 mg/l represented the inferior part of the dynamic range of interest in this study and was therefore selected to assess the performance of this SERS method toward lower concentrations. A Raman spectrum of 100 mg/l SO_2 solution was reported in Figure 43 b in black line. It demonstrated that, without the nanoparticles, the characteristic bands of SO_2 were not revealed and the only considerable peaks were those of ethanol.

The most important output from Figure 43 was the different AgNPs – SO_2 interaction depending on the size of the nanoparticles. The mix 55 nm AgNPs – SO_2 did not provoke a relevant modification of the UV-Vis spectra compared to the corresponding pure AgNPs. Conversely, the mix 4 nm AgNPs – SO_2 and the

mix 30 nm AgNPs – SO_2 showed a LSPR blue-shift. In the case of 4 nm AgNPs, this progressive blue shift was highlighted in Figure 44.

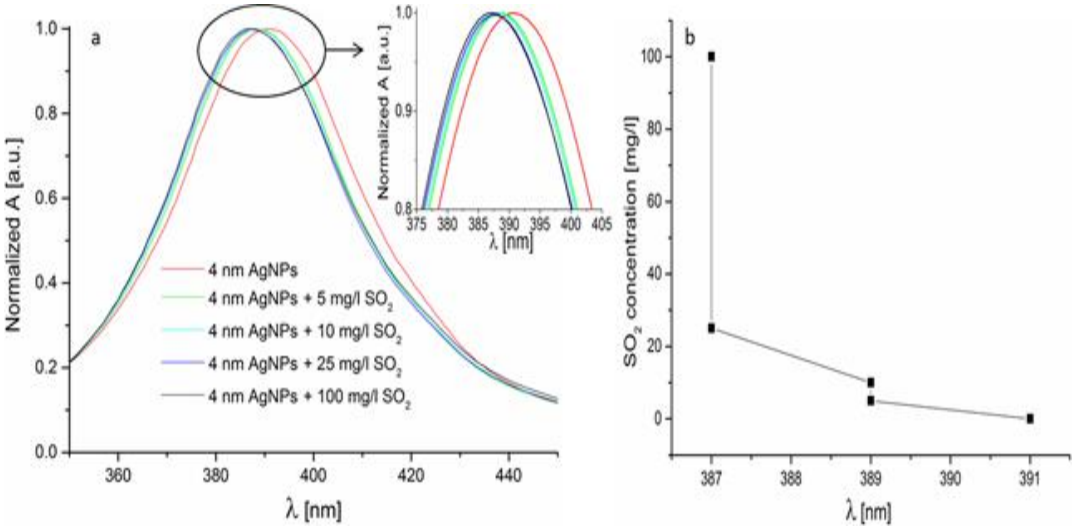


Figure 44: Progressive blue shift of 4 nm AgNPs LSPR

Figure 44: a) Progressive blue shift of LSPR in the UV-Vis spectra for the mixes of 4 nm AgNPs – SO_2 in the range 0-100 mg/l; b) Wavelengths of LSPR of 4 nm AgNPs at each SO_2 concentration point. Image taken from [47]

At SO_2 concentration of 100 mg/l, the LSPR shift was of 4 nm. To justify this experimental evidence, it had to be considered that sodium citrate was adopted as reducing and stabilizing product during the synthesis of AgNPs. As a consequence, AgNPs presented a weakly bound shell of citrate ions [67]. However, sulfur had a chemical affinity toward Ag and thus the citrate ions were exchanged with SO_2 molecules on the AgNPs surface. As a consequence, the shell was modified and the global diameter of the nanoparticles decreased, resulting in the observed blue shift. This phenomenon was probably more evident in the case of 4 nm AgNPs since the change of shell dimensions mostly affected the smallest nanoparticles. It would been interesting to try to observe this diameter shrinking of the AgNPs by TEM. Moreover, as a future perspective, a Mie-model could be used to assess if the change of the dielectric constant of the liquid medium induced by the addition of sulfites could justify the blue shift of the AgNPs.

In agreement with the UV-Vis considerations, the SERS spectra of Figure 43 b highlighted two intense peaks of SO_2. They were attributable to the following vibrational modes [314], [315]:

- the O-S-O symmetric bending mode at 620 cm^{-1},

- the S-O stretching symmetric and asymmetric modes at 928 cm^{-1}. This band presented a left shoulder due to an ethanol signal (~ 900 cm^{-1}) in the lower SERS intensity spectra.

In Table 13 the Raman peaks related to SO_2, citrates and ethanol were summarized.

Table 13: Assignment of the vibrational modes and positions of the peaks of SO_2, citrates and ethanol

Molecule	Vibrational mode	Raman shift [cm^{-1}]
SO_2	O-S-O symmetric bending [314], [315]	620
SO_2	S-O stretching symmetric and asymmetric [314], [315]	928
Citrates	CO stretching combined with OH deformation	1400
EtOH	CCO symmetric stretching [320]	~ 890
EtOH	CO stretching [320]	~ 1050
EtOH	CCO stretching [320]	~ 1100
EtOH	CH_2 deformation [320]	~ 1290
EtOH	CH_3 asymmetric deformation [320]	~ 1460

Among the SERS spectra of Figure 43 b, the highest peaks were those of 4 nm AgNPs – SO_2 mix while almost barely identifiable peaks were obtained for 55 nm AgNPs – SO_2 mix.

Probably, the 4 nm AgNPs conducted to the greatest interaction with SO_2 thank to their highest surface area compare to the other AgNPs, as reported in Table 1 of Chapter 2. As a consequence of the different behaviours of the three

AgNPs respect to the mix with SO_2, the 4 nm AgNPs were chosen for the subsequent experiments.

AgNPs – SO_2 interaction in wine simulant solution

To make the model system more similar to the real wine matrix, a wine simulant solution was exploited. In this environment, even in absence of SO_2, a considerable agglomeration of AgNPs caused the variation from yellow to red of the solution colour. Indeed, this agglomeration was evinced in the UV-Vis spectrum from the decrease of the main absorption peak intensity for 4 nm AgNPs and from the rise of a shoulder at 530 nm, as shown in Figure 45 a (solid purple line).

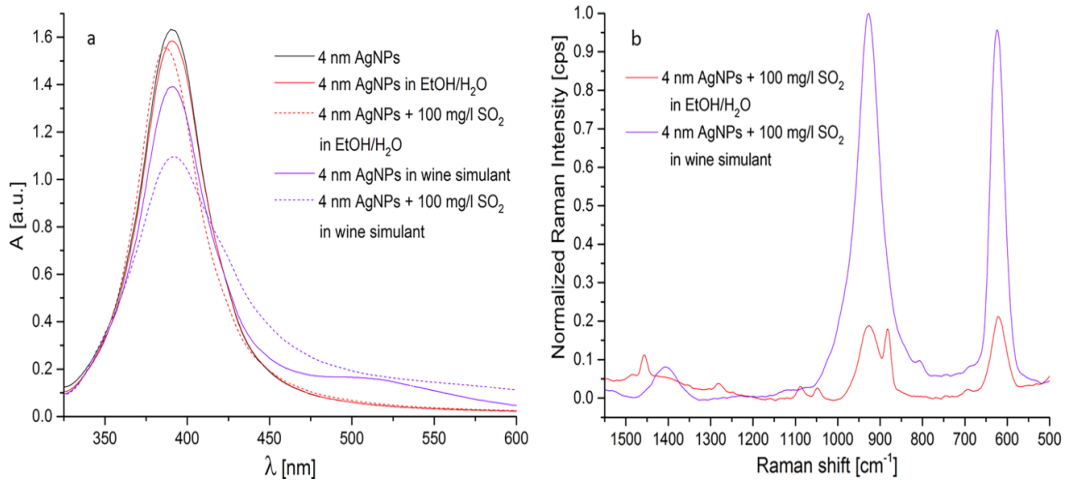


Figure 45: AgNPs – SO_2 interaction in wine simulant solution and comparison with hydroalcoholic solution

Figure 45: 4 nm AgNPs – SO_2 interactions in hydroalcoholic solution (red lines) and in wine simulant solution (purple lines). a) UV-Vis spectra of 4 nm AgNPs without SO_2 and of 4 nm AgNPs – SO_2 100 mg/l; b) Normalized SERS spectra of 4 nm AgNPs – SO_2 100 mg/l. Image taken from [47]

In presence of the 4 nm AgNPs – SO_2 mix, a strong agglomeration occurred and the colour of the wine simulant solution became dark green. This was reflected in the UV-Vis spectrum in the broadening and lowering of the absorption peak, as shown in Figure 45 a (dash purple line). In Figure 45 a, as a comparison, were also reported the spectra of dilute 4 nm AgNPs in water (black line) and of 4 nm AgNPs without SO_2 and with 100 mg/l of SO_2 in hydroalcoholic

solution (solid and dash red lines, respectively). The pH of the wine simulant solution was around 3 and influenced the AgNPs surface charge. Citrate acid presented three pK_a due to its carboxylic groups (pK_{a1} = 3.13, pK_{a2} = 4.76 and pK_{a3} = 6.34) [321]. Therefore, at the pH typical of wine, all these groups were protonated, the repulsive forces among nanoparticles were reduced and the agglomeration were promoted. Furthermore, thanks to the chemical affinity between S and Ag, a great interaction between analyte and substrate occurred, as monitored by UV-Vis spectra of Figure 45 a. This agglomeration was confirmed by SERS measurements in which the generated hot-spots provoked the enhancement of the sulfites signals (see Figure 45 b). In Figure 45 b, the SERS spectra of the mix of 4 nm AgNPs – SO_2 at 100 mg/l in the wine simulant solution was compared to the same mix in hydroalcoholic solution. It was evident that in wine simulant solution the signal was about 80 % more intense than in hydroalcoholic solution. Furthermore, in wine simulant solution, the peak at 928 cm^{-1} was not flanked by the one of ethanol, as already explained before, and another band at 1400 cm^{-1} appeared. This latter band was probably attributable to the modes of CO stretching combined with OH deformation of the citrates on the AgNPs surface.

To provide a SERS quantification of sulfites in wine simulant solution, mixes of 4 nm AgNPs with SO_2 solutions at increasing concentration from 0 to 100 mg/l were analysed. For each concentration, the measurements were repeated three times and the average spectra were shown in Figure 46.

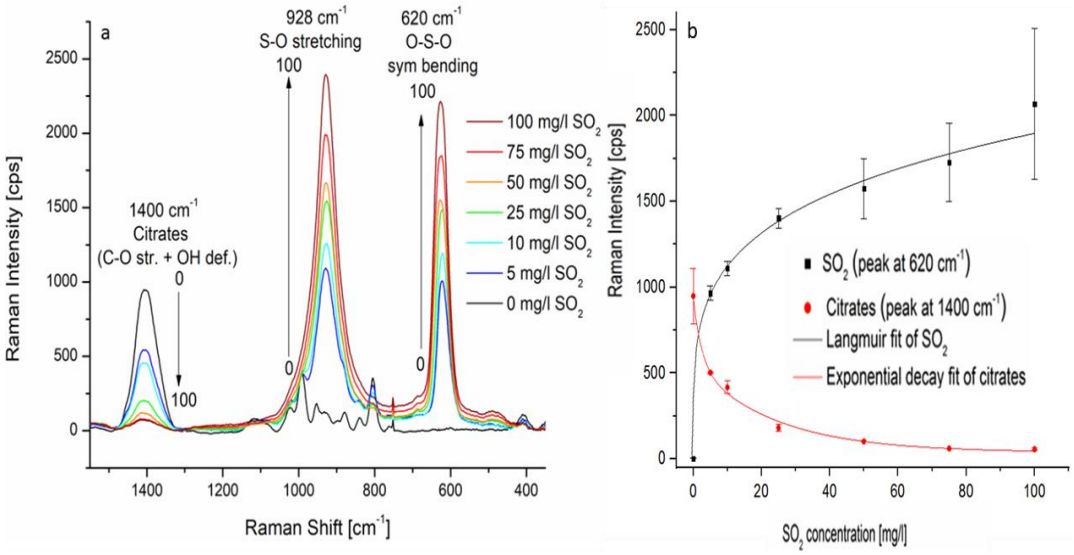


Figure 46: Quantification of SO_2 in wine simulant solution

Figure 46: a) Average SERS spectra of mix of 4 nm AgNPs – SO_2 at increasing concentration from 0 to 100 mg/l in wine simulant solution; b) Langmuir fit with standard deviations (black bars) of the Raman intensities of O-S-O symmetric bending mode at 620 cm^{-1} and exponential decay fit with standard deviations (red bars) of the Raman intensities of CO stretching combined with OH deformation of the citrates at 1400 cm^{-1}. Image taken from [47]

In Table 14 the average intensities of the two peaks related to SO_2 at different concentration were reported together with their standard deviation.

Table 14: Average SERS intensity, standard deviation and relative standard deviation (RSD) of the 620 cm^{-1} and 928 cm^{-1} peaks at increasing SO_2 concentration in wine simulant solution.

Table taken from [47]

Concentration of SO_2 [mg/l]	**Intensity at 620 cm^{-1} [cps]**	**Standard deviation [cps]**	**Relative standard deviation %**	**Intensity at 928 cm^{-1} [cps]**	**Standard deviation [cps]**	**Relative standard deviation %**
5	965.4	42.3	4.4	1003.0	44.7	4.5
10	1109.6	41.3	3.7	1131.0	39.4	3.5
25	1402.2	57.6	4.1	1424.9	32.7	2.3
50	1574.3	174.7	11.1	1656.0	188.5	11.4
75	1727.4	227.3	13.2	1827.9	256.2	14.0
100	2067.8	441.2	21.3	2193.8	484.6	22.1

For both the vibrational modes related to SO_2 (620 and 928 cm^{-1}), the intensity of the peaks increased with the concentration of SO_2 in wine simulant solution. The curve obtained by the experimental data was a Langmuir fit with 0.94 as correlation factor, as reported in Figure 46 b for peaks at 620 cm^{-1}. This kind of fit is characteristic of adsorption-desorption phenomena [322]. Otherwise, the peaks of citrate at 1400 cm^{-1} displayed an opposite trend that can be

attributable to their progressive substitution on the AgNPs surface with SO_2 molecules. It is noteworthy that beyond the SO_2 concentration of 25 mg/l the following experimental evidences were observed:

- the exponential decay fit of citrates reached a plateau,
- no more blue shift of the 4 nm AgNPs LSPR in the UV-Vis spectra occurred, as shown in Figure 44,
- the peak at 620 cm^{-1} slightly shifted in the direction of higher frequencies, as shown in Figure 47 c. This evidence could be attribute to the adsorbate-adsorbate interactions that occurred at the surface of the nanoparticles [323] and was probably related to the bending mode and not to the stretching mode (Figure 47 b) for reasons related to the directions of movement of the atoms,
- the relative standard deviation increased, as reported in Table 14 and can be observed by the standard deviation bars on the Langmuir fit of Figure 46 b. In particular, for the last three points (50, 75 and 100 mg/l), the raise of the SO_2 concentration implied a strong clustering of AgNPs which made the suspension unstable. These clusters were subjected to fluctuation over time and the density variation of them led to differences in the SERS signal intensities.

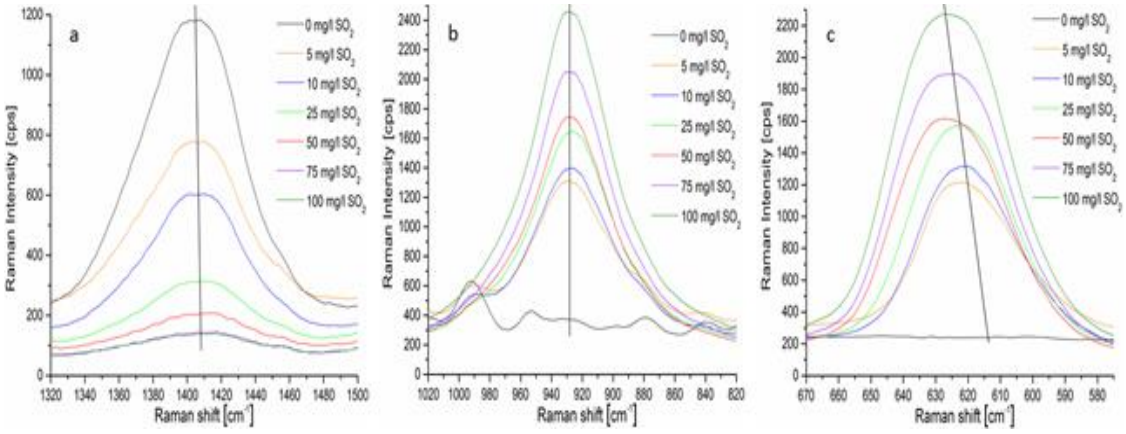


Figure 47: Details of the three SERS peaks of Figure 46 in wine simulant solution at different SO_2 concentration
Figure 47: a) Peaks at 1408 cm^{-1} of citrates, b) Peaks at 928 cm^{-1} of S-O stretching mode; c) Peaks initially at 622 cm^{-1}, and then, over 25 mg/l of SO_2, shifting at 626 cm^{-1} of O-S-O bending modes. Image taken from [47]

Putting together all these information, the SO_2 concentration of 25 mg/l could be considered as s threshold. Indeed, at this concentration, on the AgNPs surface

a sort of equilibrium between completely removed citrates and absorbed SO_2 was reached. However, since citrates had a greater steric hindrance than SO_2, their removal generated a free surface on the AgNPs. Other SO_2 molecules could be absorbed on this free surface, as demonstrated by the rise of the SERS intensity at 620 cm^{-1} and 928 cm^{-1} with the increase of the sulfites concentration. The greater proximity between the adsorbed SO_2 molecules therefore affects the bending mode and leads to the shift of the peak to 620 cm^{-1} (Figure 47 c). Overall, therefore, beyond the threshold of 25 mg/l of SO_2 the sample solution became more unstable.

Pre-cleaning of the wine samples

In real wines, the multitude of molecules found in the matrix represent a problem for the correct quantification of SO_2. Indeed, some of these chemical components can interfere with the target analyte and negatively influence its identification and quantification. For these reasons, a pre-cleaning of the wine matrices was performed by C18 SPE cartridge. On the base of its characteristics, the cartridge is able to retain interfering molecules thanks to the affinity with the functional groups of the solid sorbent packed inside it and to return a purified sample [324], [325]. This purification step is quite common for the analysis in the oenological sector [286], [326].

In this work, SPE was used for an unspecific pre-cleaning process of the wine samples in which organic compounds such as polyphenols, terpenes and many others were retained by the cartridge unlike the sulfur dioxide which passed through. To verify the percentage of SO_2 recovery, measurements using the apparatus related to the OIV method were performed before and after the SPE pre-cleaning step. A red wine was chosen for this test because this type of matrix contains more interfering molecules than the white wines. The results were reported in Table 15 and demonstrated that SO_2 were not restrained by the SPE during the pre-cleaning of the samples.

Table 15: Concentration of SO_2 in red wine before and after the SPE pre-cleaning step obtained by OIV methods.

Table taken from [47] and adapted.

Measure n°	Concentration of SO_2 before SPE [mg/l]		Concentration of SO_2 after SPE [mg/l]		Recovery %	
	Free SO_2	Combined SO_2	Free SO_2	Combined SO_2	Free SO_2	Combined SO_2
1	9.6	32.0	9.0	33.3	93	104
2	10.2	34.6	11.5	34.6	113	100
3	10.2	38.4	10.2	34.6	100	90
Average	10.0	35.0	10.2	34.1	102	98
Standard deviation	0.4	3.2	1.3	0.7	-	-
Total SO_2	45.0		44.4		99	

Interaction of wine compounds with AgNPs

As already mentioned, the presence of a multitude of chemical compounds in wine make the quantification of SO_2 more challenging compared to the simplified model of wine previously used. Although the real wine samples were pre-cleaned, only some molecules were eliminated and, for example the organic matter of the matrices were still present. The interaction of the nanoparticles with these compounds could not be neglected. Indeed, the mix 4 nm AgNPs – wine (both red and wine) rapidly switched colour from yellow of the AgNPs to dark purple of the wine mix shown in Figure 48.



Figure 48: Cuvette with 4 nm AgNPs – wine mix

Figure 48: Dark purple colour obtained when 4 nm AgNPs (yellow) were mixed with wine sample

This resulted in a severe agglomeration of the AgNPs that was evident in the new UV-Vis band at around 570 nm in Figure 49 for the case of Dolcetto red wine.

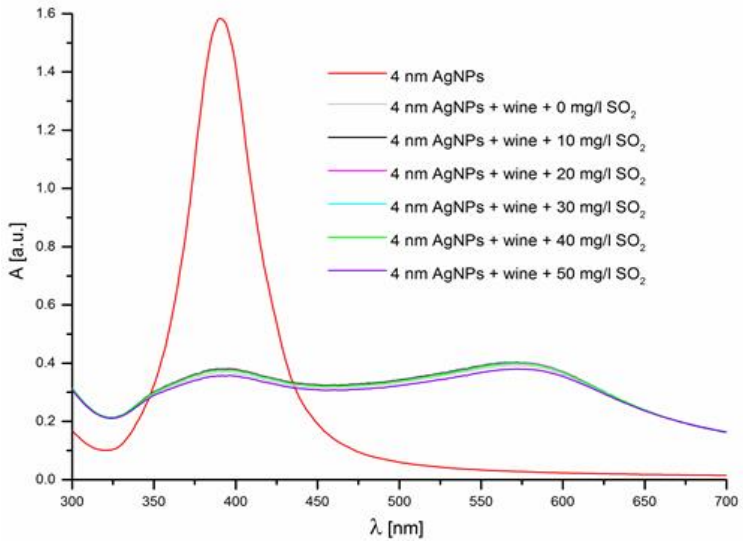


Figure 49: AgNPs – wine interaction

Figure 49: UV-Vis spectra of diluted 4 nm AgNPs and of the mix 4 nm AgNPs – Dolcetto red wine with the addition of different SO_2 concentrations. Image taken from [47]

Quantification of SO_2 in the wine samples and comparison of these results with the ones obtained by applying the official OIV OIV-OENO 591B-2018 method

The strong agglomeration that occurred when 4 nm AgNPs were mixed with wine samples resulted in SO_2 SERS peaks clearly visible. However, a not negligible variability of the SERS signals among wine samples was observed. The variability among the SERS spectra concerned the baseline, the noise signal and the peaks shape. This matrix effect could be due to the diversified organic composition of the analysed wine samples. Furthermore, even small variation of the pH value of the wine could affect the level of AgNPs agglomeration and, as a consequence, the formation of hot-spots and the intensity of the SO_2 signals. For these reasons it was not possible to exploit an unique calibration curve obtained by the wine simulant solution for all wine samples. The standard addition strategy was therefore employed for the quantification of SO_2 in red and white wines.

In Figures from 50 to 55 were reported the SERS spectra and the fits for the six wine samples analysed.

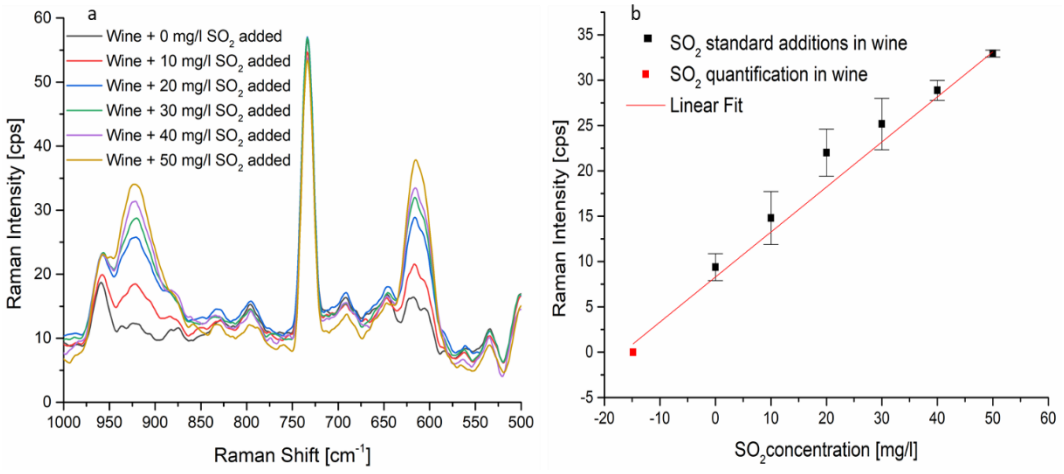


Figure 50: Quantification of total SO_2 in Chardonnay white wine by in liquid SERS method

Figure 50: a) SERS spectra of the mix 4 nm AgNPs – Chardonnay white wine with increasing concentration of SO_2; b) Linear fit of 620 cm^{-1} peaks intensities and extrapolated value of SO_2 concentration in diluted wine sample

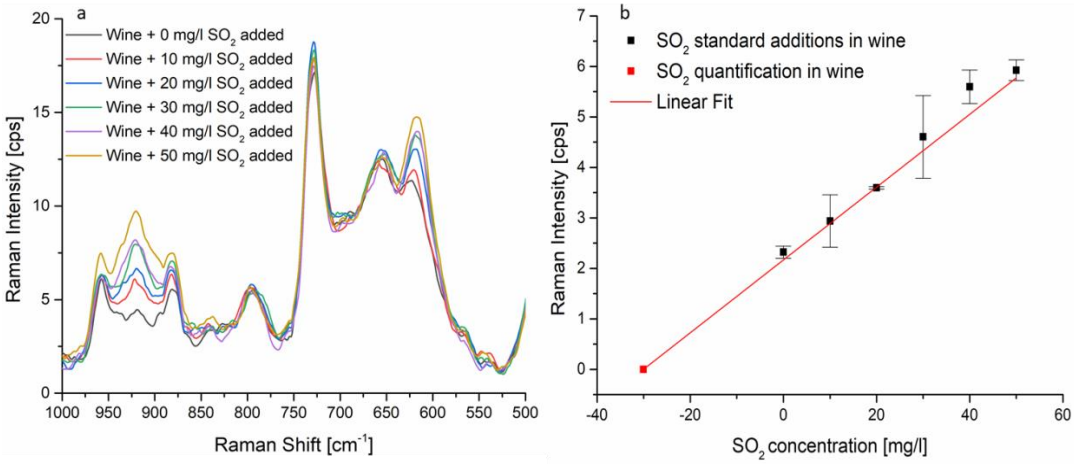


Figure 51: Quantification of total SO_2 in Grillo white wine by in liquid SERS method

Figure 51: a) SERS spectra of the mix 4 nm AgNPs – Grillo white wine with increasing concentration of SO_2; b) Linear fit of 620 cm^{-1} peaks intensities and extrapolated value of SO_2 concentration in diluted wine sample

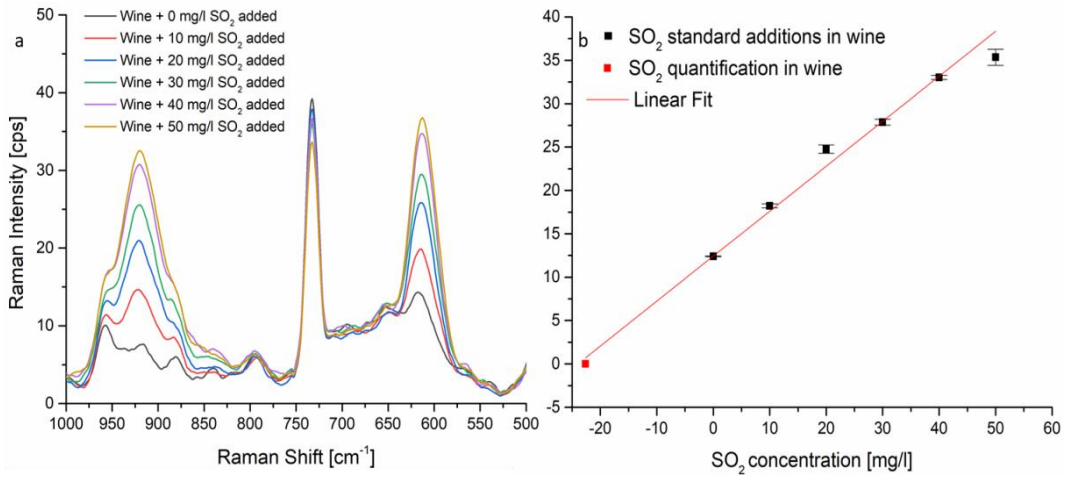


Figure 52: Quantification of total SO_2 in Favorita white wine by in liquid SERS method

Figure 52: a) SERS spectra of the mix 4 nm AgNPs – Favorita white wine with increasing concentration of SO_2; b) Linear fit of 620 cm^{-1} peaks intensities and extrapolated value of SO_2 concentration in diluted wine sample

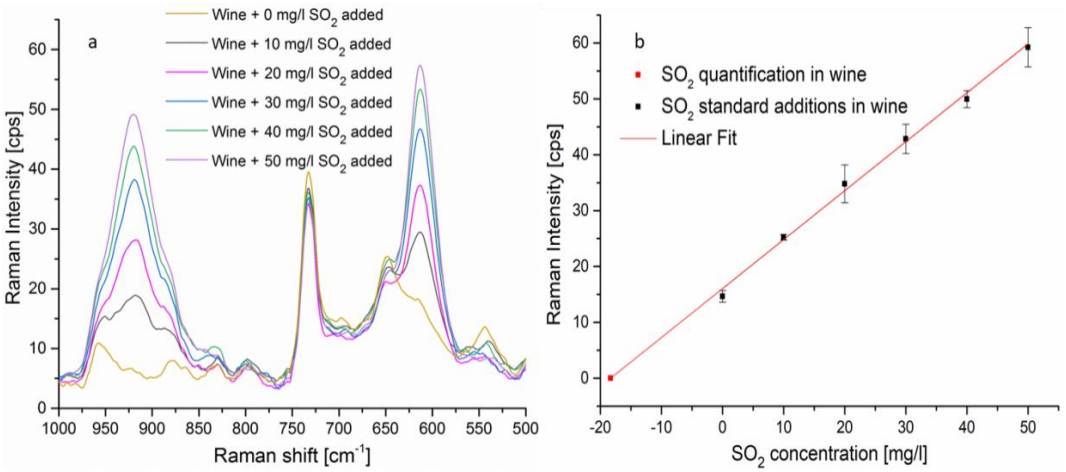


Figure 53: Quantification of total SO_2 in Dolcetto red wine by in liquid SERS method

Figure 53: a) SERS spectra of the mix 4 nm AgNPs – Dolcetto red wine with increasing concentration of SO_2; b) Linear fit of 620 cm^{-1} peaks intensities and extrapolated value of SO_2 concentration in diluted wine sample. Image taken from [47] and adapted

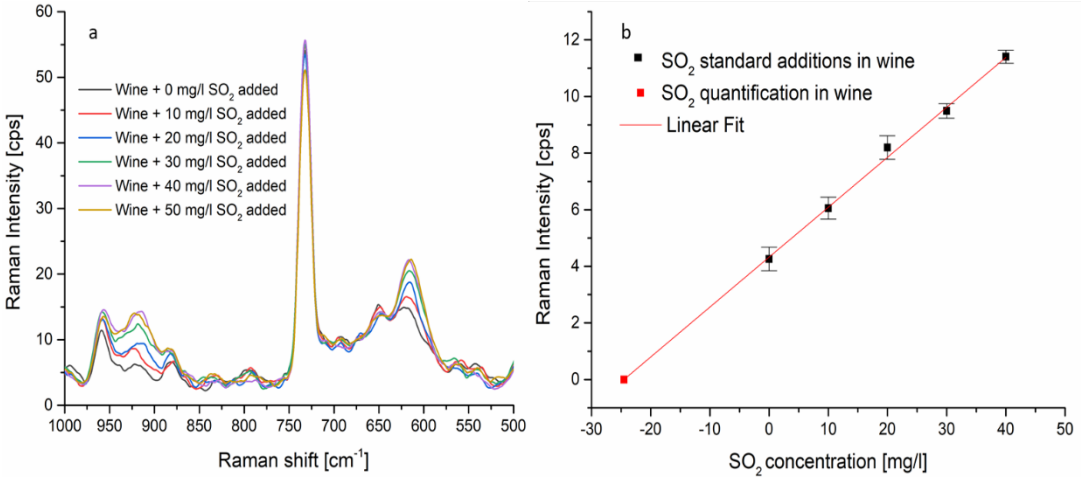


Figure 54: Quantification of total SO_2 in Chianti red wine by in liquid SERS method

Figure 54: a) SERS spectra of the mix 4 nm AgNPs – Chianti red wine with increasing concentration of SO_2; b) Linear fit of 620 cm^{-1} peaks intensities and extrapolated value of SO_2 concentration in diluted wine sample

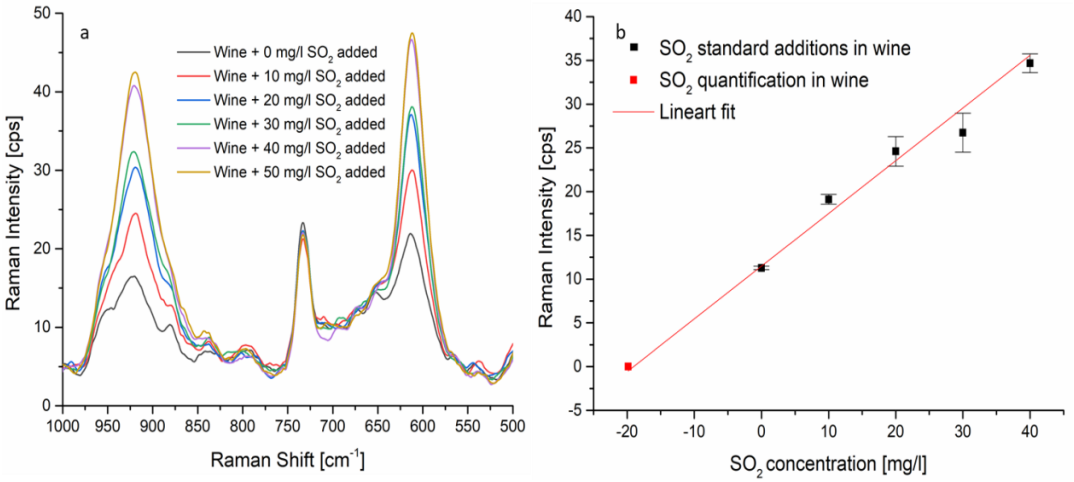


Figure 55: Quantification of total SO_2 in Freisa red wine by in liquid SERS method

Figure 55: a) SERS spectra of the mix 4 nm AgNPs – Freisa red wine with increasing concentration of SO_2; b) Linear fit of 620 cm^{-1} peaks intensities and extrapolated value of SO_2 concentration in diluted wine sample

In the part a of Figures from 50 to 55, the SERS spectra of the diluted wine sample with progressively standard addition of SO_2 from 0 to 50 mg/l are reported. It has to be considered that the wine samples were diluted of a factor of about 4 following the pre-cleaning procedure and the mix with the AgNPs. For this reason, the concentration of SO_2 added were in that narrower range. To provide the total SO_2 quantification, the intensities of the peaks at 620 cm^{-1} were considered because they were narrow and less affected by nearby peaks. In the part b of Figure from 50 to 55, the plots of these peaks as a function of the sulfur dioxide concentration are shown. As can be observed, the curves obtained by the experimental data of the real samples of wine were linear fits, instead of the Langmuir fit achieved in wine simulant solution. Indeed, thanks to the dilution of the wine samples, the range of concentration of the additions of SO_2 was 0 – 50 mg/l. This range covered the initial part of the Langmuir curve which was approximately linear. From each linear fit, the concentration of SO_2 in the diluted wine sample was extrapolated, as illustrated in the part b of Figure from 50 to 55. To go back to the real SO_2 concentration in the wine bought at the local market, the extrapolated value was multiplied for the dilution factor of 4.14. The SO_2 concentration results achived by this innovative in liquid SERS method for the six wine samples were reported in Table 16. However, the linear fit slope was different for each wine and, thus, a specific LOD was calculated for all the six analysed wine samples (Table 16).

The official OIV-OENO 591B-2018 method [292] was conducted in parallel at CREA of Asti on the same wine samples and the results achived were summarized in Table 16. This OIV method was considered, in this case, as a reference in the comparison between the two techniques.

Table 16: SO_2 quantifications in red and white wines by the proposed in liquid SERS method and by the official OIV-OENO 591B-2018 method.
Table taken from [47]

Wine	SERS LOD [mg/l]	SO_2 by SERS [mg/l]	Standard deviation [mg/l]	SO_2 by OIV method [mg/l]	Standard deviation [mg/l]	Error %
Chardonnay	9.6	61.4	1.0	64.0	3.7	4.1
Grillo	0.6	124.5	9.2	111.4	2.6	11.8
Favorita	0.6	72.7	3.9	78.0	2.5	6.8
Dolcetto	1.5	71.1	3.2	70.4	1.9	1.0
Chianti	3.9	101.5	9.3	97.9	2.0	3.7
Freisa	1.1	82.2	5.0	81.1	2.6	1.4

The comparison of the results achived by the two techniques attested a good agreement in the SO_2 quantification, as shown in Figure 56. Furthermore, all the wine samples were complient with the legal limits for SO_2 concentrations.

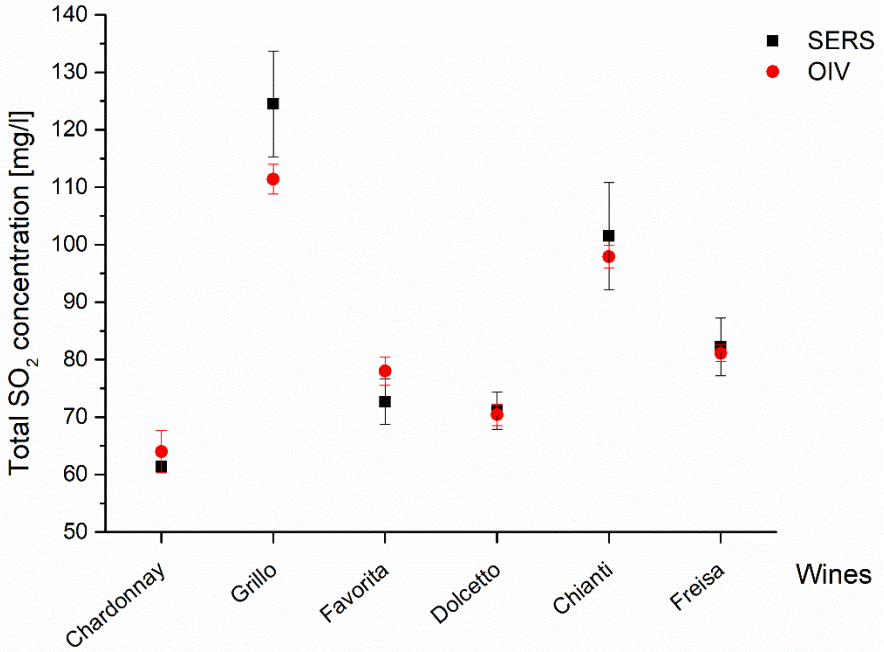


Figure 56: The comparison of the results

Figure 56: Concentrations obtained for total SO_2 in the three white wines (Chardonnay, Grillo and Favorita) and in the three red wines (Dolcetto, Chianti and Freisa) by the new in liquid SERS method and by the OIV-OENO 591B-2018 method

Taking the OIV method as a reference, the percentage errors obtained by the proposed SERS method were lower than 5 % in most cases and only for Grillo white wine was higher than 10 %. Considering only the standard deviations of the measurements carried out by the two techniques, the validity of the proposed in liquid SERS method was provided.

The errors in the quantification of SO_2 by SERS method can be attributable to numerous factors:

- First of all, the sample was subject to variation over time due to the fast agglomeration of the AgNPs. The clustering of the nanoparticles led to precipitation of the agglomerates. This inhomogeneity of the samples affected the stability of the SERS signal during the measurement. To try to overcome this problem, the AgNPs – SO_2 mixes for wine samples analyses were prepared just before the measurement and the SERS measurements were carried out in the shortest possible time (approximately 1 minute);

- The free form of SO_2 is a volatile and evaporate from the samples. This phenomenon was not relevant during the a single SERS measurement, since it last few seconds, but it could be significant throughout the entire measurement campaign on the same sample. Moreover, the wine samples were opened at CREA, where the measurements with the official OIV method were performed, and transported at INRiM where they were analysed the day after. The amount of volatilized SO_2 depended on the conditions of conservation and trasport of the samples, which were the same for all of them, and on the fraction of buond SO_2 in the wines, which was the non volatile part that strictly depended on the composition of wines. In order to minimazed the evaporation of SO_2, each measurement campaign was conducted in the shortest possible time which was 2 days and particular attention was paid to the transport and storage conditions. This aspect could justify the random underestimation/overestimation with respect to the official OIV method;
- The real wines contained different organic components that could interfere in the measure affecting the SO_2 quantification. This aspect could justify the random underestimation/overestimation with respect to the official OIV method;
- The rise in temperature could have influenced the measurement by promoting the SO_2 evaporation;
- The measurement uncertainty related to this SERS method was not evaluated. However, it was certainly greater than that of the official OIV method. As a conclusion, an uncertainty assessment of the total SO_2 concentration results achieved by both the methods should be done in order to reliably compare the results.

4.5.10 Conclusions and future perspectives

To evaluate the best SERS substrate for the detection of SO_2, AgNPs with nominal diameter of 4, 30 and 55 nm were tested in the most simplified version of wine, i.e. the hydroalcoholic solution. Both UV-Vis and SERS spectra showed better substrate-analyte interaction in the case of 4 nm AgNPs and thus these were selected for the subsequent analysis.

In wine simulant solution, the agglomeration of the AgNPs led to two intense SERS peaks that were directly proportional to the increase of SO_2 concentration

from 0 to 100 mg/l. The intensities trend was the characteristic absorption-desorption Langmuir fit.

In real samples of red and white wines, despite the pre-cleaning procedure adopted, the matrix effect had to be considered. Thus, a standard addition method was used. The severe agglomeration of AgNPs that occurred in wine samples allowed the determination of SO_2 concentration by SERS method. The wine samples analysed were Chardonnay, Grillo and Favorita (white wines) and Dolcetto, Chianti and Freisa (red wines). The concentration of total SO_2 in these wines were tested in parallel with the proposed in liquid SERS method and with the official OIV-OENO 591B-2018 method, here taken as a reference. The consistency of the results obtained by the two techniques provided a validation of the SERS method in wine.

The advantages of this new in liquid SERS method were the minimal pretreatment of the samples, which consistented only in a pre-cleaning procedure through a SPE cartridge, the rapidity and semplicity of the analysis and the possibility to conduct the measurement *in situ* with a portable Raman spectrometer. This last option could make this method really promising due to its possible applications in wineries.

A future perspective of this experimental activity could be a rigorous evaluation of the measurement uncertainty of total SO_2 concentration applying the in liquid SERS method. This evaluation would allow a more reliable assessment of the quality of the results. However, this detailed evaluation represents a huge challenge. Indeed, in SERS analysis, the 4 nm AgNPs – wine mix is subjected to chemical and physical degradation during the time of the measurement and this modification is caused by matrix-effects.

Chapter 5

Final conclusions and future perspectives

In recent years, numerous analytical methods have been developed in the area of contaminants and food additives and many others are currently under study in order to improve the accuracy concerning qualitative and quantitative detections with the aim to decrease the lowest detectable concentrations. During my PhD, I faced the study of two main molecules: the ochratoxin A, which is a food contaminant and in particular a mycotoxin, and the sulfur dioxide, which is a food additive and in particular an antimicrobial and antioxidant agent. For both the case studies, I tackled several analytical aspects in order to provide a broad characterization of the analytes. Furthermore, I synthetized batches of AgNPs with three nominal lateral sizes which were necessary for the research activities related to the SERS spectroscopy.

Following the order of description reported in this thesis, I briefly summarize here the results I achieved and the future perspectives for further studies and developments.

- AgNPs.

  I synthetized batches of AgNPs colloidal suspensions with three nominal diameters: 4, 30 and 55 nm. All these types of nanoparticles were characterized in terms of dimension, shape, spectral position of the LSPR and specific surface area. The 4 and 30 nm AgNPs resulted

spheroidal and homogeneously distributed, with the LSPR positioned at 391 nm and 397 nm, respectively. Most 55 nm AgNPs were spherical but some of them also had different shapes. Their LSPR was positioned at 417 nm. The specific surface area was higher for the 4 nm AgNPs and lower for 55 nm AgNPs. All these three sizes of AgNPs were tested as a substrate in the innovative in liquid SERS methods developed in my thesis;

- Ochratoxin A.

  First of all, I used the HPLC-FLD to quantify the OTA concentration in a CRM of red wine. It resulted that, despite it is the election analytical technique, some critical aspects came out. The major issue was related to the solvent evaporation step which led to the crystallization of the toxic solid OTA.

  Then, a wide range of pH (from 1 to 12.5) was investigated in order to provide a comprehensive description of the behaviour of OTA in aqueous solutions. The two pK_a of OTA were evaluated by two independent techniques: the UV-Vis spectrophotometry and the fluorescence spectroscopy. They resulted 4.4 ± 0.1 and 7.09 ± 0.01 (pK_{a1}) and 4.2 ± 0.9 and 7.0 ± 0.4 (pK_{a2}), respectively. Moreover, the most probable degradation pathway of OTA in solution under alkaline conditions was identified by experimental fluorescence maps and theoretical calculations. The degradation of OTA conducted to its fragmentation into two molecules: the phenylalanine, an amino acid, and the ochratoxin α, which is much less toxic than its precursor. However, such fragmentation happened only if the degradation process was prolonged over time and under strong alkaline condition. Thus, for this study, the condition of reversibility of the degradation pathway, which conducts again to toxic OTA, was defined. As a result, OTA samples and contaminated glassware should be handled paying greater attention. All the information acquired in this work was useful for future toxicological studies of the various forms of OTA and for the development of CRMs of this mycotoxin.

  Despite its high toxicity, a reference Raman spectrum of solid OTA was obtained in a wide spectral range. The corresponding vibrational mode has been carefully attributed to most of the peaks relative to the OTA. Then, an in liquid label-free SERS method with AgNPs as a substrate was developed for OTA identification. After many tests and parameter optimization, the main peaks identified in

the spectrum of solid OTA were found also in the SERS spectrum. The spectrum was achieved with 30 nm AgNPs and tartaric acid as an aggregating agent. This feasibility study provided a method which presented the advantages of being fast and easy. However, the sensitivity of this method was insufficient for OTA detection at the concentration typical of food matrices.

Lastly, I participated to a Secondment at the NRC – Canada focussed on culturing, isolation, and purification of ochratoxin A for reference material production, along with metrological characterization of the material. The first goal of this project was the production of pure solid OTA. I developed my expertise on fundamental techniques in fungal cultures to produce mycotoxins and I learned how to handle biological material. The final goal of the project, which is part of the BIPM's Mycotoxin Metrology Capacity Building and Knowledge Transfer (CBKT) Programme, was the production of CRMs of OTA;

- Sulfur dioxide.

  I applied the OIV-OENO 591A-2018 method in order to evaluate the recovery of free SO_2 in a wine simulant solution with a gravimetrically known concentration of this additive. The achieved recovery was of 95.5%. Moreover, a measurement comparison was conducted among nine specialized laboratories with this official method. The first output of the comparison was that this official method suffers of an underestimation of the SO_2 content in wine. Indeed, none of the participants achieved the total recovery of the analyte. The second output regarded the high variability of the results, reported with only their standard deviation, obtained by the laboratories. In this regards, a greater exchange of information and a more homogenous application of the official method is desirable.

  I carried out a rigorous evaluation of the measurement uncertainty associated to the free SO_2 concentration achieved by the official method with the INRiM apparatus. For the wine simulant used in the comparison, which presented a concentration of free SO_2 of 150.1 mg/l applying a gravimetric method as a reference, the obtained at INRiM was 143.3 mg/l with an expanded uncertainty of 3.9 mg/l. This work was in support of the official method.

  To perform all the above mentioned activities regarding SO_2, including the comparison, I produced a sample of wine simulant. This

solution can be considered as a sort of CRM candidate. Indeed, long term stability and homogeneity tests were performed. The concentration of free SO_2 as a CRM candidate was 143.3 mg/l with an expanded uncertainty of 4.8 mg/l.

In order to develop an in liquid SERS method for the quantification of total SO_2 in wine, I firstly performed tests of interaction between the three sizes of AgNPs and the SO_2 in a hydroalcoholic solution. Once defined the 4 nm AgNPs as the best substrate for this kind of analysis, the same interaction was investigated with the SO_2 in wine simulant. In this matrix, a greater interaction between the two components was observed and the vibrational peaks related to SO_2 were identified. Furthermore, the experimental data were fitted with a Langmuir function, typical of adsorption-desorption phenomena. Six wines (three red and three white) were analysed by this optimized in liquid SERS method. The results achieved by SERS were compared with the ones obtained by applying the official OIV-OENO 591B-2018 method on the same samples. The agreement between the results provided the validation of this innovative SERS technique. This method could be used for in situ analysis in the future.

Therefore, the two main subjects of my thesis, the ochratoxin A and the sulfur dioxide, were approached following schemes which presented some similarities:

- For both the analytes, I experimented the most used analytical methods (HPLC-FLD for OTA and OIV-OENO 591A-2018 method for SO_2) and some criticalities emerged;
- I developed a simple and fast in liquid SERS method for the identification/detection of these target molecules. To do this, I synthetized and tested AgNPs featured by three dimensions, choosing the more performant vs. the analytes. In the case of SO_2 this method was validated, while in the case of OTA this method resulted inadequate to reach the concentration levels close to the legal limits of OTA in food matrices;
- For both the analytes, I contributed to increase the level of knowledge concerning their characterization. About OTA, the improvement regarded a comprehensive study of its behaviour in aqueous solution in a range of pH from 1 to 12.5. In this regards, the two acid

dissociation constants were established along with the adopted experimental conditions. Furthermore, the degradation pathway of OTA under alkaline condition was defined for the first time by following the experimental findings and by comparing they with the theoretical calculations. About SO_2, I performed a rigorous evaluation of the measurement uncertainty associated to free concentration of SO_2 by the OIV-OENO 591A-2018 method. This work was in support to the OIV method. Moreover, with this work I highlighted a systematic underestimation of the free SO_2 concentration by this method. This not total recovery of SO_2 from the wine simulant was confirmed by a measurement comparison between nine specialized laboratories.

- All this PhD work was permeated by reference materials and certified reference materials. Indeed, for the study that I performed on OTA, some RMs and CRMs were used and I took part in a project with the aim of CRMs of OTA production. Regarding SO_2, since no CRM in wine was available, I conducted a feasibility study for the production of a candidate CRM of free sulfur dioxide in wine simulant.

In conclusion, some general final remarks can be outlined.

The first consideration, even if it may seem trivial, concerns the importance of characterization and knowledge of the behaviour of the substance under study. In fact, in order to develop new analytical techniques and to interpret the experimental evidence, a thorough knowledge of the analytes is necessary. For this reason, part of my thesis was dedicated to understanding the chemical-physical characteristics of the nanoparticles, used as a probe in some analytical methods, beside the studied contaminant and additive.

The second fundamental consideration regards the measurement results. To be expressed in a correct way, a result should be reported as an estimate with its uncertainty. The rigorous evaluation of the measurement uncertainty associated to a measurement result should represent a fundamental part of the measurement process. Indeed, it is a quantitative parameter which indicates the quality of a measurement results and provide an indication of the measurement reliability. However, despite the undeniable role of measurement uncertainty, this rigorous determination is sometimes omitted in laboratory of analytical chemistry. In some cases, as highlighted in my thesis work, even official methods do not provide and/or require the evaluation of the measurement uncertainty. Actually, just the

standard deviation is often preferred to more complicated and laborious uncertainty evaluation related to the particular measurement typologies. In this framework, during my PhD work I came across the different approaches of chemistry and metrology laboratory towards the measurement and the suitable expression of the measurement results. After having experienced these difficulties of interpenetration between the two visions, I believe that greater communication and a concrete commitment to amalgamate these two realities are desirable.

The third consideration pertains the key role of the reference materials and, above all, of the certified reference materials in the development of measurement processes. The development of CRMs is an increasingly present necessity in modern society. In fact, the currently available CRMs are not able to satisfy the market demand. This is at least partially due to the length, complexity and cost of the production process. Moreover, in the case of food related materials, it is necessary to consider the huge possibility of combinations deriving from the coupling of an analyte and a food matrix, without considering the concentration levels of the substances. It follows that the specificity of the chemical composition of CRMs in food matrices makes these materials perfectly suitable for the analysis for which they were designed, but raises questions about their use in conditions other than optimal ones. However, despite the difficulties that may be encountered in the production of a CRM, as also underlined in my PhD work, the development of an ever greater number of CRMs is advisable. Furthermore, the accreditation of Reference Material Producers (RMP) according to ISO 17034 is a fundamental aspect to ensure their technical competence and to guarantee the correct determination of the analytes. This kind of materials represents one of the most important intersections point between chemistry and metrology.

All the highlighted aspects contributed to improve the quality assurance and to building an ever wider sharing of knowledge and a solid guarantee for food safety.

References

[1] JCGM 200:2012, “International vocabulary of metrology – Basic and general concepts and associated terms (VIM) 3rd edition,” 2012.

[2] R. N. Fletcher, “ANCIENT METROLOGY,” vol. 19, 1968, pp. 270–277.

[3] R. J. C. Brown, “Measuring measurement – What is metrology and why does it matter?,” *Meas. J. Int. Meas. Confed.*, vol. 168, no. August 2020, p. 108408, 2021, doi: 10.1016/j.measurement.2020.108408.

[4] JCGM 100:2008, “Evaluation of measurement data — Guide to the expression of uncertainty in measurement.” 2008, [Online]. Available: http://www.bipm.org/en/publications/guides/gum.html.

[5] H. G. Semerjian and E. S. Beary, “Impact of Metrology on the Economy and Quality of Life,” 2002.

[6] D. B. Hibbert, E. H. Korte, and U. Örnemark, “Metrological and quality concepts in analytical chemistry (IUPAC Recommendations 2021),” *Pure Appl. Chem.*, vol. 93, no. 9, pp. 997–1048, 2021, doi: 10.1515/pac-2019-0819.

[7] A. N. 76 Analytical Methods Committee, “Chemical metrology,” *Anal. Methods*, vol. 8, no. 46, pp. 8119–8122, 2016, doi: 10.1039/c6ay90155g.

[8] O. Zakaria and M. F. Rezali, “Reference Materials as a Crucial Tools for Validation and Verification of the Analytical Process,” *Procedia - Soc. Behav. Sci.*, vol. 121, no. September 2012, pp. 204–213, 2014, doi: 10.1016/j.sbspro.2014.01.1121.

[9] T. P. J. Linsinger and H. Emons, “The role of reference materials in chemical metrology,” *Chimia (Aarau).*, vol. 63, no. 10, pp. 629–631, 2009, doi: 10.2533/chimia.2009.629.

[10] K. E. Sharpless *et al.*, “Standard reference materials for foods and dietary supplements,” *Anal. Bioanal. Chem.*, vol. 389, no. 1, pp. 171–178, 2007, doi: 10.1007/s00216-007-1315-y.

[11] ISO 17034:2016, “ISO 17034:2016, General requirements for the competence of reference material producers.” 2016.

[12] “https://www.imeko.org/index.php/tc23-homepage.” .

[13] “https://www.who.int/health-topics/food-safety.” .

[14] “http://www.fao.org/food-safety/background/en/.”

[15] Food and Agriculture Organization of the United Nations, “The Future of Food Safety. There is no food security without food safety.” .

[16] Keiji Fukuda, “Food safety in a globalized world,” *Bull. World Health Organ.*, p. 154831, 2015.

[17] World Health Organization (WHO), “WHO ESTIMATES OF THE GLOBAL BURDEN OF FOODBORNE DISEASES. FOODBORNE DISEASE BURDEN EPIDEMIOLOGY REFERENCE GROUP 2007-2015.” 2015.

[18] World Health Organization, “Five Keys To Safer Food Manual Safer Food Manual,” *Int. J. Environ. Res. Public Health*, vol. 6, no. 11, pp. 2833–2842, 2009, [Online]. Available: http://www.mdpi.com/1660-4601/6/11/2833/.

[19] Dipartimento per la Pubblica Informazione and Nazioni Unite, “Trasformare il nostro mondo: Agenda 2030 per lo Sviluppo Sostenibile Dipartimento per la Pubblica Informazione Nazioni Unite,” [Online]. Available: https://unric.org/it/agenda-2030/.

[20] L. A. Ribera, M. A. Palma, M. Paggi, R. Knutson, J. G. Masabni, and J. Anciso, “Economic Analysis of Food Safety Compliance Costs and Foodborne Illness Outbreaks in the United States,” *Horttechnology*, vol. 22, no. 2, pp. 150–156, 2012, doi: 10.21273/horttech.22.2.150.

[21] “https://www.who.int/news-room/events/detail/2015/04/07/default-calendar/world-health-day-2015.”

[22] G. A. Kleter and H. J. P. Marvin, “Indicators of emerging hazards and risks to food safety,” *Food Chem. Toxicol.*, vol. 47, no. 5, pp. 1022–1039, 2009, doi: 10.1016/j.fct.2008.07.028.

[23] G. Liuzzo, S. Bentley, F. Giacometti, S. Piva, and A. Serraino, “Social involvement, food safety and food security,” *Ital. J. Food Saf.*, vol. 7:7394, pp. 138–141, 2018, doi: 10.4081/ijfs.2018.7394.

[24] P. Pinstrup-Andersen, “Food security: definition and measurement,” *Food Secur.*, vol. 1, no. 1, pp. 5–7, 2009, doi: 10.1007/s12571-008-0002-y.

[25] M. A. Hussain, “Food contamination: Major challenges of the future,” *Foods*, vol. 5, no. 2, pp. 1–2, 2016, doi: 10.3390/foods5020021.

[26] CODEX, “Codex General Standard for Contaminants and Toxins in Food and Feed,” *Codex Stan 193-1995*, vol. 193, pp. 1–44, 2009.

[27] Ministero della Salute., D. S. A. E. DIPARTIMENTO DELLA SANITA’ PUBBLICA VETERINARIA, D. O. C. P. L. T. DELLA SALUTE, D. G. D. O. C. P. L. T. D. S. U. I. R. C.-F. E. BIOLOGICO, and OBIETTIVO, “OBIETTIVO STRATEGICO 2011. POTENZIAMENTO DELLA VALUTAZIONE DELLA PRESENZA DEI PRINCIPALI CONTAMINANTI AMBIENTALI CHE POSSONO INCIDERE NELLA CATENA ALIMENTARE.” 2011.

[28] “https://www.iaea.org/topics/food-contaminants.” .

[29] P. K. Rai, S. S. Lee, M. Zhang, Y. F. Tsang, and K. H. Kim, “Heavy metals in food crops: Health risks, fate, mechanisms, and management,” *Environ. Int.*, vol. 125, no. January, pp. 365–385, 2019, doi: 10.1016/j.envint.2019.01.067.

[30] “https://www.who.int/news-room/fact-sheets/detail/antibiotic-resistance.”

[31] B. Aslam *et al.*, “Antibiotic resistance: a rundown of a global crisis,” *Infect. Drug Resist.*, vol. 11, pp. 1645–1658, 2018, doi: 10.2147/IDR.S173867.

[32] C. Linhart *et al.*, “Pesticide contamination and associated risk factors at public playgrounds near intensively managed apple and wine orchards,” *Environ. Sci. Eur.*, vol. 31, no. 1, 2019, doi: 10.1186/s12302-019-0206-0.

[33] L. A. Thompson and W. S. Darwish, “Environmental Chemical Contaminants in Food: Review of a Global Problem,” *J. Toxicol.*, vol. 2019, 2019, doi: 10.1155/2019/2345283.

[34] T. Bintsis, “Microbial pollution and food safety,” *AIMS Microbiol.*, vol. 4, no. 3, pp. 377–396, 2018, doi: 10.3934/microbiol.2018.3.377.

[35] O. O. Alegbeleye, I. Singleton, and A. S. Sant’Ana, “Sources and contamination routes of microbial pathogens to fresh produce during field cultivation: A review,” *Food Microbiol.*, vol. 73, pp. 177–208, 2018, doi: 10.1016/j.fm.2018.01.003.

[36] A. Alshannaq and J. H. Yu, “Occurrence, toxicity, and analysis of major mycotoxins in food,” *Int. J. Environ. Res. Public Health*, vol. 14, no. 6, 2017, doi: 10.3390/ijerph14060632.

[37] Y. G. Zhu and G. Shaw, “Soil contamination with radionuclides and potential remediation,” *Chemosphere*, vol. 41, no. 1–2, pp. 121–128, 2000, doi: 10.1016/S0045-6535(99)00398-7.

[38] World Health Organization (WHO), “Nuclear accidents and radioactive contamination of foods,” no. March. pp. 1–5, 2011.

[39] B. Toussaint *et al.*, “Review of micro- and nanoplastic contamination in the food chain,” *Food Addit. Contam. - Part A Chem. Anal. Control. Expo. Risk Assess.*, vol. 36, no. 5, pp. 639–673, 2019, doi: 10.1080/19440049.2019.1583381.

[40] W. Fu, J. Min, W. Jiang, Y. Li, and W. Zhang, “Separation, characterization and identification of microplastics and nanoplastics in the environment,” *Sci. Total Environ.*, vol. 721, p. 137561, 2020, doi: 10.1016/j.scitotenv.2020.137561.

[41] P. B. Deepanksha Sharma, Shania Javed, Arshilekha, Prachi Saxena, P. B. Deepanksha Sharma, Shania Javed, Arshilekha, Prachi Saxena, P. S. and S. V. Divyanshu Shukla, S. Vats, and Institute, “Food additives and their effects: a mini review,” *Int. J. Curr. Res.*, vol. 10, no. 6, pp. 69999–70002, 2018.

[42] Food and Agriculture Organization of the United Nations (FAO) - World Health Organization (WHO), “General Standard For Food Additives CODEX STAND 192-1995,” *Codex Aliment. Int. Food Stand.*, pp. 1–480, 2019, [Online]. Available: http://www.fao.org/gsfaonline/docs/CXS_192e.pdf.

[43] “https://www.efsa.europa.eu/en/topics/topic/food-additives.” .

[44] R. F. Guerrero and E. Cantos-Villar, “Demonstrating the efficiency of sulphur dioxide replacements in wine: A parameter review,” *Trends Food Sci. Technol.*, vol. 42, no. 1, pp. 27–43, 2015, doi: 10.1016/j.tifs.2014.11.004.

[45] H. Vally, N. L. A. Misso, and V. Madan, “Clinical effects of sulphite additives,” *Clin. Exp. Allergy*, vol. 39, no. 11, pp. 1643–1651, 2009, doi: 10.1111/j.1365-2222.2009.03362.x.

[46] “https://www.who.int/news-room/fact-sheets/detail/food-additives.” .

[47] L. Mandrile *et al.*, "Direct quantification of sulfur dioxide in wine by Surface Enhanced Raman Spectroscopy," *Food Chem.*, vol. 326, no. May, p. 127009, 2020, doi: 10.1016/j.foodchem.2020.127009.

[48] R. P. Feyman, "There's Plenty of Room at the Bottom. An Invitation to Enter a New Field of Physics," *Eng. Sci. Mag.*, vol. XXIII, no. 5, 1960.

[49] W. M. Shume, H. C. A. Murthy, and E. A. Zereffa, "A Review on Synthesis and Characterization of Ag2O Nanoparticles for Photocatalytic Applications," *J. Chem.*, vol. 2020, 2020, doi: 10.1155/2020/5039479.

[50] B. Calderón-Jiménez, M. E. Johnson, A. R. Montoro Bustos, K. E. Murphy, M. R. Winchester, and J. R. V. Baudrit, "Silver nanoparticles: Technological advances, societal impacts, and metrological challenges," *Front. Chem.*, vol. 5, no. Feb, pp. 1–26, 2017, doi: 10.3389/fchem.2017.00006.

[51] ISO, "ISO/TS 80004-1:2015 Nanotechnologies — Vocabulary — Part 1: Core terms," 2015.

[52] Y. Asefi, "Synergistic Effect of Vitamin C with Superparamagnetic Iron Oxide Nanoparticles for Inhibiting Proliferation of Gastric Cancer Cells," vol. 12, no. 3, pp. 3215–3224, 2022.

[53] B. Yilmaz and O. Ozay, "Synthesis , Characterization and Biomedical Applications of p (HEMA-co-APTMACI) Hydrogels Crosslinked with Modified Silica Nanoparticles," vol. 12, no. 3, pp. 3664–3680, 2022.

[54] N. Kanojia, N. Sharma, N. Gupta, and S. Singh, "Applications of Nanostructured Lipid Carriers : Recent Advancements and Patent Review," vol. 12, no. 1, pp. 638–652, 2022.

[55] Y. Yu *et al.*, "Colorimetric immunoassay via smartphone based on Mn 2 + -Mediated aggregation of AuNPs for convenient detection of fumonisin B1," *Food Control*, vol. 132, no. June 2021, p. 108481, 2022, doi: 10.1016/j.foodcont.2021.108481.

[56] Y. Pan, W. Jin, and Q. Huang, "Structure , assembly and application of novel peanut oil body protein extracts nanoparticles," *Food Chem.*, vol. 367, no. June 2021, p. 130678, 2022, doi: 10.1016/j.foodchem.2021.130678.

[57] E. N. Hammad, "Purpureocillium lilacinum Mediated Biosynthesis Copper Oxide Nanoparticles with Promising Removal of Dyes," vol. 12, no. 2, pp. 1397–1404, 2022.

[58] P. Liu *et al.*, "Dual-mode fluorescence and colorimetric detection of pesticides realized by integrating stimulus-responsive luminescence with oxidase-mimetic activity into cerium-based coordination polymer nanoparticles," *J. Hazard. Mater.*, vol. 423, no. PA, p. 127077, 2022, doi: 10.1016/j.jhazmat.2021.127077.

[59] N. D. Davlatshoevich, K. M. Ashur, and B. Amondulloi, "Investigation of Structural and Optoelectronic Properties of N-Doped Hexagonal Phases of TiO 2 (TiO 2-x N x) Nanoparticles with DFT Realization : OPTIMIZATION of the Band Gap and Optical Properties for Visible-Light Absorption and Photovoltaic Applicati," vol. 12, no. 3, pp. 3836–3848, 2022.

[60] V. Cregan, "Nanoparticle synthesis via precipitation from solution," *European Consortium for Mathematics in Industry*. 2016.

[61] A. Almatroudi, "Silver nanoparticles : synthesis , characterisation and biomedical applications," *Open Life Sci.*, vol. 15, pp. 819–839, 2020.

[62] J. K. Patra and K. Baek, "Green Nanobiotechnology : Factors Affecting Synthesis and Characterization Techniques," *J. Nanomater.*, 2014.

[63] H. Heinz *et al.*, "Surface Science Reports Nanoparticle decoration with surfactants : Molecular interactions , assembly , and applications," *Surf. Sci. Rep.*, vol. 72, pp. 1–58, 2017, doi: 10.1016/j.surfrep.2017.02.001.

[64] Y. Wan *et al.*, "Quasi-spherical silver nanoparticles : Aqueous synthesis and size control by the seed-mediated Lee – Meisel method," *J. Colloid Interface Sci.*, vol. 394, pp. 263–268, 2013, doi: 10.1016/j.jcis.2012.12.037.

[65] P. C. Lee and D. Meisel, "Adsorption and surface-enhanced Raman of dyes on silver and gold sols - The Journal of Physical Chemistry (ACS Publications)," *J. Phys. Chem.*, vol. 60439, no. 50 mL, pp. 3391–3395, 1982, [Online]. Available: http://pubs.acs.org/doi/abs/10.1021/j100214a025%5Cnpapers2://publication/uuid/5A7A731B-3B42-4DAF-BF7E-9BCD8F727CE9.

[66] S. Agnihotri, S. Mukherji, and S. Mukherji, "Size-controlled silver nanoparticles synthesized over the range 5–100 nm using the same protocol and their antibacterial effica," *RSC Advences*, vol. 4, pp. 3974–3983, 2014, doi: 10.1039/c3ra44507k.

[67] Si. Dalla Marta, C. Novara, F. Giorgis, A. Bonifacio, and V. Sergo, "Optimization and Characterization of Paper-Made Surface Enhanced Raman Scattering (SERS) Substrates with Au and Ag NPs for Quantitative

Analysis," *Materials (Basel).*, vol. 10, p. 1365, 2017, doi: 10.3390/ma10121365.

[68] S. Monti, G. Barcaro, L. Sementa, V. Carravetta, and H. Ågren, "Characterization of the adsorption dynamics of trisodium citrate on gold in water solution," *RSC Adv.*, vol. 7, no. 78, pp. 49655–49663, 2017, doi: 10.1039/c7ra10759e.

[69] M. D. Abràmoff, P. J. Magalhaes, and S. J. Ram, "Image processing with ImageJ," *Biophotonics Int.*, vol. 11, no. 7, pp. 36–42, 2004.

[70] E. Petryayeva and U. J. Krull, "Localized surface plasmon resonance: Nanostructures, bioassays and biosensing-A review," *Anal. Chim. Acta*, vol. 706, no. 1, pp. 8–24, 2011, doi: 10.1016/j.aca.2011.08.020.

[71] R. X. He, R. Liang, P. Peng, and N. Y. Zhou, "Effect of the size of silver nanoparticles on SERS signal enhancement Effect of the size of silver nanoparticles on SERS signal enhancement," *J Nanopart Res*, vol. 19, p. 267, 2017, doi: 10.1007/s11051-017-3953-0.

[72] S. Hong and X. Li, "Optimal size of gold nanoparticles for surface-enhanced Raman spectroscopy under different conditions," *J. Nanomater.*, vol. 2013, 2013, doi: 10.1155/2013/790323.

[73] S. Marhaba, "Effect of Size, Shape and Environment on the Optical Response of Metallic Nanoparticles," in *Noble and Precious Metals - Properties, Nanoscale Effects and Applications*, 2012, p. Chapter 3.

[74] D. Gaspar *et al.*, "Ag and Sn Nanoparticles to Enhance the Near-Infrared Absorbance of a-Si:H Thin Films," *Plasmonics*, vol. 9, no. 5, pp. 1015–1023, 2014, doi: 10.1007/s11468-014-9709-0.

[75] F. Quan *et al.*, "Combustion synthesis and formation mechanism of silver nanoparticles," *Int. J. Mater. Res.*, vol. 109, no. 8, pp. 751–755, 2018, doi: 10.3139/146.111666.

[76] M. Chen, Y. G. Feng, X. Wang, T. C. Li, J. Y. Zhang, and D. J. Qian, "Silver nanoparticles capped by oleylamine: Formation, growth, and self-organization," *Langmuir*, vol. 23, no. 10, pp. 5296–5304, 2007, doi: 10.1021/la700553d.

[77] A. P. Craig, A. S. Franca, and J. Irudayaraj, *Vibrational spectroscopy for food quality and safety screening*. Elsevier Ltd., 2015.

[78] E. Li-Chan, J. M. Chalmers, and P. R. Griffths, "Applications of vibrational

spectroscopy in food science," in *Jhon Wiley& Sons.*, 2010.

[79] R. S. Das and Y. K. Agrawal, "Raman spectroscopy: Recent advancements, techniques and applications," *Vib. Spectrosc.*, vol. 57, no. 2, pp. 163–176, 2011, doi: 10.1016/j.vibspec.2011.08.003.

[80] A. Campion, P. Kambhampati, A. Campion, and C. Harris, "Surface-enhanced Raman scattering," vol. 27, pp. 241–250, 1998.

[81] K. Kneipp, H. Kneipp, I. Itzkan, R. R. Dasari, and M. S. Feld, "Ultrasensitive Chemical Analysis by Raman Spectroscopy," *Chem. Rev.*, vol. 99, no. 10, pp. 2957–2975, 1999, doi: 10.1021/cr980133r.

[82] T. Vo-Dinh, "Surface-enhanced Raman spectroscopy using metallic nanostructures," *TrAC - Trends Anal. Chem.*, vol. 17, no. 8–9, pp. 557–582, 1998, doi: 10.1016/S0165-9936(98)00069-7.

[83] S. Schlücker, "Surface-Enhanced Raman Spectroscopy : Concepts and Chemical Applications Angewandte," *Angew. Rev.*, vol. 53, pp. 2–42, 2014, doi: 10.1002/anie.201205748.

[84] A. Virga *et al.*, "SERS active Ag nanoparticles in mesoporous silicon : detection of organic molecules and peptide – antibody assays," *J. Raman Spectrosc*, vol. 43, pp. 730–736, 2012, doi: 10.1002/jrs.3086.

[85] N. Tran Truc Phuong *et al.*, "Rapid and sensitive detection of Rhodamine B in food using the plasmonic silver nanocube-based sensor as SERS active substrate," *Spectrochim. Acta - Part A Mol. Biomol. Spectrosc.*, vol. 263, p. 120179, 2021, doi: 10.1016/j.saa.2021.120179.

[86] K. Wang and J. Li, "Reliable SERS detection of pesticides with a large-scale self-assembled Au@4-MBA@Ag nanoparticle array," *Spectrochim. Acta - Part A Mol. Biomol. Spectrosc.*, vol. 263, p. 120218, 2021, doi: 10.1016/j.saa.2021.120218.

[87] H. Chen, H. Liu, Y. Chen, X. Li, C. Gu, and T. Jiang, "Surface-enhanced Raman scattering detection of additive by a reusable ZnO/GO/Ag hybrid substrate," *Mater. Chem. Phys.*, vol. 273, no. July, p. 125083, 2021, doi: 10.1016/j.matchemphys.2021.125083.

[88] L. Ouyang, P. Dai, L. Yao, Q. Zhou, H. Tang, and L. Zhu, "A functional Au array SERS chip for the fast inspection of pesticides in conjunction with surface extraction and coordination transferring," *Analyst*, vol. 144, pp. 5528–5537, 2019.

[89] A. P. Craig, A. S. Franca, and J. Irudayaraj, “Surface-enhanced Raman spectroscopy applied to food safety,” *Annu. Rev. Food Sci. Technol.*, vol. 4, no. 1, pp. 369–380, 2013, doi: 10.1146/annurev-food-022811-101227.

[90] G. Barzan *et al.*, “Surface Minimal Bactericidal Concentration: A comparative study of active glasses functionalized with different-sized silver nanoparticles,” *Colloids Surfaces B Biointerfaces*, vol. 204, no. January, p. 111800, 2021, doi: 10.1016/j.colsurfb.2021.111800.

[91] L. Mandrile, M. Vona, A. M. Giovannozzi, J. Salafranca, G. Martra, and A. M. Rossi, “Migration study of organotin compounds from food packaging by surface-enhanced Raman scattering,” *Talanta*, vol. 220, no. July 2020, p. 121408, 2020, doi: 10.1016/j.talanta.2020.121408.

[92] P. A. Mosier-Boss, “Review of SERS substrates for chemical sensing,” *Nanomaterials*, vol. 7, no. 6, 2017, doi: 10.3390/nano7060142.

[93] H. Dai *et al.*, “Three-dimensional TiO2 supported silver nanoparticles as sensitive and UV-cleanable substrate for surface enhanced Raman scattering,” *Sensors Actuators, B Chem.*, vol. 242, pp. 260–268, 2017, doi: 10.1016/j.snb.2016.10.085.

[94] B. N. Khlebtsov, V. A. Khanadeev, E. V. Panfilova, D. N. Bratashov, and N. G. Khlebtsov, “Gold nanoisland films as reproducible SERS substrates for highly sensitive detection of fungicides,” *ACS Appl. Mater. Interfaces*, vol. 7, no. 12, pp. 6518–6529, 2015, doi: 10.1021/acsami.5b01652.

[95] X. Liang *et al.*, “Interfacial synthesis of a three-dimensional hierarchical MoS2-NS@Ag-NP nanocomposite as a SERS nanosensor for ultrasensitive thiram detection,” *Nanoscale*, vol. 9, no. 25, pp. 8879–8888, 2017, doi: 10.1039/c7nr01891f.

[96] K. Wang, D. W. Sun, H. Pu, and Q. Wei, “Two-dimensional Au@Ag nanodot array for sensing dual-fungicides in fruit juices with surface-enhanced Raman spectroscopy technique,” *Food Chem.*, vol. 310, no. October 2019, p. 125923, 2020, doi: 10.1016/j.foodchem.2019.125923.

[97] C. Yuan *et al.*, “Single clusters of self-assembled silver nanoparticles for surface-enhanced Raman scattering sensing of a dithiocarbamate fungicide,” *J. Mater. Chem. C*, vol. 21, p. 16264, 2011, doi: 10.1039/b000000x.

[98] Z. Xiong, M. Lin, H. Lin, and M. Huang, “Facile synthesis of cellulose nanofiber nanocomposite as a SERS substrate for detection of thiram in juice,” *Carbohydr. Polym.*, vol. 189, no. February, pp. 79–86, 2018, doi:

10.1016/j.carbpol.2018.02.014.

[99] C. Novara *et al.*, "SERS active silver nanoparticles synthesized by inkjet printing on mesoporous silicon," *Nanoscale Res. Lett.*, vol. 9, no. 1, pp. 1–7, 2014, doi: 10.1186/1556-276X-9-527.

[100] M. Viehrig *et al.*, "Quantitative SERS Assay on a Single Chip Enabled by Electrochemically Assisted Regeneration: A Method for Detection of Melamine in Milk," *Anal. Chem.*, vol. 92, no. 6, pp. 4317–4325, 2020, doi: 10.1021/acs.analchem.9b05060.

[101] A. D'Agostino, A. M. Giovannozzi, L. Mandrile, A. Sacco, A. M. Rossi, and A. Taglietti, "In situ seed-growth synthesis of silver nanoplates on glass for the detection of food contaminants by surface enhanced Raman scattering," *Talanta*, vol. 216, no. December 2019, p. 120936, 2020, doi: 10.1016/j.talanta.2020.120936.

[102] E. Cara *et al.*, "Influence of the long-range ordering of gold-coated Si nanowires on SERS," *Sci. Rep.*, vol. 8, no. 1, pp. 1–10, 2018, doi: 10.1038/s41598-018-29641-x.

[103] J. Liu, Y. Hu, G. Zhu, X. Zhou, L. Jia, and T. Zhang, "Highly sensitive detection of zearalenone in feed samples using competitive surface-enhanced raman scattering immunoassay," *J. Agric. Food Chem.*, vol. 62, no. 33, pp. 8325–8332, 2014, doi: 10.1021/jf503191e.

[104] D. Chen *et al.*, "Polydopamine@Gold Nanowaxberry Enabling Improved SERS Sensing of Pesticides, Pollutants, and Explosives in Complex Samples," *Anal. Chem.*, vol. 90, no. 15, pp. 9048–9054, 2018, doi: 10.1021/acs.analchem.8b01348.

[105] Y. Zhang, Z. Wang, L. Wu, Y. Pei, P. Chen, and Y. Cui, "Rapid simultaneous detection of multi-pesticide residues on apple using SERS technique," *Analyst*, vol. 139, no. 20, pp. 5148–5154, 2014, doi: 10.1039/c4an00771a.

[106] L. Mandrile, A. M. Giovannozzi, F. Durbiano, G. Martra, and A. M. Rossi, "Rapid and sensitive detection of pyrimethanil residues on pome fruits by Surface Enhanced Raman Scattering," *Food Chem.*, vol. 244, no. July 2017, pp. 16–24, 2018, doi: 10.1016/j.foodchem.2017.10.003.

[107] Y. Wang *et al.*, "Flexible, transparent and highly sensitive SERS substrates with cross-nanoporous structures for fast on-site detection," *Nanoscale*, vol. 10, no. 32, pp. 15195–15204, 2018, doi: 10.1039/c8nr01628c.

[108] Y. Wang *et al.*, "A 3D spongy flexible nanosheet array for on-site recyclable swabbing extraction and subsequent SERS analysis of thiram," *Microchim. Acta*, vol. 186, no. 7, 2019, doi: 10.1007/s00604-019-3579-2.

[109] J. Chen *et al.*, "Flexible and Adhesive Surface Enhance Raman Scattering Active Tape for Rapid Detection of Pesticide Residues in Fruits and Vegetables," *Anal. Chem.*, vol. 88, no. 4, pp. 2149–2155, 2016, doi: 10.1021/acs.analchem.5b03735.

[110] L. Mandrile, A. M. Giovannozzi, A. Sacco, G. Martra, and A. M. Rossi, "Flexible and transparent substrates based on gold nanoparticles and TiO2 for in situ bioanalysis by surface-enhanced raman spectroscopy," *Biosensors*, vol. 9, no. 4, 2019, doi: 10.3390/bios9040145.

[111] P. Wang *et al.*, "Gecko-Inspired Nanotentacle Surface-Enhanced Raman Spectroscopy Substrate for Sampling and Reliable Detection of Pesticide Residues in Fruits and Vegetables," *Anal. Chem.*, vol. 89, no. 4, pp. 2424–2431, 2017, doi: 10.1021/acs.analchem.6b04324.

[112] A. M. Dowgiallo and D. A. Guenther, "Determination of the Limit of Detection of Multiple Pesticides Utilizing Gold Nanoparticles and Surface-Enhanced Raman Spectroscopy," *J. Agric. Food Chem.*, vol. 67, no. 46, pp. 12642–12651, 2019, doi: 10.1021/acs.jafc.9b01544.

[113] A. M. Giovannozzi, F. Rolle, M. Sega, M. C. Abete, D. Marchis, and A. M. Rossi, "Rapid and sensitive detection of melamine in milk with gold nanoparticles by Surface Enhanced Raman Scattering," *Food Chem.*, vol. 159, pp. 250–256, 2014, doi: 10.1016/j.foodchem.2014.03.013.

[114] B. Saute and R. Narayanan, "Solution-based SERS method to detect dithiocarbamate fungicides in different real-world matrices," *J. Raman Spectrosc.*, vol. 44, no. 11, pp. 1518–1522, 2013, doi: 10.1002/jrs.4387.

[115] A. I. Pérez-Jiménez, D. Lyu, Z. Lu, G. Liu, and B. Ren, "Surface-enhanced Raman spectroscopy: Benefits, trade-offs and future developments," *Chem. Sci.*, vol. 11, no. 18, pp. 4563–4577, 2020, doi: 10.1039/d0sc00809e.

[116] L. Ouyang, W. Ren, L. Zhu, and J. Irudayaraj, "Prosperity to challenges: Recent approaches in SERS substrate fabrication," *Rev. Anal. Chem.*, vol. 36, no. 1, 2017, doi: 10.1515/revac-2016-0027.

[117] S. Atumo, "A Review of Ochratoxin A Occurrence, Condition for the Formation and Analytical Methods," *Int. J. Agric. Sci. Food Technol.*, vol. 6, pp. 180–185, 2020, doi: 10.17352/2455-815x.000071.

[118] V. Pichon and A. Combès, “Selective tools for the solid-phase extraction of Ochratoxin A from various complex samples: immunosorbents, oligosorbents, and molecularly imprinted polymers,” *Anal. Bioanal. Chem.*, vol. 408, no. 25, pp. 6983–6999, 2016, doi: 10.1007/s00216-016-9886-0.

[119] J. L. Richard, “Some major mycotoxins and their mycotoxicoses-An overview,” *Int. J. Food Microbiol.*, vol. 119, no. 1–2, pp. 3–10, 2007, doi: 10.1016/j.ijfoodmicro.2007.07.019.

[120] E. Streit *et al.*, “Current situation of mycotoxin contamination and co-occurrence in animal feed focus on Europe,” *Toxins (Basel).*, vol. 4, no. 10, pp. 788–809, 2012, doi: 10.3390/toxins4100788.

[121] J. M. Wagacha and J. W. Muthomi, “Mycotoxin problem in Africa: Current status, implications to food safety and health and possible management strategies,” *Int. J. Food Microbiol.*, vol. 124, no. 1, pp. 1–12, 2008, doi: 10.1016/j.ijfoodmicro.2008.01.008.

[122] S. M. Sanzani, M. Reverberi, and R. Geisen, “Mycotoxins in harvested fruits and vegetables: Insights in producing fungi, biological role, conducive conditions, and tools to manage postharvest contamination,” *Postharvest Biol. Technol.*, vol. 122, pp. 95–105, 2016, doi: 10.1016/j.postharvbio.2016.07.003.

[123] M. E. Zain, “Impact of mycotoxins on humans and animals,” *J. Saudi Chem. Soc.*, vol. 15, no. 2, pp. 129–144, 2011, doi: 10.1016/j.jscs.2010.06.006.

[124] C. L. Berry, “The pathology of mycotoxins,” *J. Pathol.*, vol. 154, no. 4, pp. 301–311, 1988, doi: 10.1002/path.1711540405.

[125] E. M. Fox and B. J. Howlett, “Secondary metabolism: regulation and role in fungal biology,” *Curr. Opin. Microbiol.*, vol. 11, no. 6, pp. 481–487, 2008, doi: 10.1016/j.mib.2008.10.007.

[126] M. Capcarova, K. Zbynovska, A. Kalafova, J. Bulla, and P. Bielik, “Environment contamination by mycotoxins and their occurrence in food and feed: Physiological aspects and economical approach,” *J. Environ. Sci. Heal. - Part B Pestic. Food Contam. Agric. Wastes*, vol. 51, no. 4, pp. 236–244, 2016, doi: 10.1080/03601234.2015.1120617.

[127] S. C. Duarte, C. M. Lino, and A. Pena, “Mycotoxin food and feed regulation and the specific case of ochratoxin A: a review of the worldwide status,” *Food Addit. Contam.*, vol. 27, pp. 1440–1450, 2010.

[128] Food and Agriculture Organization (FAO), “Worldwide regulations for mycotoxins 2003. A compendium.,” *FAO Food Nutr. Pap.*, 2004.

[129] L.-C. Lin, P.-C. Chen, Y.-M. Fu, and D. Y.-C. Shih, “Ochratoxin A Contamination in Coffees, Cereals, Red Wines and Beers in Taiwan,” *J. Food Drug Anal.*, vol. 13, no. 1, p. 84, 2005.

[130] G. Parussolo *et al.*, “Ochratoxin A production by Aspergillus westerdijkiae in Italian-type salami,” *Food Microbiol.*, vol. 83, no. May, pp. 134–140, 2019, doi: 10.1016/j.fm.2019.05.007.

[131] K. J. Van der Merwe, P. S. Steyn, and L. Fourie, “Mycotoxins Part II the constitution of ochratoxin A, B and C, metabolites of Aspergillus ochraceus,” *Wilh. J. Chem. Soc.*, no. 7083–7088, 1965.

[132] F. Malir, V. Ostry, A. Pfohl-Leszkowicz, J. Malir, and J. Toman, “Ochratoxin A: 50 years of research,” *Toxins (Basel).*, vol. 8, no. 7, pp. 12–15, 2016, doi: 10.3390/toxins8070191.

[133] A. C. Galvis-Sánchez, A. S. Barros, and I. Delgadillo, “Method for analysis dried vine fruits contaminated with ochratoxin A,” *Anal. Chim. Acta*, vol. 617, no. 1–2, pp. 59–63, 2008, doi: 10.1016/j.aca.2008.02.065.

[134] I. Cagnasso *et al.*, “Comprehensive study on the degradation of ochratoxin A in water by spectroscopic techniques and DFT calculations,” *RSC Adv.*, vol. 9, no. 34, pp. 19844–19854, 2019, doi: 10.1039/c9ra02086a.

[135] A. E. el Khoury and A. Atoui, “Ochratoxin a: General overview and actual molecular status,” *Toxins (Basel).*, vol. 2, no. 4, pp. 461–493, 2010, doi: 10.3390/toxins2040461.

[136] M. Jalili, S. Jinap, and R. Son, “The effect of chemical treatment on reduction of aflatoxins and ochratoxin A in black and white pepper during washing,” *Food Addit. Contam. - Part A Chem. Anal. Control. Expo. Risk Assess.*, vol. 28, no. 4, pp. 485–493, 2011, doi: 10.1080/19440049.2010.551300.

[137] S. Kumar, A. K. Chaubey, and D. K. Maurya, “In vitro analysis of efficacy of chlorination in detoxifying ochratoxin A from freshly shelled sweet corn kernels spiked with toxigenic Aspergillus ochraceus strain,” vol. 3, no. 12, pp. 570–582, 2014.

[138] I. G. Gillman, T. N. Clark, and R. A. Manderville, “Oxidation of Ochratoxin A by an Fe-Porphyrin System: Model for Enzymatic Activation and DNA Cleavage,” *Chem. Res. Toxicol.*, vol. 12, pp. 1066–1076, 1999.

[139] H. Xiao *et al.*, “Toxicity of ochratoxin A, its opened lactone form and several of its analogs: Structure-activity relationships,” *Toxicol. Appl. Pharmacol.*, vol. 137, no. 2, pp. 182–192, 1996, doi: 10.1006/taap.1996.0071.

[140] R. R. Marquardt and A. A. Frohlich, “A review of recent advances in understanding ochratoxicosis.,” *J. Anim. Sci.*, vol. 70, no. 12, pp. 3968–3988, 1992, doi: 10.2527/1992.70123968x.

[141] S. Uchiyama, Y. Saito, and M. Uchiyama, “Protein-binding of Ochratoxin A and Its Extractability from Proteinous Food,” *Food Hyg. Saf. Sci. (Shokuhin Eiseigaku Zasshi)*, vol. 26, no. 6, p. 651, 1985, doi: 10.3358/shokueishi.26.651.

[142] F. S. Chu, I. Noh, and C. C. Chang, “Structural requirements for ochratoxin intoxication,” *Life Sci.*, vol. 11, no. 10, pp. 503–508, 1972.

[143] F. S. Chu, “Interaction of Ochratoxin A with Bovine Serum Albumin,” *Arch. Biochem. Biophys.*, vol. 147, pp. 359–366, 1971.

[144] M. J. Pitout, “The Effect of Ochratoxin A on Glycogen Storage in the Rat Liver,” *Toxicol. Appl. Pharmacol.*, vol. 13, pp. 299–306, 1968.

[145] EFSA Panel on Contaminants in the Food Chain (CONTAM) *et al.*, “Risk assessment of ochratoxin A in food,” *EFSA J.*, vol. 18, no. 5, 2020, doi: 10.2903/j.efsa.2020.6113.

[146] “REGULATION (EC) No. 1881/2006.” 2006.

[147] A. H. Heussner and L. E. H. Bingle, “Comparative ochratoxin toxicity: A review of the available data,” *Toxins (Basel).*, vol. 7, no. 10, pp. 4253–4282, 2015, doi: 10.3390/toxins7104253.

[148] Y. Tao *et al.*, “Ochratoxin A: Toxicity, oxidative stress and metabolism,” *Food Chem. Toxicol.*, vol. 112, no. January, pp. 320–331, 2018, doi: 10.1016/j.fct.2018.01.002.

[149] World Health Organization and INTERNATIONAL AGENCY FOR RESEARCH ON CANCER, “Monographs on the evaluation of carcinogenic risks to humans. Volume 56. Some naturally occurring substances: food items and constituents, heterocyclic aromatic amines and mycotoxins, Ochratoxin A, International Agency for Research on Cancer.” 1993.

[150] World Health Organization and INTERNATIONAL AGENCY FOR

RESEARCH ON CANCER, “MONOGRAPHS ON THE EVALUATION OF CARCINOGENIC RISKS TO HUMANS. Volume 82. Some Traditional Herbal Medicines, Some Mycotoxins, Naphthalene and Styrene.” 2002.

[151] T. H. Ha, “Recent advances for the detection of ochratoxin A,” *Toxins (Basel).*, vol. 7, no. 12, pp. 5276–5300, 2015, doi: 10.3390/toxins7124882.

[152] L. Anfossi, C. Giovannoli, and C. Baggiani, “Mycotoxin detection,” *Curr. Opin. Biotechnol.*, vol. 37, pp. 120–126, 2016, doi: 10.1016/j.copbio.2015.11.005.

[153] M. L. Savastano, I. Losito, and S. Pati, “Rapid and automatable determination of ochratoxin A in wine based on microextraction by packed sorbent followed by HPLC-FLD,” *Food Control*, vol. 68, no. 1881, pp. 391–398, 2016, doi: 10.1016/j.foodcont.2016.04.016.

[154] F. Chen, C. Luan, L. Wang, S. Wang, and L. Shao, “Simultaneous determination of six mycotoxins in peanut by high performance liquid chromatography with a fluorescence detector,” *J. Sci. Food Agric.*, vol. 97, p. 1805, 2017.

[155] C. Giovannoli, C. Passini, F. Di Nardo, L. Anfossi, and C. Baggiani, “Determination of ochratoxin A in Italian red wines by molecularly imprinted solid phase extraction and HPLC analysis,” *J. Agric. Food Chem.*, vol. 62, no. 22, pp. 5220–5225, 2014, doi: 10.1021/jf5010995.

[156] L. González-Osnaya, J. M. Soriano, J. C. Moltó, and J. Mañes, “Simple liquid chromatography assay for analyzing ochratoxin A in bovine milk,” *Food Chem.*, vol. 108, no. 1, pp. 272–276, 2008, doi: 10.1016/j.foodchem.2007.10.013.

[157] L. Monaci and F. Palmisano, “Determination of ochratoxin a in foods: State-of-the-art and analytical challenges,” *Anal. Bioanal. Chem.*, vol. 378, no. 1, pp. 96–103, 2004, doi: 10.1007/s00216-003-2364-5.

[158] N. W. Turner, S. Subrahmanyam, and S. A. Piletsky, “Analytical methods for determination of mycotoxins: A review,” *Anal. Chim. Acta*, vol. 632, no. 2, pp. 168–180, 2009, doi: 10.1016/j.aca.2008.11.010.

[159] A. Kaushik, S. K. Arya, A. Vasudev, and S. Bhansali, “Recent Advances in Detection of Ochratoxin-A,” *Open J. Appl. Biosens.*, vol. 02, no. 01, pp. 1–11, 2013, doi: 10.4236/ojab.2013.21001.

[160] C. Frenette, R. J. Paugh, M. Tozlovanu, M. Juzio, A. Pfohl-Leszkowicz,

and R. A. Manderville, “Structure-activity relationships for the fluorescence of ochratoxin A: Insight for detection of ochratoxin A metabolites,” *Anal. Chim. Acta*, vol. 617, no. 1–2, pp. 153–161, 2008, doi: 10.1016/j.aca.2007.12.030.

[161] J. Hashemi and N. Alizadeh, “Investigation of solvent effect and cyclodextrins on fluorescence properties of ochratoxin A,” *Spectrochim. Acta - Part A Mol. Biomol. Spectrosc.*, vol. 73, no. 1, pp. 121–126, 2009, doi: 10.1016/j.saa.2009.02.001.

[162] Y. V. Il’ichev, J. L. Perry, R. A. Manderville, C. F. Chignell, and J. D. Simon, “The pH-dependent primary photoreactions of ochratoxin A,” *J. Phys. Chem. B*, vol. 105, no. 45, pp. 11369–11376, 2001, doi: 10.1021/jp012683q.

[163] T. Li, B. B. Kim, T. H. Ha, Y. B. Shin, and M. G. Kim, “The effects of pH and surfactants on the absorption and fluorescence properties of ochratoxin A and zearalenone,” *Luminescence*, vol. 30, no. 7, pp. 1106–1111, 2015, doi: 10.1002/bio.2866.

[164] E. P. Meulenberg, “Immunochemical methods for ochratoxin A detection: A review,” *Toxins (Basel).*, vol. 4, no. 4, pp. 244–266, 2012, doi: 10.3390/toxins4040244.

[165] R. Gillibert, M. N. Triba, and M. Lamy De La Chapelle, “Surface enhanced Raman scattering sensor for highly sensitive and selective detection of ochratoxin A,” *Analyst*, vol. 143, no. 1, pp. 339–345, 2018, doi: 10.1039/c7an01730h.

[166] B. Shao *et al.*, “Nanogapped Au(core) @ Au-Ag(shell) structures coupled with Fe3O4 magnetic nanoparticles for the detection of Ochratoxin A,” *Anal. Chim. Acta*, vol. 1033, pp. 165–172, 2018, doi: 10.1016/j.aca.2018.05.058.

[167] D. Song, R. Yang, S. Fang, Y. Liu, F. Long, and A. Zhu, “SERS based aptasensor for ochratoxin A by combining Fe3O4@Au magnetic nanoparticles and Au-DTNB@Ag nanoprobes with multiple signal enhancement,” *Microchim. Acta*, vol. 185, no. 10, pp. 2–11, 2018, doi: 10.1007/s00604-018-3020-2.

[168] E. O. Ganbold *et al.*, “Subnanomolar detection of ochratoxin A using aptamer-attached silver nanoparticles and surface-enhanced Raman scattering,” *Anal. Methods*, vol. 6, no. 11, pp. 3573–3577, 2014, doi: 10.1039/c4ay00440j.

[169] M. Z. M. Nasir and M. Pumera, "Simultaneous Anodic and Cathodic Voltammetric Detection of Patulin and Ochratoxin A on Well-Defined Carbon Electrodes," *Electroanalysis*, vol. 27, no. 4, 2015.

[170] D. Afzali, F. Fathirad, and S. Ghaseminezhad, "Determination of trace amounts of ochratoxin A in different food samples based on gold nanoparticles modified carbon paste electrode," *J Food Sci Technol*, vol. 53, no. 1, p. 909, 2016.

[171] S. C. B. Oliveira, V. C. Diculescu, G. Palleschi, D. Compagnone, and A. M. Oliveira-Brett, "Electrochemical oxidation of ochratoxin A at a glassy carbon electrode and in situ evaluation of the interaction with deoxyribonucleic acid using an electrochemical deoxyribonucleic acid-biosensor," *Anal Chim Acta*, vol. 588, no. 2, p. 283, 2007.

[172] A. Kholová *et al.*, "Determination of Ochratoxin A and Ochratoxin B in Archived Tokaj Wines (Vintage 1959–2017) Using On-Line Solid Phase Extraction Coupled to Liquid Chromatography," *Toxins (Basel).*, vol. 12, p. 739, 2020.

[173] C. L. De Jesus, A. Bartley, A. Z. Welch, and J. P. Berry, "High incidence and levels of ochratoxin A in wines sourced from the United States," *Toxins (Basel).*, vol. 10, no. 1, pp. 1–12, 2018, doi: 10.3390/toxins10010001.

[174] V. Durguti, A. Georgieva, A. Angelov, and Z. Bajrami, "Quantitative determination of ochratoxin A in wine after the clarification and filtration," *Croat. J. Food Sci. Technol.*, vol. 6, no. 2, pp. 79–83, 2014, doi: 10.17508/cjfst.2014.6.2.03.

[175] A. Tafuri, G. Meca, and A. Ritieni, "A rapid high-performance liquid chromatography with fluorescence detection method developed to analyze ochratoxin A in wine," *J. Food Prot.*, vol. 71, no. 10, pp. 2133–2137, 2008, doi: 10.4315/0362-028X-71.10.2133.

[176] "EN 14133:2009. Foodstuffs - Determination of ochratoxin A in wine and beer - HPLC method with immunoaffinity column clean-up." 2009.

[177] B. Nemzer, D. Kalita, A. Y. Yashin, and Y. I. Yashin, "Chemical Composition and Polyphenolic Compounds of Red Wines: Their Antioxidant Activities and Effects on Human Health—A Review," *Beverages*, vol. 8, no. 1, pp. 1–18, 2022, doi: 10.3390/beverages8010001.

[178] S. H. Alarcón, L. Micheli, G. Palleschi, and D. Compagnone, "Development of an electrochemical immunosensor for ochratoxin A,"

Anal. Lett., vol. 37, no. 8, pp. 1545–1558, 2004, doi: 10.1081/AL-120037586.

[179] F. Y. H. Kutsanedzie, A. A. Agyekum, V. Annavaram, and Q. Chen, "Signal-enhanced SERS-sensors of CAR-PLS and GA-PLS coupled AgNPs for ochratoxin A and aflatoxin B1 detection," *Food Chem.*, vol. 315, no. January, p. 126231, 2020, doi: 10.1016/j.foodchem.2020.126231.

[180] R. Peró-Gascón, F. Benavente, J. Barbosa, and V. Sanz-Nebot, "Determination of acidity constants and prediction of electrophoretic separation of amyloid beta peptides," *J. Chromatogr. A*, vol. 1508, pp. 148–157, 2017, doi: 10.1016/j.chroma.2017.05.069.

[181] S. Babić, A. J. M. Horvat, D. Mutavdžić Pavlović, and M. Kaštelan-Macan, "Determination of pKa values of active pharmaceutical ingredients," *TrAC - Trends Anal. Chem.*, vol. 26, no. 11, pp. 1043–1061, 2007, doi: 10.1016/j.trac.2007.09.004.

[182] F. S. Chu and B. J. Wilson, "Studies on ochratoxins," *Crit. Rev. Toxicol.*, vol. 2, no. 4, pp. 499–524, 1973, doi: 10.3109/10408447309025706.

[183] C. De Stefano, P. Princi, C. Rigano, C. Van de Wiele, and S. Sammartano, "No Title," *Ann. Chim.*, vol. 77, pp. 643–675, 1987.

[184] "http://www.hyperquad.co.uk/HypSpec2014.htm." .

[185] P. Gans, A. Sabatini, and A. Vacca, "Hyperquad 2000.pdf," *Talanta*, vol. 43. pp. 1739–1753, 1996.

[186] R. Karoui and C. Blecker, "Fluorescence Spectroscopy Measurement for Quality Assessment of Food Systems-a Review," *Food Bioprocess Technol.*, vol. 4, no. 3, pp. 364–386, 2011, doi: 10.1007/s11947-010-0370-0.

[187] K. R. Murphy, C. A. Stedmon, D. Graeber, and R. Bro, "Fluorescence spectroscopy and multi-way techniques. PARAFAC," *Anal. Methods*, vol. 5, no. 23, pp. 6557–6566, 2013, doi: 10.1039/c3ay41160e.

[188] R. a Harshman, "Foundations of the PARAFAC procedure: Models and conditions for an 'explanatory' multimodal factor analysis," *UCLA Work. Pap. Phonetics*, vol. 16, no. 10, pp. 1–84, 1970, [Online]. Available: http://www.psychology.uwo.ca/faculty/harshman/wpppfac0.pdf.

[189] C. M. Andersen and R. Bro, "Practical aspects of PARAFAC modeling of fluorescence excitation-emission data," *J. Chemom.*, vol. 17, no. 4, pp.

200–215, 2003, doi: 10.1002/cem.790.

[190] S. Leurgans and R. T. Ross, “Multilinear models: applications in spectroscopy.,” *Stat SCi*, vol. 7, no. 3, pp. 289–310, 1992.

[191] R. T. Ross and S. Leurgans, “Component resolution using multilinear models,” *Methods Enzymol. Acad. Press*, pp. 679–700, 1995.

[192] J. A. Pople, P. M. W. Gill, and B. G. Johnson, “Kohn-Sham density-functional theory within a finite basis set,” *Chem. Phys. Lett.*, vol. 199, no. 6, pp. 557–560, 1992, doi: 10.1016/0009-2614(92)85009-Y.

[193] H. B. Schlegel, “No Title,” *Comput. Theor. Org. Chem.*, pp. 129–159, 1981.

[194] H. B. Schlegel, “Optimization of Equilibrium Geometries and Transition Structures,” *Adv. Chem. Phys.*, vol. 67, no. 2, pp. 249–286, 1982, doi: 10.1002/9780470142936.ch4.

[195] H. B. Schlegel, “An efficient algorithm for calculating ab initio energy gradients using s, p Cartesian Gaussians,” *J. Chem. Phys.*, vol. 77, no. 7, pp. 3676–3681, 1982, doi: 10.1063/1.444270.

[196] H. B. Schlegel, J. S. Binkley, and J. A. Pople, “First and second derivatives of two electron integrals over Cartesian Gaussians using Rys polynomials,” *J. Chem. Phys.*, vol. 80, no. 5, pp. 1976–1981, 1984, doi: 10.1063/1.446960.

[197] R. G. Parr and W. Yang, “Density-Functional Theory of Atoms and Molecules,” in *Oxford University Press*, 1989.

[198] J. Da Chai and M. Head-Gordon, “Long-range corrected hybrid density functionals with damped atom-atom dispersion corrections,” *Phys. Chem. Chem. Phys.*, vol. 10, no. 44, pp. 6615–6620, 2008, doi: 10.1039/b810189b.

[199] J. Da Chai and M. Head-Gordon, “Long-range corrected double-hybrid density functionals,” *J. Chem. Phys.*, vol. 131, no. 17, 2009, doi: 10.1063/1.3244209.

[200] J. Da Chai and M. Head-Gordon, “Systematic optimization of long-range corrected hybrid density functionals,” *J. Chem. Phys.*, vol. 128, no. 8, 2008, doi: 10.1063/1.2834918.

[201] J. Da Chai and M. Head-Gordon, “Optimal operators for Hartree-Fock exchange from long-range corrected hybrid density functionals,” *Chem.*

Phys. Lett., vol. 467, no. 1–3, pp. 176–178, 2008, doi: 10.1016/j.cplett.2008.10.070.

[202] B. Tian, E. S. E. Eriksson, and L. A. Eriksson, "Can range-separated and hybrid DFT functionals predict low-lying excitations? A Tookad case study," *J. Chem. Theory Comput.*, vol. 6, no. 7, pp. 2086–2094, 2010, doi: 10.1021/ct100148h.

[203] U. Salzner and A. Aydin, "Improved prediction of properties of π-conjugated oligomers with range-separated hybrid density functionals," *J. Chem. Theory Comput.*, vol. 7, no. 8, pp. 2568–2583, 2011, doi: 10.1021/ct2003447.

[204] Y. Minenkov, Å. Singstad, G. Occhipinti, and V. R. Jensen, "The accuracy of DFT-optimized geometries of functional transition metal compounds: A validation study of catalysts for olefin metathesis and other reactions in the homogeneous phase," *Dalt. Trans.*, vol. 41, no. 18, pp. 5526–5541, 2012, doi: 10.1039/c2dt12232d.

[205] A. D. Boese, "Density functional theory and hydrogen bonds: Are we there yet?," *ChemPhysChem*, vol. 16, no. 5, pp. 978–985, 2015, doi: 10.1002/cphc.201402786.

[206] A. D. McLean and G. S. Chandler, "Contracted Gaussian basis sets for molecular calculations. I. Second row atoms, Z=11–18," *J. Chem. Phys.*, vol. 72, p. 5639, 1980.

[207] R. Krishnan, J. S. Binkley, R. Seeger, and J. A. Pople, "Self-consistent molecular orbital methods. XX. A basis set for correlated wave functions," *J. Chem. Phys.*, vol. 72, 1980.

[208] A. V. Marenich, C. J. Cramer, and D. G. Truhlar, "Universal solvation model based on solute electron density and on a continuum model of the solvent defined by the bulk dielectric constant and atomic surface tensions," *J. Phys. Chem. B*, vol. 113, no. 18, pp. 6378–6396, 2009, doi: 10.1021/jp810292n.

[209] R. E. Skyner, J. L. McDonagh, C. R. Groom, T. Van Mourik, and J. B. O. Mitchell, "A review of methods for the calculation of solution free energies and the modelling of systems in solution," *Phys. Chem. Chem. Phys.*, vol. 17, no. 9, pp. 6174–6191, 2015, doi: 10.1039/c5cp00288e.

[210] J. Tomasi, B. Mennucci, and E. Cance, "The IEF version of the PCM solvation method: an overview of a new method addressed to study molecular solutes at the QM ab initio level," vol. 464, pp. 211–226, 1999.

[211] R. Gómez-Bombarelli, E. Calle, and J. Casado, “Mechanisms of lactone hydrolysis in neutral and alkaline conditions,” *J. Org. Chem.*, vol. 78, no. 14, pp. 6868–6879, 2013, doi: 10.1021/jo400258w.

[212] Y. Jin, Y. Zhu, and M. Tang, “Theoretical analysis on alkaline hydrolysis mechanisms of N-(2-methoxyphenyl) benzamide,” *Comput. Theor. Chem.*, vol. 963, no. 2–3, pp. 268–272, 2011, doi: 10.1016/j.comptc.2010.10.036.

[213] D. Cheshmedzhieva, S. Ilieva, B. Hadjieva, and B. Galabov, “The mechanism of alkaline hydrolysis of amides: A comparative computational and experimental study of the hydrolysis of N-methylacetamide, N-methylbenzamide, and acetanilide,” *J. Phys. Org. Chem.*, vol. 22, no. 6, pp. 619–631, 2009, doi: 10.1002/poc.1492.

[214] R. Bauernschmitt and R. Ahlrichs, “Treatment of electronic excitations within the adiabatic approximation of time dependent density functional theory,” *Chem. Phys. Lett.*, vol. 256, no. 4–5, pp. 454–464, 1996, doi: 10.1016/0009-2614(96)00440-X.

[215] M. E. Casida, C. Jamorski, K. C. Casida, and D. R. Salahub, “Molecular excitation energies to high-lying bound states from time-dependent density-functional response theory: Characterization and correction of the time-dependent local density approximation ionization threshold,” *J. Chem. Phys.*, vol. 108, no. 11, pp. 4439–4449, 1998, doi: 10.1063/1.475855.

[216] C. Van Caillie and R. D. Amos, “Geometric derivatives of excitation energies using SCF and DFT,” *Chem. Phys. Lett.*, vol. 308, no. 3–4, pp. 249–255, 1999, doi: 10.1016/S0009-2614(99)00646-6.

[217] C. Van Caillie and R. D. Amos, “Geometric derivatives of density functional theory excitation energies using gradient-corrected functionals,” *Chem. Phys. Lett.*, vol. 317, no. 1–2, pp. 159–164, 2000, doi: 10.1016/S0009-2614(99)01346-9.

[218] F. Furche and R. Ahlrichs, “Adiabatic time-dependent density functional methods for excited state properties,” *J. Chem. Phys.*, vol. 117, no. 16, pp. 7433–7447, 2002, doi: 10.1063/1.1508368.

[219] G. Scalmani, M. J. Frisch, B. Mennucci, J. Tomasi, R. Cammi, and V. Barone, “Geometries and properties of excited states in the gas phase and in solution: Theory and application of a time-dependent density functional theory polarizable continuum model,” *J. Chem. Phys.*, vol. 124, no. 9, 2006, doi: 10.1063/1.2173258.

[220] A. J. Cohen and N. C. Handy, “Dynamic correlation,” *Mol. Phys.*, vol. 99,

no. 7, pp. 607–615, 2001, doi: 10.1080/00268970010023435.

[221] "http://gaussian.com/uvvisplot/." .

[222] M. J. Frisch *et al.*, "Gaussian 09, Revision D.01, Gaussian, Inc., Wallingford CT." 2016.

[223] R. Verrone *et al.*, "Effect of β-cyclodextrin on spectroscopic properties of ochratoxin a in aqueous solution," *J. Incl. Phenom. Macrocycl. Chem.*, vol. 57, no. 1–4, pp. 475–479, 2007, doi: 10.1007/s10847-006-9237-4.

[224] A. Casale, P. G. Daniele, A. De Robertis, and S. Sammartano, "Ionic strength dependence of formation constants. Part XI. An analysis of literature data on carboxylate ligand complexes," *Ann. Chim.*, vol. 78, pp. 249 – 260, 1988.

[225] I. Bazin, V. Faucet-Marquis, M. C. Monje, M. El Khoury, J. L. Marty, and A. Pfohl-Leszkowicz, "Impact of pH on the stability and the cross-reactivity of ochratoxin A and citrinin," *Toxins (Basel).*, vol. 5, no. 12, pp. 2324–2340, 2013, doi: 10.3390/toxins5122324.

[226] J. Christensen, L. Nørgaard, R. Bro, and S. B. Engelsen, "Multivariate autofluorescence of intact food systems," *Chem. Rev.*, vol. 106, no. 6, pp. 1979–1994, 2006, doi: 10.1021/cr050019q.

[227] F. Y. H. Kutsanedzie, A. A. Agyekum, V. Annavaram, and Q. Chen, "Signal-enhanced SERS-sensors of CAR-PLS and GA-PLS coupled AgNPs for ochratoxin A and aflatoxin B1 detection," *Food Chem.*, vol. 315, no. March 2019, p. 126231, 2020, doi: 10.1016/j.foodchem.2020.126231.

[228] S. Rostami *et al.*, "High-throughput label-free detection of Ochratoxin A in wine using supported liquid membrane extraction and Ag-capped silicon nanopillar SERS substrates," *Food Control*, vol. 113, no. February, p. 107183, 2020, doi: 10.1016/j.foodcont.2020.107183.

[229] B. C. Galarreta, M. Tabatabaei, V. Guieu, E. Peyrin, and F. Lagugné-Labarthet, "Microfluidic channel with embedded SERS 2D platform for the aptamer detection of ochratoxin A," *Anal. Bioanal. Chem.*, vol. 405, no. 5, pp. 1613–1621, 2013, doi: 10.1007/s00216-012-6557-7.

[230] M. M. Hassan, M. Zareef, Y. Xu, H. Li, and Q. Chen, "SERS based sensor for mycotoxins detection: Challenges and improvements," *Food Chem.*, vol. 344, no. August 2020, 2021, doi: 10.1016/j.foodchem.2020.128652.

[231] W. Zhai, T. You, X. Ouyang, and M. Wang, “Recent progress in mycotoxins detection based on surface-enhanced Raman spectroscopy,” *Compr. Rev. Food Sci. Food Saf.*, vol. 20, no. 2, pp. 1887–1909, 2021, doi: 10.1111/1541-4337.12686.

[232] X. Wang *et al.*, “Sensitive and Reproducible Immunoassay of Multiple Mycotoxins Using Surface-Enhanced Raman Scattering Mapping on 3D Plasmonic Nanopillar Arrays,” *Small*, vol. 14, no. 39, pp. 1–11, 2018, doi: 10.1002/smll.201801623.

[233] Y. Li *et al.*, “Microarray surface enhanced Raman scattering based immunosensor for multiplexing detection of mycotoxin in foodstuff,” *Sensors Actuators, B Chem.*, vol. 266, pp. 115–123, 2018, doi: 10.1016/j.snb.2018.03.040.

[234] J. Yuan *et al.*, “A rapid Raman detection of deoxynivalenol in agricultural products,” *Food Chem.*, vol. 221, pp. 797–802, 2017, doi: 10.1016/j.foodchem.2016.11.101.

[235] T. T. Pan, D. W. Sun, H. Pu, and Q. Wei, “Simple Approach for the Rapid Detection of Alternariol in Pear Fruit by Surface-Enhanced Raman Scattering with Pyridine-Modified Silver Nanoparticles,” *J. Agric. Food Chem.*, vol. 66, no. 9, pp. 2180–2187, 2018, doi: 10.1021/acs.jafc.7b05664.

[236] Y. Kang, H. X. Gu, and X. Zhang, “A self-referenced method for determination of patulin by surface-enhanced Raman scattering using gold nanobipyramids as the substrate,” *Anal. Methods*, vol. 11, no. 40, pp. 5142–5149, 2019, doi: 10.1039/c9ay01366k.

[237] J. Li, H. Yan, X. Tan, Z. Lu, and H. Han, “Cauliflower-inspired 3D SERS substrate for multiple mycotoxins detection,” *Anal. Chem.*, vol. 91, no. 6, pp. 3885–3892, 2019, doi: 10.1021/acs.analchem.8b04622.

[238] B. Lin, P. Kannan, B. Qiu, Z. Lin, and L. Guo, “On-spot surface enhanced Raman scattering detection of Aflatoxin B1 in peanut extracts using gold nanobipyramids evenly trapped into the AAO nanoholes,” *Food Chem.*, vol. 307, no. September 2019, p. 125528, 2020, doi: 10.1016/j.foodchem.2019.125528.

[239] C. Fang, C. Wei, M. Xu, Y. Yuan, R. Gu, and J. Yao, “Ni@Au nanoparticles for surface enhanced Raman spectroscopy based ultrasensitive magnetic immunoassay on aflatoxin B1,” *RSC Adv.*, vol. 6, no. 66, pp. 61325–61333, 2016, doi: 10.1039/c6ra09397c.

[240] J. Ko, C. Lee, and J. Choo, “Highly sensitive SERS-based immunoassay of

aflatoxin B1 using silica-encapsulated hollow gold nanoparticles," *J. Hazard. Mater.*, vol. 285, pp. 11–17, 2015, doi: 10.1016/j.jhazmat.2014.11.018.

[241] Y. Jia, G. Zhou, P. Liu, Z. Li, and B. Yu, "Recent development of aptamer sensors for the quantification of aflatoxin B1," *Appl. Sci.*, vol. 9, no. 11, pp. 1–17, 2019, doi: 10.3390/app9112364.

[242] X. Xia *et al.*, "Dual-Terminal Stemmed Aptamer Beacon for Label-Free Detection of Aflatoxin B1 in Broad Bean Paste and Peanut Oil via Aggregation-Induced Emission," *J. Agric. Food Chem.*, vol. 66, no. 46, pp. 12431–12438, 2018, doi: 10.1021/acs.jafc.8b05217.

[243] B. Shao *et al.*, "Nanogapped Au(core) @ Au-Ag(shell) structures coupled with Fe3O4 magnetic nanoparticles for the detection of Ochratoxin A," *Anal. Chim. Acta*, vol. 1033, pp. 165–172, 2018, doi: 10.1016/j.aca.2018.05.058.

[244] Y. Zhao, Y. Yang, Y. Luo, X. Yang, M. Li, and Q. Song, "Double Detection of Mycotoxins Based on SERS Labels Embedded Ag@Au Core-Shell Nanoparticles," *ACS Appl. Mater. Interfaces*, vol. 7, no. 39, pp. 21780–21786, 2015, doi: 10.1021/acsami.5b07804.

[245] A. Foti *et al.*, "Optical aggregation of gold nanoparticles for SERS detection of proteins and toxins in liquid environment: Towards ultrasensitive and selective detection," *Materials (Basel).*, vol. 11, no. 3, 2018, doi: 10.3390/ma11030440.

[246] Y. Zhu, L. Wu, H. Yan, Z. Lu, W. Yin, and H. Han, "Enzyme induced molecularly imprinted polymer on SERS substrate for ultrasensitive detection of patulin," *Anal. Chim. Acta*, vol. 1101, pp. 111–119, 2020, doi: 10.1016/j.aca.2019.12.030.

[247] L. Wu *et al.*, "Surface-Imprinted Gold Nanoparticle-Based Surface-Enhanced Raman Scattering for Sensitive and Specific Detection of Patulin in Food Samples," *Food Anal. Methods*, vol. 12, no. 7, pp. 1648–1657, 2019, doi: 10.1007/s12161-019-01498-4.

[248] L. L. Qu *et al.*, "Thin layer chromatography combined with surface-enhanced raman spectroscopy for rapid sensing aflatoxins," *J. Chromatogr. A*, vol. 1579, pp. 115–120, 2018, doi: 10.1016/j.chroma.2018.10.024.

[249] W. Zhang *et al.*, "Multiplex SERS-based lateral flow immunosensor for the detection of major mycotoxins in maize utilizing dual Raman labels and triple test lines," *J. Hazard. Mater.*, vol. 393, no. January, p. 122348, 2020,

doi: 10.1016/j.jhazmat.2020.122348.

[250] A. Sacco, S. Mangino, C. Portesi, E. Vittone, and A. M. Rossi, “Novel Approaches in Tip-Enhanced Raman Spectroscopy: Accurate Measurement of Enhancement Factors and Pesticide Detection in Tip Dimer Configuration,” *J. Phys. Chem. C*, vol. 123, no. 40, pp. 24723–24730, 2019, doi: 10.1021/acs.jpcc.9b07016.

[251] M. W. Bredenkamp, J. L. M. Dillen, P. H. van Rooyen, and P. S. Steyn, “Crystal Structures and Conformational Analysis of Ochratoxin A and B: Probing the Chemical Structure causing Toxicity,” *J. CHEM. SOC. PERKIN TRANS. II*, p. 1835, 1989.

[252] G. Socrates, “Infrared and Raman Characteristic Group Frequencies. Tables and Charts,” in *Wiley*, 2001.

[253] S. Burikov, S. Dolenko, T. Dolenko, S. Patsaeva, and V. Yuzhakov, “Decomposition of water Raman stretching band with a combination of optimization methods,” *Mol. Phys.*, vol. 108, no. 6, pp. 739–747, 2010, doi: 10.1080/00268970903567288.

[254] B. Hernández, F. Pflüger, S. G. Kruglik, and M. Ghomi, “Characteristic Raman lines of phenylalanine analyzed by a multiconformational approach,” *J. Raman Spectrosc.*, vol. 44, no. 6, pp. 827–833, 2013, doi: 10.1002/jrs.4290.

[255] J. Binoy *et al.*, “Near-infrared Fourier transform Raman, surface-enhanced Raman scattering and Fourier transform infrared spectra and ab initio calculations of the natural product nodakenetin angelate,” *J. Raman Spectrosc.*, vol. 36, no. 1, pp. 63–72, 2005, doi: 10.1002/jrs.1272.

[256] “https://www.bipm.org/en/committees/cb/cbkt/wg/cbkt-mm-bipm#secondments-OTA.” .

[257] “www.bipm.org.” .

[258] R. D. Josephs *et al.*, “Mycotoxin Metrology CBKT Programme Programme Update CCQM-K154 . a trans -ZEN in acetonitrile,” 2019.

[259] J. Bates, A. Bahadoor, Y. Cui, J. Meija, A. Windust, and J. E. Melanson, “Certification of ochratoxin a reference materials: Calibration solutions OTAN-1 and OTAL-1 and a mycotoxin-contaminated rye flour MYCO-1,” *J. AOAC Int.*, vol. 102, no. 6, pp. 1756–1766, 2019, doi: 10.5740/jaoacint.19-0086.

[260] R. E. Peterson and A. Ciegler, “Ochratoxin A: Isolation and subsequent purification by high-pressure liquid chromatography,” *Appl. Environ. Microbiol.*, vol. 36, no. 4, pp. 613–614, 1978, doi: 10.1128/aem.36.4.613-614.1978.

[261] S. Westwood *et al.*, “RAPPORT BIPM – 2019/06. Purity Evaluation Guideline: Zearalenone. BIPM PEG-01.” 2019.

[262] P. Ribéreau-Gayon, D. Dubourdieu, B. Donèche, and A. Lonvaud, *Handbook of Enology: The Microbiology of Wine and Vinification*, vol. 1. 2006.

[263] T. Fazio and C. R. Warner, “A review of sulphites in foods: Analytical methodology and reported findings,” *Food Addit. Contam.*, vol. 7, no. 4, pp. 433–454, 1990, doi: 10.1080/02652039009373907.

[264] A. Jain and P. Mathur, “Estimation of Sulphite Levels in Food Products Available in Delhi, India,” *J. Nutr. Food Sci.*, vol. 06, no. 02, 2016, doi: 10.4172/2155-9600.1000463.

[265] M. V. Moreno-Arribas and B. B. Sualdea, *Wine Safety, Consumer Preference, and Human Health*. 2016.

[266] G. Gastaminza *et al.*, “Pickled onion-induced asthma : a model of sulfite-sensitive asthma ?,” vol. 25, pp. 698–703, 1995.

[267] S. L. Taylor, N. A. Higley, and R. K. Bush, “Sulfites in foods: Uses, analytical methods, residues, fate, exposure assessment, metabolism, toxicity, and hypersensitivity,” *Adv. Food Res.*, vol. 30, pp. 1–76, 1986, doi: 10.1016/S0065-2628(08)60347-X.

[268] A. L. Waterhouse, G. L. Sacks, and D. W. Jeffery, *Understanding Wine Chemistry*. 2016.

[269] E. Wilkes, “Practical measurement of total SO2 in wine,” *Wine Vitic. J.*, vol. V33N4, no. Spring 2018, pp. 32–34, 2018, [Online]. Available: www.winetitles.com.au/wvj.

[270] J. Moreno and R. Peinado, *Enological Chemistry*. 2012.

[271] G. Cordero-Bueso, J. Moraga, M. Ríos-Carrasco, M. Ruiz-Muñoz, and J. M. Cantoral, “Bacteriophages as an Up-and-Coming Alternative to the Use of Sulfur Dioxide in Winemaking,” *Front. Microbiol.*, vol. 10, no. January, pp. 1–12, 2020, doi: 10.3389/fmicb.2019.02931.

[272] H. K. Yildirim, “Alternative Methods of Sulfur Dioxide Used in Wine Production,” *J. Microbiol. Biotechnol. Food Sci.*, vol. 9, no. 4, pp. 675–687, 2020, doi: 10.15414/jmbfs.2020.9.4.675-687.

[273] I. Loira *et al.*, “Applications of nanotechnology in the winemaking process,” *Eur. Food Res. Technol.*, vol. 246, no. 8, pp. 1533–1541, 2020, doi: 10.1007/s00217-020-03519-7.

[274] M. T. Lisanti, G. Blaiotta, C. Nioi, and L. Moio, “Alternative Methods to SO 2 for Microbiological Stabilization of Wine,” *Compr. Rev. Food Sci. Food Saf.*, vol. 18, no. 2, pp. 455–479, 2019, doi: 10.1111/1541-4337.12422.

[275] G. A. Badea and A. O. Antoce, “Glutathione As a Possible Replacement of Sulfur Dioxide in Winemaking Technologies: a Review,” *Sci. Pap. B, Hortic.*, no. 59, pp. 123–140, 2015.

[276] European Commission, “Comission delegated Regulation (EU) 2019/934 of 12 March 2019,” *Off. J. Eur. Union*, vol. 149, no. 7.6.2019, pp. 1–52, 2019.

[277] C. S. Ough, “Determination of sulfur dioxide in grapes and wines.,” *J. Assoc. Off. Anal. Chem.*, vol. 69, no. 1, pp. 5–7, 1986, doi: 10.1093/jaoac/69.1.5.

[278] J. M. Vahl and J. E. Converse, “Ripper Procedure for Determining Sulfur Dioxide in Wine: Collaborative Study,” vol. 63, no. 2, pp. 194–199, 1980.

[279] T. M. Monro *et al.*, “Sensing free sulfur dioxide in wine,” *Sensors (Switzerland)*, vol. 12, no. 8, pp. 10759–10773, 2012, doi: 10.3390/s120810759.

[280] M. A. Segundo and A. O. S. S. Rangel, “A gas diffusion sequential injection system for the determination of sulphur dioxide in wines,” *Anal. Chim. Acta*, vol. 427, no. 2, pp. 279–286, 2001, doi: 10.1016/S0003-2670(00)01197-1.

[281] S. M. Oliveira, T. I. M. S. Lopes, I. V. Tóth, and A. O. S. S. Rangel, “Development of a gas diffusion multicommuted flow injection system for the determination of sulfur dioxide in wines, comparing malachite green and pararosaniline chemistries,” *J. Agric. Food Chem.*, vol. 57, no. 9, pp. 3415–3422, 2009, doi: 10.1021/jf803639n.

[282] A. M. G. Prieto, J. L. P. Pavón, and B. M. Cordero, “Gas diffusion and micellar catalysis in the flow injection determination of sulfite,” *Analyst*,

vol. 119, no. 11, pp. 2447–2452, 1994, doi: 10.1039/AN9941902447.

[283] C. M. N. Azevedo, K. Araki, H. E. Toma, and L. Angnes, "Determination of sulfur dioxide in wines by gas-diffusion flow injection analysis utilizing modified electrodes with electrostatically assembled films of tetraruthenated porphyrin," *Anal. Chim. Acta*, vol. 387, no. 2, pp. 175–180, 1999, doi: 10.1016/S0003-2670(99)00060-4.

[284] T. J. Cardwell, R. W. Cattrall, G. N. Chen, G. R. Scollary, and I. C. Hamilton, "Determination of free sulphur dioxide in red wine by alternating current voltammetry," *Analyst*, vol. 116, no. 3, pp. 253–256, 1991, doi: 10.1039/AN9911600253.

[285] Y. Huang, C. Zhang, X. Zhang, and Z. Zhang, "Chemiluminescence of sulfite based on auto-oxidation sensitized by rhodamine 6G," *Anal. Chim. Acta*, vol. 391, no. 1, pp. 95–100, 1999, doi: 10.1016/S0003-2670(99)00179-8.

[286] Y. Xiong, Q. Wang, X. Li, S. Fang, and M. Duan, "Total Sulfur Dioxide Determination in Red Wine by Suppressed Ion Chromatography with In-Sample Oxidation and SPE," *Chromatographia*, vol. 81, no. 7, pp. 1003–1011, 2018, doi: 10.1007/s10337-018-3538-9.

[287] M. Koch, R. Köppen, D. Siegel, A. Witt, and I. Nehls, "Determination of total sulfite in wine by ion chromatography after in-sample oxidation," *J. Agric. Food Chem.*, vol. 58, no. 17, pp. 9463–9467, 2010, doi: 10.1021/jf102086x.

[288] X. F. Yang, X. Q. Guo, and Y. B. Zhao, "Novel spectrofluorimetric method for the determination of sulfite with rhodamine B hydrazide in a micellar medium," *Anal. Chim. Acta*, vol. 456, no. 1, pp. 121–128, 2002, doi: 10.1016/S0003-2670(02)00005-3.

[289] A. Pérez-Ponce, S. Garrigues, and M. De la Guardia, "Direct determination of total SO2 in musts and wines by vapour phase Fuorier trasform infrared spectrometry," *Química Analítica*, vol. 19, pp. 151–158, 2000.

[290] V. J. Smith, "Determination of Sulfite Using a Sulfite Oxidase Enzyme Electrode," *Anal. Chem.*, vol. 59, no. 18, pp. 2256–2259, 1987, doi: 10.1021/ac00145a010.

[291] OIV (2018a), "Resolution OIV-OENO 591A-2018. Free sulphur dioxide – Update to method OIV-MA-AS323-04A. https://www.oiv.org/public/medias/6437/oiv-oeno-591a-2018-en.pdf Last accessed 2021-07-28." 2018.

[292] OIV (2018b), “Resolution OIV-OENO 591B-2018. Total sulphur dioxide – Update to method OIV-MA-AS323-04A. https://www.oiv.org/public/medias/6438/oiv-oeno-591b-2018-en.pdf Last accessed 2021-07-28.” 2018.

[293] OIV, “Resolution OENO 377/2009. Method OIV-MA-AS323-04B.” 2009.

[294] OIV, “Resolution OENO 377/2009. Method OIV-MA-AS323-04C,” 2009.

[295] W. Horwitz, “Evaluation of Analytical Methods Used for Regulation of Foods and Drugs,” *Anal. Chem.*, vol. 54, no. 1, pp. 67A-76A, 1982, doi: 10.1021/ac00238a765.

[296] W. Horwitz, L. R. Kamps, and K. W. Boyer, “Quality assurance in the analysis of foods and trace constituents.,” *J. Assoc. Off. Anal. Chem.*, vol. 63, no. 6, pp. 1344–1354, 1980, doi: 10.1093/jaoac/63.6.1344.

[297] UNI-ISO 13528:2016, “UNI-ISO 13528:2016.” .

[298] I. Cagnasso *et al.*, “RT INRIM 15/2021. Confronto di misura sulla determinazione della concentrazione dell’anidride solforosa libera in una soluzione di similvino.” 2021.

[299] P. Scafidi, A. Pisciotta, D. Patti, P. Tamborra, R. Di Lorenzo, and M. G. Barbagallo, “Effect of artificial shading on the tannin accumulation and aromatic composition of the Grillo cultivar (Vitis vinifera L.),” *BMC Plant Biol.*, vol. 13, no. 1, 2013, doi: 10.1186/1471-2229-13-175.

[300] O. Corona, M. Squadrito, and A. Tirelli, “Factors affecting the spectrophotometric quantification of flavonoids in wine,” *Ital. J. Food Sci.*, vol. 31, no. 3, pp. 459–469, 2019, doi: 10.14674/IJFS-1336.

[301] V. Ivanova-Petropulos, D. Petruševa, and S. Mitrev, “Rapid and Simple Method for Determination of Target Organic Acids in Wine Using HPLC-DAD Analysis,” *Food Anal. Methods*, vol. 13, no. 5, pp. 1078–1087, 2020, doi: 10.1007/s12161-020-01724-4.

[302] H. Kahlert, G. Meyer, and A. Albrecht, “Colour maps of acid–base titrations with colour indicators: how to choose the appropriate indicator and how to estimate the systematic titration errors,” *ChemTexts*, vol. 2, no. 2, pp. 1–28, 2016, doi: 10.1007/s40828-016-0026-4.

[303] I. Cagnasso *et al.*, “Evidence of a systematic underestimation of free sulfur dioxide by the aeration-oxidation method approved by OIV,” *Measurement*, vol. 194, no. December 2021, p. 111047, 2022, doi:

10.1016/j.measurement.2022.111047.

[304] L. Molognoni, H. Daguer, I. R. dos Santos, and J. De Dea Lindner, "Influence of method validation parameters in the measurement uncertainty estimation by experimental approaches in food preservatives analysis," *Food Chem.*, vol. 282, pp. 147–152, 2019, doi: 10.1016/j.foodchem.2018.12.115.

[305] A. M. H. van der Veen and M. G. Cox, "Getting started with uncertainty evaluation using the Monte Carlo method in R," *Accredit. Qual. Assur.*, vol. 26, no. 3, pp. 129–141, 2021, doi: 10.1007/s00769-021-01469-5.

[306] JCGM 101:2008, "Evaluation of measurement data — Supplement 1 to the 'Guide to the expression of uncertainty in measurement' — Propagation of distributions using a Monte Carlo method," vol. JCGM 101:2. 2008.

[307] J. Meija *et al.*, "Atomic weights of the elements 2013 (IUPAC Technical Report)," *Pure Appl. Chem.*, vol. 88, no. 3, pp. 265–291, 2016, doi: 10.1515/pac-2015-0305.

[308] R. De Levie, "Explicit Expressions of the General Form of the Titration Curve in Terms of Concentration," *J. Chem. Educ.*, vol. 70, no. 3, pp. 209–217, 1993.

[309] D. A. Ahumada Forigua and J. Meija, "Solution to titration endpoint challenge," *Anal. Bioanal. Chem.*, vol. 411, no. 17, pp. 3705–3706, 2019, doi: 10.1007/s00216-019-01800-7.

[310] D. A. Ahumada Forigua and J. Meija, "Titration endpoint challenge," *Anal. Bioanal. Chem.*, vol. 411, no. 1, pp. 1–2, 2019, doi: 10.1007/s00216-018-1430-y.

[311] EURACHEM /CITAC Guide CG 4, "Quantifying Uncertainty in Analytical Measurements, Third Edition," *QUAM:2012.P1*. 2012, doi: 10.3329/jbas.v41i2.35494.

[312] A. Possolo, A. M. H. Van Der Veen, J. Meija, and D. B. Hibbert, "Interpreting and propagating the uncertainty of the standard atomic weights (IUPAC Technical Report)," *Pure Appl. Chem.*, vol. 90, no. 2, pp. 395–424, 2018, doi: 10.1515/pac-2016-0402.

[313] U. C. E. I. 17034:2017, "UNI CEI EN ISO 17034:2017, Requisiti generali per la competenza dei produttori di materiali di riferimento." 2017.

[314] M. Chen, H. Yang, L. Rong, and X. Chen, "A gas-diffusion microfluidic

paper-based analytical device (μPAD) coupled with portable surface-enhanced Raman scattering (SERS): Facile determination of sulphite in wines," *Analyst*, vol. 141, no. 19, pp. 5511–5519, 2016, doi: 10.1039/c6an00788k.

[315] Z. Deng, X. Chen, Y. Wang, E. Fang, Z. Zhang, and X. Chen, "Headspace thin-film microextraction coupled with surface-enhanced raman scattering as a facile method for reproducible and specific detection of sulfur dioxide in wine," *Anal. Chem.*, vol. 87, no. 1, pp. 633–640, 2015, doi: 10.1021/ac503341g.

[316] A. Malengo and F. Pennecchi, "A weighted total least-squares algorithm for any fitting model with correlated variables," *Metrologia*, vol. 50, no. 6, pp. 654–662, 2013, doi: 10.1088/0026-1394/50/6/654.

[317] "https://www.itl.nist.gov/div898/handbook/pmd/section1/pmd143.htm." .

[318] T. Lafarge and A. Possolo, "The NIST uncertainty machine," *NCSLI Meas.*, vol. 10, no. 3, pp. 20–27, 2015.

[319] A. Shrivastava and V. Gupta, "Methods for the determination of limit of detection and limit of quantitation of the analytical methods," *Chronicles Young Sci.*, vol. 2, no. 1, p. 21, 2011, doi: 10.4103/2229-5186.79345.

[320] A. Emin, A. Hushur, and T. Mamtimin, "Raman study of mixed solutions of methanol and ethanol," *AIP Adv.*, vol. 10, no. 6, 2020, doi: 10.1063/1.5140722.

[321] M. Papagianni, "Advances in citric acid fermentation by Aspergillus niger: Biochemical aspects, membrane transport and modeling," *Biotechnol. Adv.*, vol. 25, no. 3, pp. 244–263, 2007, doi: 10.1016/j.biotechadv.2007.01.002.

[322] D. G. Kinniburgh, "General Purpose Adsorption Isotherms," *Environ. Sci. Technol.*, vol. 20, no. 9, pp. 895–904, 1986, doi: 10.1021/es00151a008.

[323] S. Coluccia, M. Baricco, L. Marchese, G. Martra, and A. Zecchina, "Surface morphology and reactivity towards CO of MgO particles: FTIR and HRTEM studies," *Spectrochim. Acta Part A Mol. Spectrosc.*, vol. 49, no. 9, pp. 1289–1298, 1993, doi: 10.1016/0584-8539(93)80036-A.

[324] M. Dziadas and H. H. Jeleń, "Analysis of terpenes in white wines using SPE-SPME-GC/MS approach," *Anal. Chim. Acta*, vol. 677, no. 1, pp. 43–49, 2010, doi: 10.1016/j.aca.2010.06.035.

[325] J. F. Picron, M. Herman, E. Van Hoeck, and S. Goscinny, "Analytical

strategies for the determination of pyrrolizidine alkaloids in plant based food and examination of the transfer rate during the infusion process," *Food Chem.*, vol. 266, no. December 2017, pp. 514–523, 2018, doi: 10.1016/j.foodchem.2018.06.055.

[326] O. Corona, M. Squadrito, G. Vento, A. Tirelli, and R. Di Stefano, "Over-evaluation of total flavonoids in grape skin extracts containing sulphur dioxide," vol. 172, pp. 537–542, 2015, doi: 10.1016/j.foodchem.2014.09.125.